รายงานวิจัยฉบับสมบูรณ์

โครงการ การสังเคราะห์และการศึกษาคุณลักษณะ สมบัติทางไดอิเล็กตริก และการตอบสนองทางไฟฟ้าในวัสดุเซรามิก $(Na_{1/3}Ca_{1/3}Ln_{1/3})Cu_3Ti_4O_{12}$: Ln = La^{3+}, Bi^{3+}, Sm^{3+}, Gd^{3+}, Y^{3+}, Yb^{3+}, Nd^{3+}, และ Dy^{3+}

Synthesis, Characterization, Dielectric Properties, and Electrical Response in $(Na_{1/3}Ca_{1/3}Ln_{1/3})Cu_3Ti_4O_{12}$ Ceramics: Ln = La^{3+}, Bi^{3+}, Sm^{3+}, Gd^{3+}, Y^{3+}, Yb^{3+}, Nd^{3+}, and Dy^{3+}

โดย ผศ.ดร.ประสิทธิ์ ทองใบ และคณะ

เดือน ปี ที่เสร็จโครงการ

มิถุนายน 2558

สัญญาเลขที่ TRG5680047

รายงานวิจัยฉบับสมบูรณ์

โครงการ การสังเคราะห์และการศึกษาคุณลักษณะ สมบัติทางไดอิเล็กตริก และการตอบสนองทางไฟฟ้าในวัสดุเซรามิก $(Na_{1/3}Ca_{1/3}Ln_{1/3})Cu_3Ti_4O_{12}$: Ln = La^{3+}, Bi^{3+}, Sm^{3+}, Gd^{3+}, Y^{3+}, Yb^{3+}, Nd^{3+}, และ Dy^{3+}

Synthesis, Characterization, Dielectric Properties, and Electrical Response in $(Na_{1/3}Ca_{1/3}Ln_{1/3})Cu_3Ti_4O_{12}$ Ceramics: Ln = La^{3+}, Bi^{3+}, Sm^{3+}, Gd^{3+}, Y^{3+}, Yb^{3+}, Nd^{3+}, and Dy^{3+}

ผู้วิจัย	สังกัด
1. ผศ.ดร. ประสิทธิ์ ทองใบ	มหาวิทยาลัยขอนแก่น
2. ศาสตราจารย์ ดร. สันติ แม้นศิริ	มหาวิทยาลัยเทคโนโลยีสุรนารี

สนับสนุนโดยสำนักงานกองทุนสนับสนุนการวิจัย
และมหาวิทยาลัยขอนแก่น

ACKNOWLEDGEMENTS

This work was financially supported by the Thailand Research Fund (TRF) and Khon Kaen University, Thailand (Grant number TRG5680047). The authors would like to thank the Electron Microscopy Unit, Faculty of Science, Khon Kaen University, for providing SEM facilities. The authors would like to thank the National Metal and Materials Technology Center (MTEC) for providing SEM facilities and Impedance analyzer facilities. The authors would like to thank the Thailand Center of Excellence in Physics (ThEP) for providing XPS facilities.

Asst. Prof.Dr. Prasit Thongbai

Abstract

Project Code : TRG5680047

Project Title : Synthesis, Characterization, Dielectric Properties, and Electrical Response in $(Na_{1/3}Ca_{1/3}Ln_{1/3})Cu_3Ti_4O_{12}$ Ceramics: Ln = La^{3+}, Bi^{3+}, Sm^{3+}, Gd^{3+}, Y^{3+}, Yb^{3+}, Nd^{3+}, and Dy^{3+}

Investigator : Asst. Prof.Dr. Prasit Thongbai

E-mail Address : pthongbai@kku.ac.th; prasitphysics@hotmail.com

Project Period : 2 years

The aims of this research work are to seek a new giant dielectric material system of $(Na_{1/3}Ca_{1/3}\mathbf{Ln}_{1/3})Cu_3Ti_4O_{12}$ (**Ln**=La^{3+}, Bi^{3+}, Sm^{3+}, Y^{3+}, and Yb^{3+} ions) and to improve the dielectric properties of $CaCu_3Ti_4O_{12}$-based ceramics. Ceramic samples were prepared by solid state reaction method and combustion route. Phase composition and crystal structure were characterized by X-ray diffraction (XRD) technique. Scanning electron microscope (SEM) coupled with an energy dispersive X-ray spectroscopy (EDS) was used to characterize the ceramic microstructure. The dielectric properties were investigated as functions of frequency and temperature. $(Na_{1/3}Ca_{1/3}\mathbf{Ln}_{1/3})Cu_3Ti_4O_{12}$ ceramics with **Ln** = Bi^{3+}, Y^{3+}, and Yb^{3+} exhibited high dielectric permittivity (ε') and low loss tangent ($\tan\delta$). Interestingly, $Na_{1/3}Ca_{1/3}Bi_{1/3}Cu_3Ti_4O_{12}$ exhibited a low $\tan\delta$~0.038 and high ε'~2.5×10^4 with good temperature stability. For $CaCu_3Ti_4O_{12}$-based ceramics, a novel strategy to improve the dielectric and non-Ohmic properties that deliberately created composite systems of $CaCu_{3-x}\mathbf{A}_xTi_4O_{12}/CaTiO_3$ and $CaCu_3Ti_{4-x}\mathbf{B}_xO_{12}/CaTiO_3$ (**A** = Mg, Zn and **B** = Sn, Zr) was carried out. These ceramics were prepared by using starting nominal formulas of $Ca_2Cu_{2-x}\mathbf{A}_xTi_4O_{12}$ and $Ca_2Cu_2Ti_{4-x}\mathbf{B}_xO_{12}$, respectively. The greatly reduced $\tan\delta$ and improved non-Ohmic properties were successfully accomplished, which were attributed to the improved electrical properties of the grain boundaries. Investigation to further extremely enhance ε' is important for fabricating ultra-small size capacitors with very high performance.

Keywords : Dielectric properties; Capacitor; Impedance spectroscopy.

บทคัดย่อ

รหัสโครงการ: TRG5680047

ชื่อโครงการ: การสังเคราะห์และการศึกษาคุณลักษณะ สมบัติทางไดอิเล็กตริก และการตอบสนองทางไฟฟ้าในวัสดุเซรามิก $(Na_{1/3}Ca_{1/3}Ln_{1/3})Cu_3Ti_4O_{12}$: Ln = La^{3+}, Bi^{3+}, Sm^{3+}, Gd^{3+}, Y^{3+}, Yb^{3+}, Nd^{3+}, และ Dy^{3+}

ชื่อนักวิจัย : ผศ.ดร.ประสิทธิ์ ทองใบ
สถาบัน : มหาวิทยาลัยขอนแก่น

E-mail Address: pthongbai@kku.ac.th; prasitphysics@hotmail.com

ระยะเวลาโครงการ: 2 ปี

งานวิจัยนี้ ได้ดำเนินการศึกษาวิจัยใน 2 แนวทางหลัก คือ การสังเคราะห์และศึกษาค้นคว้าวัสดุไจแอนต์ไดอิเล็กตริกกลุ่มใหม่ตามสูตรเคมี $(Na_{1/3}Ca_{1/3}\mathbf{Ln}_{1/3})Cu_3Ti_4O_{12}$ (**Ln**=La^{3+}, Bi^{3+}, Sm^{3+}, Y^{3+}, and Yb^{3+} ions) และการศึกษาวิธีการปรับปรุงสมบัติทางไดอิเล็กตริกของวัสดุเซรามิกกลุ่ม $CaCu_3Ti_4O_{12}$ โดยสังเคราะห์วัสดุเซรามิกด้วยวิธีปฏิกิริยาสถานะของแข็ง องค์ประกอบเฟสและโครงสร้างผลึกของวัสดุได้ศึกษาโดยใช้เทคนิค XRD และใช้เทคนิค SEM-EDS สำหรับศึกษาโครงสร้างทางจุลภาคของวัสดุเซรามิก ในขณะที่สมบัติทางไดอิเล็กตริกได้ศึกษาในช่วงอุณหภูมิและความถี่ต่างๆ ผลการวิจัยพบว่าวัสดุเซรามิก $(Na_{1/3}Ca_{1/3}\mathbf{Ln}_{1/3})Cu_3Ti_4O_{12}$ (**Ln** = Bi^{3+}, Y^{3+} และ Yb^{3+}) สามารถแสดงค่า ε' ที่สูงมาก ($\varepsilon' \approx 10^4$) อีกทั้งยังมีค่า tanδ ต่ำอีกด้วย โดยที่ 20 °C และที่ความถี่ 1 kHz วัสดุเซรามิก $Na_{1/3}Ca_{1/3}Bi_{1/3}Cu_3Ti_4O_{12}$ มีค่า tanδ~0.038 และมีค่า $\varepsilon' \sim 2.5\times10^4$ รวมทั้งมีความเสถียรกับอุณหภูมิในช่วงกว้างอีกด้วย ในงานวิจัยนี้ยังได้ศึกษาปรับปรุงวัสดุเซรามิกกลุ่ม $CaCu_3Ti_4O_{12}$ ด้วยแนวทางใหม่ โดยใช้วิธีการสังเคราะห์วัสดุคอมโพสิต $CaCu_{3-x}\mathbf{A}_xTi_4O_{12}/CaTiO_3$ และ $CaCu_3Ti_{4-x}\mathbf{B}_xO_{12}/CaTiO_3$ (**A** = Mg, Zn และ **B** = Sn, Zr) เพียงขั้นตอนเดียวจากสูตรเคมี $Ca_2Cu_{2-x}\mathbf{A}_xTi_4O_{12}$ และ $Ca_2Cu_2Ti_{4-x}\mathbf{B}_xO_{12}$ ตามลำดับ โดยสามารถลดค่า tanδ ได้อย่างมาก รวมทั้งยังสามารถเพิ่มคุณสมบัติทางด้านความไม่เป็นเชิงเส้นทางไฟฟ้าได้อีกด้วย ซึ่งเป็นผลเนื่องจากการเปลี่ยนแปลงสมบัติทางไฟฟ้าที่ขอบเกรนที่ดีขึ้น การพัฒนาต่อยอดเพื่อเพิ่มค่า ε' ให้มีค่าสูงอย่างทวีคูณเป็นงานวิจัยที่สำคัญยิ่งในอนาคต สำหรับการพัฒนาตัวเก็บประจุไฟฟ้าขนาดจิ๋วที่เปี่ยมไปด้วยประสิทธิภาพสูง

คำหลัก : สมบัติทางไดอิเล็กตริก; ตัวเก็บประจุไฟฟ้า; อิมพีแดนซ์

TABLE OF CONTENTS

TABLE OF CONTENTS (Cont.)

LIST OF TABLES

LIST OF FIGURES

LIST OF FIGURES (Cont.)

LIST OF FIGURES (Cont.)

LIST OF FIGURES (Cont.)

LIST OF FIGURES (Cont.)

LIST OF FIGURES (Cont.)

CHAPTER I

INTRODUCTION

1.1 Introduction to the research problem and its significance

In recent years, $CaCu_3Ti_4O_{12}$ (CCTO) gained considerable attention due to abnormal high dielectric constants (ε'~10^3—10^5) over the temperature range from 100 to 600 K and its apparent nonlinear current—voltage (current density—electric field, *J*—*E*) properties [1—16]. These ceramics are so called "*giant dielectric materials*". By considering the dielectric and nonlinear electrical properties of these perovskite—type materials, it is believed that these ceramics are promising materials for many applications. Normally, the degree of electronic device miniaturization utilizing capacitive components is decided by the ε' value of a dielectric material. The size of such devices can be reduced by replacing dielectric layers with a relative high—dielectric material. However, the loss tangent ($\tan\delta$) of CCTO and related materials is still too large ($\tan\delta$ > 0.05 at 1 kHz), making them unsuitable for capacitor applications. Therefore, reduction of $\tan\delta$ value is an important and urgent issue requiring investigation.

The dielectric properties of *Ln*—doped CCTO ceramics have been widely investigated, where *Ln* is lanthanide metal ions such as La^{3+} [18—23], Y^{3+} [22,23], Gd^{3+} [22—24], Eu^{3+} [23,25], and Nd^{3+} [26]. All of these doping ions have an influence on the microstructure and dielectric properties as well as the nonlinear current—voltage behavior of CCTO ceramics. Some doping ions can reduce significantly $\tan\delta$ of CCTO ceramics. La^{3+} substitution into CCTO can reduce $\tan\delta$ to be less than 0.03 [19]. However, the reduction of $\tan\delta$ is usually accompanied by a decrease in ε' value (~2,000-3,000). Generally, the perovskite structure can be considered highly flexible. For $ACu_3Ti_4O_{12}$ compounds (e.g., CCTO) [27], the octahedra have tilted to produce square planar sites. As a result, the structure of CCTO becomes very rigid. The space for the Ca^{2+} cations in CCTO structure is therefore essentially fixed. As well known, the ionic radius of doping ions is one of the most important parameters to determine the incorporation site. It was found that lattice parameters of some closely related $Ln_{2/3}Cu_3Ti_4O_{12}$ (especially for *Ln* = Eu^{3+} (7.390 Å), La^{3+} (7.417 Å), Nd^{3+} (7.400 Å), Tb^{3+}

(7.383 Å), Dy^{3+} (7.379 Å), Y^{3+} (7.378 Å), Gd^{3+} (7.388 Å), and Sm^{3+} (7.394 Å)) compounds and CCTO (7.391 Å) are nearly the same in value [27]. This indicates that Eu^{3+}, Gd^{3+}, and Sm^{3+} ions can perfectly substitute into Ca^{2+} sites in CCTO structure.

Besides CCTO—based ceramics, there are several brief reports on the giant dielectric properties of related oxides in the family of $(Na_{1/2}Ln)Cu_3Ti_4O_{12}$ compounds, where Ln is lanthanide metal ions. These related compounds conclude of $Na_{1/2}Bi_{1/2}$ [28—32], $Na_{1/2}La_{1/2}$ [33], $Na_{1/2}Y_{1/2}$ [34]. As reported by Subramanian *et al*. [1], it was found that only CCTO exhibits a giant value of the dielectric constant (ε'~10,286 at 100 kHz). The values of ε' for other materials in this $ACu_3Ti_4O_{12}$ material system were found to be considerably lower than 3600 at 100 kHz. Further investigation revealed that by varying sintering conditions, some $(Na_{1/2}Ln)Cu_3Ti_4O_{12}$ ceramics could exhibit very high ε' values, on the order of 10^4, as was observed in CCTO ceramics [28—34]. These are of approximately the same magnitude as values of ε' exhibited by CCTO materials.

Notably, many types of these $(Na_{1/2}Ln)Cu_3Ti_4O_{12}$ ceramics can exhibit good dielectric properties. For example, it was found that $(Na_{1/2}Bi_{1/2})Cu_3Ti_4O_{12}$ [29] and La—doped $(Na_{1/2}Bi_{1/2})Cu_3Ti_4O_{12}$ ceramics [30] exhibited good dielectric properties. These materials showed high ε' (13,495 and 10,200 at 10 kHz, respectively) and low $\tan\delta$ (0.031 and 0.022 at 10 kHz, respectively). $(Na_{1/2}La_{1/2})Cu_3Ti_4O_{12}$ ceramics can also exhibit high ε' of 6,100—8,700 with $\tan\delta$ values of 0.073—0.114 at 1 kHz [33]. The lowest $\tan\delta$ value observed in $(Na_{1/2}La_{1/2})Cu_3Ti_4O_{12}$ ceramics was 0.032 at 10 kHz. These results indicate that the $(Na_{1/2}Ln)Cu_3Ti_4O_{12}$ ceramic system is one of dielectric material systems with potential for capacitor applications.

It was observed that the ceramic microstructure of $(Na_{1/2}Ln)Cu_3Ti_4O_{12}$ ceramics is highly dense, consisting of small grain sizes with narrow distribution size. It was clearly proved that these ceramics compounds as well as CCTO ceramics are electrically heterogeneous, consisting of semiconducting grains and insulating grain boundaries [3]. High density of insulating grain boundary layer is obtained in a ceramic that possesses a highly dense microstructure with small grains. Reduction of grain size to increase the grain boundary density is one of the most effective methods to greatly reduce the low–frequency values of $\tan\delta$ of dielectric ceramic materials. Therefore, it is important to seek new giant dielectric materials that process small and fine grains. It is likely that the grain growth rate of $(Na_{1/2}Ln)Cu_3Ti_4O_{12}$ compounds is lower than that of

CCTO ceramics. Abnormal grain growth cannot be exhibited in these compounds; while, this behavior is usually observed in CCTO ceramics. Although the mechanism of microstructure evolution of $(Na_{1/2}Ln)Cu_3Ti_4O_{12}$ compounds is still unclear, different types and valent states of cations in A-site of $(Na_{1/2}Ln)Cu_3Ti_4O_{12}$ compounds may be another one important factor that can cause an influence on the microstructure evolution. Therefore, incorporation of various types with different valent states (+1, 2+, and +3) in A-site (e.g., Ca-site for $CaCu_3Ti_4O_{12}$) of $ACu_3Ti_4O_{12}$ structure may increase a degree of disorder in structure. It is also possible that heavy ions with high atomic mass such as La^{3+}, Bi^{3+}, Sm^{3+}, Gd^{3+}, Y^{3+}, Yb^{3+}, Nd^{3+}, and Dy^{3+} may be a primary cause to inhibit the grain boundary mobility due to a solute drag effect. As a result, the grain growth rate of these compounds is inhibited, producing a fine-grained microstructure. Thus, giant dielectric properties can be improved and modified.

In the first part of this research project, $(Na_{1/3}Ca_{1/3}Ln_{1/3})Cu_3Ti_4O_{12}$ ceramics, where Ln = La^{3+}, Bi^{3+}, Sm^{3+}, Gd^{3+}, Y^{3+}, Yb^{3+}, Nd^{3+}, and Dy^{3+}, are synthesized by using a standard solid state reaction method. The phase formation and microstructure of the sintered ceramics are investigated. The dielectric properties and electrical nonlinear current-voltage characteristics are investigated systematically.

Generally, lowering σ_{dc} to reduce low-frequency tanδ can be done by enhancing the resistances of internal interfaces in CCTO-based compounds. These could be the interface between grains or the interface between a CCTO grain and a second phase particle. Enhancement may be accomplished by (1) doping CCTO with suitable metal ions to intrinsically improve electrical properties of grain boundaries [38-41], (2) altering Ca^{2+} and Cu^{2+} molar ratios to produce CCTO/$CaTiO_3$ (CTO) composites [42-47], (3) filling oxygen vacancies at grain boundaries [48], among others. Unfortunately, improved dielectric properties of CCTO produced using these strategies rarely result in materials that fulfill all of the requirements of electronic applications, *i.e.*, high ε', low tanδ, and dielectric response with good temperature stability. It was also found that most of the metal ion substitutions or other strategies, which have been successfully used to improve a particular dielectric property, simultaneously worsen other important dielectric properties of CCTO. For example, a large decrease in tanδ (~0.02 at 1 kHz) observed in a binary compound system of $Ca_2Cu_2Ti_4O_{12}$ (consisting of 33.3 mol% of CCTO and 66.7 mol% of CTO) caused a large decrease in ε' (~2×10^3) [44,49]. Given a very low-tanδ value of CCTO/CTO, with its low-ε' value are still acceptable values for

use in capacitor applications compared to commercial $BaTiO_3$ and $Pb(Sc_{1/2}Ta_{1/2})O_3$ ceramics [49]. Unfortunately, the condition of $\Delta\varepsilon'(\%) < \pm 15\%$ within CCTO/CTO exists only in a narrow temperature range of -60 to 90 ^{o}C [44,45]. Hence, these properties are consistent with the EIA temperature standard for application in X5R capacitor only, but not for X7R or X8R capacitors [50]. It is very important to note the advantages of CCTO/CTO composite ceramics. First, this composite system can be synthesized using a one—step process from a nominal composition of $Ca_2Cu_2Ti_4O_{12}$ [xxx]. Second, this composite ceramic showed no piezoelectricity, which is advantageous to reduce mechanical damage in ac operation [49]. Third, its sintering temperature is lower than that of $BaTiO_3$ [44,49]. Thus, it is better if all of the dielectric properties of $Ca_2Cu_2Ti_4O_{12}$ ceramics can simultaneously be improved. This will support progress in communications technology. Enhanced ε', reduced tanδ, and increased $\Delta\varepsilon'(\%)$ are valuable for enhancing volumetric efficiency, reducing dissipation of stored energy into heat, and extending the temperature use range of capacitors, respectively.

Interestingly, it was found that substitution of suitable ions such as Mg^{2+} [51], Zn^{2+} [52], La^{3+} [53], Bi^{3+} [54], Sn^{4+} [55], and Zr^{4+} [39] can reduce low-frequency tanδ values of CCTO ceramics. Although these tanδ values were still slightly higher than the standard value, these behaviors are rarely found in CCTO ceramics. We hypothesize that substitution of theses ions into $Ca_2Cu_2Ti_4O_{12}$ ceramics may enhance the overall dielectric properties. Therefore, the aim of this part for this research work is to provide a novel strategy to improve the overall dielectric properties of CCTO-based ceramics by substitution of Mg^{2++}, Zn^{2+}, La^{3+}, Bi^{3+}, Sn^{4+}, and Zr^{4+} ions to the composite system of $Ca_2Cu_2Ti_4O_{12}$.

1.2 Literature review

Figure 1.2.1 shows the structure of $CaCu_3Ti_4O_{12}$ compound. The structure of $CaCu_3Ti_4O_{12}$ has been determined from neutron powder diffraction data [36], indexing in space group *Im3* (No. 204) at 100 and 35 K to study the possible occurrence of a ferroelectric phase transition. It was found that there is no indication of any phase transition in the $CaCu_3Ti_4O_{12}$. The structure remains cubic and centric down to 35 K [1].

In general, the perovskite structure with formula of AMO_3 is considered highly flexible. Thus, the perovskite structure can accommodate a large range of A cation sizes through tilting of MO_6 octahedra such as TiO_6 for $BaTiO_3$ compound. If the TiO_6

octahedra have tilted to produce square planar sites for three quarters of the A cations (such as in $ACu_3Ti_4O_{12}$ compounds), the structure will be very rigid. The space for the A cations is therefore essentially fixed, and the twelve equal A–O distances must be very close to 2.6 Å. Thus, only Ca and Cd ions can be filled in the A-site of the $ACu_3Ti_4O_{12}$ compounds [27].

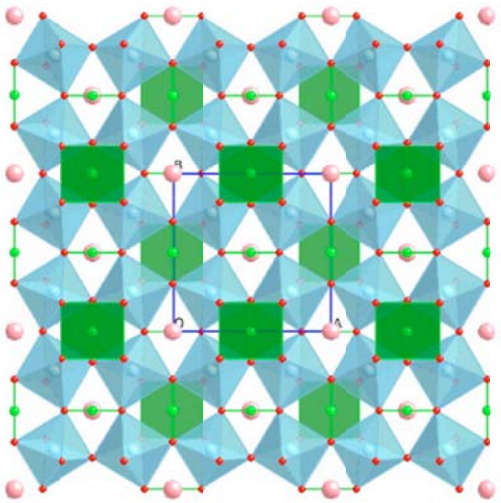

Figure 1.2.1 The *Im*3 average crystal structure of $CaCu_3Ti_4O_{12}$ in projection along $\langle 001 \rangle$ showing the tilted TiO_6 octahedral network as well as the CuO_4 square planar coordination of the Cu ions [35].

There are several brief reports on the giant dielectric properties of related oxides in the family of $(Na_{1/2}Ln)Cu_3Ti_4O_{12}$ compounds, where Ln is lanthanide metal ions. These related compounds conclude of $Na_{1/2}Bi_{1/2}$ [28—32], $Na_{1/2}La_{1/2}$ [33], $Na_{1/2}Y_{1/2}$ [34]. As reported by Subramanian *et al*. [1], it was found that only $CaCu_3Ti_4O_{12}$ exhibits a giant value of the dielectric constant (ε'~10,286 at 100 kHz). The values of ε' for other materials in this $ACu_3Ti_4O_{12}$ material system were found to be considerably lower than 3600 at 100 kHz. Ferrarelli *et al.* [37] have found that $Na_{1/2}Bi_{1/2}Cu_3Ti_4O_{12}$ ceramic can also exhibit a giant dielectric constant of about 10^4 at room temperature just as observed in $CaCu_3Ti_4O_{12}$ ceramics. As demonstrated in Fig. 1.2.2, the dielectric constant of the $Na_{1/2}Bi_{1/2}Cu_3Ti_4O_{12}$ is slightly higher than that of the $CaCu_3Ti_4O_{12}$ ceramic. Unfortunately, the authors did not provide the values of $\tan\delta$ for these two ceramics [37]. However, according to this observation, it is expected that other related

$(Na_{1/2}Ln)Cu_3Ti_4O_{12}$ compounds may produce a high dielectric constant as observed in $CaCu_3Ti_4O_{12}$ ceramics.

Ren *et al.* [29] reported the effect of sintering conditions on the dielectric properties of $Na_{1/2}Bi_{1/2}Cu_3Ti_4O_{12}$ ceramics. They found that a high dielectric constant value of about 13,495 with very low dielectric loss 0.031 was obtained in the $Na_{1/2}Bi_{1/2}Cu_3Ti_4O_{12}$ ceramic sintered at 1000 ^{o}C for 7.5 h. It is interesting that this ceramics also showed an excellent temperature stability of dielectric constant values (-4.00 to -0.69%) in the temperature range of -50 - 150 ^{o}C. As shown in Fig. 1.2.3, the dielectric properties of $Na_{1/2}Bi_{1/2}Cu_3Ti_4O_{12}$ ceramics sintered at various temperatures for 5 h are depended on the sintering temperatures.

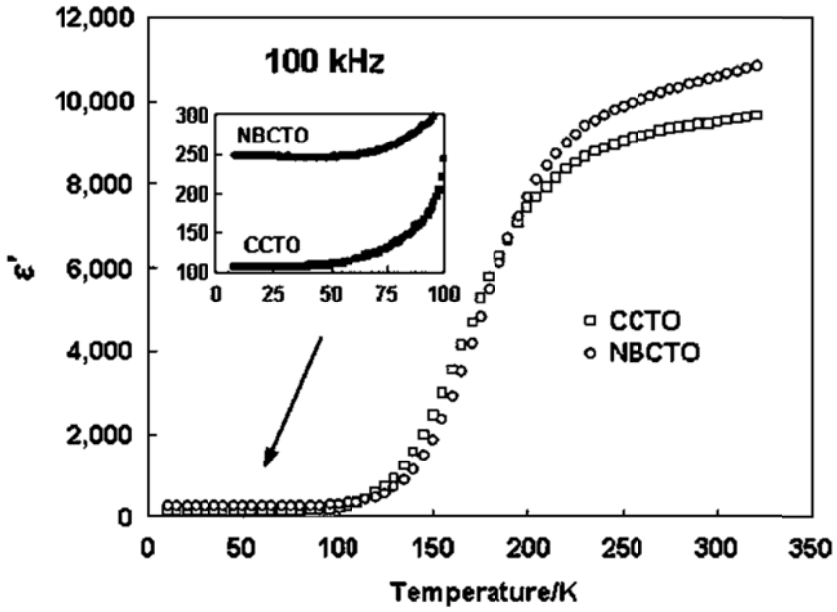

Figure 1.2.2 Variation of permittivity at 100 kHz for $Na_{1/2}Bi_{1/2}Cu_3Ti_4O_{12}$ and $CaCu_3Ti_4O_{12}$ ceramics [37].

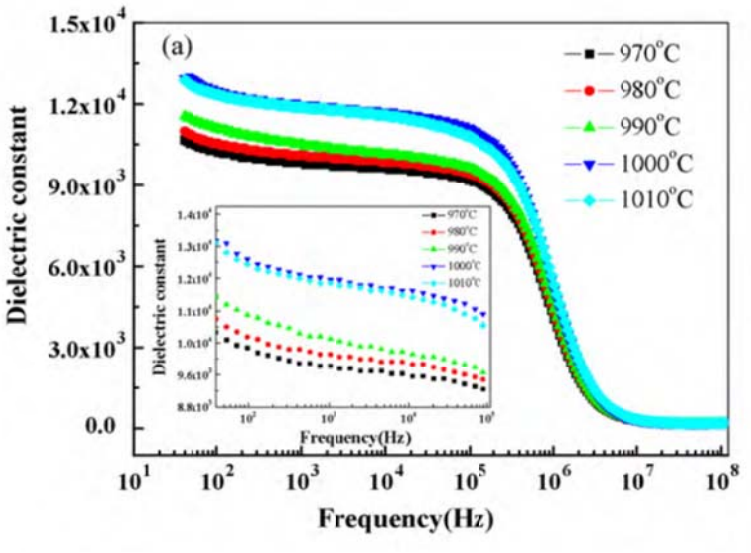

Figure 1.2.3 Frequency dependence of dielectric constant for specimens prepared at different temperatures for 5 h [29].

Recently, we found that $Na_{1/2}La_{1/2}Cu_3Ti_4O_{12}$ ceramics can exhibit good dielectric properties just as observed in $Na_{1/2}Bi_{1/2}Cu_3Ti_4O_{12}$ ceramics [15]. High dielectric constant values and low tanδ (0.032–0.038 at 10 kHz) were observed in $Na_{1/2}La_{1/2}Cu_3Ti_4O_{12}$ ceramics. Moreover, we also found that the $Na_{1/2}La_{1/2}Cu_3Ti_4O_{12}$ ceramics can also exhibit nonlinear current-voltage properties as observed in $CaCu_3Ti_4O_{12}$ ceramics. As shown in Fig. 1.2.4, the $Na_{1/2}La_{1/2}Cu_3Ti_4O_{12}$ ceramics exhibit non-Ohmic properties, and shows very high breakdown electric field strength of 4.40 and 2.87 kV cm^{-1}. The overall dielectric and nonlinear electrical properties of $Na_{1/2}Bi_{1/2}Cu_3Ti_4O_{12}$ and $Na_{1/2}La_{1/2}Cu_3Ti_4O_{12}$ ceramics are likely to better than that of $CaCu_3Ti_4O_{12}$ ceramics. These results may be associated with the fine-grained ceramic microstructure of the samples, as revealed in Figs. 1.2.5 and 1.2.6. Obviously, an abnormal grain growth is not observed in these two figures for $Na_{1/2}Bi_{1/2}Cu_3Ti_4O_{12}$ and $Na_{1/2}La_{1/2}Cu_3Ti_4O_{12}$ ceramics. Microstructures of both ceramics are dense and consist of small grain sizes.

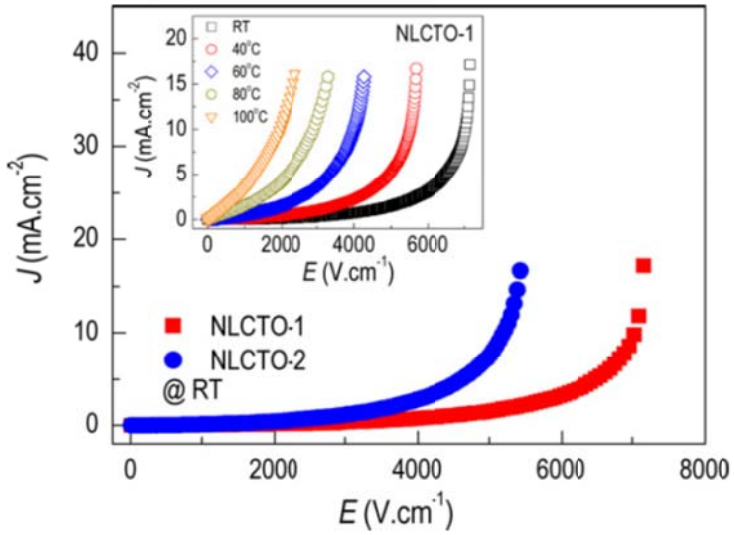

Figure 1.2.4 Non-Ohmic characteristics (J vs. E) for $Na_{1/2}La_{1/2}Cu_3Ti_4O_{12}$ ceramics sintered at different temperatures [15].

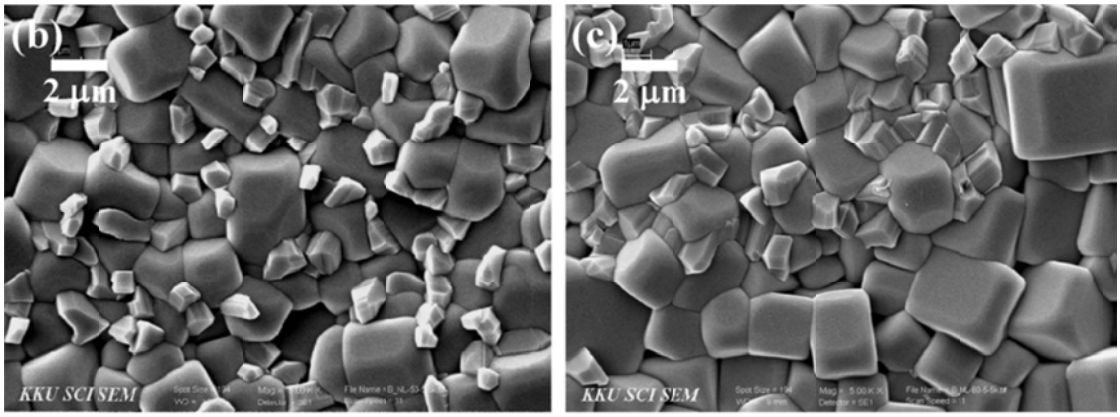

Figure 1.2.5 SEM images of surface morphologies of $Na_{1/2}La_{1/2}Cu_3Ti_4O_{12}$ ceramics sintered at (a) 1080 °C and (b) 1090 °C for 5 h [15].

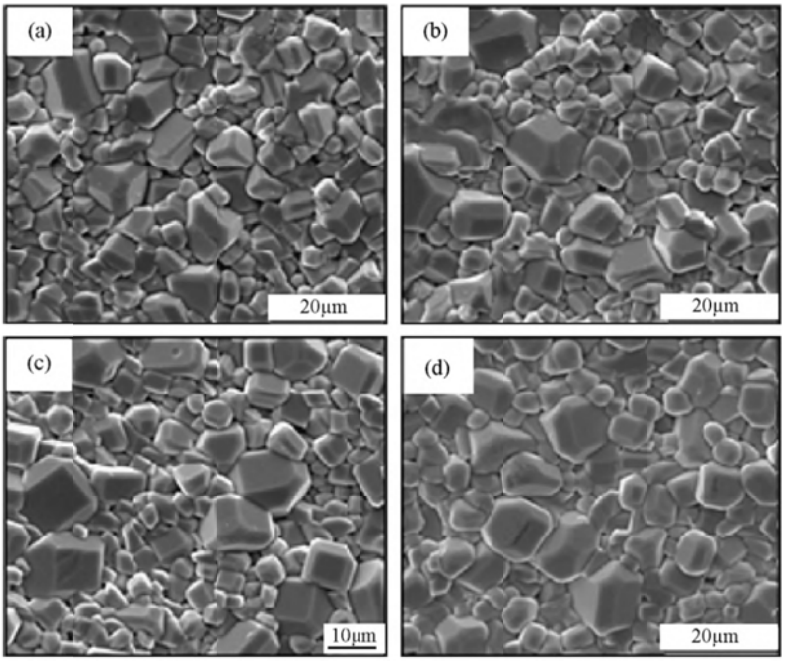

Figure 1.2.6 SEM images of surface morphologies of $Na_{1/2}Bi_{1/2}Cu_3Ti_4O_{12}$ ceramics sintered at (a) 970, (b) 980, (c) 990 and (d) 1000 ^{o}C for 5 h [15].

References

[1] M.A. Subramanian, D. Li, N. Duan, B.A. Reisner, A.W. Sleight, J. Solid State Chem. 151 (2000) 323.

[2] S.–Y. Chung, I.-D. Kim, S.-J.L. Kang, Nature Mat. 3 (2004) 774.

[3] J. Liu, C.-G. Duan, W.-G, Yin, W.N. Mei, R.W. Smith, J.R. Hardy, Phys. Rev. B 70 (2004) 144106.

[4] L. Liu, H. Fan, P. Fang, X. Chen, Mat. Res. Bull. 43 (2008) 1800.

[5] P. Lunkenheimer, S. Krohns, R. Fichtl, S.G. Ebbinghaus, A. Reller, A. Loidl, Eur. Phys. J. Special Topics 180 (2010) 61.

[6] H. Ren, P. Liang, Z. Yang, Mat. Res. Bull. 45 (2010) 1608.

[7] Z.Y. Liu, X.M. Li, J.Q. Wu, J. Am. Ceram. Soc. 95 (2012) 476.

[8] W.C. Ribeiro, R.G.C. Araújo, P.R. Bueno, Appl. Phys. Letts. 98 (2011) 132906.

[9] W. Somphan, N. Sangwong, T. Yamwong, P. Thongbai, J. Mater. Sci.: Mater. Electron. (2011), DOI 10.1007/s10854-011-0578-4.

[10] M. Li, D.C. Sinclair, A.R. West, J. Appl. Phys. 109 (2011) 084106.

[11] A. Rajabtabar-Darvishi, W .Li, O. Sheikhnejad-Bishe, L. Wang, X. Li, N. Li, W. Fei, Trans. Nonferrous. Met. Soc. Chaina 21 (2011) 400.

[12] J. Yuan, Y.-H. Lin, H. Lu, B. Cheng, C.-W. Nan, J. Am. Ceram. Soc. 94 (2011) 1966.

[13] T. Li, K. Fang, J. Hao, Y. Xue, Z. Chen, Mater. Sci. Eng. B 176 (2011) 171.

[14] J.L. He, F.C. Luo, J. Hu, Y.-H. Lin, Sci. China Tech. Sci. 54 (2011) 2506.

[15] P. Thongbai, T. Yamwong, S. Maensiri, Mat. Res. Bull. 47 (2012) 432.

[16] P. Thongbai, B. Putasaeng, T. Yamwong, S. Maensiri, J. Mater. Sci.: Mater. Electron. 23 (2012) 795.

[17] S. Jesurani, S. Kanagesan, K. Ashok, J. Sol-Gel Sci. Technol. (2012) DOI 10.1007/s10971-012-2862-z.

[18] B.S. Prakash, K.B.R. Varma, J. Mater. Sci.: Mater. Electron. 17 (2006) 899.

[19] L. Feng, X. Tang, Y. Yan, X. Chen, Z. Jiao, G. Cao, Phys. Stat. Sol. (a) 203 (2006) 22.

[20] B. Cheng, Y.-H. Lin, J. Yuan, J. Cai, C.-W. Nan, X. Xiao, J. He, J. Appl. Phys. 106 (2009) 034111.

[21] S. Jin, H. Xia, Y. Zhang, Ceram. Int. 35 (2009) 309.

[22] C. Mu, H. Zhang, Y. Liu, Y. Song, P. Liu, J. rare Earths 28 (2010) 43.

[23] L. Liu, L. Fang, Y. Huang, Y. Li, D. Shi, S. Zheng, S. Wu, C. Hu, J. Appl. Phys. 110 (2011) 094101.

[24] R. Kashyap, O.P. Thakur, R.P. Tandon, Ceram. Int. 38 (2012) 3029.

[25] T. Li, Y. Xue, Z. Chen, F. Chang, Mater. Sci. Eng. B 158 (2009) 58.

[26] Y. Wang, L. Ni, X.M. Chen, J. Mater. Sci.: Mater. Electron. 22 (2011) 345.

[27] M.A. Subramanian, A.W. Sleight, Solid State Sci. 4 (2002) 347.

[28] M.C. Ferrarelli, T.B. Adams, A. Feteira, D.C. Sinclair, A.R. West, Appl. Phys. Lett. 89 (2006) 212904.

[29] H. Ren, P. Liang, Z. Yang, Mater. Res. Bull. 45 (2010) 1608.

[30] Z. Yang, H. Ren, X. Chao, P. Liang, Mater. Res. Bull. 47 (2012) 1273.

[31] B. Xu, J. Zhang, Z. Tian, S.L. Yuan, Mater. Lett. 75 (2012) 87.

[32] Y. Qiu, Z.Z. Ma, S.X. Huo, H.N. Duan, Z.M. Tian, S.L. Yuan, L. Chen, J. Mater. Sci.: Mater. Electron. 23 (2012) 1587.

[33] P. Thongbai, T. Yamwong, S. Maensiri, Mater. Res. Bull. 47 (2012) 432.

[34] W. Somphan, N. Sangwong, T. Yamwong, P. Thongbai, J. Mater. Sci.: Mater. Electron. 23 (2012) 1229.

[35] Y. Liu, R. L. Withers, X. Y. Wei, Phys. Rev. B 72 (2005) 134104.

[36] B. Bochu, M. N. Deschizeaux, J. C. Joubert, J. Solid State Chem. 29 (1979) 291.

[37] M. C. Ferrarelli, T. B. Adams, A. Feteira, D. C. Sinclair, A. R. West, Appl. Phys. Lett. **89** (2006) 212904.

[38] E.A. Patterson, S. Kwon, C.-C. Huang, D.P. Cann, Appl. Phys. Lett. 87 (2005) 182911.

[39] Z. Yang, L. Zhang, X. Chao, L. Xiong, J. Liu, J. Alloys Compd. 509 (2011) 8716-8719.

[40] P. Liang, X. Chao, F. Wang, Z. Liu, Z. Yang, J. Am. Ceram. Soc. 96 (2013) 3883-3890.

[41] P. Thongbai, B. Putasaeng, T. Yamwong, V. Amornkitbamrung, S. Maensiri, J. Alloys Compd. 582 (2014) 747-753.

[42] L. Ramajo, R. Parra, J.A. Varela, M.M. Reboredo, M.A. Ramírez, M.S. Castro, J. Alloys Compd. 497 (2010) 349-353.

[43] T. Li, K. Fang, J. Hao, Y. Xue, Z. Chen, Mater. Sci. Eng. B 176 (2011) 171-176.

[44] P. Thongbai, B. Putasaeng, T. Yamwong, S. Maensiri, J. Alloys Compd. 509 (2011) 7416-7420.

[45] M.A. Ramírez, P.R. Bueno, E. Longo, J.A. Varela, J. Phys. D: Appl. Phys. 41 (2008) 152004.

[46] M.A. Ramírez, P.R. Bueno, R. Tararam, A.A. Cavalheiro, E. Longo, J.A. Varela, J. Phys. D: Appl. Phys. 42 (2009) 185503.

[47] J. Jumpatam, P. Thongbai, B. Kongsook, T. Yamwong, S. Maensiri, Mater. Lett. 76 (2012) 40-42.

[48] R. Yu, H. Xue, Z. Cao, L. Chen, Z. Xiong, J. Eur. Ceram. Soc. 32 (2012) 1245-1249.

[49] W. Kobayashi, I. Terasaki, Appl. Phys. Lett. 87 (2005) 032902.

[50] A.J. Moulson, J.M. Herbert, Electroceramics : materials, properties, applications, 2nd ed., Wiley, West Sussex ; New York, 2003.

[51] M. Li, G. Cai, D.F. Zhang, W.Y. Wang, W.J. Wang, X.L. Chen, J. Appl. Phys. 104 (2008) 074107.

[52] D. Xu, C. Zhang, Y. Lin, L. Jiao, H. Yuan, G. Zhao, X. Cheng, J. Alloys Compd. 522 (2012) 157-161.

[53] L. Feng, X. Tang, Y. Yan, X. Chen, Z. Jiao, G. Cao, physica status solidi (a) 203 (2006) R22-R24.

[54] F. Luo, J. He, J. Hu, Y.-H. Lin, J. Appl. Phys. 105 (2009) 076104.

[55] L. Ni, X.M. Chen, X.Q. Liu, Mater. Chem. Phys. 124 (2010) 982-986.

1.3 Objectives

1.3.1 To synthesize the $(Na_{1/3}Ca_{1/3}Ln_{1/3})Cu_3Ti_4O_{12}$ ceramics, where Ln = La^{3+}, Bi^{3+}, Sm^{3+}, Gd^{3+}, Y^{3+}, Yb^{3+}, Nd^{3+}, and Dy^{3+}.

1.3.2 To study the structure and microstructure of the sintered $(Na_{1/3}Ca_{1/3}Ln_{1/3})Cu_3Ti_4O_{12}$ ceramics.

1.3.3 To seek new giant dielectric materials with high performance properties: high dielectric constant, low loss tangent, and good temperature stability.

1.3.4 To improve the dielectric properties of $CaCu_3Ti_4O_{12}$-based ceramics by fabricating $CaCu_3Ti_4O_{12}/CaTiO_3$ composites in which were substituted by La^{3+}, Bi^{3+}, Mg^{2+}, Zn^{2+}, Sn^{4+}, and Zr^{4+} ions.

1.3.5 To explain the giant dielectric behavior and nonlinear electrical properties of all the synthesized ceramic samples.

1.4 Scope of research

1.4.1 $(Na_{1/3}Ca_{1/3}Ln_{1/3})Cu_3Ti_4O_{12}$ ceramics, where Ln = La^{3+}, Bi^{3+}, Sm^{3+}, Gd^{3+}, Y^{3+}, Yb^{3+}, Nd^{3+}, and Dy^{3+}, were prepared by solid state reaction method and combustion route.

1.4.2 $CaCu_{3-x}\mathbf{A}_xTi_4O_{12}/CaTiO_3$ (**A** = Mg, Zn), $CaCu_3Ti_{4-x}\mathbf{B}_xO_{12}/CaTiO_3$ (**B** = Sn, Zr), and $Ca_{1-x}\mathbf{C}_xCu_3Ti_4O_{12}/CaTiO_3$ (**C** = La, Bi) composites were prepared by solid state reaction method.

1.4.3 The microstructure, phase composition, and valent states of the sintered ceramics were characterized by using the SEM-EDS, XRD, and XPS techniques, respectively.

1.4.4 The dielectric properties were investigated in the frequency range of 10^2-10^7 Hz and temperature range from -70 to 220 ^oC.

1.4.5 The nonlinear current-voltage properties were investigated at room temperature.

CHAPTER II

RESEARCH METHODOLOGY

2.1 Sample Preparation

2.1.1 $(Na_{1/3}Ca_{1/3}Ln_{1/3})Cu_3Ti_4O_{12}$ ceramics (Ln = La^{3+}, Bi^{3+}, Sm^{3+}, Gd^{3+}, Y^{3+}, Yb^{3+}, Nd^{3+}, and Dy^{3+})

In this part of the research work, $(Na_{1/3}Ca_{1/3}Ln_{1/3})Cu_3Ti_4O_{12}$ ceramics, where Ln = La^{3+}, Bi^{3+}, Sm^{3+}, Gd^{3+}, Y^{3+}, Yb^{3+}, Nd^{3+}, and Dy^{3+}, were prepared by a solid state reaction method. $CaCO_3$ (99.95% purity), CuO (99.9% purity), TiO_2 (99.9% purity), La_2O_3 (>99% purity), Y_2O_3 (>99% purity), Yb_2O_3 (>99% purity), Sm_2O_3 (>99% purity), Gd_2O_3 (>99% purity), Dy_2O_3 (>99% purity), Nd_2O_3 (>99% purity), and Bi_2O_3 (>99% purity), were used as starting raw materials. First, stoichiometric amounts of the raw materials were weighted to produce $(Na_{1/3}Ca_{1/3}Ln_{1/3})Cu_3Ti_4O_{12}$. Second, the mixture was ball milled in ethanol for 24 h. Next, the mixed slurry was dried and calcined at 900 ^{o}C for 6-15 h. Then, the calcined powder was ground and pressed into pellets of 9.5 mm in diameter and ~1 mm in thickness by uniaxial compression at 200 MPa. Finally, these pellets were sintered at 1050—1100 ^{o}C for 1—30 h using heating and cooling rates of 5 ^{o}C/min.

2.1.2 $CaCu_{3-x}A_xTi_4O_{12}/CaTiO_3$ (A = Mg, Zn), $CaCu_3Ti_{4-x}B_xO_{12}/CaTiO_3$ (B = Sn, Zr), and $Ca_{1-x}C_xCu_3Ti_4O_{12}/CaTiO_3$ (C = La, Bi)

In this part of the research work, $CaCu_{3-x}\mathbf{A}_xTi_4O_{12}/CaTiO_3$ (**A** = Mg, Zn), $CaCu_3Ti_{4-x}\mathbf{B}_xO_{12}/CaTiO_3$ (**B** = Sn, Zr), and $Ca_{1-x}\mathbf{C}_xCu_3Ti_4O_{12}/CaTiO_3$ (**C** = La, Bi) were prepared by a solid state reaction method. These three compound systems were prepared using nominal chemical compositions of $Ca_2Cu_{2-x}\mathbf{A}_xTi_4O_{12}$, $Ca_2Cu_2Ti_{4-x}\mathbf{B}_xO_{12}$, and $Ca_{2-x}\mathbf{C}_xCu_2Ti_4O_{12}$ (x = 0, 0.05, 0.10, 0.20, and 0.30), respectively. $CaCO_3$ (99.95% purity), CuO (99.9% purity), TiO_2 (99.9% purity), MgO (99.99% purity), ZnO (99.99% purity), Bi_2O_3 (>99% purity), La_2O_3 (>99% purity), SnO_2 (>99% purity), and ZrO_2 (>99% purity) were used as starting raw materials. A stoichiometric mixture of the starting materials for each composition was ball-milled in ethanol for 24 h using ZrO_2 balls. The mixed slurries were dried and then calcined at 900 ^{o}C for 15 h. The calcined powders were ground and pressed into pellets (without a binder) of 9.5 mm diameter and ~1.0

mm thickness by uniaxial compression at 200 MPa. Finally, these pellets were sintered at 1100 ^{o}C for 6-24 h.

2.2 Characterization techniques

X-ray diffraction (XRD) (Philips PW3040, The Netherlands) was used to characterize the crystal structure and phase composition of all powders and sintered ceramics. Scanning electron microscopy (SEM) (LEO 1450VP, UK and Hitachi S-3400, Japan) coupled with energy–dispersive X–ray spectrometry (EDS) was used to characterize the microstructure of the synthesized ceramics. Valence states of cations in the sintered ceramics were investigated using x–ray photoelectron spectroscopy (XPS) (AXIS Ultra DLD, UK). Transmission electron microscopy (TEM) (FEI Tecnai G^{2}, Eindhoven, The Netherlands) was used to characterize the morphologies of the prepared powders.

2.3 Dielectric and nonlinear current-voltage measurements

Dielectric properties of the samples were measured using an Agilent E4980A Precision LCR Meter and Agilent 4294A Precision LCR Meter over the frequency range from 10^{2} to 10^{7} Hz and at an oscillation voltage of 0.5 V. The measurements were performed over the temperature range from -70 to 200 ^{o}C. Each measured temperature was kept constant with an accuracy of $\pm$1 ^{o}C. Current–voltage measurements were made at room temperature using a high voltage measurement unit (Keithley Model 247). Prior to measurements, Au electrodes were sputtered on each pellet face at a current of 25 mA for 8 min using a Polaron SC500 sputter coating unit. Current–voltage measurements were made at room temperature using a high voltage measurement unit (Keithley Model 247). Prior to measurements, Au electrodes were sputtered on each pellet face at a current of 25 mA for 8 min using a Polaron SC500 sputter coating unit. The breakdown electric field (E_b) was achieved at J = 1 mA.cm^{-2}. The nonlinear coefficient (α) values were calculated from the following formula:

$$\alpha = \frac{\log(J_2 / J_1)}{\log(E_2 / E_1)} \qquad (2.3.1)$$

where E_1 and E_2 are, respectively, the electric fields corresponding to J_1 = 1 and J_2 = 10 mA.cm^{-2}.

The complex impedance (Z^*) was calculated from the relation,

$$\varepsilon^* = \varepsilon' - i\varepsilon'' = \frac{1}{i\omega C_0 Z^*} = \frac{1}{i\omega C_0 (Z' - iZ'')}, \quad (2.3.2)$$

where ε' and ε'' are, respectively, the real (dielectric constant) and imaginary parts (dielectric loss) of the complex permittivity (ε^*). Z' and Z'' are the real part and imaginary parts of Z^*, respectively. ω is the angular frequency ($\omega=2\pi f$) and $i = \sqrt{-1}$. $C_0 = \varepsilon_0 S/d$ is the empty cell capacitance, where S is the sample area, d is the sample thickness, and ε_0 is the permittivity of free space, ε_0 = 8.854×10^{-12} F/m. The complex admittance (Y^*) of the samples was calculated from the relation,

$$Y^* = Y' + jY'' = \frac{1}{Z^*}, \quad (2.3.3)$$

where Y' and Y'' are the real part and imaginary parts of Y^*, respectively.

CHAPTER III
RESULTS AND DISCUSSION

3.1 $(Na_{1/3}Ca_{1/3}Ln_{1/3})Cu_3Ti_4O_{12}$ ceramics (Ln = La^{3+}, Bi^{3+}, Sm^{3+}, Gd^{3+}, Y^{3+}, Yb^{3+}, Nd^{3+}, and Dy^{3+})

In this part of the research work, $(Na_{1/3}Ca_{1/3}Ln_{1/3})Cu_3Ti_4O_{12}$ ceramics (Ln = La^{3+}, Bi^{3+}, Sm^{3+}, Gd^{3+}, Y^{3+}, Yb^{3+}, Nd^{3+}, and Dy^{3+}) were synthesized. It was found that pure phase can be achieved in the $(Na_{1/3}Ca_{1/3}Bi_{1/3})Cu_3Ti_4O_{12}$, $(Na_{1/3}Ca_{1/3}Y_{1/3})Cu_3Ti_4O_{12}$, $(Na_{1/3}Ca_{1/3}Yb_{1/3})Cu_3Ti_4O_{12}$, $(Na_{1/3}Ca_{1/3}La_{1/3})Cu_3Ti_4O_{12}$, and $(Na_{1/3}Ca_{1/3}SM_{1/3})Cu_3Ti_4O_{12}$ compounds. Unfortunately, the main phase of the $(Na_{1/3}Ca_{1/3}Gd_{1/3})Cu_3Ti_4O_{12}$, $(Na_{1/3}Ca_{1/3}Nd_{1/3})Cu_3Ti_4O_{12}$, and $(Na_{1/3}Ca_{1/3}Dy_{1/3})Cu_3Ti_4O_{12}$ cannot be produced by using a solid state reaction method. A large amount of impurities were detected in these compounds.

The best dielectric properties were achieved in the $(Na_{1/3}Ca_{1/3}Bi_{1/3})Cu_3Ti_4O_{12}$ (NCBCTO) ceramics. According to this part of the research, a new approach to achieve a novel perovskite ceramic compound, $ACu_3Ti_4O_{12}$, is demonstrated. A-sites in the $ACu_3Ti_4O_{12}$ structure were occupied by Na^{+}, Ca^{2+}, and Bi^{3+} each at a level of ~33.3 at.%, leading to formation of $Na_{1/3}Ca_{1/3}Bi_{1/3}Cu_3Ti_4O_{12}$. This ceramic exhibited a low loss tangent ($\tan\delta$~0.038) and a high ε' value of ~2.5×10^4 at 1 kHz with good temperature stability. The high-frequency dielectric relaxation behavior showed activation energies of 0.110-0.121 eV. Nonlinear *J-E* characteristics were observed, indicating the existence of Schottky barriers at grain boundaries. Valence states of Cu cations (*i.e.*, Cu^{+}, Cu^{2+}, and Cu^{3+}) in $Na_{1/3}Ca_{1/3}Bi_{1/3}Cu_3Ti_4O_{12}$ ceramic were investigated using X-ray photoelectron spectroscopy. Impedance spectroscopy analysis revealed that $Na_{1/3}Ca_{1/3}Bi_{1/3}Cu_3Ti_4O_{12}$ was electrically heterogeneous and comprised of semiconducting grains and insulating grain boundaries. Interfacial polarization at the insulating layer of grain boundaries was suggested to be the origin of this high dielectric response. Details of the experimental results and discussion are as follows:

Figure 3.1.1 shows the surface morphologies of NCBCTO ceramics sintered under different conditions. Abnormal grain growth was observed in all samples. Large grain sizes of ~10-20 μm and fine grains with sizes of 2-5 μm were observed. The

overall surface morphologies of the NCBCTO ceramics were similar to those observed in $[Na^{+}_{1/2}Ln^{3+}_{1/2}]Cu_3Ti_4O_{12}$ rather than like CCTO ceramics [1-6].

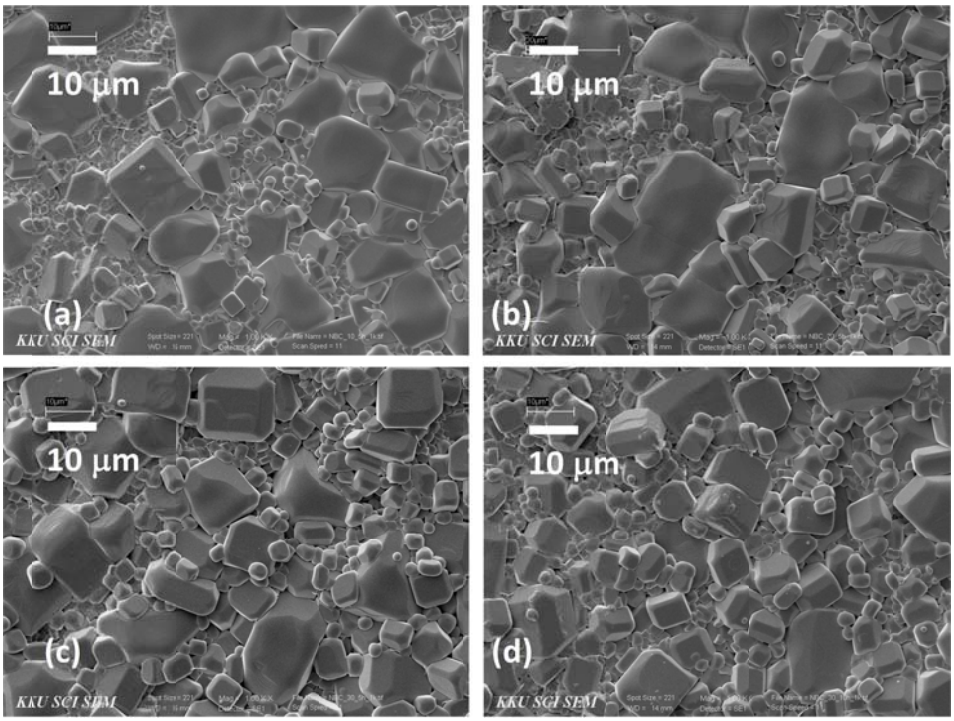

Figure 3.1.1 SEM images of un-polished surface of NCBCTO ceramics sintered at different conditions: (a) 1060 °C for 5 h, (b) 1070 °C for 5 h, (c) 1080 °C for 5 h, and (d) 1080 °C for 10 h.

From the nominal formula of $Na_{1/3}Ca_{1/3}Bi_{1/3}Cu_3Ti_4O_{12}$, there are at least two possible mechanisms of the phase formation. A two—phase composite system of CCTO—$Na_{1/2}Bi_{1/2}Cu_3Ti_4O_{12}$ could form. Alternatively, a single phase may form following the nominal composition by random distribution of Na^{+}, Ca^{2+}, and Bi^{3+} ions in A—sites of the crystal lattice. To clarify, the XRD technique was used to determine phase composition(s). As shown in Fig. 3.12(a), all of the XRD patterns indicated a single phase. However, it is difficult to differentiate CCTO and $Na_{1/2}Bi_{1/2}Cu_3Ti_4O_{12}$ phases because their lattice parameters are very close (7.391 and 7.412 Å, respectively) [7]. Thus, splitting of XRD peaks could not be observed using our X—ray spectrometer instrument. It is notable that these XRD patterns confirm the formation of a $CaCu_3Ti_4O_{12}$—like structure (JCPDS 75—2188). All diffraction peaks in XRD patterns for NCBCTO ceramics are well indexed based on the body—centered cubic structure within

space group *Im*3. Lattice parameters were calculated and found to be 7.40074, 7.4001, 7.3960, and 7.3966 Å for NCBCTO ceramics sintered at 1060 °C for 5 h, 1070 °C for 5 h, 1080 °C for 5 h, and 1080 °C for 10 h, respectively. It was observed that these lattice parameter values were intermediate between the corresponding values of CCTO and $Na_{1/2}Bi_{1/2}Cu_3Ti_4O_{12}$.

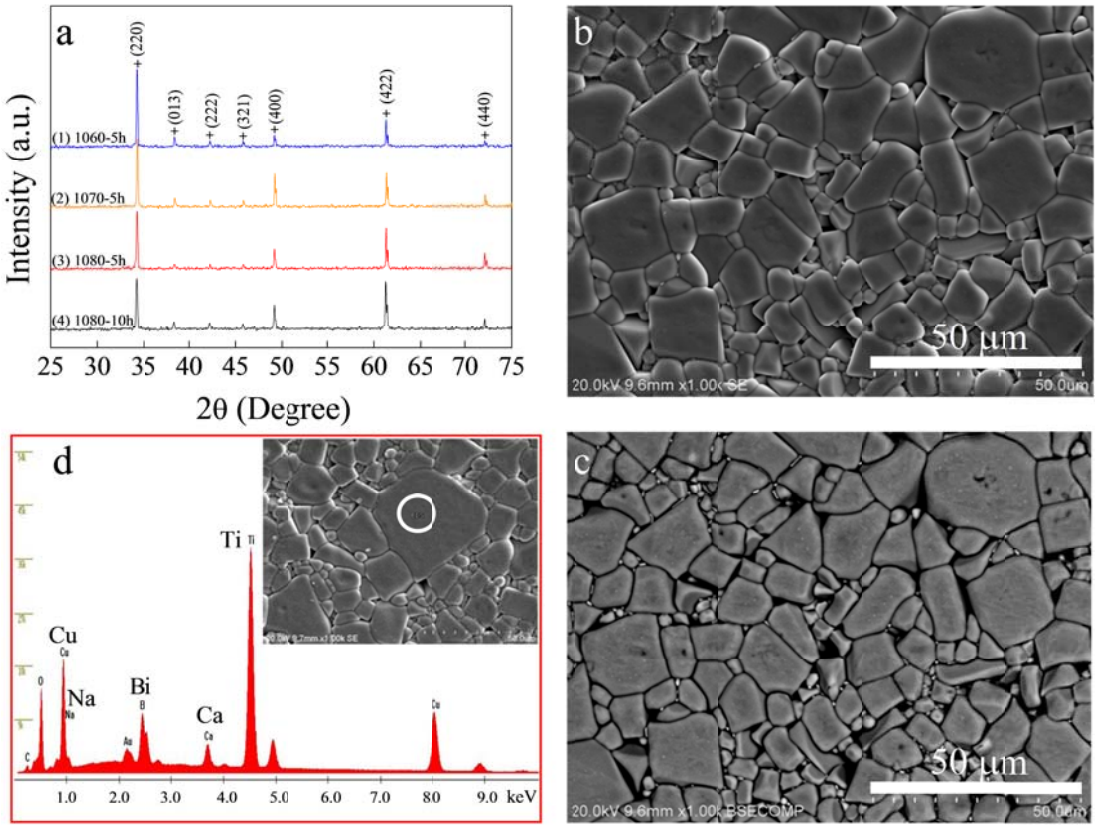

Figure 3.1.2 (a) XRD patterns of NCBCTO ceramics. (b-c) Secondary electron and backscattered SEM images of polished surfaces of the NCBCTO ceramic sintered at 1060 °C for 5 h. (d) EDS spectrum detected in the circle area, as shown in its inset.

As seen in Figs. 3.1.2(b) and (c), the SEM images of the polished surfaces in the same area showed no difference in contrast in the backscattered SEM image [Fig. 3.1.2(c)]. This may indicate a single phase in the NCBCTO ceramic. The microstructure was characterized using an EDS technique. The results are shown in Fig. 3.1.2(d). It was found that the EDS peaks of all metal elements (i.e., Na, Ca, Bi, Cu, Ti) were

detected at the same point (as marked in the circle area). These results indicate that Na^{+}, Ca^{2+}, and Bi^{3+} ions may well randomly occupy A-sites in the $ACu_3Ti_4O_{12}$ lattice structure.

As depicted in Fig. 3.1.3, all the sintered ceramics exhibited giant dielectric properties with $\varepsilon' \sim 1.5\text{-}2.75\times10^4$ at frequencies less than 10^5 Hz as was observed in CCTO ceramics and some $ACu_3Ti_4O_{12}$ compounds [1, 8-12]. The frequency dependence of tanδ at 20 °C is demonstrated in the inset of Fig. 3.1.3. Based on the experimental results of the current study, the optimal sintering condition was 1060 °C for 5 h, resulting in values of $\varepsilon' \sim 2.59\times10^4$ and tanδ~0.038 at 1 kHz. ε′ decreased as the sintering temperature was increased. This is similar to that reported in published literature for $Na_{1/2}Bi_{1/2}Cu_3Ti_4O_{12}$ ceramics [1]. At 1 kHz, tanδ values of NCBCTO ceramics sintered at 1060 °C for 5 h, 1070 °C for 5 h, 1080 °C for 5 h, and 1080 °C for 10 h were approximately 0.038, 0.046, 0.067, and 0.057, respectively. The overall frequency dependence of ε′ and tanδ behavior were similar to those observed in many compounds in the $ACu_3Ti_4O_{12}$ family.

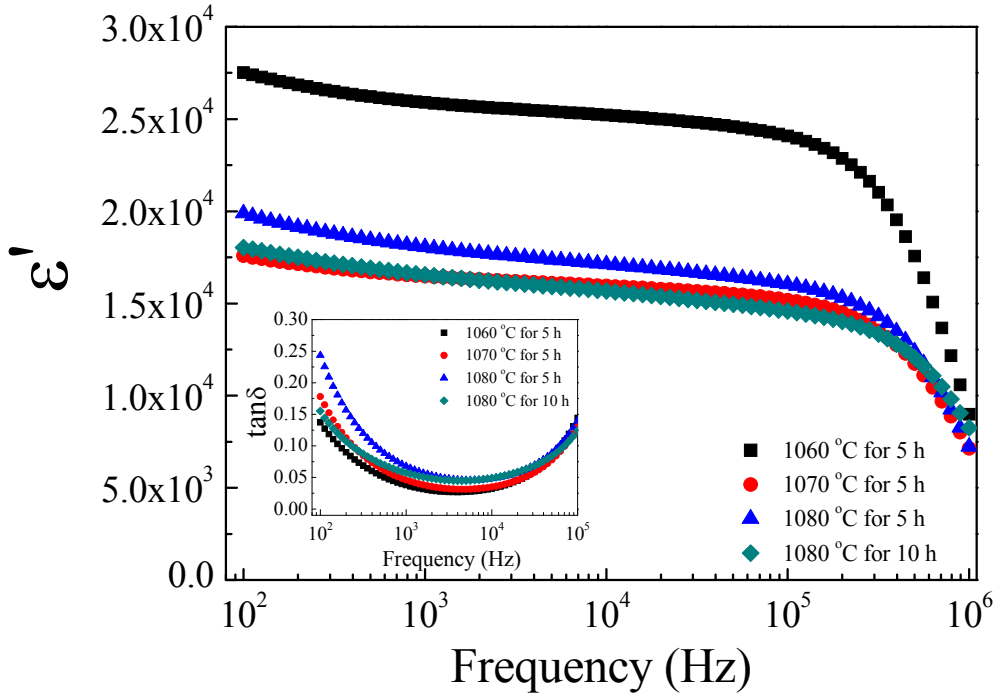

Figure 3.1.3 Variation in ε′ with frequency at 20 °C for NCBCTO ceramics sintered at different conditions; inset shows tanδ as a function of frequency at 20 °C.

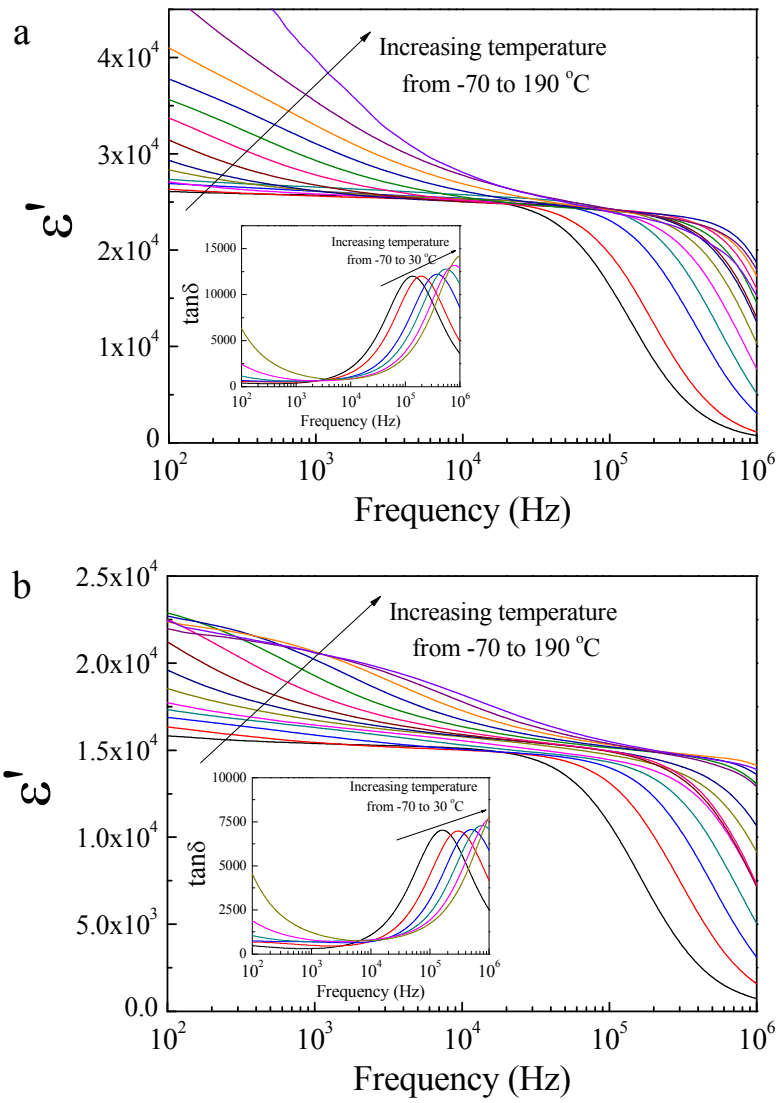

Figure 3.1.4 Frequency dependence of ε′ at various temperatures of the NCBCTO ceramics sintered at (a) 1060 °C and (b) 1080 °C for 10 h; their insets show the frequency dependence of tanδ in a temperature range from -70 to 30 °C.

As can be seen in Fig. 3.1.4, the frequency dependence of ε′ for NCBCTO ceramics at different temperatures showed three main parts of dielectric relaxation processes. Three plateau-like features in the plots of ε′ vs. frequency were observed in the temperature range from -70 to 190 °C, especially for the NCBCTO ceramic sintered at 1080 °C for 10 h [Fig. 3.1.14(b)]. The first plateau at low frequencies was observed at the highest temperatures, whereas the high frequency plateau can only be seen in

parts at the lowest temperature measured. The first plateau in a low-frequency range is attributed to an sample-electrode interface response, while the high frequency plateau is originated from the bulk response. At intermediate frequencies, the primary plateau is obvious. This is attributed to the dielectric response of the grain boundaries [13, 14]. The dielectric responses of these three parts were clearly shown by Li *et al* [14]. A step-like decrease in ε' and a concurrent appearance of tanδ-relaxation peaks [as shown in the insets] were observed. Both of a step-like decrease in ε' and tanδ peak shift to higher frequencies with increasing temperature, indicating to thermally activated dielectric relaxation process. This dielectric relaxation process is usually observed in CCTO and related ceramics [2, 11, 15, 16]. The primary dielectric relaxation process is referred to Maxwell-Wagner relaxation. According to the Maxwell-Wagner model, Liu *et al* [17]. demonstrated that the dielectric relaxation behavior was governed by the electrical response of the grains. It was found that the high-frequency bulk relaxation activation energies of the NCBCTO ceramics sintered at 1060 ^{o}C for 5 h, 1070 ^{o}C for 5 h, 1080 ^{o}C for 5 h, and 1080 ^{o}C for 10 h were 0.110, 0.116, 0.113, and 0.121 eV, respectively. These bulk values are comparable to those observed in CCTO (0.103 eV) [18], $Bi_{2/3}Cu_3Ti_4O_{12}$ (0.095 eV) [17], and $Na_{1/2}Y_{1/2}Cu_3Ti_4O_{12}$ ceramics (0.112 eV) [12].

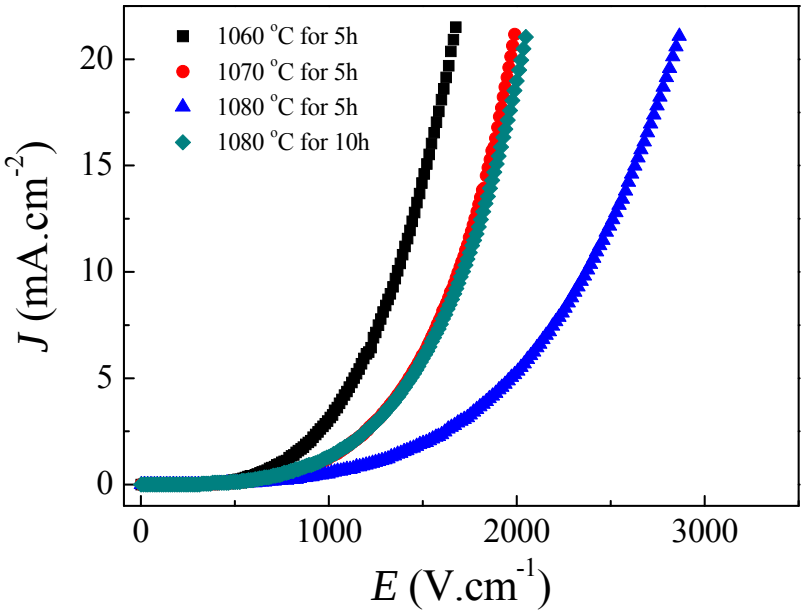

Figure 3.1.5 Nonlinear *J-E* characteristics of NCBCTO ceramics at room temperature.

Nonlinear electrical behavior was also observed in NCBCTO ceramics, as shown in Fig. 3.1.5. The breakdown electric field strength (E_b) was obtained at a current density of J = 1 mA.cm^{-2}. The nonlinear coefficient (α) was calculated in the range of J = 1-10 mA.cm^{-2}. The values of α in NCBCTO ceramics sintered at 1060 °C for 5 h, 1070 °C for 5 h, 1080 °C for 5 h, and 1080 °C for 10 h were found to be 3.67, 3.72, 3.19, and 3.74, respectively. E_b values were 569, 739, 836, and 704 V.cm^{-2}, respectively. The nonlinear properties of NCBCTO ceramics slightly changed with sintering conditions. However, these values were still too low for practical application in varistor devices.

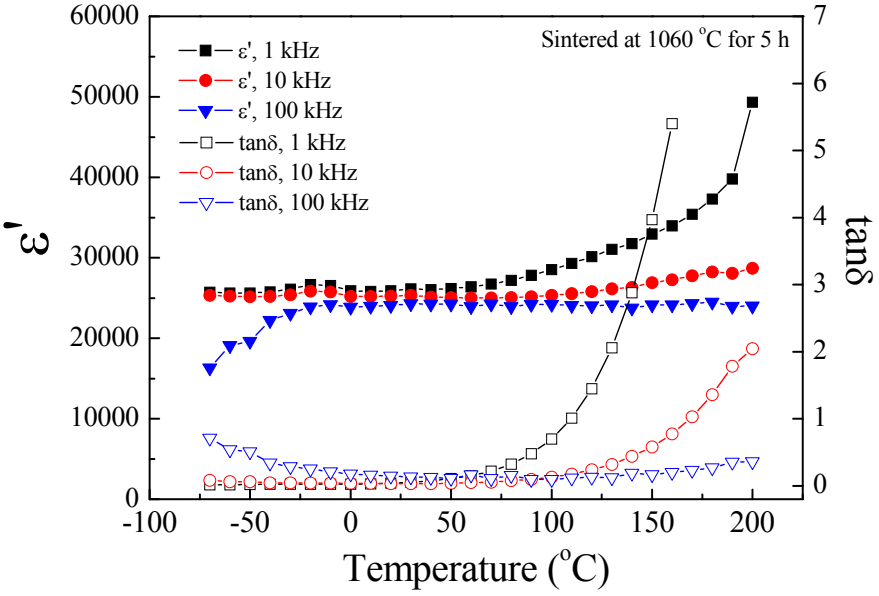

Figure 3.1.6 Temperature dependence of ε′ and tanδ at selected frequencies of the NCBCTO ceramic sintered at 1060 °C for 5 h.

To describe the dielectric and electrical properties of NCBCTO ceramics, the ceramic sample with the best dielectric properties was selected for further investigation. The temperature dependences of ε′ and tanδ of the NCBCTO ceramic sintered at 1060 °C for 5 h are shown in Fig. 3.1.6. At 20 °C and 1 kHz, ε′ and tanδ values of this NCBCTO ceramic were 2.59×10^4 and 0.038, respectively. Moreover, ε′ was slightly dependent upon temperature in the range from -70 to 110 °C with a temperature coefficient less than ±15% (at 1 kHz). According to previous reports [1, 3], at 10 kHz, $Na_{1/2}Bi_{1/2}Cu_3Ti_4O_{12}$ and La-doped $Na_{1/2}Bi_{1/2}Cu_3Ti_4O_{12}$ ceramics showed high ε′ values of

~1.34×10^4 and ~1.02×10^4 and low tanδ of ~0.031 and 0.022, respectively. In these two materials, ε′ at 10 kHz was slightly dependent upon temperature in the ranges of -50 - 150 °C and -60-120 °C, respectively. It was found that at 10 kHz, high ε′ (~1.1×10^4) and low tanδ (~0.033) with good thermal stability of ε′ in the range of -60 - 150 °C were achieved in $Y_{2/3}Cu_3Ti_4O_{12}$ ceramics.[11] To compare the dielectric properties with other $ACu_3Ti_4O_{12}$ ceramics, ε′ and tanδ values as well as the temperature coefficient of the NCBCTO ceramic at 10 kHz were evaluated, *i.e.*, ε′~2.52×10^4, tanδ~0.032, and temperature coefficient less than ±15% in the range of -70 - 200 °C. These results produced better dielectric properties in the NCBCTO ceramic than other $ACu_3Ti_4O_{12}$ ceramics.

Impedance spectroscopy was used to study the electrical properties of grains and grain boundaries to elucidate possible mechanisms resulting in the giant dielectric response of NCBCTO ceramics. According to the brick–work layer model for polycrystalline electroceramics [13, 14], an equivalent circuit consisting of two parallel resistor-capacitor (*R*-*C*) elements connected in series was presented. For CCTO ceramics, one *R*-*C* element represents the electrical response of semiconducting grains and other represents the electrical response of grain boundaries. It is notable that the impedance data of all the ceramic samples were calculated by considering the ratio of area of electrode/pellet thickness. As can be seen in Fig. 3.1.7 and its inset, the diameter of the large semicircle arc of the impedance complex plane plot (Z^*) decreased with increasing temperature. This indicated that the total resistance decreased as temperature increased. The total resistance might be governed by the grain boundary resistance (R_{gb}) or R_{gb} combined with the electrode interface resistance (R_{gb}+R_e). Generally, the grain (bulk) and grain boundary responses can each be described by a parallel *R*–*C* element, whereas the macroscopic dielectric response is usually represented by a series connection of two *R*–*C* elements [13]. To clarify, impedance data were fitted to a single *R*–*C* parallel circuit using the modified equation for a Z^* plot [17],

$$Z^* = \frac{R_{gb}}{1+\left(i\omega R_{gb}C_{gb}\right)^{\alpha}}, \qquad (3.1.1)$$

where C_{gb} is the capacitance of the grain boundaries, α is a constant parameter ($0 < \alpha \leq 1$), and ω is the angular frequency of an applied electric field. As shown in Fig. 3.1.7 and its inset, Z^* plots of the experimental data in the temperature range of 100 - 170 ^{o}C are well fitted by Eq. (3.1.1). This indicates that there are no two overlapping arcs of R_{gb} and R_e. Thus, the large semicircle arc of Z^* plots at various temperatures is attributed to the grain boundary response only. The conduction activation energy of the grain boundary determined by variation in R_{gb} was found to be 0.551 eV. The nonzero intercept of the high-frequency impedance data was also observed (not shown). Therefore, one can conclude that NCBCTO ceramics are electrically heterogeneous, consisting of conductive and insulating elements. These are the electrical properties of grains and grain boundaries, respectively. Thus, it is reasonable to suggest that the giant dielectric response of NCBCTO ceramics may be caused by the interfacial polarization at the grain boundaries. Under an applied electric field, charges inside the semiconducting grains were forced to move accumulating at the insulating grain boundaries, producing a strong interfacial polarization. This is responsible for the observed giant dielectric properties of NCBCTO ceramics.

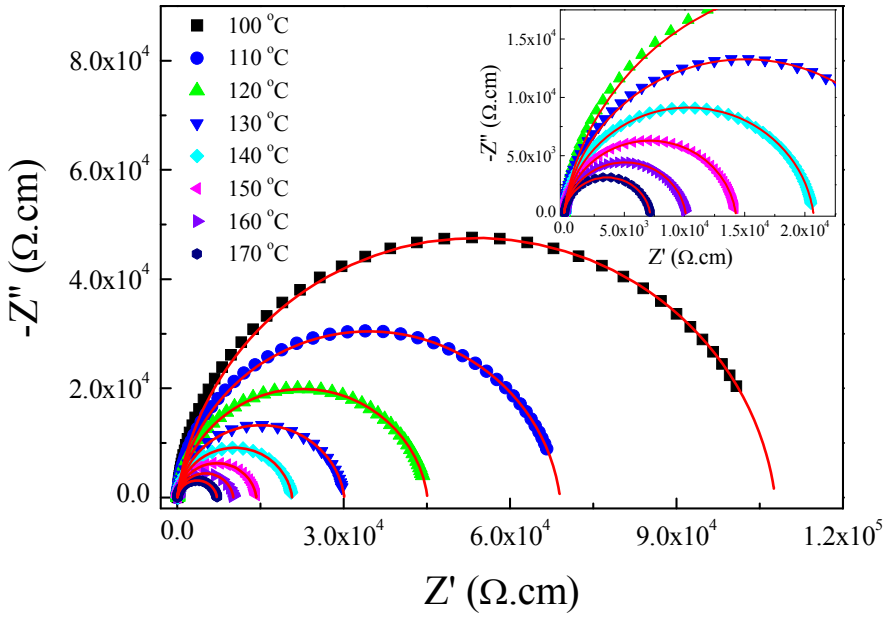

Figure 3.1.7 Impedance complex plan plot (Z^*) at different temperatures for the NCBCTO ceramic sintered at 1060 ^{o}C for 5 h; the inset is an expanded view near the origin for high frequency data. The solid curves are the fitted data using Eq. (3.1.1).

The oxidation states of polyvalent cations were investigated using an XPS technique. Fig. 3.1.8 shows the XPS spectrum of Cu2*p* regions of the NCBCTO ceramic. The Cu_{2p} peak region was divided into three peaks using Gaussian-Lorentzian profile fitting. The highest peak height represents Cu^{2+}. The other two peaks at lower and higher binding energies were produced by Cu^{+} and Cu^{3+}, respectively [18-20]. The XPS spectrum also indicated the presence of Ti^{3+} in the NCBCTO ceramic. Polyvalent cations, i.e., Cu^{+}, Cu^{3+}, and Ti^{3+} ions, may have a remarkable effect on the electrical semiconducting properties of grains. For CCTO ceramics, *n*-type semiconductor characteristic of the grains was confirmed by measuring the thermoelectric power with a negative Seebeck coefficient value [21]. Thus, it is reasonable to suggest that the conduction mechanism inside the *n*-type semiconducting grains of the NCBCTO ceramics is primarily due to electron hopping between $Cu^{+} \leftrightarrow Cu^{2+}$ and $Ti^{3+} \leftrightarrow Ti^{4+}$ sites.

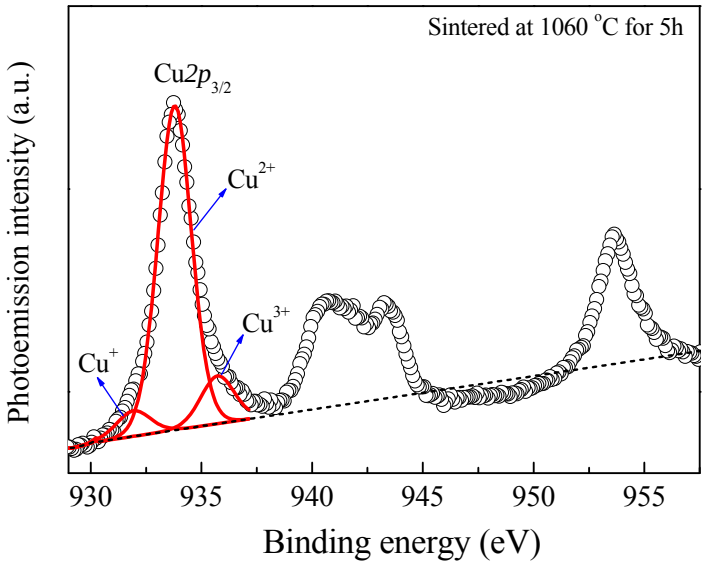

Figure 3.1.8 XPS spectrum of the NCBCTO ceramic sintered at 1060 °C for 5 h.

The microstructures of other $(Na_{1/3}Ca_{1/3}\boldsymbol{Ln}_{1/3})Cu_3Ti_4O_{12}$ ceramics were characterized using SEM technique. As shown in Fig. 3.1.9, the microstructure of the $(Na_{1/3}Ca_{1/3}\boldsymbol{Ln}_{1/3})Cu_3Ti_4O_{12}$ ceramics, where ***Ln*** = La^{3+}, Sm^{3+}, Y^{3+}, and Yb^{3+} consisted of grains and grain boundaries. The mean grain sizes of these ceramics are smaller than that of the NCBCTO ceramics. Residual pores were observed in the microstructures of the $(Na_{1/3}Ca_{1/3}\mathbf{Y}_{1/3})Cu_3Ti_4O_{12}$ and $(Na_{1/3}Ca_{1/}\mathbf{Sm}_{1/3})Cu_3Ti_4O_{12}$ ceramics.

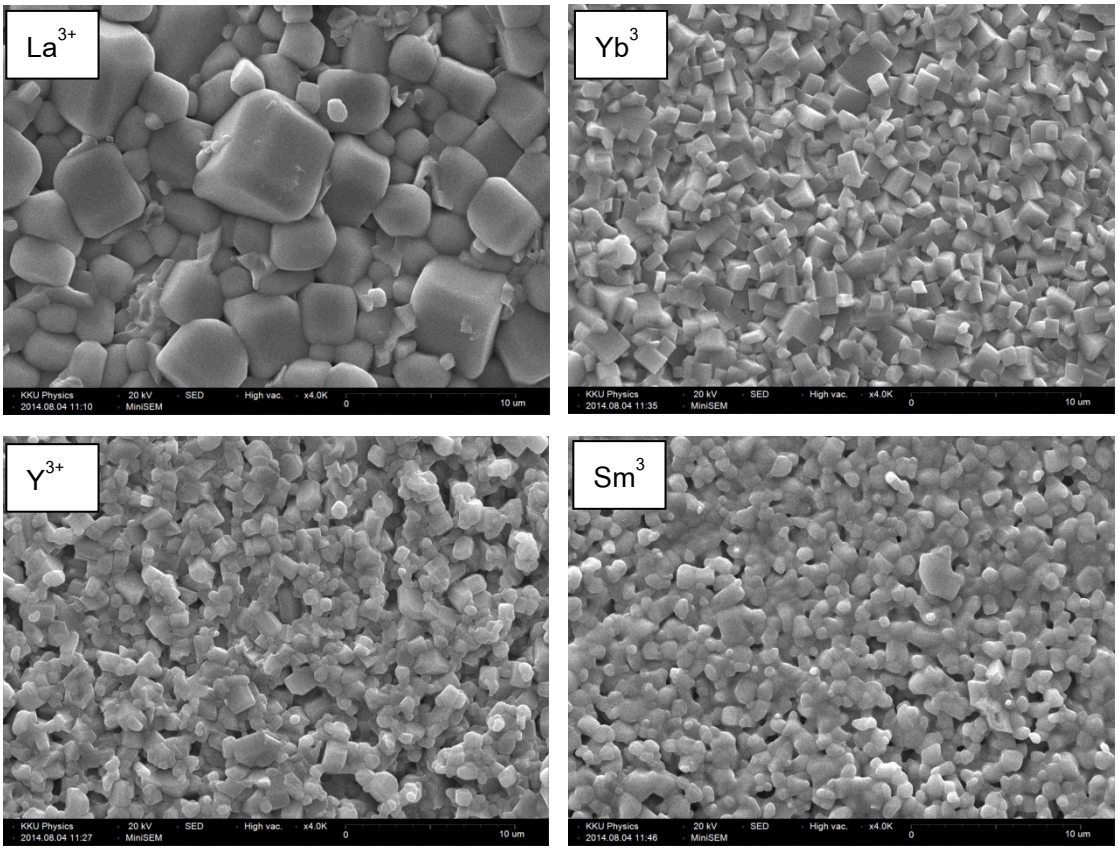

Figure 3.1.9 SEM images of $(Na_{1/3}Ca_{1/3}\boldsymbol{Ln}_{1/3})Cu_3Ti_4O_{12}$, where ***Ln*** = La^{3+}, Sm^{3+}, Y^{3+}, and Yb^{3+}.

The dielectric properties at room temperature of the $(Na_{1/3}Ca_{1/3}\mathbf{Y}_{1/3})Cu_3Ti_4O_{12}$ ceramics sintered at various conditions are illustrated in Figs. 3.1.10 and 3.1.11. According to the capacitance values, ε' values were calculated and found to be in the range of 10^4 at the frequency of 1 kHz. Notably, low tanδ values of about 0.03 at 1 kHz were obtained in the $(Na_{1/3}Ca_{1/3}\mathbf{Y}_{1/3})Cu_3Ti_4O_{12}$ ceramics sintered at 1100 ^{o}C for 15 h and 1110 ^{o}C for 10 h. This is the interesting result, in which was successfully accomplished from this research work. It was also found that ε' was slightly dependent on temperature in the range of -70 to 110 ^{o}C (does not show). Unfortunately, tanδ values of other ceramics were larger than 0.05, which are unsuitable for capacitor applications. Thus, we did not focus on these materials. The origin of the observed giant dielectric response in this ceramic was attributed to the interfacial polarization at the grain boundaries, just as occurred in CCTO ceramics.

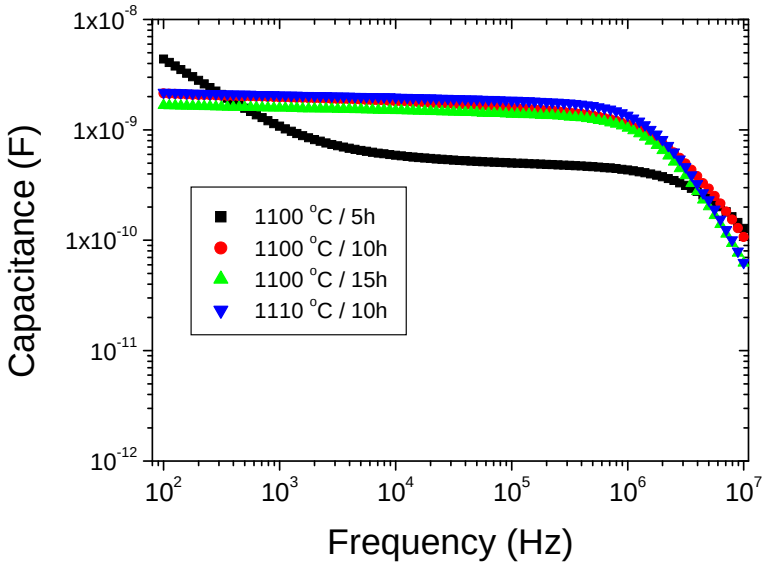

Figure 3.1.10 Capacitance values as a function of frequency at room temperature of the $(Na_{1/3}Ca_{1/3}Y_{1/3})Cu_3Ti_4O_{12}$ ceramics sintered at 1100 °C for different sintering times.

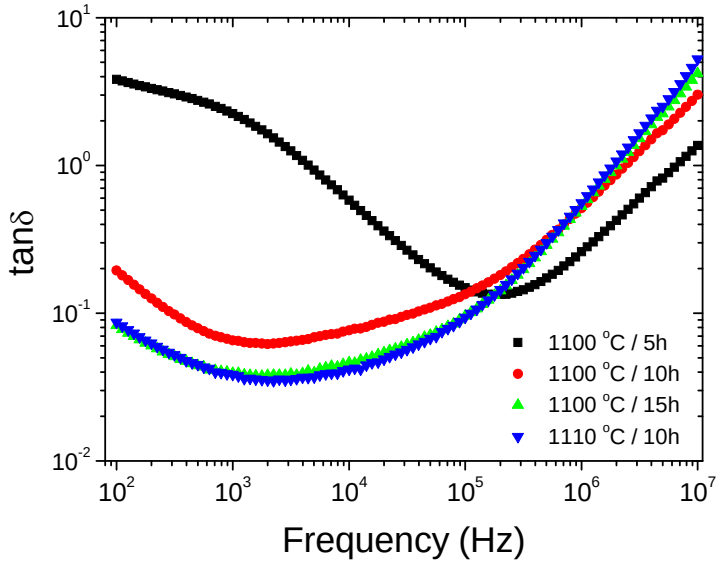

Figure 3.1.11 tanδ values as a function of frequency at room temperature of the $(Na_{1/3}Ca_{1/3}Y_{1/3})Cu_3Ti_4O_{12}$ ceramics sintered at 1100 °C for different sintering times.

References

[1] H. Ren, P. Liang, Z. Yang, Mater. Res. Bull. 45 (2010) 1608-1613.

[2] P. Thongbai, T. Yamwong, S. Maensiri, Mater. Res. Bull. 47 (2012) 432-437.

[3] Z. Yang, H. Ren, X. Chao, P. Liang, Mater. Res. Bull. 47 (2012) 1273-1277.

[4] P. Liang, X. Chao, Z. Yang, J. Appl. Phys. 116 (2014) 044101.

[5] Z. Liu, X. Chao, Z. Yang, J. Mater. Sci.: Mater. Electron. 25 (2014) 2096-2103.

[6] P. Liang, Y. Li, F. Li, X. Chao, Z. Yang, Mater. Res. Bull. 52 (2014) 42-49.

[7] M.A. Subramanian, A.W. Sleight, Solid State Sci. 4 (2002) 347-351.

[8] M.A. Subramanian, D. Li, N. Duan, B.A. Reisner, A.W. Sleight, J. Solid State Chem. 151 (2000) 323-325.

[9] W. Hao, J. Zhang, Y. Tan, W. Su, J. Am. Ceram. Soc. 92 (2009) 2937-2943.

[10] Z. Yang, L. Zhang, X. Chao, L. Xiong, J. Liu, J. Alloys Compd. 509 (2011) 8716-8719.

[11] P. Liang, Z. Yang, X. Chao, Z. Liu, J. Am. Ceram. Soc. 95 (2012) 2218-2225.

[12] W. Somphan, N. Sangwong, T. Yamwong, P. Thongbai, J. Mater. Sci.: Mater. Electron. 23 (2012) 1229-1234.

[13] R. Schmidt, M.C. Stennett, N.C. Hyatt, J. Pokorny, J. Prado-Gonjal, M. Li, D.C. Sinclair, J. Eur. Ceram. Soc. 32 (2012) 3313-3323.

[14] M. Li, Z. Shen, M. Nygren, A. Feteira, D.C. Sinclair, A.R. West, J. Appl. Phys. 106 (2009) 104106.

[15] S. Krohns, P. Lunkenheimer, S.G. Ebbinghaus, A. Loidl, J. Appl. Phys. 103 (2008) 084107.

[16] R. Jia, X. Zhao, J. Li, X. Tang, Mater. Sci. Eng. B 185 (2014) 79-85.

[17] J. Liu, C.-G. Duan, W.-G. Yin, W. Mei, R. Smith, J. Hardy, Phys. Rev. B 70 (2004) 144106.

[18] L. Ni, X.M. Chen, J. Am. Ceram. Soc. 93 (2010) 184-189.

[19] R. Yu, H. Xue, Z. Cao, L. Chen, Z. Xiong, J. Eur. Ceram. Soc. 32 (2012) 1245-1249.

[20] W. Somphan, P. Thongbai, T. Yamwong, S. Maensiri, Mater. Res. Bull. (2013).

[21] S.-Y. Chung, I.-D. Kim, S.-J.L. Kang, Nat. Mater. 3 (2004) 774-778.

3.2 $CaCu_{3-x}Mg_xTi_4O_{12}/CaTiO_3$

In this part of the research work, a novel strategy to improve the dielectric and non-Ohmic properties of $CaCu_3Ti_4O_{12}$ ceramics that deliberately created a binary-phase system of $CaCu_{3-x}Mg_xTi_4O_{12}/CaTiO_3$ was proposed and can be performed with a starting nominal formula of $Ca_2Cu_{2-x}Mg_xTi_4O_{12}$. Mg^{2+} doping ions were preferentially incorporated only into the $CaCu_3Ti_4O_{12}$ phase. Substitution of Mg^{2+} into $CaCu_3Ti_4O_{12}/CaTiO_3$ can cause a significant increase in dielectric permittivity and a large reduction of the loss tangent to <0.015 at 1 kHz; while, retaining excellent temperature dielectric-stability. Sintering time had a slight influence on the dielectric properties, but remarkable effects upon the nonlinear electrical properties of $CaCu_{3-x}Mg_xTi_4O_{12}/CaTiO_3$ ceramics. Degradation of nonlinear properties with increased sintering time is suggested to be the result of the dominant effect of oxygen vacancies. Impedance spectroscopy analysis demonstrated that improved dielectric and nonlinear properties could be attributed to the enhanced electrical responses of $CaCu_3Ti_4O_{12}$-$CaTiO_3$ and $CaCu_3Ti_4O_{12}$-$CaCu_3Ti_4O_{12}$ interfaces resulting from Mg^{2+} doping ions. Details of the experimental results and discussion are as follows:

An Mg-doped $Ca_2Cu_2Ti_4O_{12}$ ceramics with a nominal chemical composition of $Ca_2Cu_{2-x}Mg_xTi_4O_{12}$ (x = 0, 0.05, 0.10, 0.20, and 0.30) ceramics were synthesized. These materials are referred to as the CCTO/CTO, Mg05, Mg10, Mg20, and Mg30 ceramics, respectively. Finally, the composite ceramics were sintered at 1100 ^{o}C for 6 and 24 h.

Figure 3.2.1 shows the XRD patterns of $Ca_2Cu_{2-x}Mg_xTi_4O_{12}$ (x = 0, 0.05, 0.10, 0.20, and 0.30) ceramics sintered for 24 h. All of the 24h samples (as well as the 6h samples) consisted of two phases of CCTO (JCPDS 75-2188) and CTO (JCPDS 82-0231). This result is similar to that reported in the literature [1-8]. According to the nominal formula of $Ca_2Cu_2Ti_4O_{12}$, two phases of ~33.3 mol% of CCTO and ~66.7 mol% of CTO should be formed due to the imbalance between Ca^{2+} and Cu^{2+} ions. This is confirmed by a Rietveld quantitative analysis of a $Ca_2Cu_2Ti_4O_{12}$ ceramic as reported in the literature [2]. The ionic radius of Ca^{2+} is much larger than that of Cu^{2+}. As a result, Ca^{2+} cannot enter into Cu^{2+} sites in a planar square to form $Ca(CaCu_2)Ti_4O_{12}$ structure. Interestingly, no impurity related to Mg^{2+} doping ions was observed. This likely indicates the formation of a solid solution between the Mg^{2+} doping ions and CCTO, CTO or both. To clarify this, lattice parameters (a) of the CCTO phase in all composite ceramics were calculated and are summarized in Table 3.2.1. These values showed no significant

change even through the Mg^{2+} concentration was increased to x = 0.3. There are two possible mechanisms that may be responsible for this observation. First, Cu^{2+} might form a solid solution with CTO phase, leading to an unchanged lattice parameter value of the CCTO structure. Second, Mg^{2+} ions might replace Cu^{2+} sites in the CCTO phase, forming a solid solution with the CCTO phase. In the latter explanation, the *a* value of a CCTO phase is unchanged due to the same ionic radii of Mg^{2+} (r_4=0.57 Å) and Cu^{2+} (r_4=0.57 Å) ions [9].

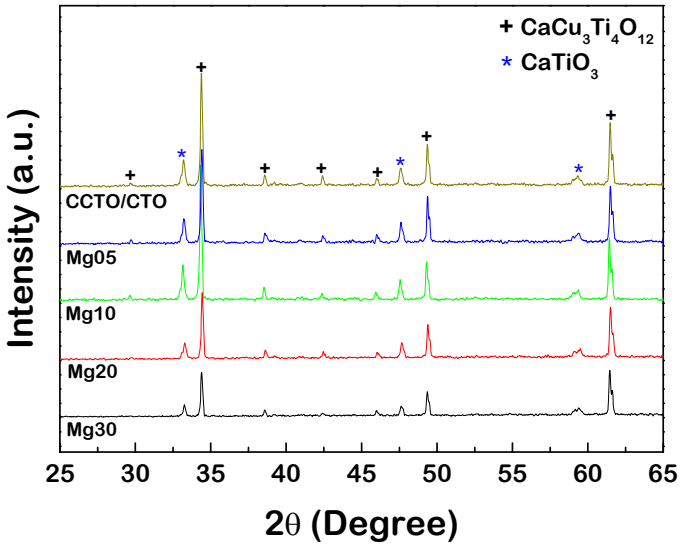

Figure 3.2.1 XRD patterns of CCTO/CTO and Mg-doped CCTO/CTO composite ceramics sintered for 24 h.

Figures 3.2.2(a-e) and 3.2.2(f-j) show backscattered SEM images of the polished 24h samples and 6h samples, respectively. Two phases with different contrasts were observed, *i.e.*, darker and lighter phases. This observation is consistent with the XRD result and similar to those reported in the literature for un-doped $Ca_2Cu_2Ti_4O_{12}$ ceramics [1, 2, 4]. As shown in Figures 3.2.3(a) and (b), the darker and lighter phases are clearly CTO and CCTO phases, respectively. Only the EDS peaks corresponding to Ca, Ti, and O appeared in the EDS spectra measured in the darker region. All possible EDS peaks for Ca, Cu, Ti, O, and Mg were detected in the lighter CCTO phase. This clearly indicates that Mg^{2+} doping ions preferentially form solid solution only within the CCTO phase. Therefore, it is likely that Mg^{2+} ions were substituted into Cu^{2+} sites in the CCTO phase. Thus, it is reasonable to suggest that the

prepared $Ca_2Cu_{2-x}Mg_xTi_4O_{12}$ ceramics consist of ~33.3 mol% of $CaCu_{3-x}Mg_xTi_4O_{12}$ (x = 0, 0.05, 0.10, 0.20, 0.30) and ~66.7 mol% of CTO.

Table 3.2.1 Lattice parameter (a), ε' and tanδ (at 1 kHz and 30 °C), resistance at GBs (R_{gb}) at 120 °C, nonlinear coefficient (α), and breakdown field strength (E_b).

Sample	a (Å)	ε'	tanδ	R_{gb} (MΩ.cm)	α	E_b (V/cm)
Sintered for 6 h						
CCTO/CTO	7.388	2,182	0.023	0.62	13.1	8,211
Mg05	7.386	3,372	0.014	0.83	11.9	7,811
Mg10	7.382	3,298	0.011	1.52	20.7	10,221
Mg20	7.390	2,748	0.015	2.62	18.5	10,869
Mg30	7.390	3,550	0.014	1.77	27.2	8,859
Sintered for 24 h						
CCTO/CTO	7.389	1,877	0.075	0.33	9.9	5,817
Mg05	7.391	6,824	0.020	0.17	7.3	3,452
Mg10	7.391	5,201	0.011	0.72	8.1	5,088
Mg20	7.391	4,903	0.017	0.78	7.5	4,486
Mg30	7.395	4,810	0.023	0.46	9.5	5,700

As shown in Figs. 3.2.2(a) and 3.2.2(f), the distribution of CCTO and CTO phases in the microstructures of the CCTO/CTO samples sintered for 24 and 6 h is quite uniform. The mean grain sizes of the CCTO phase in the CCTO/CTO samples sintered for 24 and 6 h were estimated to be ~2.90±0.97 and ~3.07±0.77 μm, respectively; whereas, the mean grain sizes of the CTO phase are of about ~1.96±0.48 and ~2.09±0.47 μm, respectively. The sintering time has no significant influence on the microstructural evolution of CCTO/CTO composites. It is worth noting that the mean grain sizes of CCTO phase in the CCTO/CTO samples are smaller than the mean grain size of ~7 μm for the sample sintered at 1050°C for 0.5 h sintered using a microwave sintering method [10]. Ramirez *et al* [1, 2]. found that the CCTO/CTO ceramic sintered at 1100 °C for 3 h using a conventional furnace exhibited two different grain size distributions for the CCTO phase with mean grain sizes of d = 10-15 and 3-4 μm. Grain sizes of the CTO phase of the CCTO/CTO composites sintered using a microwave and conventional furnace were found to be ~2 and ~4 μm, respectively. These values are

closed to grain sizes of ~2-3 μm of the CTO phase in the CCTO/CTO samples presented in this work.

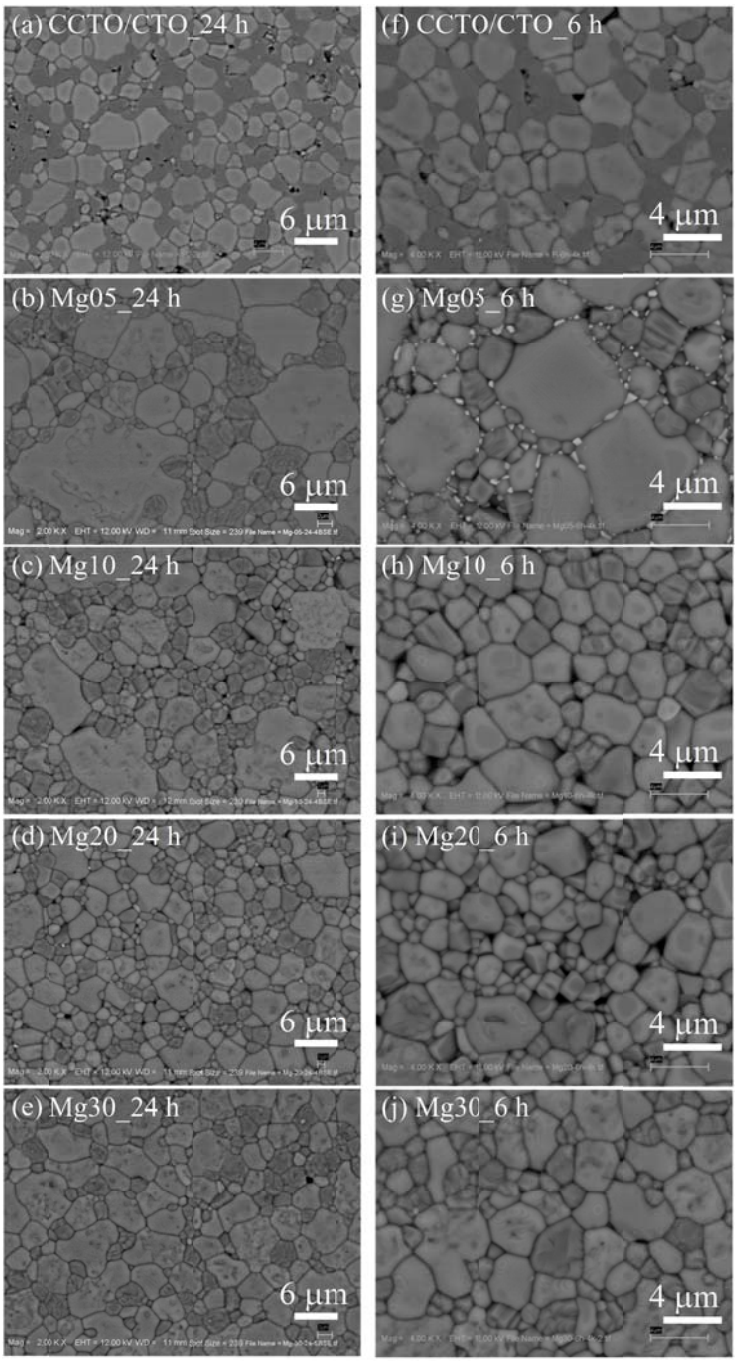

Figure 3.2.2 (a-e) Backscattered SEM images of polished—surfaces of CCTO/CTO, Mg05, Mg10, Mg20, and Mg30 samples sintered for 24 h, respectively. (f-j) Backscattered SEM images of polished—surfaces of CCTO/CTO, Mg05, Mg10, Mg20, and Mg30 samples sintered for 6 h, respectively.

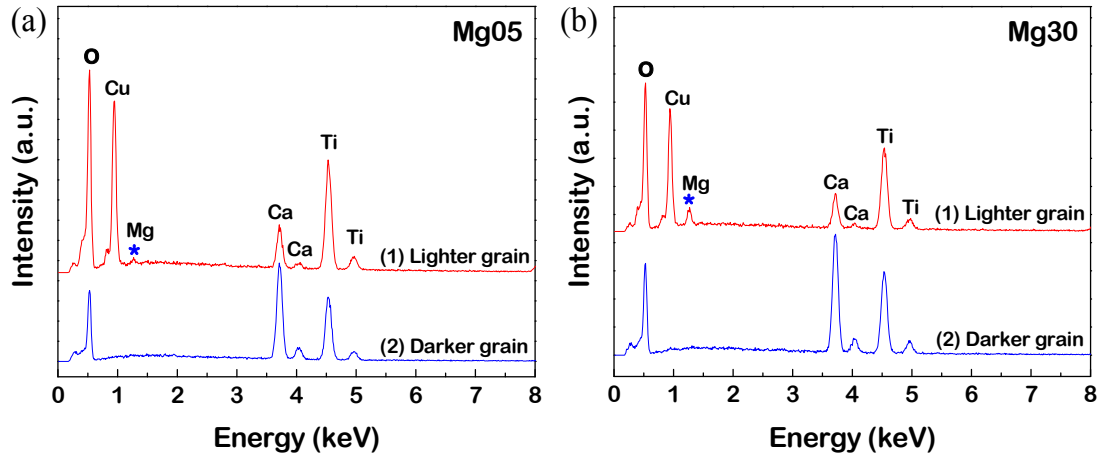

Figure 3.2.3 EDS spectra of the (a) Mg05 and (b) Mg30 samples detected at a darker and lighter regions.

After doping adding Mg^{2+} ions with x =0.05 and 0.10 (sintered for 24 h), some grains of the CCTO phase increased to sizes of ~8-20 μm with the mean grain size of ~11.1±4.6 μm for the Mg05 sample. For the Mg05 sample sintered for 6 h, large grain sizes of the CCTO phase were also observed with the mean grain size of ~4.74±2.46 μm. The mean grain sizes of the CTO phase in the Mg05 samples sintered for 24 and 6 h were estimated to be ~3.61±0.95 and ~2.42±0.69 μm, respectively. For the samples sintered for 24 h with x=0.20-0.30 and the samples sintered for 6 h with x=0.10-0.30, the grain sizes of CCTO and CTO phases become homogeneous. Morphologies of both CCTO and CTO phases of these samples were well dispersed and separate from each other. Large clusters of CTO grains no longer appeared. The mean grain sizes of the CCTO and CTO phases in the Mg10, Mg20, and Mg30 samples sintered for 24 h were estimated to be ~4.82±2.7 and ~2.66±0.74 μm, ~3.09±1.04 and ~2.08±0.39 μm, and ~5.11±1.4 and ~3.12±0.68 μm, respectively. For the 6h samples, the mean grain sizes of the CCTO and CTO phases in these compositions were ~3.03±0.86 and ~2.14±0.54 μm, ~2.65±0.72 and ~1.75±0.32 μm, and ~3.12±0.98 and ~1.88±0.61 μm, respectively.

Grain sizes of the CTO phase in these samples showed slight change. As reported by Ni and Chen [11], the mean grain size of CCTO ceramics was increased by doping with Mg^{2+}. This indicates the ability of Mg^{2+} doping ions to increase the sintering rate of CCTO ceramics through the liquid phase sintering mechanism. In CCTO-based

ceramic oxides, the grain growth is widely accepted to be primarily caused by the liquid phase sintering mechanism [12, 13]. It is possible that, during the sintering, the formation of MgO-related liquid phase in the microstructures of Mg^{2+}-doped CCTO/CTO composites occurred. Liquid phases have long been referred as a primary cause of abnormal grain growth. Usually, physical and chemical inhomogeneities, such as inhomogeneous packing of powders and non-uniform distribution of dopants, can result in local variation in the microstructure [14]. This was considered a main cause of abnormal grain growth. Thus, it is likely that the abnormal grain growth of CCTO phase in the Mg05 (sintered for 6 and 24 h) and Mg10 (sintered for 24 h) composite samples may be caused by a local liquid phase sintering because of non-uniform distribution of Mg^{2+} doping ions in the green body of composites. The local liquid phase sintering produces inequalities in the GB mobility, resulting in the initiation of abnormal growth [14]. When the concentration of Mg^{2+} doping ions increased, it may be well distributed throughout the compacted powders. On heating, equalities in the GB mobility are approximately equal throughout the composite microstructure, leading to a normal grain growth. Thus, homogeneous microstructure of the composite ceramics with high concentration of Mg^{2+} was achieved in this way.

Figures 3.2.4(a-b) and their insets show the frequency dependence of ε' and $\tan\delta$ at 30 ^{o}C for the 6h and 24h samples, respectively. Interestingly, ε' values of all the samples were independent of frequency in the range from 10^2 to 10^5 Hz. ε' values of all Mg-doped CCTO/CTO ceramics were higher than for un-doped ceramics. It is worth noting that a low-frequency $\tan\delta$ of CCTO/CTO was remarkably reduced by doping with Mg^{2+}. ε' and $\tan\delta$ (1 kHz and 30 ^{o}C) of all composite ceramics are summarized in Table 3.2.1. ε' values of the un-doped CCTO/CTO samples sintered for 6 and 24 h are close to the ε' value of ~1800 for a sample sintered at 1090 ^{o}C for 24 h, as first reported by Kobayashi and Terasaki [15]. However, these two values are larger than the ε' value of ~1300 for the sample sintered at 1050 ^{o}C for 0.5 h sintered using a microwave sintering method [10]. Ramirez *et al* [1], found ε'~2960 at 1 kHz for CCTO/CTO ceramic sintered at 1100 ^{o}C for 3 h using a conventional furnace. According to our previous work [5], ε'~2104 at 1 kHz was obtained in a CCTO/CTO ceramic sintered at 1050 ^{o}C for 10 h. These indicate that the sintering method and sintering conditions have an influence on ε' of a CCTO/CTO ceramic system.

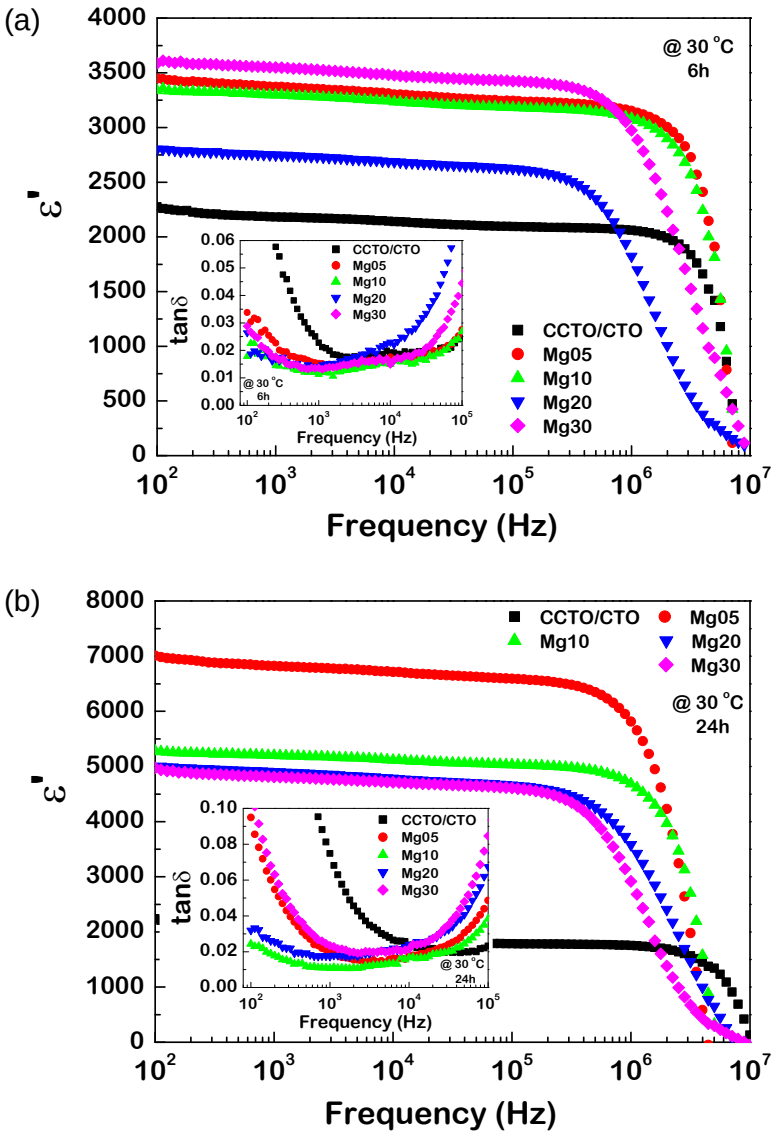

Figure 3.2.4 Frequency dependence of ε' for the ceramic samples sintered for (a) 6 and (b) 24 h; their insets show tanδ as a function of frequency.

Interestingly, ε' values of the Mg^{2+}-doped CCTO/CTO composites sintered for 24 h were about 2-3 times larger than that of the un-doped ceramics. Notably, their tanδ values were reduced by factors of 3-6. It was seen that after increasing sintering time from 6 to 24 h, ε' of Mg-doped CCTO/CTO composites increased by a factor of 1.5-2 over that of samples sintered for 6 h, while tanδ slightly changed. At 10^2 Hz, the values of tanδ at 30°C of the CCTO/CTO, Mg05, Mg10, Mg20, and Mg30 samples sintered at 1100°C for 6 h were found to be 0.118, 0.034, 0.018, 0.026, and 0.029,

respectively, while tanδ values of the 24h samples were 0.303, 0.095, 0.024, 0.032, and 0.107, respectively. For the 6h and 24h samples, tanδ values at the low frequency of 10^2 Hz for all Mg-doped CCTO/CTO composites were significantly reduced compared to the un-doped CCTO/CTO samples sintered for the same time. As is well known, dc conduction in dielectric materials leads to an apparently high value of low-frequency tanδ at room temperature and higher [16], *i.e.*, $\tan\delta \approx \sigma_{dc} / \omega\varepsilon_0\varepsilon_s'$, where ε_s' is the dielectric permittivity in a low-frequency range. This large reduction in tanδ is therefore attributed to a strong reduction of σ_{dc} in these samples.

For the 6h samples, the Mg30 sample exhibited the highest ε'; while, ε' of the Mg30 sample was found to be highest among the 24h samples. It is widely believed that the giant ε' of CCTO ceramics is attributed to the interfacial polarization at the GBs through the internal barrier layer capacitor (IBLC) effect [17-22]. This polarization is likely to be a cause of high dielectric response in CCTO/CTO composites as well. According to the IBLC model, ε' is associated with the area of insulating GB layer between grains, which is approximately equal to the mean grain size, and the GB capacitance that related to the intrinsic GB dielectric permittivity. Schmidt *et al* [20]. found that the GB dielectric permittivity strongly increased with sintering temperature. They have suggested this observation as a result of chemical changes, even though it is difficult to detect significant changes in defect chemistry. By using this model, a higher value of ε' for the Mg30 sample (sintered for 6 h) should be primarily attributed to stronger enhanced dielectric response of the GBs. For the 24h samples, the mean grain size of the Mg05 samples is much larger than those of other samples. Thus, ε' of the Mg05 sample might be dominated by the grain size effect over the improved electrically active of interfaces.

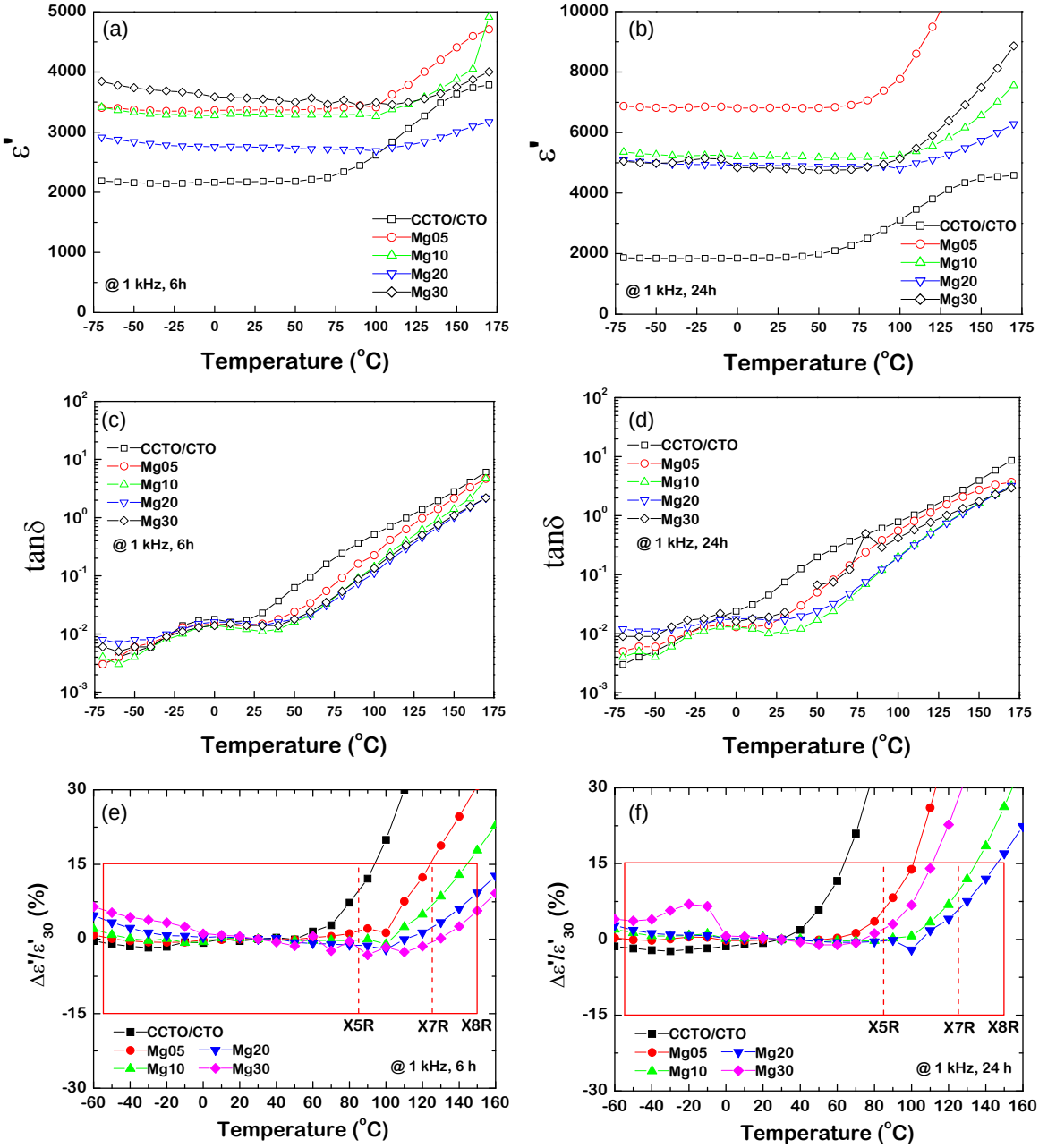

Figure 3.2.5 (a-b) Temperature dependence of ε' for the composite ceramics sintered for 6 and 24 h, respectively. (c-d) Temperature dependence of tanδ for the composite ceramics sintered for 6 and 24 h, respectively. (e-f) Temperature coefficient of ε' at 10^3 Hz for the composite ceramics sintered for 6 and 24 h, respectively: ε'_{30} is the dielectric permittivity at 30 °C.

The temperature dependencies of ε' at 1 kHz for all the 6h and 24h samples are shown in Figures 3.2.5(a) and (b), respectively. When the temperature is higher than 100 $^{\circ}$C, ε' rapidly increases in value. The temperature dependence of ε' in un-doped CCTO/CTO ceramics was similar to that observed in CCTO ceramics [11, 23-25]. Mg^{2+} substitution into CCTO/CTO ceramics not only caused an increase in ε' and reduction of tanδ, but also can contribute to the temperature stability of ε'. The temperature dependencies of tanδ at 1 kHz for all the 6h and 24h samples are shown in Figs. 3.2.5(c) and (d), respectively. When the temperature is higher than 100 $^{\circ}$C, tanδ is higher than 0.1 for Mg-doped CCTO/CTO composites. The large increase in tanδ at high temperatures is consistent with the increase in ε'. It is likely that the large value of tanδ in a high temperature range is one of the most serious problems for using CCTO-based compounds in high temperatures. Further investigation is needed to improve high-temperature tanδ of CCTO ceramics.

As shown in Fig. 3.2.5(e), for the 6h samples, the conditions of $\Delta\varepsilon' < \pm 15\%$ for the CCTO/CTO, Mg05, Mg10, Mg20, and Mg30 samples were found to be in the temperature ranges of -60°C - 90°C, -60°C - 120°C, -60°C - 140°C, -60°C - 160°C, and -60°C - 170°C, respectively. Dielectric properties of these samples satisfy the EIA X5R, X5R, X7R, X8R, and X8R standard capacitor specifications, respectively. It is worth noting that the temperature stability of ε' in CCTO-based compounds satisfying the X8R capacitor requirement was rarely reported [26, 27]. Thus, substitution of Mg^{2+} into a $Ca_2Cu_2Ti_4O_{12}$ binary system is one of the most effective and interesting methods to improve the overall dielectric performance of CCTO ceramics, making them suitable for practical application in capacitors.

As shown in Fig. 3.2.5(f), conditions where $\Delta\varepsilon' < \pm 15\%$ for the 24h samples were in the temperature ranges of -60°C - 60°C, -60°C - 100°C, -60°C - 130°C, -60°C - 140°C, and -60°C - 110°C, respectively. When the sintering time was increased to 24 h, the temperature stability of the un-doped CCTO/CTO sample greatly decreased, putting its properties out of the standard specification. Furthermore, the temperature stability of each Mg^{2+}-doped CCTO/CTO composite also decreased as the sintering time increased to 24 h. $\Delta\varepsilon'(\%)$ values of the Mg05, Mg10, Mg20, and Mg30 samples satisfy the X5R, X7R, X7R, and X5R capacitor applications, respectively. Notably, for the Mg10 and Mg20 samples, ε' increased more than 2 times with high temperature stability, whereas tanδ was reduced by factors of ≈4-6.

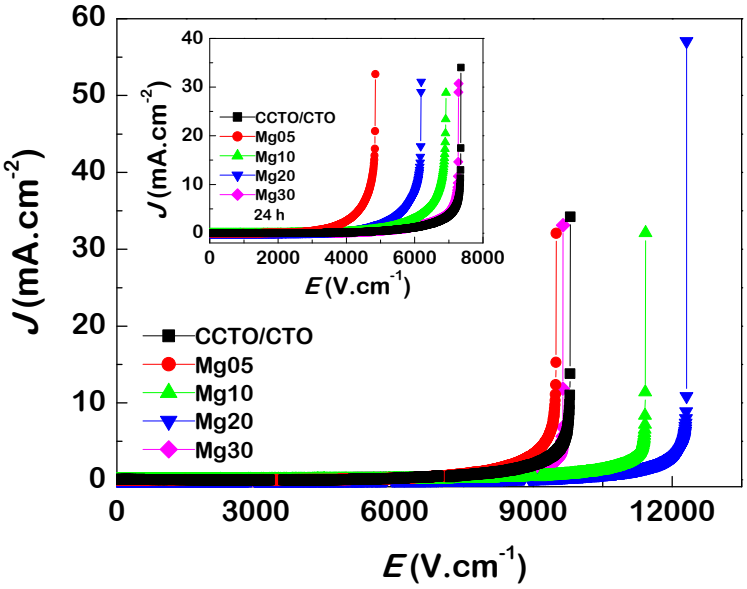

Figure 3.2.6 *J-E* curves of the composite ceramics sintered for 6 h; inset shows *J-E* curves of the ceramics sintered for 24 h.

Figure 6 and its inset demonstrate the nonlinear electrical characteristics of the 6 h and 24 h samples, respectively. All the composite ceramics exhibited nonlinear *J-E* behavior. Two important parameters (α and E_b) of all the composites were calculated from these curves and are summarized in Table 3.2.1. The overall non-Ohmic results revealed that values of α and E_b for the 24 h samples slightly changed with Mg^{2+} concentration. This is in contrast to their dielectric properties. E_b and α values were reduced by increasing sintering time. Interestingly, an α value of 27.2 observed for the Mg30 sample sintered for 6 h is much larger than that of the CCTO/CTO sample (α=13.1). This result indicates that Mg^{2+} doping ions had significant effects on both the dielectric and nonlinear electrical properties of CCTO/CTO composites sintered for 6 h. The high value of α=27.2 for the Mg30 sample can be compared to values of 29.67 and 25.3 achieved in a Tb-doped CCTO ceramic [28] and VO_2 (3 mol%)-added (66.7 mol%)CCTO/(33.7 mol%)CTO ceramic [8]. However, these values are much lower than the value of 42 for un-doped CCTO/CTO ceramic sintered at 1100^{o}C for 3 h reported by Ramirez *et al* [1]. It is worth noting that α of CCTO-based ceramics is strongly dependent on the rate increase of applied voltage [29]. α was found to decrease when this rate was increased. In this work, the rate of increase in an applied voltage was 1.33 V/s. Unfortunately, rate of voltage increase used in other work to

measure *J-E* characteristics of CCTO/CTO composites has not been reported. Therefore, the large difference in α values in many reports might be due to different rates of voltage increase used in these studies.

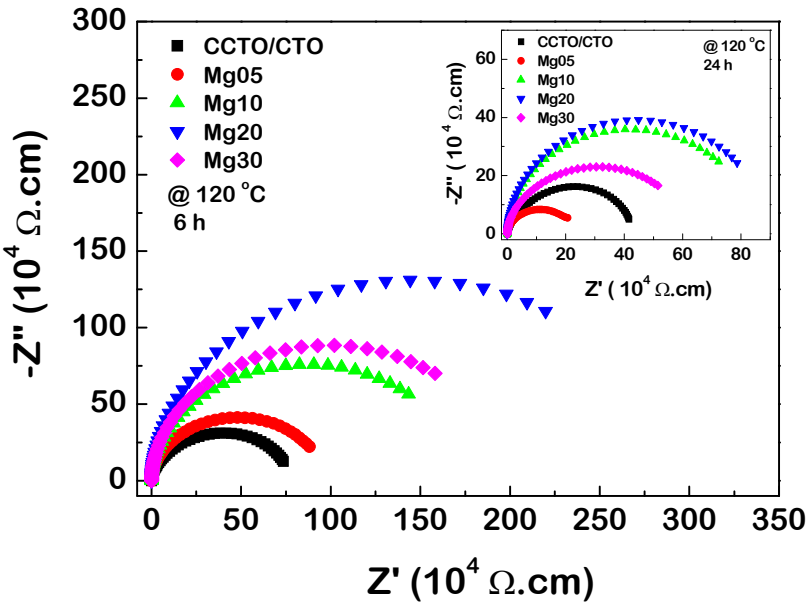

Figure 3.2.7 Impedance complex plane (Z*) plots at 120 °C for the composites sintered for 6 h; inset shows Z* plots at 120 °C for the composites sintered for 24 h.

To elucidate the possible mechanism(s) of the nonlinear properties and dielectric response in Mg^{2+}-doped CCTO/CTO composites, impedance spectroscopy was used to study electrical responses inside the grains and at internal interfaces. Figure 7 and its inset show impedance complex plane (Z*) plots at 120°C for 6h and 24h samples, respectively. The total resistance (R_{tot}) was estimated from the diameter of a large semicircle arc of the CCTO/CTO ceramic enhanced by doping with Mg^{2+}, except for the Mg05 sample sintered for 24 h [17]. Generally, R_{tot} is governed by the resistance of GBs (R_{gb}) [17, 30]. In this CCTO/CTO composite system, GBs or interfaces between grains consist of interfaces between CCTO-CCTO grains, CCTO-CTO grains, and CTO-CTO grains. The R_{gb} values determined at 120°C for all the samples are summarized in Table 3.2.1. According to the microstructure analysis, Mg^{2+} doping ions prefer to form solid solution only within CCTO phase. Thus, the molar ratio and volume fraction of the CTO phase of each composition should ideally be the same. Thus, the difference in R_{gb}

values indicated a significant effect of Mg^{2+} doping ions upon the electrical responses of internal interfaces.

According to the previous work of Ramirez *et al*. [2], using electrostatic force microscopy (EFM), it was clearly shown that CCTO-CTO and CCTO-CCTO interfaces were electrically active, indicating the presence of potential barriers. However, a CTO-CTO interface was electrically inactive. This indicates the important role of Cu atoms in generating potential barriers. Mg^{2+} doping ions might improve the electrical responses of these active interfaces. This is because of undetectable Mg^{2+} doping ions in CTO grains, which make the CTO-CTO interfaces electrically inactive. The improved electrically active of interfaces can cause increases in both R_{gb} and E_b of 6 h samples. This indicates to the effect of Mg^{2+} doping ions on the intrinsic properties of the interfaces (GBs) of the CCTO/CTO composites.

Generally, both the intrinsic and geometric properties of the GBs of CCTO ceramics are key factors determining their overall properties. The geometric properties of the GBs are also important as well and cannot be ignored. Using the geometric approach, the increase in the GB density due to the reduction in grain size can cause enhancement of R_{gb} and E_b. For the 6h samples, as shown in Table 3.2.1, it is clear that variations of R_{gb} and E_b values of the Mg05, Mg10, Mg20, and Mg30 samples are both closely related to the changes in their mean grain sizes. The geometric approach cannot describe the difference in values of R_{gb} between the un-doped CCTO/CTO sample and Mg-doped CCTO/CTO samples (especially for the Mg05 sample). As mentioned above, the increase in R_{gb} of the Mg05 sample compared to the CCTO/CTO sample is mainly attributed to the improved intrinsic properties of the GBs, which may be caused by the modified electrically active interfaces. These results indicate that both the geometric and intrinsic properties of the GBs have a remarkable effect on the electrical properties of the CCTO/CTO composites.

For the 24h samples, changes in R_{gb} and E_b values of the CCTO/CTO and Mg05 samples are both correlated with the variation of their grain sizes. R_{gb} and E_b values of the CCTO/CTO sample were reduced as the mean grain size increased for the Mg05 sample. Interestingly, variation of R_{gb} values of the Mg05, Mg10, Mg20, and Mg30 samples sintered for 24 h are closely correlated with the changes in their mean grain sizes just as observed in the Mg-doped CCTO/CTO composites sintered for 6 h. Note that, both of the 6h and 24h samples, R_{gb} of the Mg30 samples is lower than that

of the Mg20 samples. This result is primarily attributed to the increase in the mean grain size of the Mg30 samples. Variation of E_b values of the Mg05, Mg10, Mg20, and Mg30 samples cannot be explained by using the geometric approach. Generally, the formation mechanism of electrostatic barrier at GBs of traditional metal oxide non-Ohmic materials and CCTO ceramics is closely related the oxygen content at GBs [10, 31]. As shown in Table 3.2.1, E_b and α values of each sample were reduced by increasing sintering time from 6 to 24 h. The concentration of oxygen vacancy at GBs of the ceramic composites sintered for 24 h may be higher than that of the 6h samples, resulting in the degradation of nonlinear properties. This indicates that the effect of oxygen vacancies on the nonlinear properties in the 24h samples is dominant.

It was observed that the E_b value of the Mg30 sample is larger than that of the Mg20 sample; while, the mean grain size of the Mg30 sample is larger than of the Mg20 sample. It is possible that substitution of Mg^{2+} ions into CCTO/CTO composites with a suitable high-concentration might suppress the existence of oxygen vacancies at the GBs during sintering process at high temperatures and long reaction time. This can retain a high value of E_b. However, further work is needed to explore the exact origin of this observation.

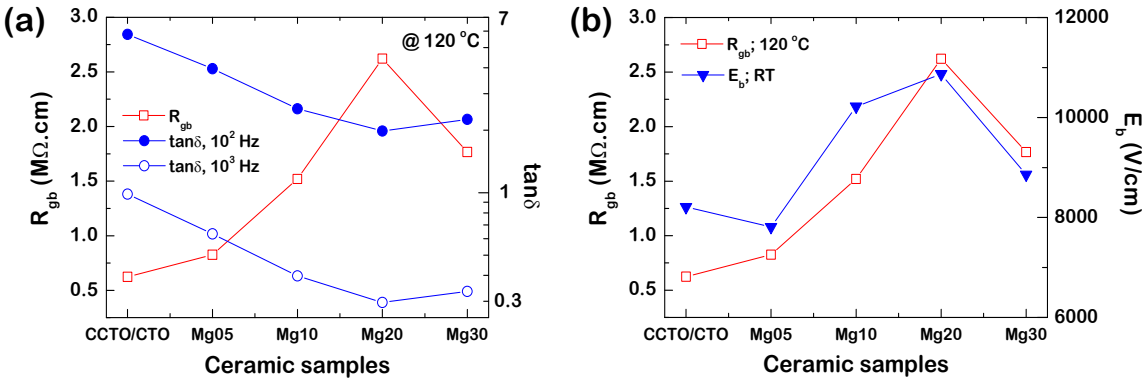

Figure 3.2.8 (a) Correlation between R_{gb} and tanδ at 120 °C of composite ceramics sintered for 6 h. (b) Correlation between R_{gb} (at 120°C) and E_b (measured at room temperature) of composite ceramics sintered for 6 h.

As mentioned above, a high value of low-frequency tanδ at high temperatures is primarily caused by long-range migration of charges (σ_{dc}) of CCTO/CTO composites. This is governed by σ_{gb}. Thus, a low-frequency tanδ value should be inversely proportional to R_{gb}, as clearly seen in Fig. 3.2.8(a). With increasing Mg^{2+} concentration, tanδ values decreased while those of R_{gb} increased. With increasing Mg^{2+} concentration (x = 0.20 to 0.30), tanδ increased as R_{gb} decreased. Although R_{gb} values at 30^{o}C for all the samples could not be calculated, it is reasonable to suggest that a reduction of tanδ at 30^{o}C for Mg^{2+}-doped CCTO/CTO composites can be attributed to enhancement of R_{gb}, as a result of the presence of Mg^{2+} doping ions. As shown in Fig. 3.2.8(b), although E_b of the Mg05 sample is slightly lower than that of the un-doped CCTO/CTO composite, a correlation between R_{gb} and E_b likely exists. From the results in Fig. 3.2.8, it is clearly demonstrated that a low-frequency tanδ value of CCTO-based compounds was closely related to resistances of internal interfaces. However, for the R_{gb}-E_b relationship, these two parameters may not be correlated with each other. As shown in the inset of Fig. 3.2.6 and in Table 3.2.1, E_b values of all the Mg^{2+}-doped CCTO/CTO composites sintered for 24 h were found to be lower than those of the un-doped CCTO/CTO sample. On the other hand, the R_{gb}-tanδ relationship is still quite similar to that observed in the 6 h samples. This means that E_b or nonlinear properties may not have any relationship to R_{gb} or tanδ. As reported by Ramirez et al. [2], E_b and α values of a CCTO/CTO composite that possessed higher volume fraction of CTO phase were less than those of the values obtained in a sample with a lower CTO volume fraction. For the 24 h samples, E_b and α were slightly changed by variation in the concentration of Mg^{2+}. It is possible that the effect of oxygen vacancies in the 24 h samples is more dominant than the effect of Mg^{2+}-modified GB response. This may make some electrically active interfaces weakly active or inactive. Evidence of a strong effect of oxygen vacancies on low-frequency tanδ values is clearly observed in the inset of Fig. 3.2.4(b).

References

[1] M.A. Ramírez, P.R. Bueno, E. Longo, J.A. Varela, J. Phys. D: Appl. Phys. 41 (2008) 152004.

[2] M.A. Ramírez, P.R. Bueno, R. Tararam, A.A. Cavalheiro, E. Longo, J.A. Varela, J. Phys. D: Appl. Phys. 42 (2009) 185503.

[3] B. Cheng, Y.-H. Lin, H. Yang, J. Lan, C.-W. Nan, X. Xiao, J. He, J. Am. Ceram. Soc. 92 (2009) 2776-2779.

[4] J. Jumpatam, P. Thongbai, B. Kongsook, T. Yamwong, S. Maensiri, Mater. Lett. 76 (2012) 40-42.

[5] P. Thongbai, B. Putasaeng, T. Yamwong, S. Maensiri, J. Alloys Compd. 509 (2011) 7416-7420.

[6] L.H. Oliveira, E.C. Paris, W. Avansi, M.A. Ramirez, V.R. Mastelaro, E. Longo, J.A. Varela, X.M. Chen, J. Am. Ceram. Soc. 96 (2013) 209-217.

[7] T. Li, K. Fang, J. Hao, Y. Xue, Z. Chen, Mater. Sci. Eng. B 176 (2011) 171-176.

[8] L. Ramajo, R. Parra, J.A. Varela, M.M. Reboredo, M.A. Ramírez, M.S. Castro, J. Alloys Compd. 497 (2010) 349-353.

[9] R.D. Shannon, Acta Cryst. A32 (1976) 751-767.

[10] M.A. Ramirez, P.R. Bueno, J.A. Varela, E. Longo, Appl. Phys. Lett. 89 (2006) 212102.

[11] L. Ni, X.M. Chen, Solid State Commun. 149 (2009) 379-383.

[12] K.-M. Kim, S.-J. Kim, J.-H. Lee, D.-Y. Kim, J. Eur. Ceram. Soc. 27 (2007) 3991-3995.

[13] J.J. Romero, P. Leret, F. Rubio-Marcos, A. Quesada, J.F. Fernández, J. Eur. Ceram. Soc. 30 (2010) 737-742.

[14] M.N. Rahaman, Sintering of ceramics, CRC Press, Boca Raton, FL, 2008.

[15] W. Kobayashi, I. Terasaki, Appl. Phys. Lett. 87 (2005) 032902.

[16] J. Wu, C.-W. Nan, Y. Lin, Y. Deng, Phys. Rev. Lett. 89 (2002) 217601.

[17] D.C. Sinclair, T.B. Adams, F.D. Morrison, A.R. West, Appl. Phys. Lett. 80 (2002) 2153.

[18] E.A. Patterson, S. Kwon, C.-C. Huang, D.P. Cann, Appl. Phys. Lett. 87 (2005) 182911.

[19] J. Li, R. Jia, X. Tang, X. Zhao, S. Li, J. Phys. D: Appl. Phys. 46 (2013) 325304.

[20] R. Schmidt, M.C. Stennett, N.C. Hyatt, J. Pokorny, J. Prado-Gonjal, M. Li, D.C. Sinclair, J. Eur. Ceram. Soc. 32 (2012) 3313-3323.

[21] Z. Yang, L. Zhang, X. Chao, L. Xiong, J. Liu, J. Alloys Compd. 509 (2011) 8716-8719.

[22] P. Thongbai, B. Putasaeng, T. Yamwong, V. Amornkitbamrung, S. Maensiri, J. Alloys Compd. 582 (2014) 747-753.

[23] M. Li, G. Cai, D.F. Zhang, W.Y. Wang, W.J. Wang, X.L. Chen, J. Appl. Phys. 104 (2008) 074107.

[24] Y. Li, P. Liang, X. Chao, Z. Yang, Ceram. Int. 39 (2013) 7879-7889.

[25] L. Ni, X.M. Chen, J. Am. Ceram. Soc. 93 (2010) 184-189.

[26] S.F. Shao, J.L. Zhang, P. Zheng, C.L. Wang, J.C. Li, M.L. Zhao, Appl. Phys. Lett. 91 (2007) 042905.

[27] S. Vangchangyia, T. Yamwong, E. Swatsitang, P. Thongbai, S. Maensiri, Ceram. Int. 39 (2013) 8133-8139.

[28] P. Thongbai, J. Boonlakhorn, B. Putasaeng, T. Yamwong, S. Maensiri, J. Am. Ceram. Soc. 96 (2013) 379-381.

[29] Z.-Y. Lu, X.-M. Li, J.-Q. Wu, M. Winter, J. Am. Ceram. Soc. 95 (2012) 476-479.

[30] T.B. Adams, D.C. Sinclair, A.R. West, J. Am. Ceram. Soc. 89 (2006) 3129-3135.

[31] R. Yu, H. Xue, Z. Cao, L. Chen, Z. Xiong, J. Eur. Ceram. Soc. 32 (2012) 1245-1249.

3.3 $CaCu_{3-x}Zn_xTi_4O_{12}/CaTiO_3$

The aim of this part is to provide a new strategy to enhance the dielectric performance of CCTO/CTO composites by doping with Zn^{2+}. $CaCu_{3-x}Zn_xTi_4O_{12}/CaTiO_3$ composites with strongly enhanced ε' and lower $\tan\delta$ can be synthesized from a binary compound system with a nominal composition of $Ca_2Cu_{2-x}Zn_xTi_4O_{12}$, where x=0, 0.2, and 0.3, which were referred to as CCTO/CTO, CCTO/CTO_Zn1, and CCTO/CTO_Zn2 composites, respectively.

The important results of this part are that the dielectric and nonlinear properties of a composite system derived from $Ca_2Cu_2Ti_4O_{12}$ were greatly improved by doping with Zn^{2+} to deliberately create $CaCu_{3-x}Zn_xTi_4O_{12}/CaTiO_3$ composites. $Ca_2Cu_{1.8}Zn_{0.2}Ti_4O_{12}$ composition can exhibit an enhanced ε'~6,513, with a strong reduction of $\tan\delta$ to ~0.015 (at 1 kHz). The nonlinear coefficient and breakdown field strength were significantly enhanced. The maximum stored energy density was very high, 39.4 kJ/m^3. The dielectric and nonlinear properties were described based on the effect of Zn^{2+} substitution upon electrical response of internal interfaces. Details of the experimental results and discussion are as follows:

The XRD patterns of $Ca_2Cu_{2-x}Zn_xTi_4O_{12}$ ceramics are shown in Fig. 3.3.1. All the samples consisted of CCTO (JCPDS 75-2188) and CTO phases (JCPDS 82-0231). This observation is similar to those reported in the literature [1-4]. Considering the nominal formula of $Ca_2Cu_2Ti_4O_{12}$, phases of CCTO (~33.3 mol%) and CTO (~66.7 mol%) should be formed. This was further confirmed by a Rietveld quantitative analysis [2]. The reason for this is that the ionic radius of Ca^{2+} is much larger than that of Cu^{2+}. Thus, Ca^{2+} cannot enter into Cu^{2+} sites in a planar square to create a $Ca(CaCu_2)Ti_4O_{12}$ structure. Interestingly, an impurity phase related to Zn^{2+} doping ions was not observed. Lattice parameters (*a*) of the CCTO phase were calculated and found to be 7.3893, 7.3929, and 7.4002 Å for CCTO/CTO, CCTO/CTO_Zn1, and CCTO/CTO_Zn2 composites, respectively. The increase in the value of *a* for the CCTO phase may be due to different ionic radii being formed between Zn^{2+} (r_4=0.60 Å) and Cu^{2+} (r_4=0.57 Å) ions [5].

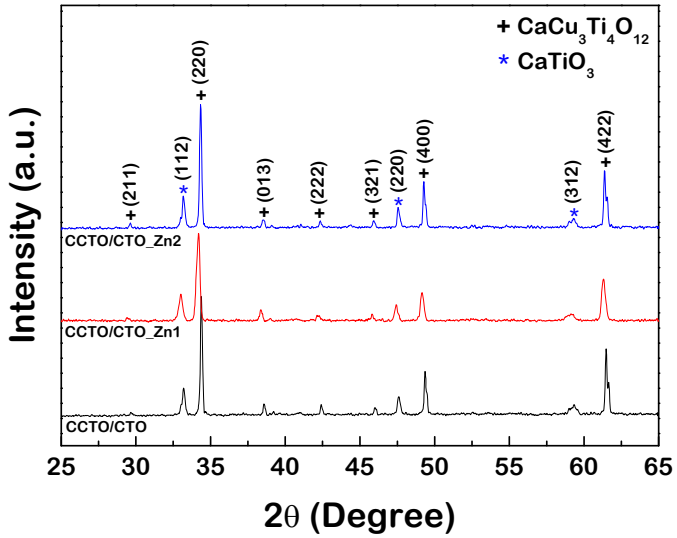

Figure 3.3.1 XRD patterns of $Ca_2Cu_{2-x}Zn_xTi_4O_{12}$ (x = 0, 0.20, and 0.30) ceramics.

Figures 3.3.2(a-c) show backscattered SEM images of the polished CCTO/CTO, CCTO/CTO_Zn1, and CCTO/CTO_Zn2 composites, respectively. Darker and lighter phases were observed, which is consistent with the XRD results and similar to those reported in the literature for un-doped $Ca_2Cu_2Ti_4O_{12}$ ceramics [2, 4]. Figure 3.3.2(d) reveals unpolished surface of the CCTO/CTO_Zn2 composite, showing the smooth and rough surfaces, which were expected as CCTO and CTO phases [4], respectively.

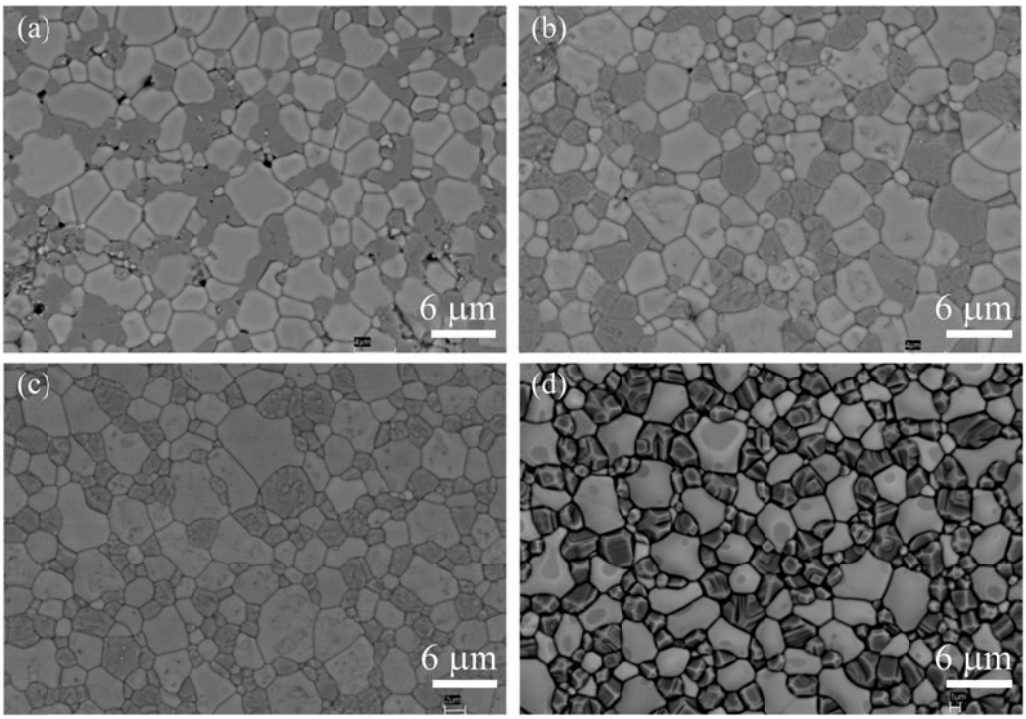

Figure 3.3.2 Backscattered SEM images of polished surfaces of (a) CCTO/CTO, (b) CCTO/CTO_Zn1, and (c) CCTO/CTO_Zn2 composites. (d) Backscattered SEM image of unpolished surface of CCTO/CTO_Zn2 composite.

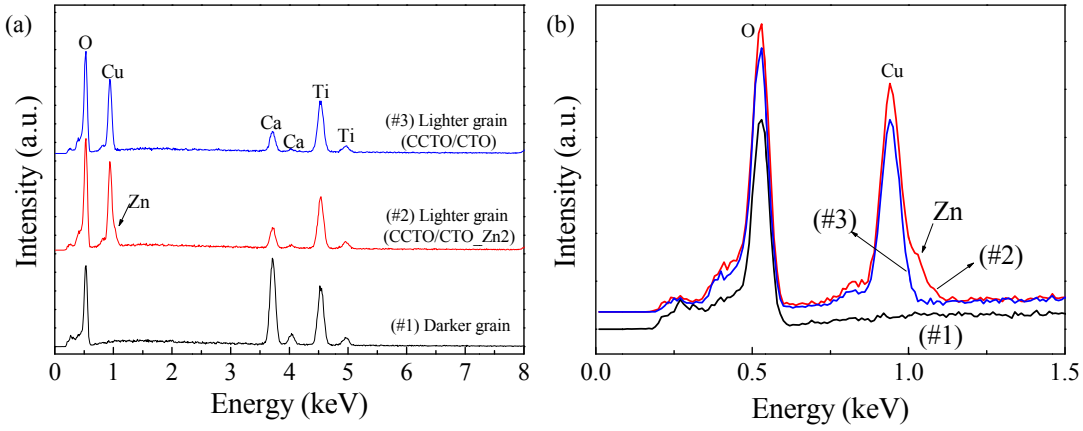

Figure 3.3.3 (a) EDS spectra of CCTO/CTO and CCTO/CTO_Zn2 composites. (b) Enlarged view of (a).

As seen in Fig. 3.3.3(a) for the EDS spectra (spectra (#1)-(#3)) of the CCTO/CTO and CCTO/CTO_Zn2 composites, the lighter and darker phases are clearly CCTO and CTO phases, respectively. Grain sizes of CCTO and CTO phases are slightly changed. Notably, highly dense microstructure of CCTO/CTO composites was obtained by doping with Zn^{2+}. However, the EDS peak of Zn cannot be observed in either phase. This was due to similarity of values of the energy of the X-ray emissions for L_{α} of Cu^{2+} (~0.929 keV) and Zn^{2+} (~1.011 keV) ions. In Fig. 3.3.3(b), the shoulder of EDS-Cu peak detected at the lighter grain of the CCTO/CTO_Zn2 composite was observed. This indicates to Zn^{2+} ions, which were preferentially substituted into Cu^{2+} sites but only in the CCTO phase. It was estimated that the $Ca_2Cu_{2-x}Mg_xTi_4O_{12}$ ceramics prepared in the current study consisted of ~33.3 mol% of $CaCu_{3-x}Mg_xTi_4O_{12}$ (x = 0, 0.20, and 0.30) and ~66.7 mol% of CTO.

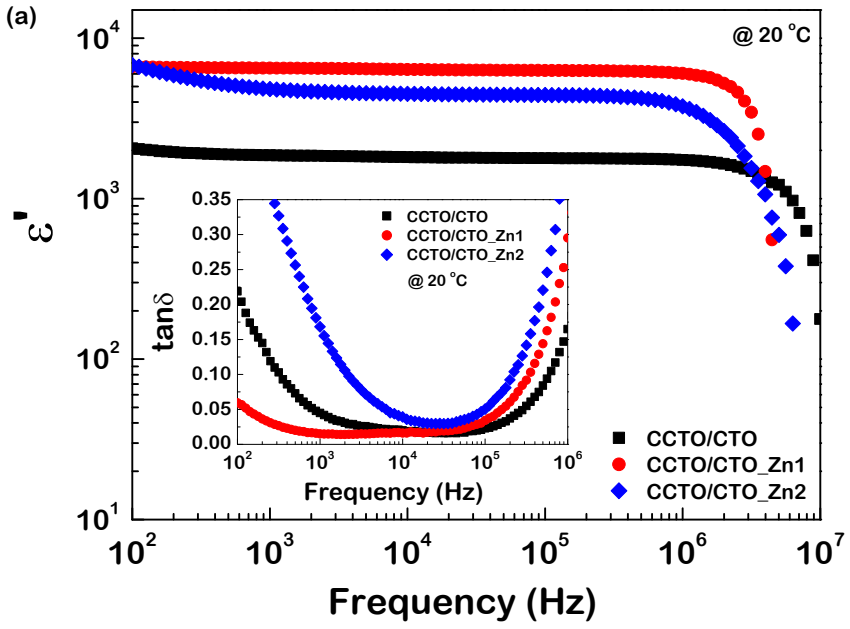

Figure 3.3.4 Frequency dependence of ε' at 20°C for $Ca_2Cu_{2-x}Zn_xTi_4O_{12}$ (x = 0, 0.20, and 0.30) ceramics; inset shows tanδ at 20°C.

As shown in Fig. 3.3.4, ε' at 20°C of the CCTO/CTO and CCTO/CTO_Zn1 composites was independent of frequency in the range from 10^2 to 10^6 Hz. Notably, ε' of CCTO/CTO composites was strongly enhanced by doping with Zn^{2+}, whereas, tanδ was significantly reduced [inset of Fig. 3.3.4]. The ε' values at 20 °C and 1 kHz of

CCTO/CTO, CCTO/CTO_Zn1, and CCTO/CTO_Zn2 composites were found to be 1863, 6513, and 4821, respectively. Values of tanδ were found to be 0.045, 0.015, and 0.168, respectively. It was noted that ε' of the CCTO/CTO composite sample was close to the ε' value of ~1800 for a sample sintered at 1090 $^{\circ}$C for 24 h as was reported in the literature [6]. Interestingly, the CCTO/CTO_Zn1 composite exhibited a greatly enhanced ε' with a significantly reduced tanδ. High performance dielectric properties of the CCTO/CTO_Zn1 composite can be comparable to that observed in $CaCu_{3-x}La_{2x/3}Ti_4O_{12}$ ceramics (ε'~7500 and tanδ~0.02 at 1 kHz) [7].

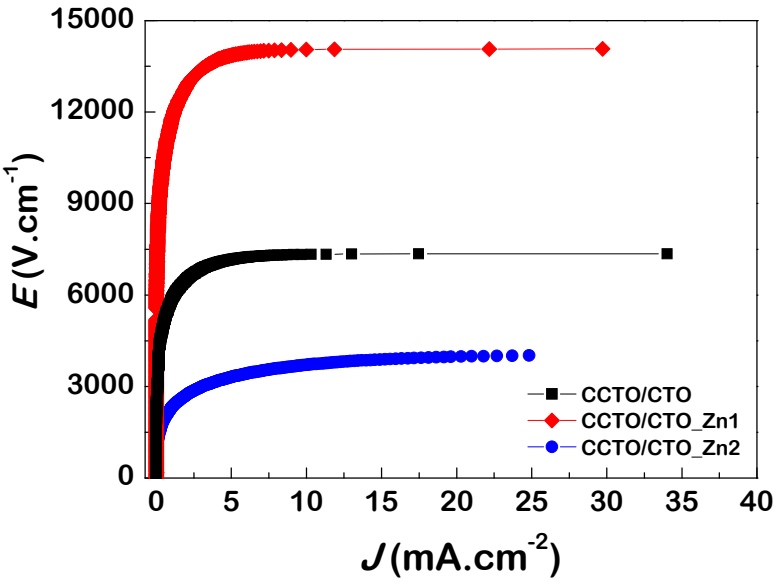

Figure 3.3.5 Nonlinear properties of $Ca_2Cu_{2-x}Zn_xTi_4O_{12}$ ceramics.

The effect of Zn^{2+} doping ions on non-Ohmic properties of CCTO/CTO composites was also investigated. The results are shown in Fig. 3.3.5. All the composite ceramics of the current study exhibited nonlinear *E*-*J* behavior. α and E_b of the CCTO/CTO, CCTO/CTO_Zn1 and CCTO/CTO_Zn2 composites were calculated and found to be 9.89 and 5,817 V/cm, 12.43 and 11,689 V/cm, and 4.77 and 2,295 V/cm, respectively. Interestingly, improved nonlinear electrical properties were achieved in the CCTO/CTO_Zn1 composite. Zn^{2+} doping ions had significant influences on both the dielectric and nonlinear electrical properties of CCTO/CTO composites. Generally, the energy density (*U*) performance of capacitors can be expressed as $U = \varepsilon'\varepsilon_0 E_b^2 / 2$. The

maximum stored energy densities of the CCTO/CTO, CCTO/CTO_Zn1, and CCTO/CTO_Zn2 composites were 2.52, 39.40, and 1.12 kJ/m^3, respectively. The high *U* value of the CCTO/CTO_Zn1 composite was equal to that observed in a CCTO/$CuAl_2O_4$ composite [8]. This is the highest *U* value among CCTO-based oxides that has ever been reported.

Using electrostatic force microscopy (EFM) [2], it was clearly shown that CCTO-CCTO and CCTO-CTO interfaces were electrically active. This indicated the presence of potential barriers at these interfaces. However, a CTO-CTO interface was electrically inactive. Enhancement of non-Ohmic properties of the CCTO/CTO_Zn1 composite was therefore attributed to the improved electrical response of these interfaces, resulting from substitution of Zn^{2+}. Higher concentrations of Zn^{2+} doping ions caused degradation of nonlinear properties in the CCTO/CTO_Zn2 composite. This result is similar to that reported in literature for Zn-doped CCTO ceramics with high Zn^{2+} content [9]. It was reported that ε' and E_b of the CCTO/CTO system decreased as the content of the CTO phase increased [2]. For CCTO ceramics, the giant ε' response is now widely accepted to be caused by the interfacial polarization at the CCTO-CCTO interface [10, 11]. Therefore, a strong increase in ε' of Zn-doped CCTO/CTO composites may be primarily caused by the enhanced electrical response at the CCTO-CCTO interface alone. This is reasonable because ε' of CCTO/CTO was found to be slightly dependent upon sintering temperature [3]. Although the mechanism responsible for these observations is still unclear, this work provides an important novel route to strongly enhance the dielectric response and non-Ohmic properties of CCTO-based ceramics.

References

[1] M.A. Ramírez, P.R. Bueno, J.A. Varela, E. Longo, Appl. Phys. Lett. 89 (2006) 212102.

[2] M.A. Ramírez, P.R. Bueno, R. Tararam, A.A. Cavalheiro, E. Longo, J.A. Varela, J. Phys. D: Appl. Phys. 42 (2009) 185503.

[3] P. Thongbai, B. Putasaeng, T. Yamwong, S. Maensiri, J. Alloys Compd. 509 (2011) 7416-7420.

[4] J. Jumpatam, P. Thongbai, B. Kongsook, T. Yamwong, S. Maensiri, Mater. Lett. 76 (2012) 40-42.

[5] R.D. Shannon, Acta Cryst. A32 (1976) 751-767.

[6] W. Kobayashi, I. Terasaki, Appl. Phys. Lett. 87 (2005) 032902.

[7] S.F. Shao, J.L. Zhang, P. Zheng, C.L. Wang, J.C. Li, M.L. Zhao, Appl. Phys. Lett. 91 (2007) 042905.

[8] J. Li, R. Jia, X. Tang, X. Zhao, S. Li, J. Phys. D: Appl. Phys. 46 (2013) 325304.

[9] D. Xu, C. Zhang, Y. Lin, L. Jiao, H. Yuan, G. Zhao, X. Cheng, J. Alloys Compd. 522 (2012) 157-161.

[10] D.C. Sinclair, T.B. Adams, F.D. Morrison, A.R. West, Appl. Phys. Lett. 80 (2002) 2153.

[11] S.-Y. Chung, I.-D. Kim, S.-J.L. Kang, Nat. Mater. 3 (2004) 774-778.

3.4 $CaCu_3Ti_{4-x}Zr_xO_{12}/CaTiO_3$

In this part of the research work, a composite system of $CaCu_3Ti_4O_{12}/CaTiO_3$ **doped** with Zr^{4+} was deliberately created using a one-step processing method. Investigation of the microstructural evolution and electrical responses of internal interfaces of Zr^{4+}-doped $CaCu_3Ti_4O_{12}/CaTiO_3$ composites was performed to clarify the exact nature of its high dielectric response. Grain sizes of the $CaCu_3Ti_4O_{12}$ phase in the $CaCu_3Ti_4O_{12}/CaTiO_3$ microstructure were largely increased by doping with Zr^{4+}, resulting in an increase in ε' (at 10^3 Hz) from 1.86×10^3 to 1.03×10^4. This is in complete contrast to observations of a single phase of Zr^{4+}-doped $CaCu_3Ti_4O_{12}$. This observation confirmed an extrinsic effect as the origin of high dielectric properties of $CaCu_3Ti_4O_{12}/CaTiO_3$ composites, rather than intrinsic factors. The macroscopic dielectric relaxation was well described by the Maxwell-Wagner relaxation model. Furthermore, changes of the loss tangent resulting from different doping levels of Zr^{4+} correlated well with variation of the resistance of insulating internal interfaces. Experimental results gave an important clue indicating that electrical responses of internal interfaces were the cause of the giant dielectric response in the $CaCu_3Ti_4O_{12}$ material system.

A solid state reaction method was used to prepare Zr-doped $Ca_2Cu_2Ti_4O_{12}$ ceramics with a nominal chemical composition of $Ca_2Cu_2Ti_{4-x}Zr_xO_{12}$, where x = 0, 0.05, 0.10, 0.20, and 0.30 (abbreviated as CCTO/CTO, Zr05, Zr10, Zr20, and Zr30 ceramics, respectively). Details of experimental results and discussion are as follows:

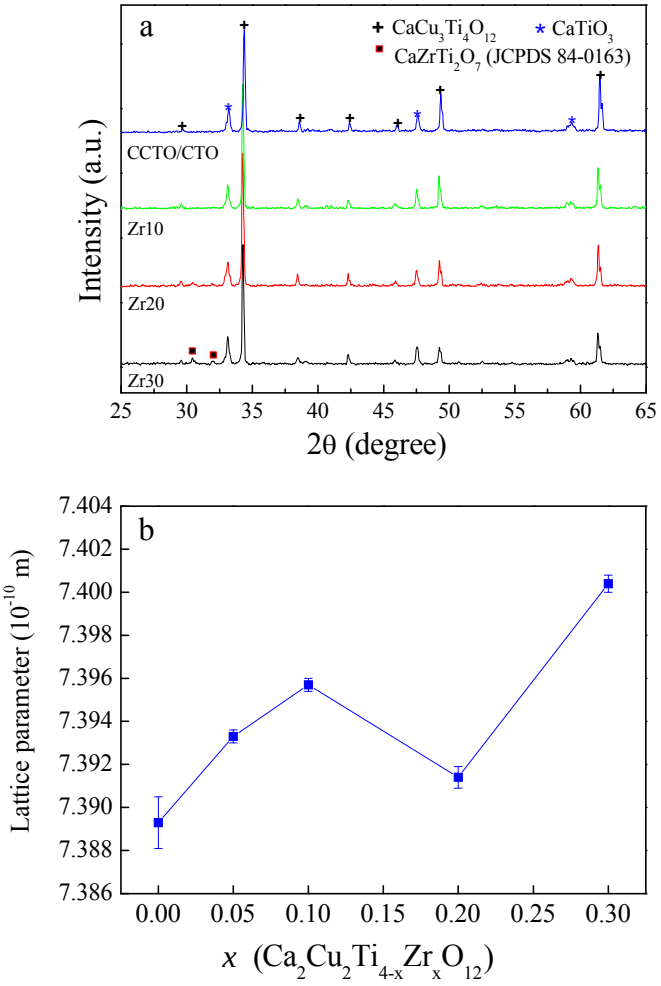

Figure 3.4.1 (a) XRD patterns of $Ca_2Cu_2Ti_{4-x}Zr_xO_{12}$ ceramics. (b) Lattice parameter of CCTO phase in $Ca_2Cu_2Ti_{4-x}Zr_xO_{12}$ composites as a function of doping level (x).

Ceramics with a nominal composition of $Ca_2Cu_2Ti_4O_{12}$ consisted of two phases, *i.e.*, CCTO and CTO at concentrations of ~33.3 and ~66.7 mol%, respectively [2, 3]. In Fig. 3.2.1(a), CCTO (JCPDS 75-2188) and CTO (JCPDS 82-0231) phases appear in all the XRD patterns of $Ca_2Cu_2Ti_{4-x}Zr_xO_{12}$ (x=0-0.3) compositions, which is similar to that reported in literature [2-9]. The XRD result confirms creation of CCTO/CTO composite system. An impurity phase was not detected in the XRD patterns of the CCTO/CTO, Zr05, and Zr30 samples. This indicates substitution of Zr^{4+} into the Ti^{4+} sites of the CCTO phase. However, an impurity phase of $CaZrTi_2O_7$ (JCPDS 84-0163) was also observed in the XRD patterns of the Zr20 and Zr30 samples. This indicates a limited solid solution of Zr^{4+} in CCTO and/or CTO phases. CCTO phase lattice parameters in

the CCTO/CTO, Zr05, Zr10, Zr20, and Zr30 composite samples were calculated by using Cohen's least mean square method and found to be 7.3893±0.0012, 7.3933±0.0003, 7.3957±0.0003, 7.3914±0.0005, and 7.4004±0.0004 Å, respectively. These calculated values are comparable to the 7.391 Å value for CCTO crystal structure (JCPDS 75-2188) and published values of ≈7.391 Å [3, 8, 10-20]. Lattice parameter calculations indicated an enlarged unit cell in the CCTO phase. As shown in Fig. 3.4.1(b), lattice parameters of CCTO phase in $Ca_2Cu_2Ti_{4-x}Zr_xO_{12}$ compositions tends to increase with increasing concentration of Zr^{4+} doping ions (x), except for the Zr02 sample for x = 0.2.

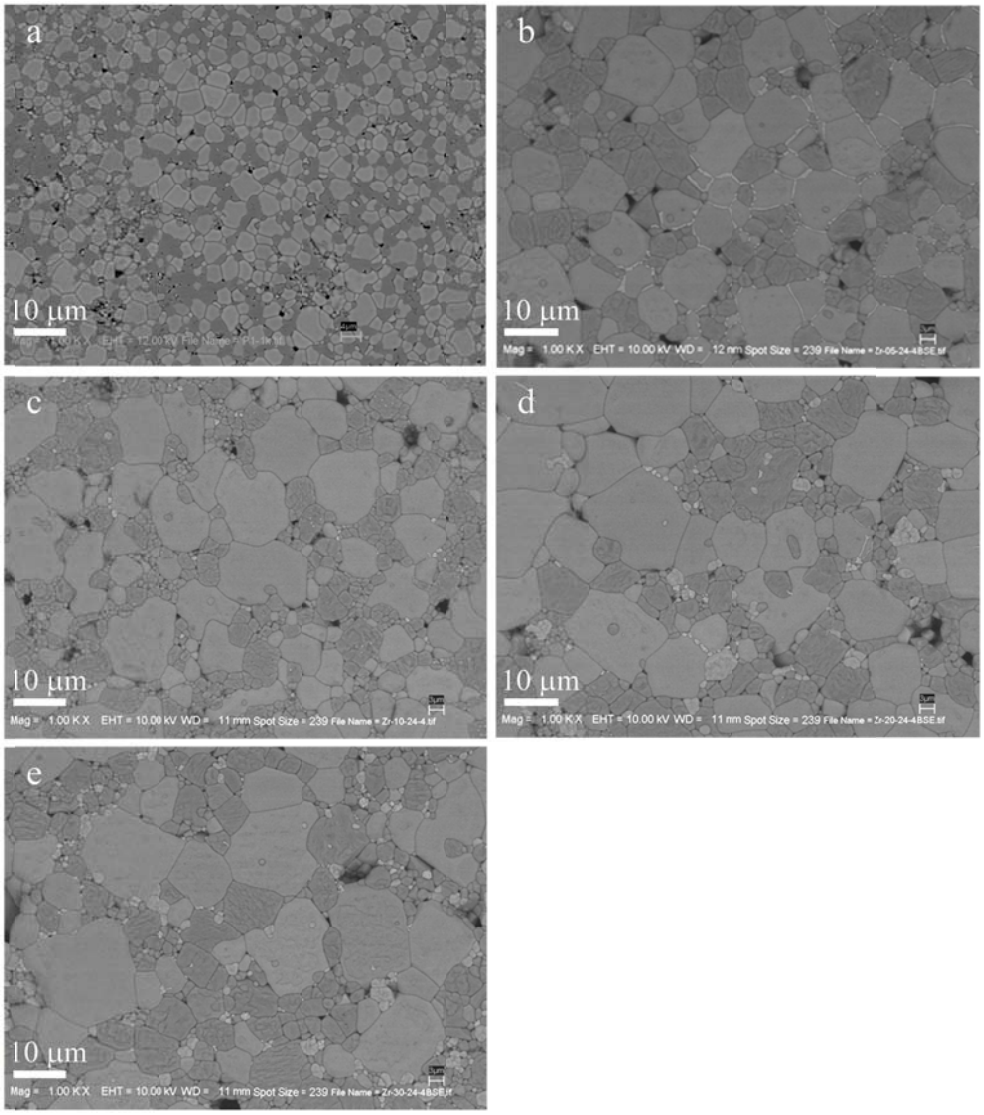

Figure 3.4.2 Backscattered SEM images of polished-surfaces of (a) CCTO/CTO, (b) Zr05, (c) Zr10, (d) Zr20, and (e) Zr30 samples.

As depicted in the backscattered SEM images of Fig. 3.4.2, all the sintered ceramics consisted of at least two phases with different contrasts. According to previous work [5, 9], brighter and darker grains in CCTO/CTO composites were clearly shown to be CCTO and CTO phases, respectively. In Figs. 3.4.3(a) and 3.4.3(b), EDS spectra detected at the darker (point 1) and brighter (point 2) grains clearly indicate CTO and CCTO phases, respectively. This is supported by published literature [5, 9]. Only EDS peaks of Ca, Ti, and O were observed in the darker grain (point 1). In the brighter grain (point 2), a small intensity Zr EDS-peak was observed as well as the main Ca, Cu, Ti, and O EDS—peaks. This indicates that some portion of the Zr^{4+} ions was substituted into the CCTO phase. As shown in Figs. 3.4.2(d) and 3.4.2(e), there is another phase in addition to CCTO and CTO that appeared in the microstructure of the Zr20 and Zr30 samples. The observation of this third phase is consistent with their XRD patterns. In Fig. 3.4.3(b), the EDS spectrum detected in this phase (point 3 in Fig. 3.4.3(a)) confirmed the existence of Ca, Zr, Ti, and O atoms in the impurities. Thus, it is reasonable to infer that this phase was $CaZrTi_2O_7$, as it appeared in the XRD patterns.

According to the microstructure analysis shown in Figs. 3.4.2 and 3.4.3, grain sizes of the CTO and CCTO phases in Zr^{4+}-doped CCTO/CTO (Z-CCTO/CTO) composites were much larger than those observed in the CCTO/CTO composite. The mean grain sizes of the CCTO phase in the CCTO/CTO, Zr05, Zr10, Zr20, and Zr30 samples were found to be 2.9±0.97, 9.04±3.44, 10.99±3.75, 13.40±3.75, and 13.54±5.22 μm, respectively. The mean grain sizes of the CTO phase in these samples were 1.96±0.48, 6.22±2.13, 4.63±1.79, 5.85±2.28, and 6.29±2.21 μm, respectively. These results are particularly interesting in light of previous work [14, 15], where substitution of Zr^{4+} into a single phase CCTO ceramic caused a great decrease in the mean grain size. Here, a small portion of Ca, Zr, Ti, and O reacted to form a new $CaZrTi_2O_7$ phase. Formation of a $CaZrTi_2O_7$ phase might cause an excess of CuO-rich phase within the microstructure. The grain growth of CCTO ceramics is correlated with liquid phase sintering [21, 22]. A slight excess of CuO in the starting CCTO composition could promote the grain growth rate in a single phase of CCTO ceramics. The CuO-rich phase was believed to be a source of a liquid phase that existed during the sintering process of CCTO ceramics. Therefore, the larger grain growth in Z-CCTO/CTO composites may be attributed to the existence of a slight excess of CuO in their microstructure. The density of all the samples was measured by the Archimedes

method. The relative densities of the CCTO/CTO, Zr05, Zr10, Zr20, and Zr30 samples were calculated and found to be 88.93, 91.33, 91.49, 89.93, and 88.96 %, respectively.

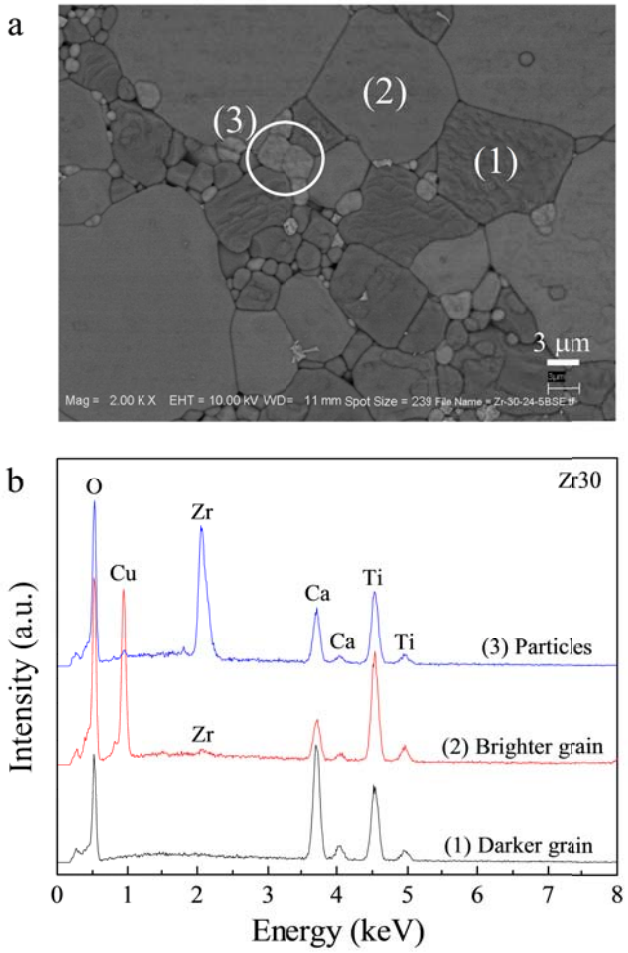

Figure 3.4.3 (a) Backscattered SEM image of polished-surfaces of Zr30 sample, showing EDS testing points at different phases. (b) EDS spectra detected at different points on the surface of the Zr03 sample.

Table 3.4.1 ε' and tanδ (at 1 kHz and 20 °C), activation energy for dielectric relaxation (E_a), activation energy for conduction inside grain (E_g), resistance of CCTO grain at 20 °C (R_g), estimated capacitance of GB at room temperature (C_{gb}), nonlinear coefficient (α), and electric breakdown field strength (E_b) at room temperature for ceramic samples.

Samples	ε'	tanδ	E_a (eV)	E_g (eV)	R_g (Ω.cm)	C_{gb} (nF)	α	E_b (V/cm)
CCTO/CTO	1,863	0.045	0.122	0.098	~160	~0.72	9.9	5,817
Zr05	8,501	0.193	0.137	0.122	~110	~2.75	3.2	519
Zr10	10,355	0.442	0.139	0.119	~120	~2.98	2.8	396
Zr20	7,073	0.089	0.144	0.125	~230	~2.28	4.1	973
Zr30	4,610	0.038	0.157	0.144	~500	~1.49	3.5	917

Figure 3.4.4 shows the frequency dependence of ε' and tanδ at 20 °C for all samples of the current study. The values of ε' at f = 1 kHz are summarized in Table 3.4.1. The inset of Fig. 5(a) demonstrates the values ε' at 10^3 and 10^4 Hz as a function of doping level. ε'~1,863 of the CCTO/CTO sample was comparable to the value 1,800 first reported by Kobayashi and Terasaki [4], and others [8]. According to microstructural analyses, it is likely that the Zr05 and Zr10 samples consisted of CTO and CCTO phases with concentrations roughly estimated to be about 66.7 and 33.3 mol%, respectively. This is the same as in the CCTO/CTO composite. The Zr20 and Zr30 samples consisted of three phases with an additional $CaZrTi_2O_7$ phase. According to previous work [14, 15, 23], it was found that substitution of Zr^{4+} ions into CCTO ceramics caused a large decrease in ε' values. According to simple mixing models that excluded the effect of interfacial interaction between the two phases [4], ε' of the Z-CCTO/CTO composite system should be reduced compared to the un-doped CCTO/CTO composite. This is because ε' of the un-doped CCTO grains in the CCTO/CTO composite was expected to be larger than that of the Zr-doped CCTO grains in the $CaCu_3Ti_{4-x}Zr_xO_{12}/CaTiO_3$ composites. Interestingly, ε' at $f < 10^5$ Hz of CCTO/CTO composites was strongly enhanced by doping with Zr^{4+}, as clearly seen in the inset of Fig. 3.4.3(a). The dielectric response in Z-CCTO/CTO composite system

could not be described by simple mixing models or a mixing law such as the Maxwell-Garnett model, Bruggeman self-consistent effective medium model, and Lichtenecker's logarithmic law [4, 24]. This result strongly suggested that the high dielectric response of a CCTO/CTO system as well as in CCTO ceramics was not primarily due to intrinsic effects. Obviously, a high dielectric response should be caused by an electrical response of internal interfaces such as the CCTO-CCTO interface, CCTO-CTO interface, and/or domain boundaries in the large grains of CCTO. Therefore, a strongly enhanced ε' in Z-CCTO/CTO system may be attributed to the modified electrical response at these internal interfaces caused by Zr^{4+} doping ions.

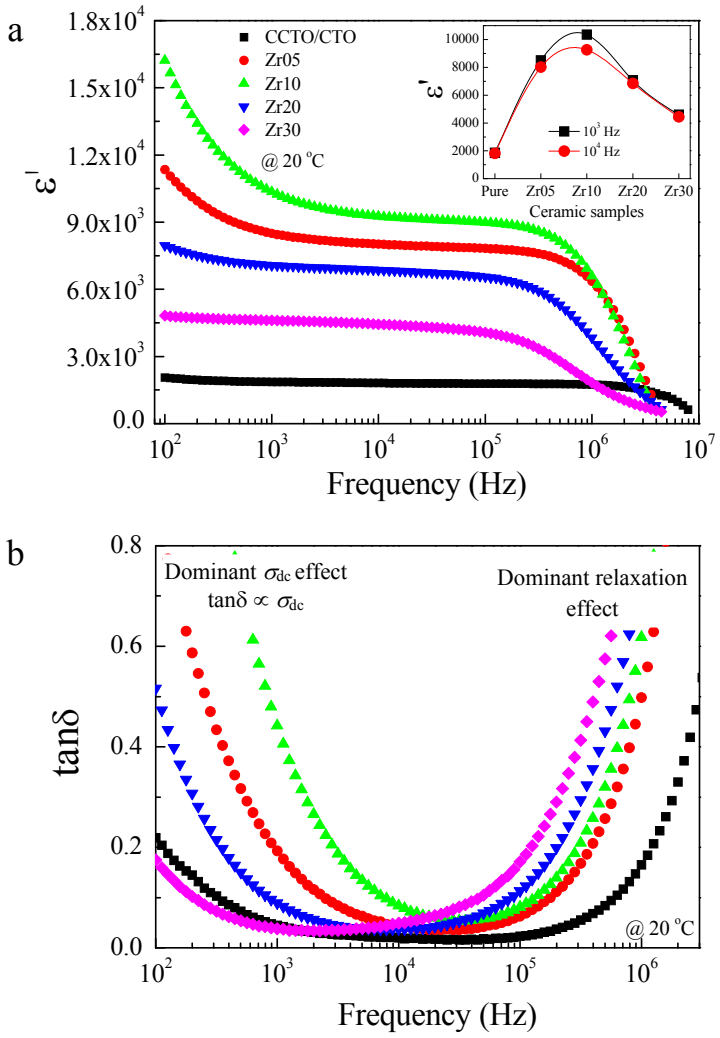

Figure 3.4.4 (a) ε' and (b) tanδ of $Ca_2Cu_2Ti_{4-x}Zr_xO_{12}$ ceramic at 20 °C over a measured frequency range; inset of (a) shows ε' as a function of doping level at 10^3 and 10^4 Hz.

The frequency dependence of tanδ at 20 °C and tanδ values (at f = 1 kHz) are shown in Fig. 3.4.4(b) and Table 3.4.1, respectively. Over the range of f = 10^2-10^4 Hz, tanδ of all samples increased rapidly with decreasing frequency. This was mainly due to the effect dc conduction in the bulk ceramics [22, 25]. A low-frequency tanδ of $Ca_2Cu_2Ti_{4-x}Zr_xO_{12}$ ceramics increased as x increased from 0-0.1. Then, it decreases as x was further increased from 0.2 to 0.3. Interestingly, the Zr30 sample exhibited improved dielectric properties with ε′~4,610 and a reduced tanδ ~ 0.038. When f >10^5 Hz, tanδ of all samples rapidly increased with increasing frequency. This was clearly due to the dielectric relaxation process [25].

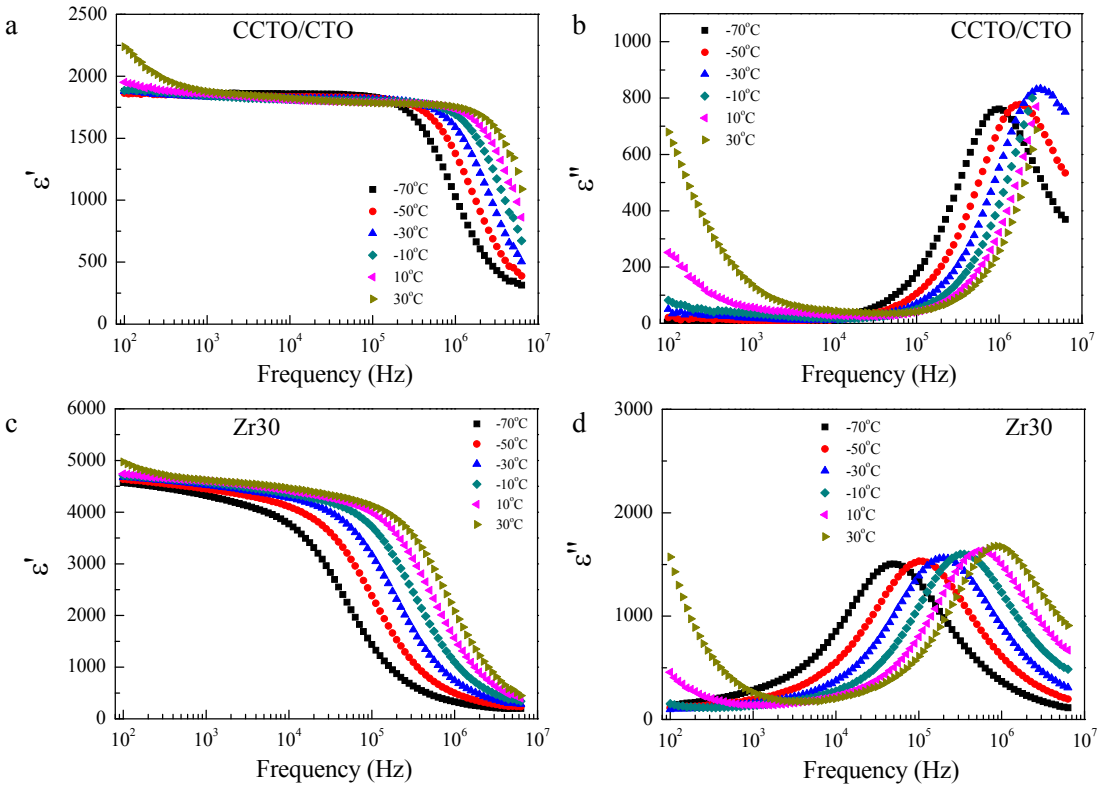

Figure 3.4.5 Frequency dependence of (a,c) ε′ and (b,d) ε′′ at various temperatures over the range of -70—30 °C for the CCTO/CTO and Zr30 samples.

To study the effect of Zr^{4+} substitution upon the dielectric relaxation mechanism in the CCTO/CTO composites, the frequency dependence of ε′ and ε′′ (ε′′=ε′tanδ) at different temperatures was investigated. As shown in Fig. 3.4.5, the frequency-dependence characteristics of the CCTO/CTO and Zr30 samples were quite similar. At

-70 °C, a sudden drop in ε' at a relatively high-frequency was observed. This was accompanied with the ε'' peak. Frequencies at which rapidly decreasing ε' and ε''-peaks were observed, shifted to higher frequencies with increasing temperature. This result indicates a thermally activated dielectric relaxation mechanism. The activation energy (E_a) required for this thermally activated relaxation could be calculated using the Arrhenius law [26],

$$f_{\max,\varepsilon'} = f_0 \exp(\frac{-E_a}{k_B T}), \tag{3.4.1}$$

where $f_{\max,\varepsilon'}$ is the frequency at which the ε'' peak ($\varepsilon''_{\max}$) was observed, T is absolute temperature (K), k_B is the Boltzmann constant, and f_0 is a constant term.

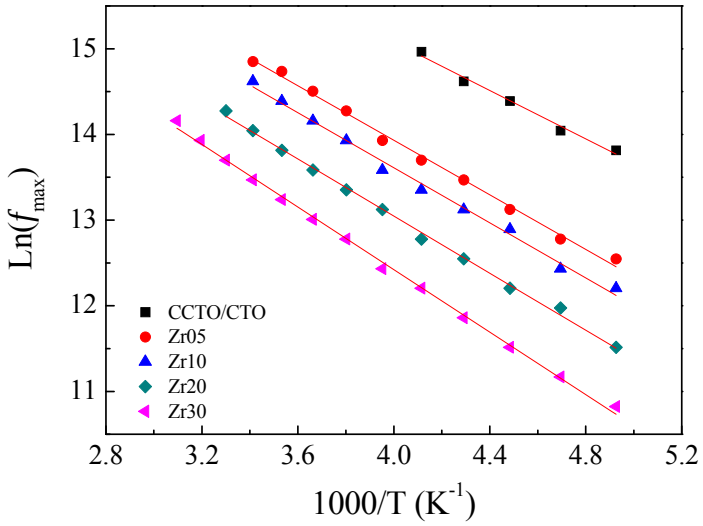

Figure 3.4.6 Arrhenius plots of temperature dependence of f_{max}.

As shown in Fig. 3.4.6, the temperature dependence of $f_{\max,\varepsilon'}$ is linearly well fitted by Eq. (3.4.1). According to the fitted results, E_a values were calculated and found to be 0.122±0.007, 0.137±0.003, 0.139±0.004, 0.144±0.002, and 0.157±0.002 eV for the CCTO/CTO, Zr05, Zr10, Zr20, and Zr30 composite samples, respectively. E_a tended to slightly increase with increasing Zr^{4+} concentration. As shown in Figs. 3.4.5 and 3.4.6, at a particular temperature, the $f_{\max,\varepsilon'}$ value of CCTZO/CTO composites decreased with increasing Zr^{4+} dopant concentration. For example, $f_{\max,\varepsilon'}$ values at -70 °C for the CCTO/CTO, Zr05, Zr10, Zr20, and Zr30 samples were obtained and found to

be 1.0×10^6, 2.8×10^5, 2.0×10^5, 1.0×10^5, and 0.5×10^5 Hz, respectively. This indicated the effects of Zr^{4+} doping ions on the dielectric relaxation behavior of CCTO/CTO composite systems. It is notable that the current study is the first report of dielectric relaxation behavior in CCTO/CTO composite systems. E_a~0.122 eV for the CCTO/CTO sample was slightly higher than the value of a single CCTO phase system. Thus, the origins of the dielectric relaxation mechanism in CCTO/CTO composites and CCTO ceramics might have resulted from a similar cause.

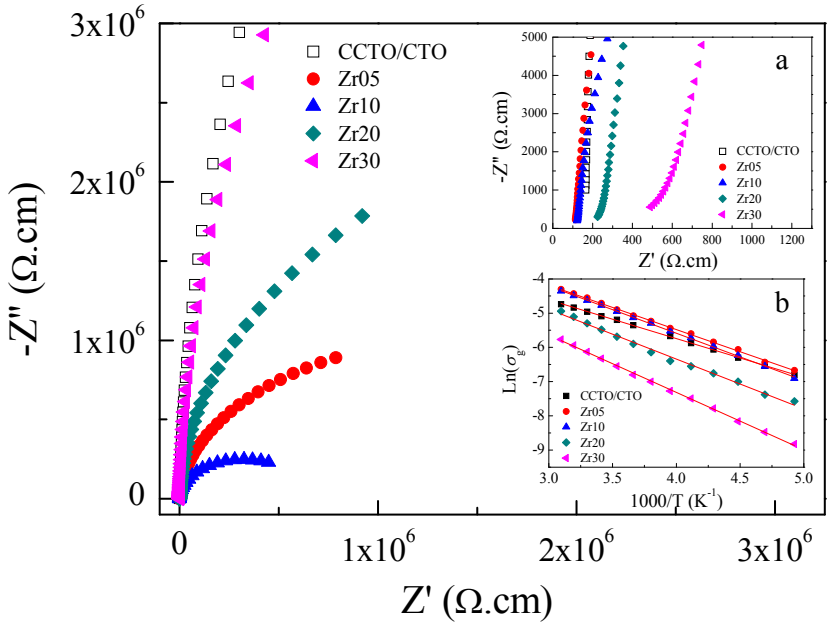

Figure 3.4.7 Impedance complex plane plot (Z^*) at 20 °C for $Ca_2Cu_2Ti_{4-x}Zr_xO_{12}$ ceramics; inset (a) shows an expanded view of the high—frequency data close to the origin, and inset (b) the Arrhenius plots of temperature dependence of σ_g.

Using the M-W relaxation model [27, 28], the macroscopic relaxation time ($\tau = 1/2\pi f_{\max,\varepsilon'}$) was derived and estimated to correlate with the microscopic parameters of grain resistance (R_g) and GB capacitance (C_{gb}), *i.e.*, $\tau \approx R_g C_{gb}$. Furthermore, it was demonstrated that E_a should be nearly the same value as the activation energy of conduction inside the semiconducting grains (E_g) [27]. For clarification, the dielectric relaxation behavior in Zr-CCTO/CTO composites was related to the M-W relaxation type. This was performed using impedance spectroscopy (IS) to investigate the electrical parameters of internal interfaces (or GB) and in the grain interior at different

temperatures. IS data were interpreted based on the brick-work layer model [29]. In Fig. 3.4.7, the observed incomplete semicircular arcs (at 20 ^{o}C) indicate to the electrical response of insulating internal interfaces [29, 30] of CCTO-CCTO and CCTO-CTO interfaces, as described by Ramirez and co-workers [3]. They used electrostatic force microscopy (EFM) to show that these two interfaces were electrically active, while the CTO-CTO interface was electrically inactive. Thus, the total resistance is governed by the resistance of these internal interfaces (R_{int} or R_{gb}). The nonzero intercept on Z′ axis at high frequency data indicated the electrical response in the semiconducting part of CCTO/CTO composites [inset (a) of Fig. 3.4.7], which is the electrical response of CCTO grains [31]. Concurrently, the CTO phase is well known as a good insulator. In inset (b) of Fig. 3.4.7, the temperature dependence of R_g follows the Arrhenius law [27]. $R_g = R_0\exp(E_g/k_BT)$ or $\sigma_g = \sigma_0\exp(E_g/k_BT)$, where, R_0 and σ_0 are constant parameters and σ_g is the grain conductivity. E_g values were calculated and found to be 0.098±0.001, 0.112±0.001, 0.119±0.001, 0.125±0.003, and 0.144±0.001 eV for the CCTO/CTO, Zr05, Zr10, Zr20, and Zr30 samples, respectively. Both E_g and E_b of the Zr-CCTO/CTO composites increased as Zr^{4+} concentration increased. This result might indicate the dielectric relaxation in CCTO/CTO composite system was of the M-W relaxation type [27].

To further investigate the relationship between the macroscopic τ values obtained from the dielectric relaxation peak of ε'' and the product of R_gC_{gb}, C_{gb} values were calculated from the M′′-*f* plots. From the magnitude of the maximum value of $M''(f)$ (M''_{max}), it can be shown that $f_{max,M''} = 1/2\pi RC$ and $M''_{max} = C_0/2C$ [1]. As seen in Fig. 3.4.8(a) for the Zr20 sample, the height of M''_{max} is nearly independent of temperature. These values are proportional to the reciprocals of the associated capacitance. This result indicated that capacitance related to observed M''_{max} only weakly depended on temperature. The calculated values of capacitances at various temperatures for all samples are shown in Fig. 3.4.8(b). The capacitance values of Zr-CCTO/CTO composites were in the range of ≈1.5-3.0 nF. According to the brick-work layer model for CCTO polycrystalline ceramics [29], it reasonable to suggest that these capacitance values were a result of the dielectric response of the insulating internal interfaces or C_{gb} [30]. The grain capacitance (C_g) of CCTO is usually in the order of 10^{-12} F (or pF) [1, 29]. Only C_{gb} values of the Zr05 and Zr10 samples were calculated at 20 ^{o}C, which were found to be 2.75 and 2.98 nF, respectively. Due to a small variation

in temperature dependence of C_{gb}, the C_{gb} values at 20 °C of other samples were roughly estimated and are summarized in Table 3.4.1. The effect of Zr^{4+} doping ions on the value of C_{gb} of CCTO/CTO composites is clearly seen in the inset of Fig. 3.4.8(b). Obviously, variations of C_{gb} values are consistent with observed variation of ε', as demonstrated in the inset of Fig. 3.4.4(a). The dielectric response of CCTO/CTO composite systems might be caused by the dielectric responses at internal interfaces. The values of R_gC_{gb} were calculated using R_g values at 20 °C and the estimated values of C_{gb} at 20 °C.

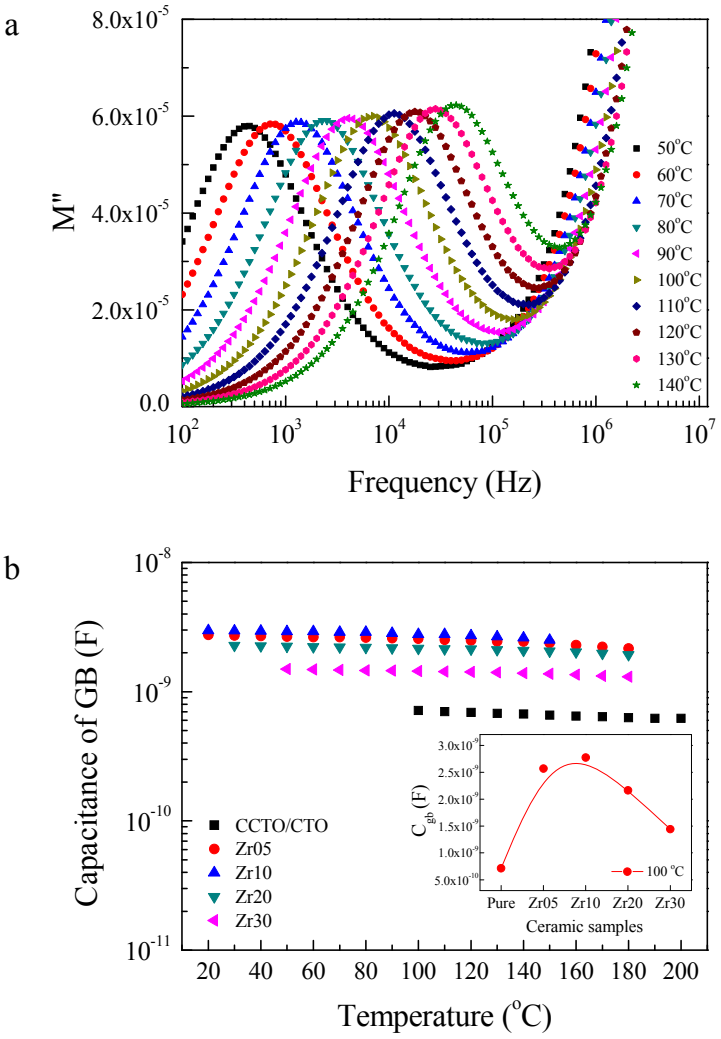

Figure 3.4.8 (a) Frequency dependence of M'' of the Zr20 sample at various temperatures over the range of 50-140 °C. (b) Capacitance values of $Ca_2Cu_2Ti_{4-x}Zr_xO_{12}$ ceramics at different temperatures; the inset demonstrates C_{gb} values at 100 °C as a function of doping level.

As shown in Fig. 3.4.9, variations of macroscopic τ values are consistent with R_gC_{gb} values. The R_gC_{gb} value of the Z-CCTO/CTO composites increased with increasing Zr^{4+} dopant concentration. Therefore, the dielectric relaxation behavior in CCTO/CTO composite systems may be due the M-W relaxation type, which is related to interfacial or space charged polarization [27, 28]. Interfacial polarization at the internal interfaces of CCTO-CCTO and CCTO-CTO interfaces is a major cause of the observed high dielectric response in CCTO/CTO composites. Changes in ε′ in the Z-CCTO/CTO composites likely resulted from modified electrical polarization at the internal interfaces. A much larger grain size of the Z-CCTO/CTO composites than un-doped CCTO/CTO composite gave rise to the space charged sheet region. This enhances polarization intensity, increases ε′ magnitude of the Z-CCTO/CTO composites compared to that of CCTO/CTO samples. The decrease in ε′ of the Zr20 and Zr30 samples compared to those values of the Zr05 and Zr10 samples was attributed to the incorporation of a $CaZrTi_2O_7$ phase.

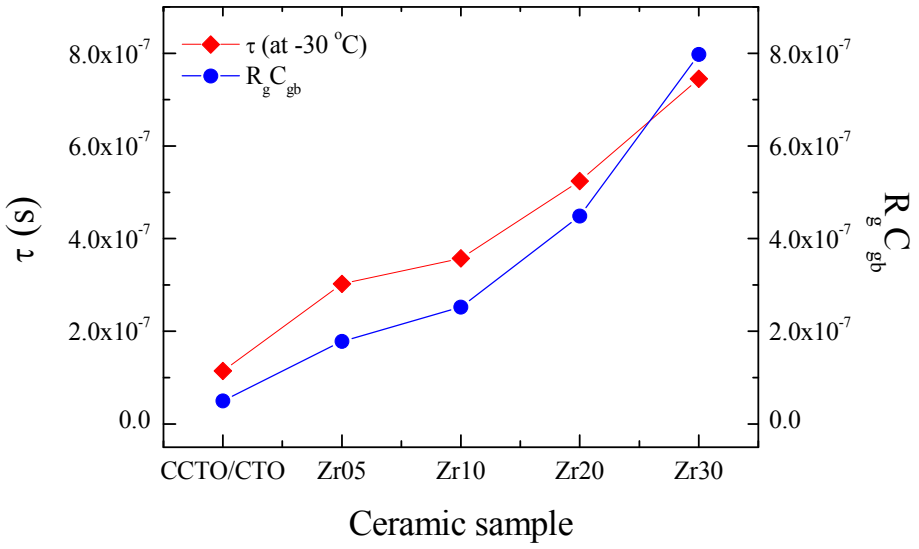

Figure 3.4.9 Relationship between τ (calculated from $\tau=1/\omega_{max}$) at -30 °C and the product of R_g and C_{gb} (R_gC_{gb} values) at 20 °C of $Ca_2Cu_2Ti_{4-x}Zr_xO_{12}$ ceramics.

To study the effect of insulating internal interfaces on tanδ of Zr-CCTO/CTO composites, the relationship between tanδ and R_{gb} was investigated. As shown in Fig. 3.4.7, R_{gb} at 20°C of Zr-CCTO/CTO composites tended to decrease strongly when

increasing Zr^{4+} concentration from 1.25 and 2.5 at.% (for Zr05 and Zr10 samples, respectively), indicating a decrease in R_{gb}. When the concentration of Zr^{4+} was further increased to 5.0-7.5 at.% for Zr20 and Zr30 samples, respectively, R_{gb} increased. This result is consistent with variations in tanδ as a function of Zr^{4+} concentration.

The effect of Zr^{4+} doping ions on the non-Ohmic properties of CCTO/CTO composites at room temperature was investigated. As illustrated in Fig. 13.4.0, E_b of nonlinear *J-E* curves was greatly reduced by substitution of Zr^{4+}. E_b and α values are provided in Table 3.4.1. The nonlinear properties of Z-CCTO/CTO composites were strongly degraded when compared to the un-doped CCTO/CTO samples. From SEM images, it is clear that one of the most important factors that remarkably decreases E_b is the larger mean grain sizes of the CCTO phase. This was especially true for the Zr05 and Zr10 samples when compared to the CCTO/CTO sample [31]. The increase in E_b values after further increasing Zr^{4+} concentrations may have resulted from the third $CaZrTi_2O_7$ phase. It is notable that *J-E* curves of the Zr20 and Zr30 samples were almost identical in the range of J = 0-5 mA/cm^2. The large increase in the mean grain size of CCTO phase reduced insulating GB density, resulting in a reduction of E_b [31]. Another important factor may be due to the interface of CCTO-$CaZrTi_2O_7$, but this is of lesser magnitude.

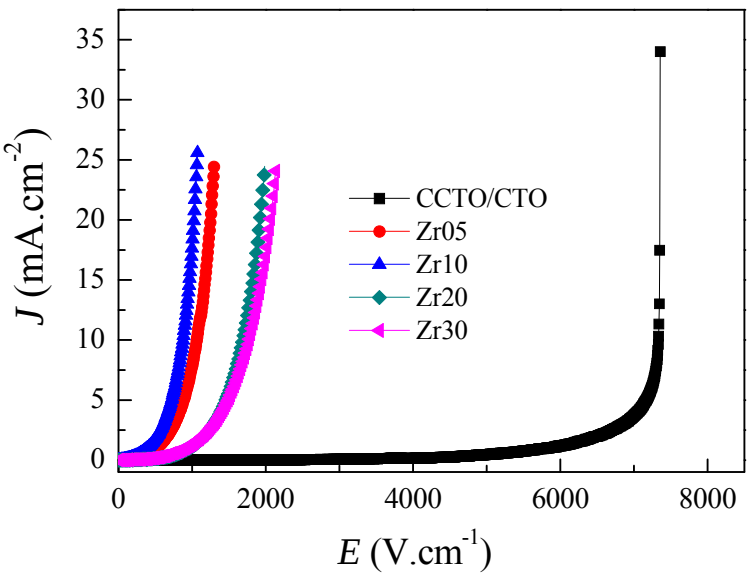

Figure 3.4.10 *J-E* characteristics at room temperature of $Ca_2Cu_2Ti_{4-x}Zr_xO_{12}$ ceramics.

References

[1] [1] J. Zang, M. Li, D.C. Sinclair, W. Jo, J. Rödel, J. Am. Ceram. Soc. (2014) n/a-n/a.

[2] M.A. Ramírez, P.R. Bueno, J.A. Varela, E. Longo, Appl. Phys. Lett. 89 (2006) 212102.

[3] M.A. Ramírez, P.R. Bueno, R. Tararam, A.A. Cavalheiro, E. Longo, J.A. Varela, J. Phys. D: Appl. Phys. 42 (2009) 185503.

[4] W. Kobayashi, I. Terasaki, Appl. Phys. Lett. 87 (2005) 032902.

[5] M.A. Ramírez, P.R. Bueno, E. Longo, J.A. Varela, J. Phys. D: Appl. Phys. 41 (2008) 152004.

[6] L. Ramajo, R. Parra, J.A. Varela, M.M. Reboredo, M.A. Ramírez, M.S. Castro, J. Alloys Compd. 497 (2010) 349-353.

[7] M.A. Ramírez, R. Parra, M.M. Reboredo, J.A. Varela, M.S. Castro, L. Ramajo, Mater. Lett. 64 (2010) 1226-1228.

[8] P. Thongbai, B. Putasaeng, T. Yamwong, S. Maensiri, J. Alloys Compd. 509 (2011) 7416-7420.

[9] J. Jumpatam, P. Thongbai, B. Kongsook, T. Yamwong, S. Maensiri, Mater. Lett. 76 (2012) 40-42.

[10] M.A. Subramanian, A.W. Sleight, Solid State Sci. 4 (2002) 347-351.

[11] Y. Liu, Q. Chen, X. Zhao, J. Mater. Sci.: Mater. Electron. 25 (2014) 1547-1552.

[12] S. Vangchangyia, T. Yamwong, E. Swatsitang, P. Thongbai, S. Maensiri, Ceram. Int. 39 (2013) 8133-8139.

[13] P. Thongbai, S. Vangchangyia, E. Swatsitang, V. Amornkitbamrung, T. Yamwong, S. Maensiri, J. Mater. Sci.: Mater. Electron. 24 (2013) 875-883.

[14] Q.G. Chi, L. Gao, X. Wang, J.Q. Lin, J. Sun, Q.Q. Lei, J. Alloys Compd. 559 (2013) 45-48.

[15] L. Zhang, Y. Wu, X. Guo, Z. Wang, Y. Zou, J. Mater. Sci.: Mater. Electron. 23 (2012) 865-869.

[16] L. Ni, X.M. Chen, J. Am. Ceram. Soc. 93 (2010) 184-189.

[17] L. Ni, X.M. Chen, Solid State Commun. 149 (2009) 379-383.

[18] H. Yu, H. Liu, H. Hao, D. Luo, M. Cao, Mater. Lett. 62 (2008) 1353-1355.

[19] L. Liu, H. Fan, P. Fang, X. Chen, Mater. Res. Bull. 43 (2008) 1800-1807.

[20] S.-H. Hong, D.-Y. Kim, H.-M. Park, Y.-M. Kim, J. Am. Ceram. Soc. 90 (2007) 2118-2121.

[21] K.-M. Kim, S.-J. Kim, J.-H. Lee, D.-Y. Kim, J. Eur. Ceram. Soc. 27 (2007) 3991-3995.

[22] S. Vangchangyia, E. Swatsitang, P. Thongbai, S. Pinitsoontorn, T. Yamwong, S. Maensiri, V. Amornkitbamrung, P. Chindaprasirt, J. Am. Ceram. Soc. 95 (2012) 1497-1500.

[23] E.A. Patterson, S. Kwon, C.-C. Huang, D.P. Cann, Appl. Phys. Lett. 87 (2005) 182911.

[24] Z.M. Dang, Y. Shen, C.W. Nan, Appl. Phys. Lett. 81 (2002) 4814.

[25] J. Wu, C.-W. Nan, Y. Lin, Y. Deng, Phys. Rev. Lett. 89 (2002) 217601.

[26] W. Li, R.W. Schwartz, A. Chen, J. Zhu, Appl. Phys. Lett. 90 (2007) 112901.

[27] J. Liu, C.-G. Duan, W.-G. Yin, W. Mei, R. Smith, J. Hardy, Phys. Rev. B 70 (2004) 144106.

[28] J. Liu, C.-g. Duan, W.N. Mei, R.W. Smith, J.R. Hardy, J. Appl. Phys. 98 (2005) 093703.

[29] D.C. Sinclair, T.B. Adams, F.D. Morrison, A.R. West, Appl. Phys. Lett. 80 (2002) 2153.

[30] T. Adams, D. Sinclair, A. West, Phys. Rev. B 73 (2006) 094124.

[31] S.-Y. Chung, I.-D. Kim, S.-J.L. Kang, Nat. Mater. 3 (2004) 774-778.

3.5 $CaCu_3Ti_{4-x}Sn_xO_{12}/CaTiO_3$

In this part of the research work, $CaCu_3Ti_{4-x}Sn_xO_{12}/CaTiO_3$ composites were prepared using a solid state reaction method employing a simple one-step process. A minor phase of $CaTiO_3$ grains was very well dispersed into the $CaCu_3Ti_4O_{12}$ matrix and these two phases were clearly separated from each other in $CaTiO_3/CaCu_3Ti_4O_{12}$. The grain size of the $CaCu_3Ti_4O_{12}$ phase was largely enhanced by Sn^{4+} doping. Furthermore, $CaTiO_3$ grains were also found inside the enlarged $CaCu_3Ti_4O_{12}$ grains. The microstructural evolution can be described based upon liquid phase sintering and the pinning effect by second-phase particles. The dielectric permittivity of $CaCu_3Ti_{4-x}Sn_xO_{12}/CaTiO_3$ was greatly enhanced from $\sim 2\times10^3$ to $\sim 0.6\text{-}1.3\times10^4$ at 10^3 Hz, while, the loss tangent was still too low. The nonlinear properties were degraded as

a main result of microstructural evolution. These results strongly indicated an extrinsic effect upon both of the giant dielectric response and nonlinear properties of $CaCu_3Ti_4O_{12}$-based compounds.

$CaCu_3Ti_{4-x}Sn_xO_{12}/CaTiO_3$ composites were prepared by using a starting nominal formula of $Ca_2Cu_2Ti_{4-x}Sn_xO_{12}$, where x=0, 0.1, 0.20, and 0.30. These were abbreviated as CCTO/CTO, Sn10, Sn20, and Sn30 composites, respectively. Details of experimental results and discussion are as follows:

Figure 3.5.1 shows the XRD patterns of the composite ceramics sintered for 6 h with nominal compositions of $Ca_2Cu_2Ti_{4-x}Sn_xO_{12}$ (x=0-0.3). Two phases of CCTO (JCPDS 75-2188) and CTO (JCPDS 82-0231) were detected in all samples, indicating the existence of a CCTO/CTO composite system as reported in published literature [1-5]. Impurity phases were not observed in the XRD patterns of the composites sintered for 6 and 24 h. Thus, Sn^{4+} could substitute into Ti^{4+} sites in CCTO and/or CTO structures. The lattice parameters (a) of the CCTO phase of CCTO/CTO, Sn10, Sn20, and Sn30 composites sintered for 6 h were found to be 7.4040, 7.4066, 7.4057, and 7.4098 Å, respectively. Lattice parameter (a) values of the composites sintered for 24 h were found to be 7.3891, 7.4011, 7.3958, and 7.4075 Å, respectively. Values of a tended to increase with increasing Sn^{4+} content. This might be due to the larger ionic radius of Sn^{4+} (0.69 Å) compared to Ti^{4+} (0.605 Å) [6].

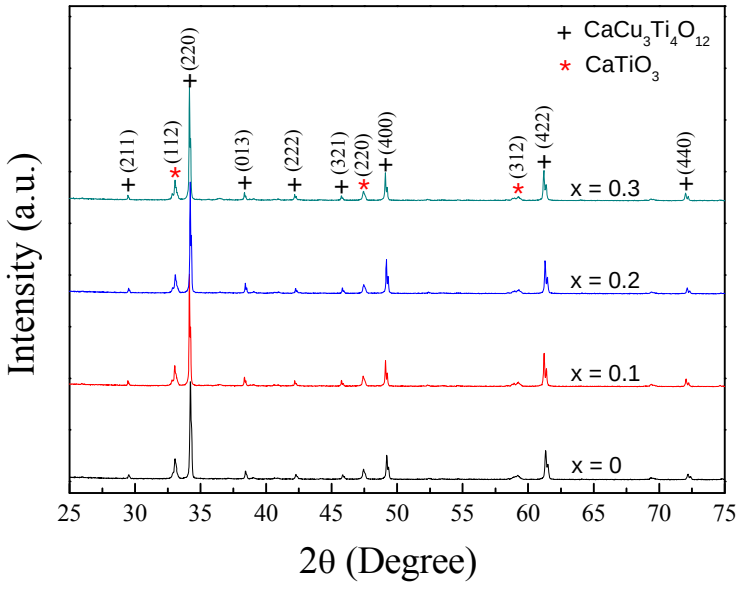

Figure 3.5.1 XRD patterns of $Ca_2Cu_2Ti_{4-x}Sn_xO_{12}$ (x=0-0.3) ceramics sintered for 6 h.

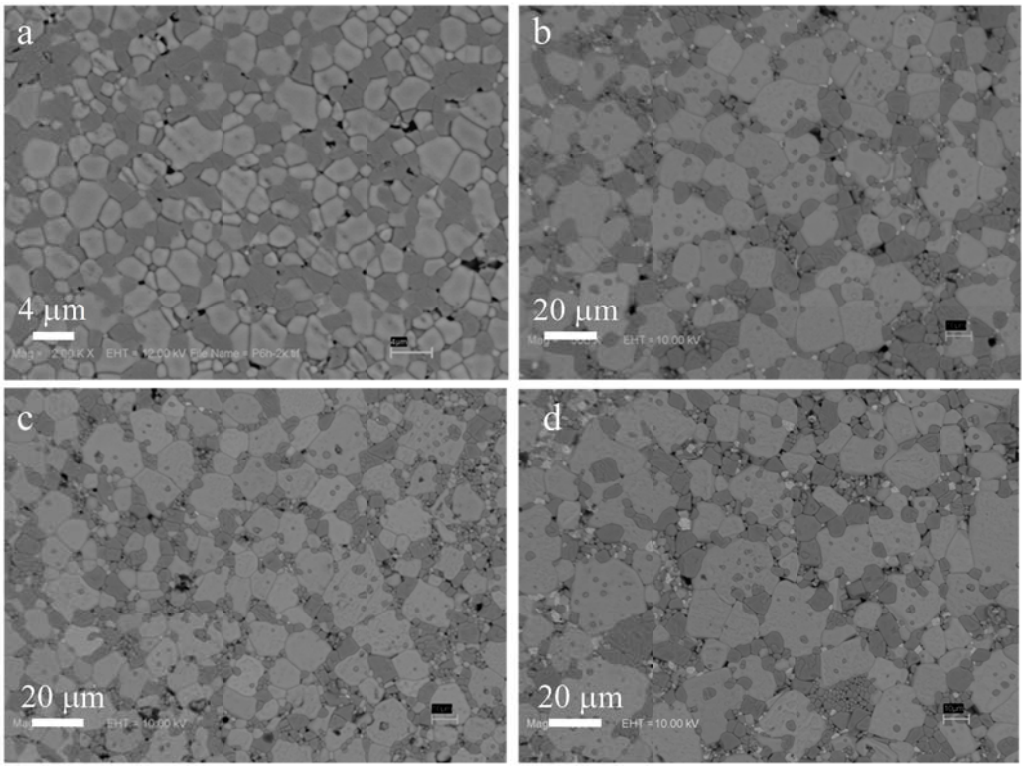

Figure 3.5.2 Backscattered SEM images of (a) CCTO/CTO, (b) Sn10, (c) Sn20, and (d) Sn30 samples sintered for 6 h.

Figures 3.5.2(a-d) show backscattered SEM images of polished surfaces of all composite samples sintered for 6 h. In each sample, at least two phases with different contrasts were observed, supporting the XRD results. Both the darker and lighter phases in CCTO/CTO composites were enhanced by Sn^{4+} doping. Fig. 3.5.3 shows EDS spectra of the Sn30 composite measured in darker and lighter contrast regions, clearly indicating CTO and CCTO phases. This result is similar to that reported in published literature [1,3-5]. In the lighter grains, a small intensity EDS-peak of Sn was detected as well as main EDS-peaks for Ca, Cu, Ti, and O. The EDS-peak for Sn was not observed in the darker CTO grain. This indicated that a relatively large portion of the Sn^{4+} ions were substituted into the CCTO phase. Note that the microstructural evolution in the composite samples sintered for 24 h (does not show) is similar to that observed in the samples sintered for 6 h.

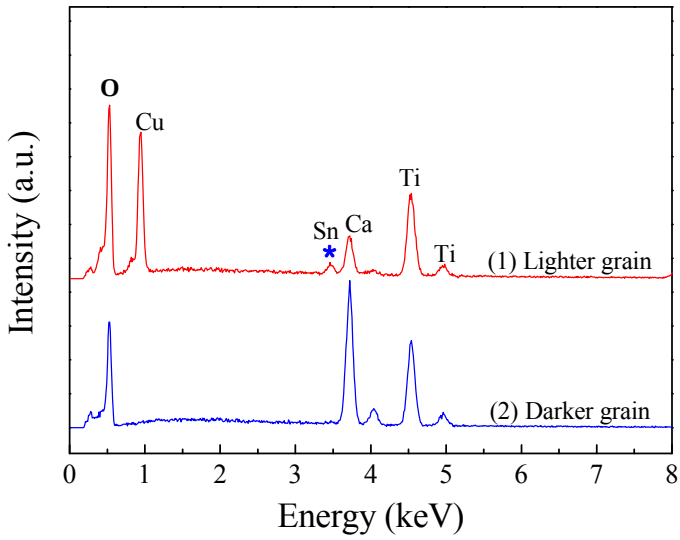

Figure 3.5.3 EDS spectra of Sn30 sample detected at darker and lighter phases.

As shown in Fig. 3.5.2, the grain sizes of the CCTO and CTO phases in CCTO/CTO composites (both of the composites sintered for 6 and 24 h) was greatly enlarged by Sn^{4+} doping. The mean grain sizes of the CCTO phase in the CCTO/CTO, Sn10, Sn20, and Sn30 composites sintered for 6 h were of ~3.1, ~18.0, ~17.0, and ~19.8 μm, respectively. The mean grain sizes of the composites sintered for 24 h were of ~2.9, ~16.9, ~17.4, and ~21.5 μm, respectively. This is completely different from that observed in the Sn-doped single phase CCTO [7,8]. As shown in Fig. 3.5.2(d), white spots were observed in the microstructure of the Sn30 samples. This was confirmed to be an impurity of the Cu-rich phase.

Generally, dispersion of solid particles in a polycrystalline ceramic matrix, i.e., one in which these particles are insoluble and immobile, can decrease the grain growth rate by the pinning effect. This is because grain boundary mobility was reduced. If there is a sufficient content of particles, grain boundary migration of the sintered polycrystalline ceramic will be pinned when it encounters the particles [9]. For a $Ca_2Cu_2Ti_4O_{12}$ composition, the calcined powder consisted of CCTO and CTO particles with volume fractions of ~0.66 and ~0.34, respectively [2]. The average grain sizes of the un-doped CCTO/CTO composites sintered for 6 and 24 h were nearly the same in value. According to the Zener model [9], limiting grain size ($G_L=2\alpha r/3f$, where α is geometrical shape factor) is only proportional to inclusion particle size (r) and inversely

proportional to the inclusion volume fraction (*f*). This result indicates that the grain growth of the CCTO matrix phase was sufficiently inhibited by (f = 0.34) CTO particles.

It was also observed that small CTO particles (darker grains) appeared in the large CCTO grains of Sn-doped CCTO/CTO composites. This observation indicated that grain boundary mobility of Sn-doped CCTO/CTO composites cannot be pinned by CTO particles. This supports the hypothesis that liquid phase sintering may be a primary cause of the microstructural changes in Sn-doped CCTO/CTO composites. This is because enhanced grain boundary mobility due to the existence of the liquid phase in the green body during sintering process is the primary factor responsible for increasing grain growth rate of polycrystalline ceramics. In this case, grain boundaries can break away from some small particles of the CTO phase, retaining these particles internally within the CCTO grains. Normally, the grain growth of a single phase CCTO ceramic is correlated with liquid phase sintering [10]. The Cu-rich related phase is generally believed to be a source of a liquid phase during the sintering process. Therefore, the observed Cu-rich particles in Sn-doped CCTO/CTO composites may be an important clue to explaining the large increase in the mean grain size of CCTO phase. In polycrystalline ceramics, a metal doping ion may react with a small portion of the major phase to form a eutectic liquid. The eutectic temperature of SnO_2-CuO was found to be ~940 ^{o}C [11]. Thus, it is strongly suggested that the eutectic liquid phase of the SnO_2-CuO system has a remarkable influence on the increase mean grain size of the CCTO phase in Sn-doped CCTO/CTO composites.

According to previous work, substitution of Sn^{4+} into a single phase CCTO caused a large decrease in the mean grain size and resulting ε' values [7, 8]. The cause of the decrease in ε' was suggested to be intrinsic factors inside the grains. The nanosized barrier layer capacitor model and mixed-valent structure model were proposed to describe the giant dielectric response in CCTO ceramics. In these two models, a high ε' value was not strongly correlated with the electrical response at grain boundaries. In the case of Sn-doped CCTO/CTO composites, substitution of Sn^{4+} ions into Ti^{4+} sites in the CCTO structure can cause a decrease in ε' of the CCTO phase. In the absence of the dominant electrical response of internal interfaces or grain boundaries, the effective ε' of CCTO/CTO composites should decrease if the ε' value of the CTO phase was not greatly enhanced by Sn^{4+} doping.

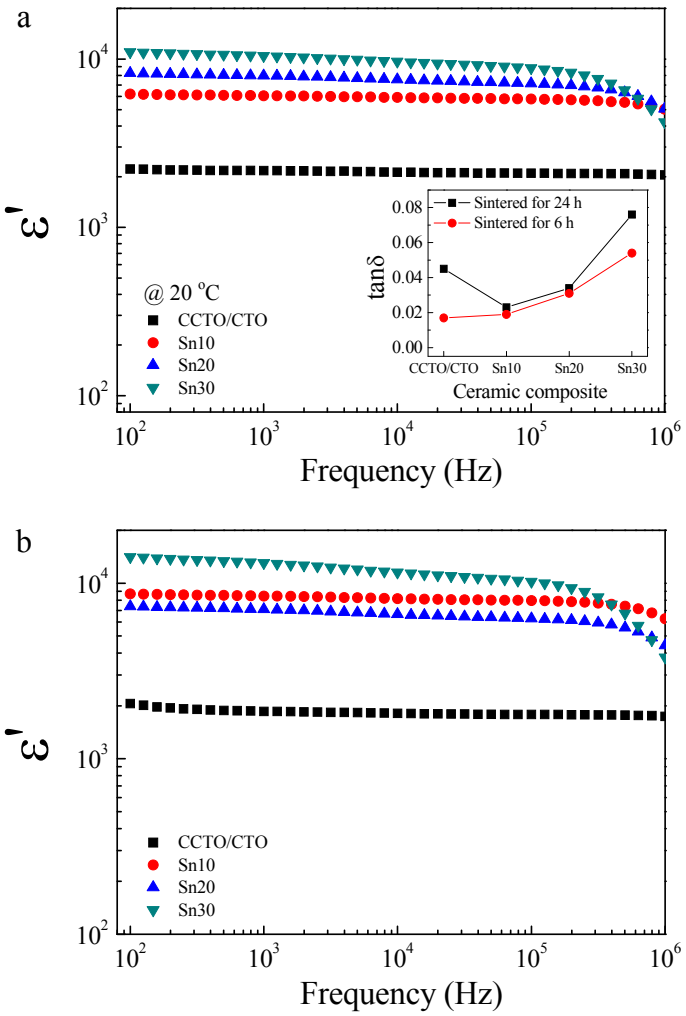

Figure 3.5.4 ε′ as a function of frequency at 20 °C for the composites sintered at 1100 °C for (a) 6 h and (b) 24 h; inset of (a) shows tanδ as a function of dopant content.

However, in this current study, ε′ of CCTO/CTO composites was greatly increased by Sn^{4+} doping, as shown in Figures 3.5.4(a) and 3.5.4(b). The ε′ values at 20 °C and 1 kHz of the CCTO/CTO, Sn10, Sn20, and Sn30 samples sintered for 6 h were approximately 2173, 6057, 7968, and 10435, respectively. Concurrently, ε′ values of the samples sintered for 24 h were 1863, 8457, 7097, and 13036, respectively. The discrepancy between the expected and experimental results may indicate a strong effect of Sn^{4+} doping ions upon the enhanced dielectric response at grain boundaries in CCTO/CTO composites. Based upon the experimental results of the current study, the intrinsic effect can be excluded from possible mechanisms contributing to the

enhancement of ε′ values of Sn-doped CCTO/CTO composites. This observation strongly suggests that the high dielectric response in CCTO/CTO composites does not originate from intrinsic effects inside the grains. In the inset of Fig. 3.5.4(a), tanδ was slightly changed by Sn^{4+} doping ions. The values of tanδ at 20 °C and 1 kHz of the CCTO/CTO, Sn10, Sn20, and Sn30 samples sintered for 6 h were approximately 0.017, 0.019, 0.031, and 0.054, respectively. However, tanδ values of the samples sintered for 24 h were found to be 0.045, 0.023, 0.034, and 0.076, respectively. Notably, high-ε′ and low-tanδ values were achieved in the Sn-doped CCTO/CTO composite system.

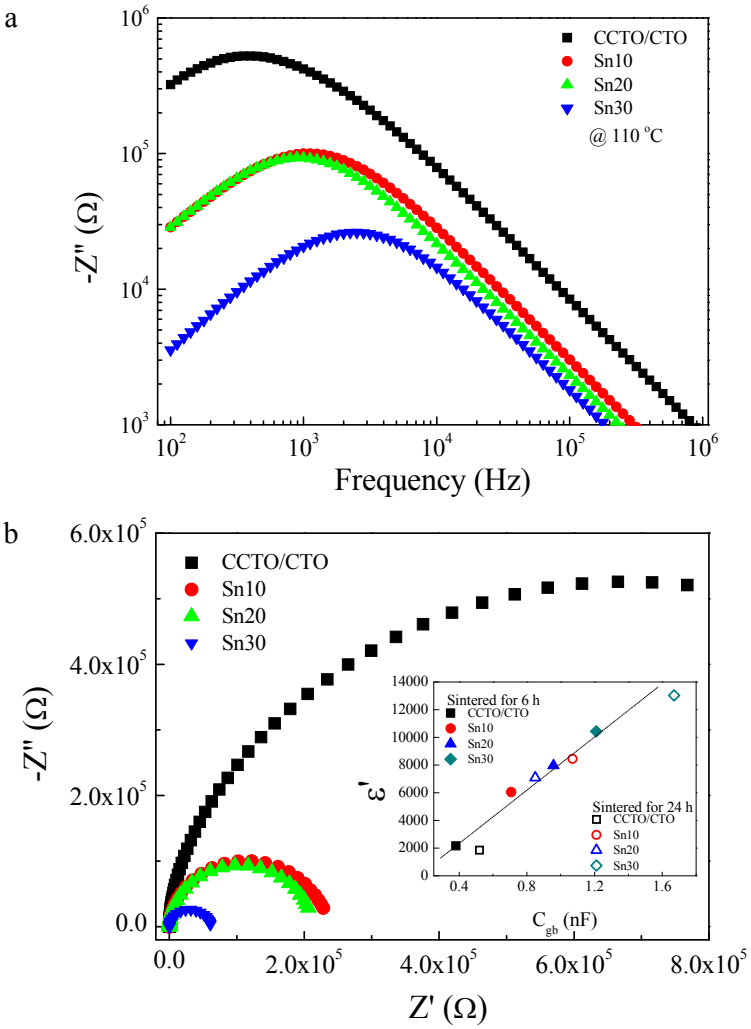

Figure 3.5.5 (a) Frequency dependence of -Z′′ of $Ca_2Cu_2Ti_{4-x}Sn_xO_{12}$ ceramics sintered for 6 h. (b) Impedance complex plane plot (Z^*) at 110 °C of $Ca_2Cu_2Ti_{4-x}Sn_xO_{12}$ ceramics sintered for 6 h; inset shows the dependence of ε′ on C_{gb} for $Ca_2Cu_2Ti_{4-x}Sn_xO_{12}$ ceramics.

Although the grain sizes of CCTO ceramics may not be a primary factor contributing to their very high ε' values, it is still one of the most significant parameters influencing the dielectric properties of many polycrystalline ceramics. Most recent investigation revealed that variation of ε' values in CCTO ceramics has a close relationship to their mean grain size [12-17]. Recently, we found that largely reduced grain size of CCTO ceramics did not result in a decrease in their ε' values [18]. Thus, the enhanced grain size of Sn-doped CCTO/CTO composites may be a slight effect contributing to the overall enhanced ε' values. For single phase CCTO ceramics, high ε' values were shown to correlate with the capacitance of the grain boundary (C_{gb}) [13, 19]. Thus, the enhanced ε' values of Sn-doped CCTO/CTO composites may originate from the improved electrical response of internal interfaces.

Impedance spectroscopy was therefore used to characterize the electrical responses of the CCTO grains and internal interfaces of Sn-doped CCTO/CTO composites. Based upon the brick–work layer model [19], the electrical structure model can be described by an equivalent circuit consisting of two parallel resistor–capacitor (*RC*) elements connected in series. In the current study, one *RC* element represents the electrical response of semiconducting grains of the CCTO phase, consisting of grain resistance (R_g) and capacitance of grains (C_g). The other represents the insulating layer of internal interfaces, consisting of the resistance and capacitance of internal interfaces (R_{int} and C_{int}). It was clearly shown that CCTO-CTO and CCTO-CCTO interfaces were electrically active, indicating the presence of potential barriers [1], whereas, a CTO-CTO interface was electrically inactive [1]. Thus, the electrical response of internal interfaces in Sn-doped CCTO/CTO composite system is likely to result from CCTO-CTO and CCTO-CCTO interfaces. Figure 3.5.5(a) shows the frequency dependence of the imaginary part ($-Z''$) of the complex impedance at 110 ^{o}C for all composites sintered for 6 h. Relaxation peaks were observed at high temperatures, which are generally attributed to be the electrical responses of internal interfaces [20,21]. The resistance of the internal interfaces, R_{int}, (or R_{gb}) can be calculated from the peak height (Z''_{max}) using the relationship $Z''_{max} = R_{gb}/2$. The peak height decreased with increasing Sn^{4+} content, indicating a reduction in R_{gb}. The decrease in R_{gb} of a CCTO/CTO composite due to the effect of Sn^{4+} doping ions is clearly illustrated in Fig. 3.5.5(b). The diameter of a semicircle arc of the CCTO/CTO sample decreased with increasing Sn^{4+} dopant concentration. R_{gb} values at 110 ^{o}C of the CCTO/CTO, Sn10, Sn20, and Sn30 samples

sintered for 6 h were approximately 1.05×10^{6}, 2.01×10^{5}, 1.87×10^{5}, and 5.24×10^{4} Ω, respectively. R_{gb} values of the samples sintered for 24 h were found to be 5.45×10^{5}, 1.67×10^{5}, 6.63×10^{5}, and 4.77×10^{4} Ω, respectively. The result achieved in the composites sintered for 6 h is consistent with the observed increase in tanδ as the Sn^{4+} dopant concentration was increased. Reduction of R_{gb} results in the enhancement of tanδ [13]. However, the decrease in tanδ of the Sn10 sample compared to the CCTO/CTO sample sintered for 24 h cannot be explained by the effect of R_{gb}. According to impedance spectroscopic analysis, the capacitance of internal interfaces (or C_{gb}) can be calculated using the relationship $C_{gb} = 1/2\pi f_{max}R_{gb}$, where f_{max} is the frequency at which Z''_{max} occurred. At 110 °C, C_{gb} values of the CCTO/CTO, Sn10, Sn20, and Sn30 samples sintered for 6 h were approximately 0.38, 0.71, 0.96, and 1.21 nF, respectively. C_{gb} values of the composites sintered for 24 h were found to be 0.52, 1.07, 0.85, and 1.67 nF, respectively. These C_{gb} values of each composite sample are consistent with their ε′ values, as clearly seen in the inset of Fig. 3.5.5(b). A clear correlation of ε′ and C_{gb} was observed. This result supports the hypothesis that an enhanced ε′ value of Sn-doped CCTO/CTO composites is likely caused by improved electrical response at the grain boundaries.

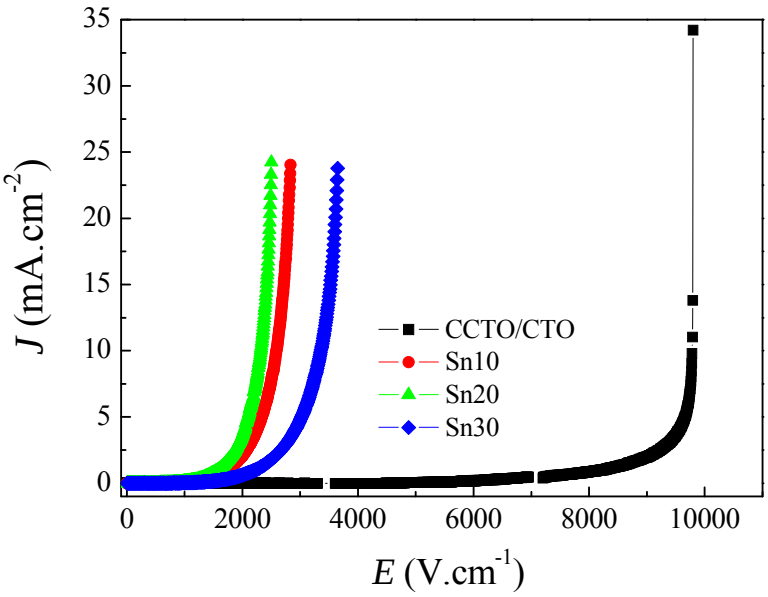

Figure 3.5.6 Nonlinear *J-E* characteristics of $Ca_2Cu_2Ti_{4-x}Sn_xO_{12}$ ceramics sintered for 6 h at room temperature.

Figure 3.5.6 illustrates the effect of Sn^{4+} on the nonlinear *J-E* characteristics of CCTO/CTO composites sintered for 6 h. α values of the CCTO/CTO, Sn10, Sn20, and Sn30 samples were found to be 13.1, 5.68, 6.04, and 5.56, respectively, whereas, α values of the composites sintered for 24 h were 9.90, 6.40, 5.66, and 6.75 respectively. The E_b value of CCTO/CTO composites sintered for 6 and 24 h was strongly reduced, as shown in Fig. 3.5.6. Clearly, the nonlinear *J-E* properties of CCTO/CTO composites were degraded by Sn^{4+} doping. Although it is quite difficult to clarify the mechanism that affects different nonlinear *J-E* properties among Sn-doped CCTO/CTO composites, the different *J-E* properties of the un-doped CCTO/CTO and doped samples were primarily due to the greatly enlarged grain size in the CCTO phase. This can cause a decrease in the number of active CCTO-CCTO and CTO-CCTO interfaces, leading to degradation of nonlinear electrical properties.

According to our previous report for the Zn-doped CCTO/CTO composite system [3], a large increase in ε' without any significant changes in the shape and mean grain size was observed. Concurrently, the nonlinear *J-E* properties were significantly improved by Zn^{2+} doping. This may be dominated by the intrinsic factor of the grain boundaries rather than the geometric factor. In the case of a Sn-doped CCTO/CTO composite system, obviously, the geometric properties of the microstructure (*i.e.*, grain boundaries) is the primary factor contributing to the variation in nonlinear *J-E* properties. It was suggested that Zn^{2+} doping ions may improve the electrical response at the CCTO-CCTO interface, increasing the value of ε'. For CCTO ceramics, interfacial polarization at the grain boundary (*i.e.,* CCTO–CCTO interface) is widely thought to be the origin of a giant ε' [12, 14, 19, 22]. Therefore, a greatly increased ε' in Sn-doped CCTO/CTO composites might have resulted from stronger interfacial polarization at internal interfaces or grain boundaries rather than the intrinsic dielectric response inside CCTO grains. This resulted from the enlarged grain size of the CCTO phase coupled with the primary factor of enhanced electrical responses at interfaces, giving rise to increased capacitance values of the active interfaces.

References

[1] M.A. Ramírez, P.R. Bueno, R. Tararam, A.A. Cavalheiro, E. Longo, J.A. Varela, J. Phys. D: Appl. Phys. 42 (2009) 185503.

[2] W. Kobayashi, I. Terasaki, Appl. Phys. Lett. 87 (2005) 032902.

[3] J. Jumpatam, B. Putasaeng, T. Yamwong, P. Thongbai, S. Maensiri, J. Am. Ceram. Soc. 97 (2014) 2368-2371.

[4] J. Jumpatam, B. Putasaeng, T. Yamwong, P. Thongbai, S. Maensiri, J. Eur. Ceram. Soc. 34 (2014) 2941-2950.

[5] M.A. Ramírez, R. Parra, M.M. Reboredo, J.A. Varela, M.S. Castro, L. Ramajo, Mater. Lett. 64 (2010) 1226-1228.

[6] R.D. Shannon, Acta Cryst. A32 (1976) 751-767.

[7] L. Ni, X.M. Chen, X.Q. Liu, Mater. Chem. Phys. 124 (2010) 982-986.

[8] W.C. Ribeiro, R.G.C. Araújo, P.R. Bueno, Appl. Phys. Lett. 98 (2011) 132906.

[9] M.N. Rahaman, Ceramic processing and sintering, 2nd ed., M. Dekker, New York, 2003.

[10] K.-M. Kim, S.-J. Kim, J.-H. Lee, D.-Y. Kim, J. Eur. Ceram. Soc. 27 (2007) 3991-3995.

[11] N. Dolet, J.M. Heintz, L. Rabardel, M. Onillon, J.P. Bonnet, J. Mater. Sci. 30 (1995) 365-368.

[12] T.B. Adams, D.C. Sinclair, A.R. West, Adv. Mater. 14 (2002) 1321-1323.

[13] S. De Almeida-Didry, C. Autret, A. Lucas, C. Honstettre, F. Pacreau, F. Gervais, J. Eur. Ceram. Soc. 34 (2014) 3649-3654.

[14] L. Ni, X.M. Chen, X.Q. Liu, R.Z. Hou, Solid State Commun. 139 (2006) 45-50.

[15] L. Liu, H. Fan, P. Fang, X. Chen, Mater. Res. Bull. 43 (2008) 1800-1807.

[16] L.F. Xu, T. Cheng, R.L. Wang, H.B. Xiao, G.Z. Liu, C.P. Yang, J. Mater. Sci.: Mater. Electron. 25 (2013) 817-823.

[17] Y. Yang, X. Wang, B. Liu, J. Mater. Sci.: Mater. Electron. 25 (2014) 146-151.

[18] K. Meeporn, T. Yamwong, S. Pinitsoontorn, V. Amornkitbamrung, P. Thongbai, Ceram. Int. 40 (2014) 15897-15906.

[19] R. Schmidt, M.C. Stennett, N.C. Hyatt, J. Pokorny, J. Prado-Gonjal, M. Li, D.C. Sinclair, J. Eur. Ceram. Soc. 32 (2012) 3313-3323.

[20] J. Liu, C.-G. Duan, W.-G. Yin, W. Mei, R. Smith, J. Hardy, Phys. Rev. B 70 (2004) 144106.

[21] Y. Liu, Q. Chen, X. Zhao, J. Mater. Sci.: Mater. Electron. 25 (2014) 1547-1552.

[22] S. Kwon, C.-C. Huang, E.A. Patterson, D.P. Cann, E.F. Alberta, S. Kwon, W.S. Hackenberger, Mater. Lett. 62 (2008) 633-636.

3.6 $Ca_{1-x}La_xCu_3Ti_4O_{12}/CaTiO_3$

In this part of the research work, the influences of La^{3+} substitution on the dielectric properties and formation of Schottky barriers at internal interfaces of a $Ca_2Cu_2Ti_4O_{12}$ ($CaTiO_3/CaCu_3Ti_4O_{12}$) composite system were investigated. It was found that electrostatic potential barrier height was greatly reduced by doping with La^{3+}, leading to a large decrease in the total resistance of internal interfaces between grains. This observation was attributed to the creation of conduction electrons, which were possibly induced by electrical charge compensation of La^{3+} substitution into Ca^{2+} sites. Variations in the dielectric properties of La^{3+}-doped $CaTiO_3/CaCu_3Ti_4O_{12}$ composite ceramics and nonlinear properties can be described based on the electrical responses at the internal interfaces between $CaCu_3Ti_4O_{12}$-$CaCu_3Ti_4O_{12}$ grains and $CaTiO_3$-$CaCu_3Ti_4O_{12}$ grains. Influence of possible charge compensation due to different levels of La^{3+} dopant on the formation of potential barriers was discussed.

Ceramics with nominal compositions of $Ca_2Cu_2Ti_4O_{12}$ (La-0), $Ca_{1.95}La_{0.05}Cu_2Ti_4O_{12}$ (La-05), and $Ca_{1.7}La_{0.3}Cu_2Ti_4O_{12}$ (La-30) were prepared by a solid state reaction method and sintered at 1100 °C for 24 h. Details of experimental results and discussion are as follows:

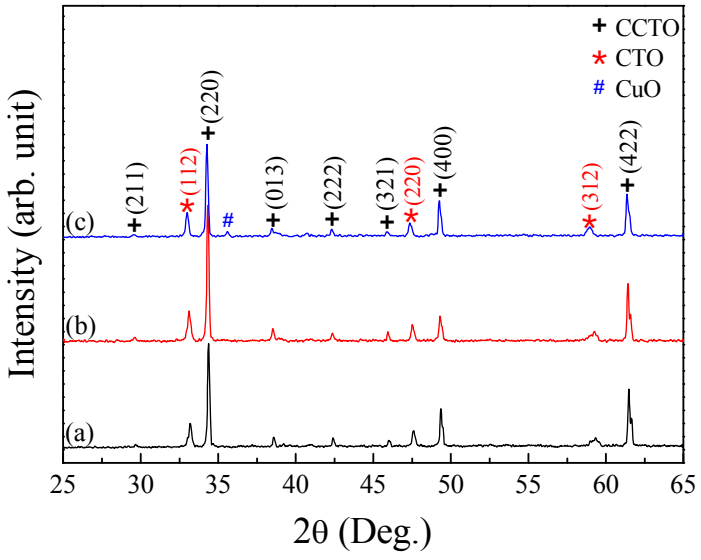

Figure 3.6.1 XRD patterns of (a) $Ca_2Cu_2Ti_4O_{12}$ (La-0 sample), (b) $Ca_{1.95}La_{0.05}Cu_2Ti_4O_{12}$ (La-05 sample), and (c) $Ca_{1.7}La_{0.3}Cu_2Ti_4O_{12}$ (La-30 sample) ceramics.

The XRD patterns of $Ca_{2-x}La_xCu_2Ti_4O_{12}$ (x = 0, 0.05, and 0.30) compositions are shown in Fig. 3.6.1. It is clearly seen that all of the ceramic compositions consisted of two main phases, CCTO (JCPDS 75-2188) and CTO (JCPDS 82-0231), forming a composite system of CCTO/CTO. These XRD patterns are similar to those reported in the literature for $Ca_2Cu_2Ti_4O_{12}$ ceramics [1-4]. An impurity phase of CuO was observed in the La-30 samples. This may be due to the decomposition of CuO from the lattice [5]. Theoretically, a ceramic that was prepared using a starting composition of $Ca_2Cu_2Ti_4O_{12}$ should consist of ~33.3 mol% of CCTO and ~66.7 mol% of CTO. This was experimentally confirmed by a Rietveld quantitative analysis [2]. Formation of a CCTO/CTO composite system was due to the much larger ionic radius of Ca^{2+} than of Cu^{2+}. Therefore, excess Ca^{2+} ions could not be substituted into Cu^{2+} sites in a planar square to create a $Ca(CaCu_2)Ti_4O_{12}$ structure. Lattice parameters of the CCTO phases of La-0, La-05 and La-30 samples were calculated and found to be 7.3891, 7.3928, and 7.3943 Å, respectively. The lattice parameter of CCTO phase in the CCTO/CTO composites increased with increasing La^{3+} doping concentration. The increase in the lattice parameter may be attributed to the different ionic radii between Ca^{2+} and La^{3+} ions.

Figure 3.6.2 and its insets show ε' and $\tan\delta$ at 20 ^{o}C as a function of frequency for the La-0, La-05, and La-30 samples. In a low frequency range of 10^2-10^3 Hz, ε' of the La-doped samples was much higher than that of the un-doped sample. ε' values at 10^2 Hz for the La-0, La-05, and La-30 samples were found to be 2060, 11162, and 6378, respectively. It was observed that these high ε' values in a low frequency range decreased as the frequency was increased from 10^2 to 10^3 Hz. This result indicates the dominant effect of dc conduction and/or low-frequency dielectric relaxation [6]. As shown in the inset of Fig. 3.6.2, $\tan\delta$ greatly increased as frequency was decreased. However, the increase in $\tan\delta$ was not exponentially. Conversely, the magnitude of the $\tan\delta$ relaxation peak was not large. Therefore, the frequency dependence of $\tan\delta$ in a low—frequency range was affected by the combined effects of dc conduction and a relaxation process [7]. $\tan\delta$ values of La-0, La-05, and La-30 samples at 10^2 Hz were found to be 0.219, 0.517, and 2.971, respectively. $\tan\delta$ of CCTO/CTO composites increased with increasing La^{3+} doping concentration. Variations in $\tan\delta$ with changing concentration of La^{3+} were not consistent with changes in ε'.

Generally, variations in the properties of CCTO ceramics were consistent with each other. Increases in ε' of CCTO ceramics were usually accompanied by an increase in tanδ [8]. This result can be described by considering interfacial polarization at GBs. High ε' values are attributed to large polarization intensity at the interfaces between adjacent grains, which are insulating GBs. Concurrently, a large polarization intensity indicates a high density of accumulated charges at GBs, driven by an external electric field. High concentrations of mobile charges inside semiconducting grains are a source of space charges. Conversely, high concentrations of charges not only contribute to polarization intensity and ε', but also increase the possibility of leaked current in bulk ceramics. This is a major cause of high tanδ. Therefore, the dielectric response behavior in La^{3+}-doped CCTO/CTO composites might be significantly influenced by the electrical characteristics of GBs as well.

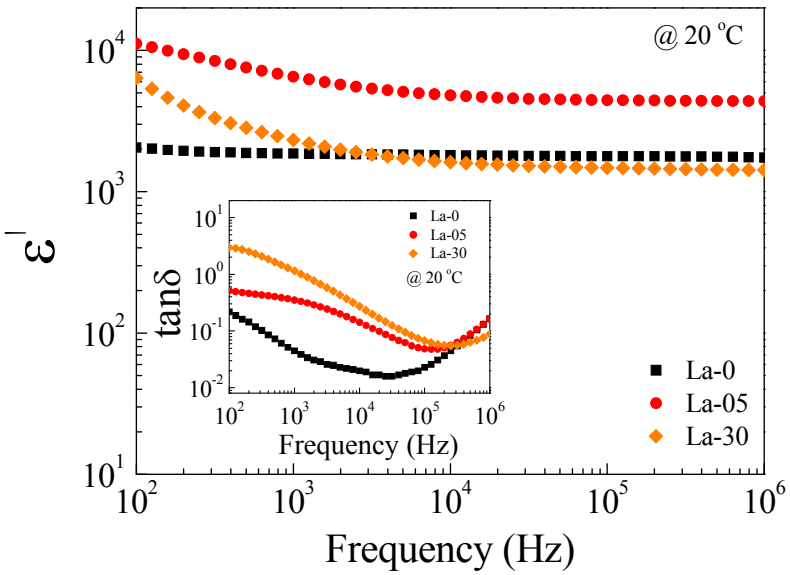

Figure 3.6.2 ε' at 20 °C in the frequency range of 10^2-10^6 Hz for all samples; the inset shows the frequency dependence of tanδ.

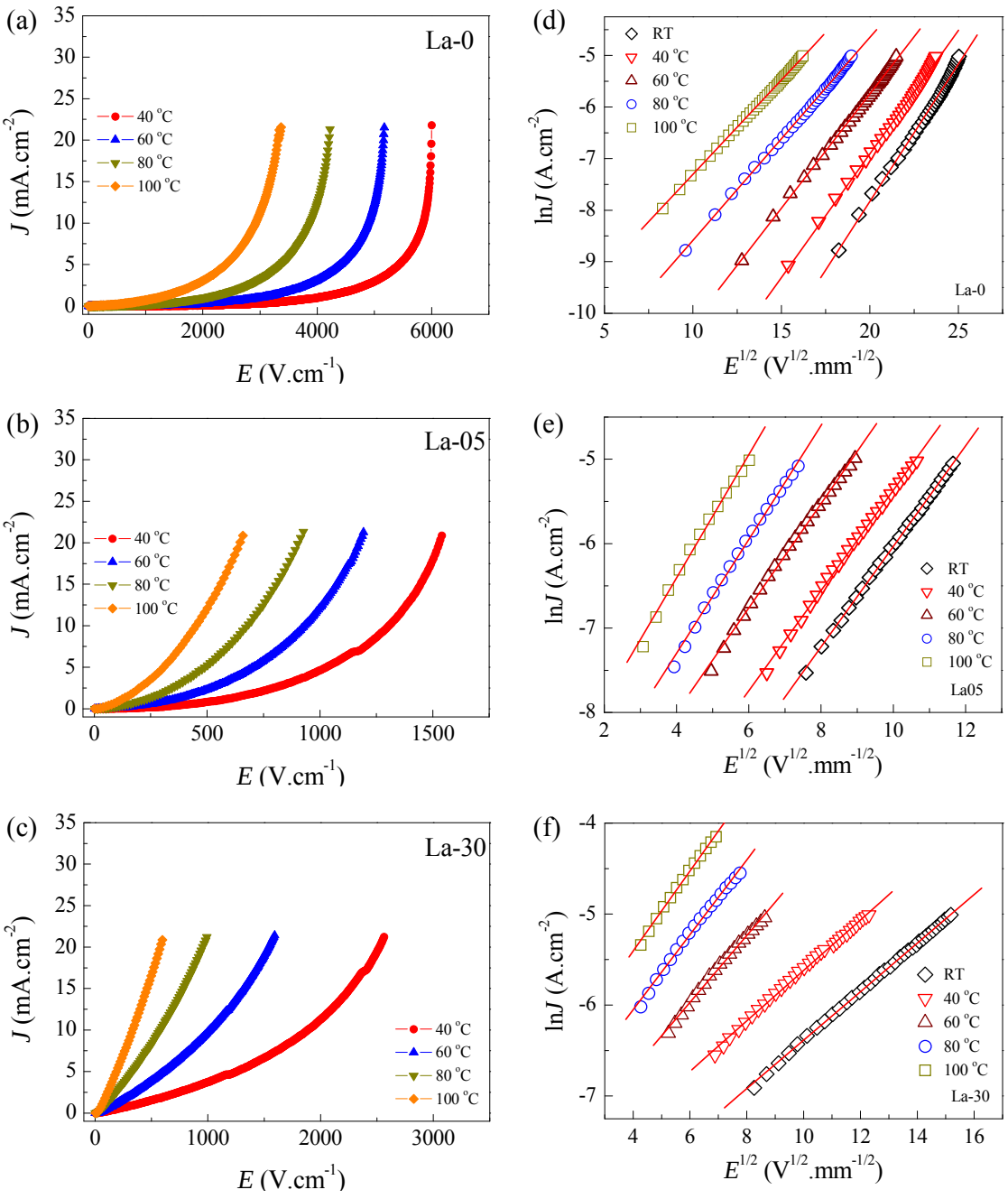

Figure 3.6.3 (a-c) Nonlinear *J-E* characteristics at various temperatures for La-0, La05, and La30 samples, respectively. (d-f) Plots of ln*J* vs. $E^{1/2}$.

In the current study, the effects of La^{3+} doping on the *J-E* characteristics of CCTO/CTO composites were investigated. Figure 3.6.3 shows the nonlinear *J-E* properties of the study samples at different temperatures. E_b values at room temperature of the La-0, La-05, and La-30 samples were found to be 4811, 732, and

665 V/cm, respectively. α values of the same samples at room temperature were found to be 7.66, 3.14, and 1.62, respectively. The nonlinear properties of CCTO/CTO composites were degraded as La^{3+} ions were substituted for Ca^{2+} sites. According to a previous work [9], substitution of La^{3+} into CCTO with nominal chemical compositions of $Ca_{1-3x/2}La_xCu_3Ti_4O_{12}$ (x=0-0.09) caused a decrease in dc conduction activation energy when x>0.05. Cheng et al. [10] found an increase in E_b in $Ca_{1-3x/2}La_xCu_3Ti_4O_{12}$ as La^{3+} concentration increased. From these two studies, the molar ratio of Ca^{2+} was adjusted to obtain an electrical charge equilibrium and thus freed electrons since an aliovalent dopant was not expected. In the current study, electronic charge compensation by conduction electrons may have existed due to La^{3+} ions being substituted into Ca^{2+} sites. This may have been the primary cause of the degradation of nonlinear properties. Ramirez *et al*. [2] used electrostatic force microscopy (EFM) to characterize possible electrical responses in a CCTO/CTO composite system. They found that a CTO-CTO interface was electrically inactive, while CCTO-CTO and CCTO-CCTO interfaces were electrically active. This indicates the presence of potential barriers.

To study the effect of La^{3+} doping ions on the formation of electrostatic potential barriers at internal interfaces of CCTO/CTO composites, nonlinear *J-E* properties were determined at different temperatures. As shown in Figs. 3.6.3(a-c), E_b linearly decreased with increasing temperature. This indicated the influence of temperature upon the electrostatic potential barriers at internal interfaces. According to previous work [10-14], the electrical response of GBs (CCTO-CCTO interfaces) for a single phase CCTO polycrystalline ceramic clearly resulted from the Schottky effect. It was also further suggested that the potential barriers at CCTO-CTO interfaces were also Schottky-type barriers [2]. Therefore, electrical conduction at CCTO-CCTO and CCTO-CTO interfaces in the pre-breakdown region should be due to thermion emission of the Schottky barrier [10,14]. This emission is usually affected by the electric field (E) and temperature (T). Variations of J with E and T will follow the relationship [13]:

$$\ln J = \frac{\beta E^{1/2}}{k_B T} + \left[\ln AT^2 - \frac{\Phi_B}{k_B T} \right] \qquad (3.6.1)$$

where Φ_B is the Schottky potential-energy barrier height at the GBs, A is the Richardson constant, and β is a constant related to the potential barrier width. The last term on the right hand side of Eq. (3.6.1) is expressed as:

$$\ln J_0 = \ln AT^2 - \frac{\Phi_B}{k_B T}. \quad (2)$$

Values of lnJ_0 at various temperatures were calculated from the plots of ln$J$ vs. $E^{1/2}$ by linearly fitting data at E = 0. Figures 3.6.3(d-f) show the fitted results, indicating a good linear relationship between ln$J$ vs. $E^{1/2}$. Using Eq. (3.6.2), Φ_B values for all the samples were calculated by fitting data of the plots of lnJ_0 vs. 1000/T.

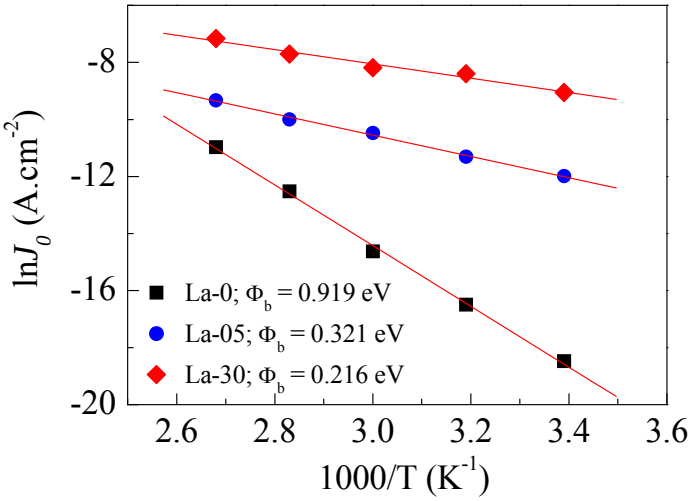

Figure 3.6.4 Plots of lnJ_0 vs. 1000/T for all samples; the solid lines are results fitted to Eq. (3.6.2).

As shown in Fig. 3.6.4, a good linear relationship between J_0 and temperature was observed. Values of Φ_B were approximately 0.919, 0.321, and 0.216 eV for the La-0, La-05, and La-30 samples, respectively. It is notable that $\Phi_B \approx$ 0.919 eV for the La-0 (CCTO/CTO) sample can be comparable to that observed in the CCTO/CTO composite prepared by a simple thermal decomposition method (0.856 eV) [15]. This value is also comparable to that observed in $Na_{1/2}Sm_{1/2}Cu_3Ti_4O_{12}$ ceramics (0.925-0.964 eV) [16]. Φ_B of CCTO/CTO composites was greatly reduced by doping with La^{3+}. This means that La^{3+} doping ions have an effect on the formation of electrostatic potential barriers at

CCTO-CTO and CCTO-CCTO interfaces. For a single phase of CCTO ceramics, the Schottky barrier at GBs can be expressed as [12]:

$$\Phi_B = \frac{qN_s^2}{8\varepsilon_0\varepsilon' N_d}, \tag{3.6.3}$$

where N_s and N_d are the acceptor (surface charge) concentration and the charge carrier concentration in semiconducting grains (*i.e.*, CCTO grains), respectively. ε' is the relative permittivity of materials, and q is the electronic charge. Using Eq. (3.6.3), it is possible that the strong reduction of Φ_B observed in CCTO/CTO composites can be attributed to either an increase in N_d or a large decrease in N_s. Generally, an increase in N_d can cause a decrease in resistance of grain interiors (R_g). In Ta^{5+} and Nb^{5+}-doped CCTO ceramic systems [17], it was found that Ta^{5+} and Nb^{5+} doping ions had no significant effect on R_g of CCTO ceramics. Thus, the observed strong decrease in potential barriers at GBs of these materials was not related to any change of N_d and other proposed mechanism. Charge compensation mechanisms were investigated in nominal compositions of $La_xCa_{1-3x/2}Cu_3Ti_4O_{12}$ and $La_xCa_{1-x}Cu_3Ti_4O_{12}$ [9]. It was clearly shown that in the latter material, electrical compensation was found to be conduction electrons.

In the current study, impedance spectroscopy was used to investigate the electrical properties of grains and GBs. As shown in Fig. 3.6.5(a), at 20 ^{o}C, the diameter of a large semicircle arc in the plot of the complex impedance plane (Z*) of CCTO/CTO composites decreased with increasing La^{3+} dopant concentration. This result indicated a large reduction of the total resistance at internal interfaces [18], *i.e.*, GBs between CCTO-CCTO grains and CTO-CCTO grains [2]. The insets (1) and (2) of Fig. 3.6.5(a) show the nonzero intercept on the Z′ axis of the impedance spectra in a high-frequency range at 20 and -70 ^{o}C, respectively. The resistances of semiconducting grains or R_g values of CCTO/CTO composites can be estimated from these nonzero intercepts [18]. At -70 ^{o}C, R_g values of ~200 Ω.cm for the La-05 and La-30 samples were much lower than R_g~500 Ω.cm for the La-0 sample (un-doped CCTO/CTO composites). R_g values at various temperatures in the range from -70 to 30 oC for all the samples are shown in Fig. 3.6.5(b). This result indicates that N_d values of the La-05 and La-30 samples were enhanced. Thus, substitution of La^{3+} ions to Ca^{2+} sites was

electrically compensated by conduction electrons. As demonstrated in Fig. 3.6.5(b), R_g decreases with increasing temperature. It was found that the temperature dependence of R_g follows the Arrhenius law:

$$R_g = R_0 \exp\left(\frac{E_g}{k_B T}\right), \tag{3.6.4}$$

where E_g is the activation energy for conduction in the grain interiors, R_0 is a constant term, T is absolute temperature (K), and k_B is Boltzmann constant. The temperature dependence of R_g is well fitted by Eq. (3.6.4). E_g values of the La-0, La-05, and La-30 samples were calculated from the fitted result and found to be 94, 74, and 69 meV, respectively.

According to Eq. (3.6.3), the strong decrease in observed Φ_B values for the La-05 and La-30 samples can be attributed to the increase in charge carrier concentration in the semiconducting grains compared to the La-0 sample. It is important to note that Φ_B of the La-30 sample was slightly reduced further to 0.216 eV. This observation is similar to that observed in Ta^{5+} and Nb^{5+}-doped CCTO systems [17]. R_g values of these two samples were nearly the same in value. R_g of the La-30 sample was slightly larger than that of the La-05 sample. This result means that N_d did not increase even though La^{3+} dopant concentration was further increased from x = 0.05 to 0.3. Charge compensation for La^{3+} substituted to Ca^{2+} sites by conduction electrons no longer occurred when La^{3+} concentration was increased to a higher level of 15 mol% (x = 0.3). In contrast, the ionic compensation by cation vacancies may have occurred in grain interiors, just as it occurred in La^{3+}-doped $BaTiO_3$ [19]. Chung et al. [17] proposed that at GBs, the positive charge of the dopant cations could efficiently make compensation of the negative charge of unknown acceptors without the creation of electrons or cation vacancies in this region. Consequently, the number of active acceptor states at GBs (CCTO-CCTO and/or CTO-CCTO interfaces) that contribute to the formation of potential barriers decreases with La^{3+} addition. It is notable that the large increase in ε' of the La-05 sample compared to the La-0 sample (un-doped CCTO/CTO composite) might be due to a high intensity of interfacial polarization at the internal interfaces. Conversely, the decrease in ε' of the La-30 sample might be due to its low Φ_B value. It is possible that this potential barrier height of the La-30 sample was not sufficient to completely

restrict the motion of conduction electrons within the grains. Most of them can move across GBs. Thus, the intensity of polarization at interfaces decreased, leading to a decrease in ε'. This is consistent with its tanδ value, which was highest among these three composites under study. Such a high value of tanδ was primarily caused by a dc current that resulted from a high concentration of conduction electrons across GBs.

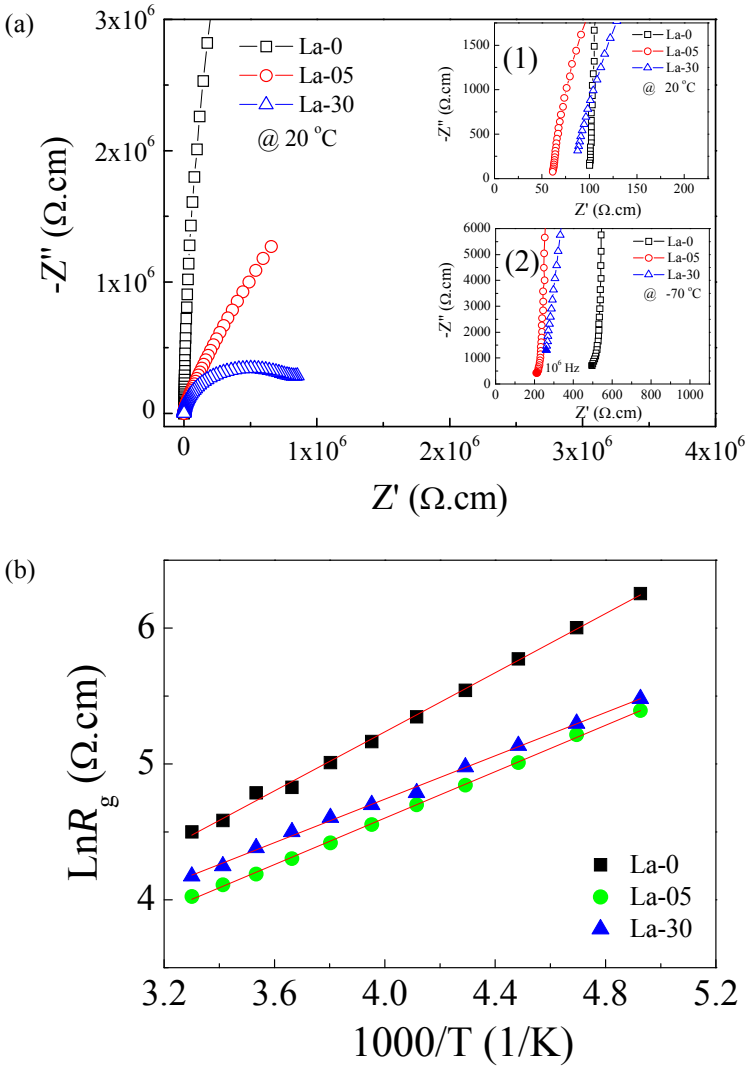

Figure 3.6.5 (a) Comparison of impedance complex plane (Z^*) plots at 20 °C for all samples; insets (1) and (2) show high-frequency data close to the origin at 20 and -70 °C, respectively. (b) Temperature dependence of R_g of all ceramic samples.

References

[1] P. Thongbai, B. Putasaeng, T. Yamwong, S. Maensiri, J. Alloys Compd. 509 (2011) 7416-7420.

[2] M.A. Ramírez, P.R. Bueno, R. Tararam, A.A. Cavalheiro, E. Longo, J.A. Varela, J. Phys. D: Appl. Phys. 42 (2009) 185503.

[3] L. Ramajo, R. Parra, J.A. Varela, M.M. Reboredo, M.A. Ramírez, M.S. Castro, J. Alloys Compd. 497 (2010) 349-353.

[4] J. Jumpatam, B. Putasaeng, T. Yamwong, P. Thongbai, S. Maensiri, J. Eur. Ceram. Soc. (2014) http://dx.doi.org/10.1016/j.jeurceramsoc.2014.1004.1037.

[5] T.B. Adams, D.C. Sinclair, A.R. West, J. Am. Ceram. Soc. 89 (2006) 2833–2838.

[6] S. Vangchangyia, E. Swatsitang, P. Thongbai, S. Pinitsoontorn, T. Yamwong, S. Maensiri, V. Amornkitbamrung, P. Chindaprasirt, J. Am. Ceram. Soc. 95 (2012) 1497-1500.

[7] P. Lunkenheimer, S. Krohns, S. Riegg, S.G. Ebbinghaus, A. Reller, A. Loidl, The European Physical Journal Special Topics 180 (2010) 61-89.

[8] P. Thongbai, B. Putasaeng, T. Yamwong, S. Maensiri, J. Mater. Sci.: Mater. Electron. 23 (2012) 795-801.

[9] A.K. Dubey, P. Singh, S. Singh, D. Kumar, O. Parkash, J. Alloys Compd. 509 (2011) 3899-3906.

[10] B. Cheng, Y.-H. Lin, J. Yuan, J. Cai, C.-W. Nan, X. Xiao, J. He, J. Appl. Phys. 106 (2009) 034111.

[11] S.-Y. Chung, I.-D. Kim, S.-J.L. Kang, Nat. Mater. 3 (2004) 774-778.

[12] T. Adams, D. Sinclair, A. West, Phys. Rev. B 73 (2006) 094124.

[13] Y.-H. Lin, J. Cai, M. Li, C.-W. Nan, J. He, J. Appl. Phys. 103 (2008) 074111.

[14] J. Yuan, Y.-H. Lin, H. Lu, B. Cheng, C.-W. Nan, J. Am. Ceram. Soc. 94 (2011) 1966-1969.

[15] J. Jumpatam, P. Thongbai, B. Kongsook, T. Yamwong, S. Maensiri, Mater. Lett. 76 (2012) 40-42.

[16] W. Somphan, P. Thongbai, T. Yamwong, S. Maensiri, Mater. Res. Bull. (2013).

[17] S.-Y. Chung, J.-H. Choi, J.-K. Choi, Appl. Phys. Lett. 91 (2007) 091912.

[18] R. Schmidt, M.C. Stennett, N.C. Hyatt, J. Pokorny, J. Prado-Gonjal, M. Li, D.C. Sinclair, J. Eur. Ceram. Soc. 32 (2012) 3313-3323.

[19] F.D. Morrison, D.C. Sinclair, A.R. West, J. Am. Ceram. Soc. 84 (2001) 474-476.

3.7 $Ca_{1-x}Bi_xCu_3Ti_4O_{12}/CaTiO_3$

In this part of the research work, the effects of Bi^{3+} doping ions on the microstructure and dielectric properties of $CaCu_3Ti_4O_{12}/CaTiO_3$ (CCTO/CTO) composites prepared by using a conventional solid state reaction method were investigated. Microstructure analysis revealed that Bi^{3+} doping ions can be substituted into Ca^{2+} sites in both the CCTO and CTO phases. It is notable that the value of ε' at 1 kHz and 30 ^{o}C of the CCTO/CTO composite was greatly increased to 4.1×10^4 by doping with Bi^{3+} ions, compared to the un-doped sample ($\varepsilon'\sim1.8\times10^3$). Non-Ohmic properties of Bi^{3+}-doped CCTO/CTO composites were also investigated. The electrical responses of grains and internal interfaces were investigated using impedance spectroscopy. Strongly enhanced dielectric responses and variation in nonlinear electrical properties can be well described based on the electrical responses at internal interfaces of the composites.

$Ca_2Cu_2Ti_4O_{12}$ (CCTO/CTO), $Ca_{1.95}Bi_{0.05}Cu_2Ti_4O_{12}$ (Bi_05), $Ca_{1.90}Bi_{0.10}Cu_2Ti_4O_{12}$ (Bi_10), and $Ca_{1.7}Bi_{0.30}Cu_2Ti_4O_{12}$ (Bi_30) were prepared by using a solid state reaction method and sintered in air at 1100 ^{o}C for 24 h at heating and cooling rates of 5 ^{o}C/min. Details of experimental results and discussion are as follows:

The XRD patterns of Bi-doped CCTO/CTO composites are illustrated in Fig. 3.7.1. It is clearly seen that all of the composite samples consisted of two phases of CTO (JCPDS 82-0231) and CCTO (JCPDS 75-2188). This result is similar to those reported in the literature [1-4]. Considering the nominal formula of $Ca_2Cu_2Ti_4O_{12}$, ~66.7 mol% of CTO and ~33.3 mol% of CCTO should be created during the sintering process due to an imbalance between Ca^{2+} and Cu^{2+} ions. The creation of CCTO/CTO composites was confirmed by a Rietveld quantitative analysis of synthesized $Ca_2Cu_2Ti_4O_{12}$ ceramics as reported in the literature [1]. The formation can be explained as follows. Due to a relatively large ionic radius of Ca^{2+} compared to that of Cu^{2+}, Ca^{2+} cannot enter into Cu^{2+} sites in a planar square to form a $Ca(CaCu_2)Ti_4O_{12}$ structure [3,4].

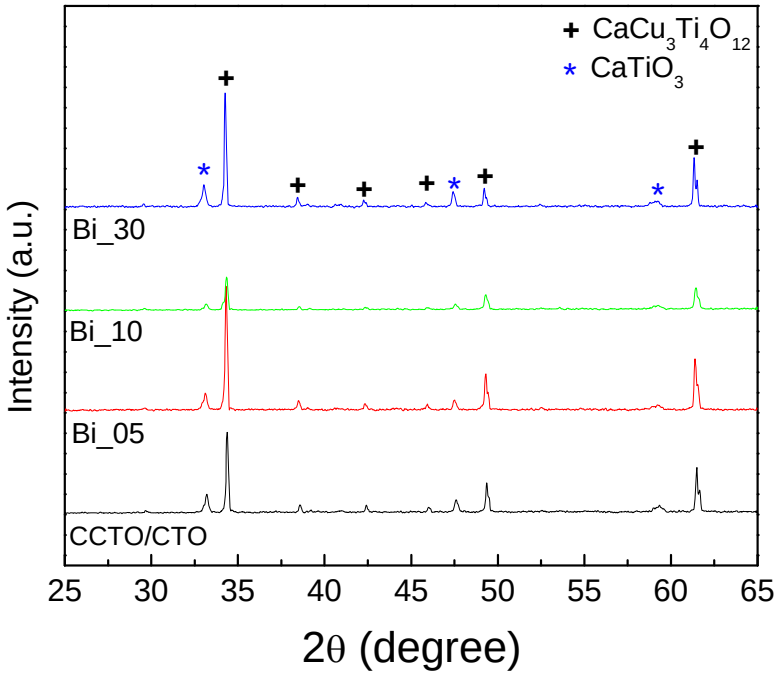

Figure 3.7.1 XRD patterns of Bi-doped CCTO/CTO composites.

Figure 3.7.2 shows surface morphologies of CCTO/CTO and Bi-doped CCTO/CTO composites. It was found that some grains in the microstructure of Bi-doped CCTO/CTO grew rapidly. This indicates that an abnormal grain growth occurred in the Bi-doped CCTO/CTO composites [5]. Such grain growth may be related to the liquid phase sintering behavior as a result of a Bi-related liquid phase. This is reasonable because the melting point of Bi_2O_3 is lower than the sintering temperature of CCTO/CTO composites (1100 ^{o}C). As revealed in the insets of Figs. 3.7.2(a) and 3.7.2(b) for the backscattered SEM images, two phases with different contrasts were observed, *i.e.*, darker and lighter phases in the CCTO/CTO sample. This observation is consistent with the XRD results and similar to those reported in the literature for un-doped CCTO/CTO [1, 3, 4]. The darker and lighter phases were CTO and CCTO phases, respectively [1, 3, 4]. However, varying contrast could not be clearly observed in the Bi_05 sample as well as in other Bi-doped CCTO/CTO samples. As depicted in Figs. 3.7.33(a) and 3.7.3(b), EDS peaks corresponding to Bi, Ca, Ti, and O appeared in the EDS spectra measured in a small grain (point 2). All EDS peaks for Bi, Ca, Cu, Ti, and O were detected in the larger grain. This clearly indicates that Bi^{3+} doping ions preferentially formed solid solution within both the CCTO and CTO phases.

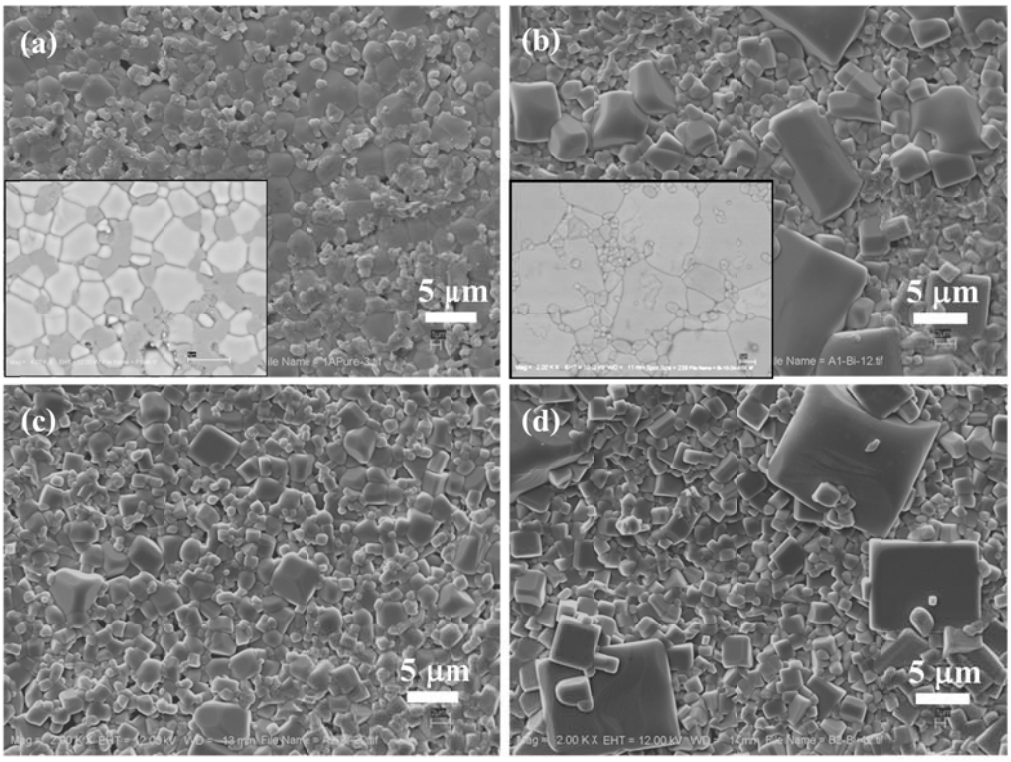

Figure 3.7.2 SEM images of (a) CCTO/CTO, (b) Bi_05, (c) Bi_10, and (d) Bi_30 samples; insets of (a) and (b) are backscattered SEM images of the CCTO/CTO and Bi_05 samples.

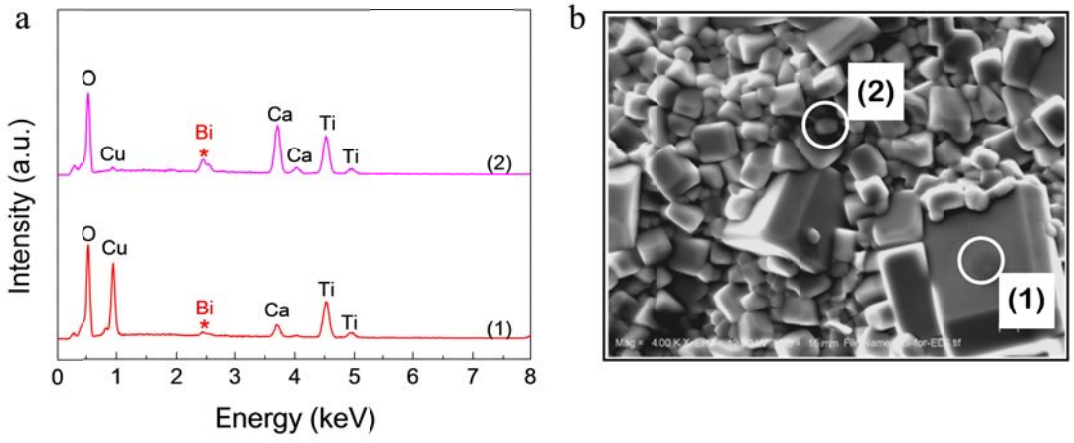

Figure 3.7.3 (a) EDS spectra of a Bi_30 sample detected at different regions on the surface of the sample. (b) SEM image of Bi_30 sample showing EDS-detection points.

Figure 3.7.4 and its inset show the frequency dependence of ε' and tanδ at 30 ^{o}C, respectively. Clearly, Bi^{3+} doping ions have a great influence on the dielectric properties of CCTO/CTO composites. The values of ε' and tanδ of CCTO/CTO composites were strongly enhanced by doping with Bi^{3+}. This is likely due to the enhanced dielectric responses of internal interfaces [6]. At 30 ^{o}C and 1 kHz, the ε' values of the CCTO/CTO, Bi_05, Bi_10, and Bi_30 samples were found to be 1877, 19153, 41468, and 6458, respectively. Variation in tanδ due to substituted Bi^{3+} ions was similar to that observed in the change in ε'. Fig. 3.7.5 shows the temperature dependence of ε'. It was observed that ε' values of all the samples increased with increasing temperature. The increase in ε' at high temperatures for CCTO ceramics is usually observed. This may be related to the effect of dc conduction in the bulk sintered ceramic composites [7]. It is notable that strong increases in ε' were observed in the Bi_05 and Bi_30 samples.

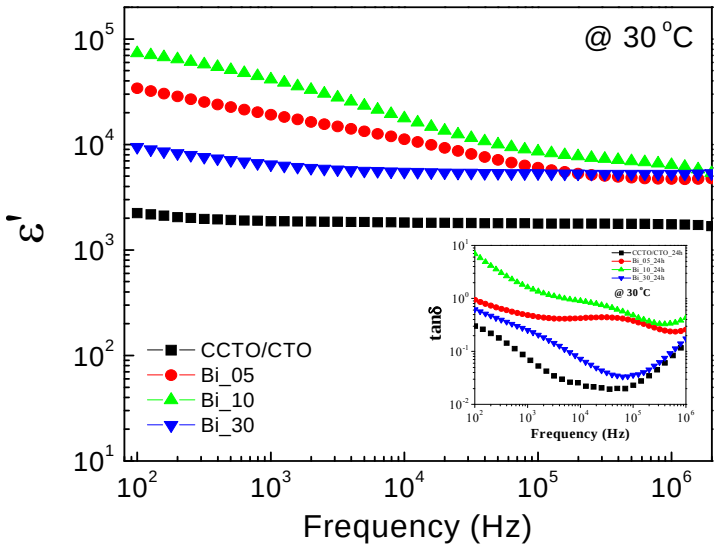

Figure 3.7.4 Frequency dependence of ε' at 30 ^{o}C for Bi-doped CCTO/CTO composites; inset depicts tanδ as a function of frequency at 30 ^{o}C.

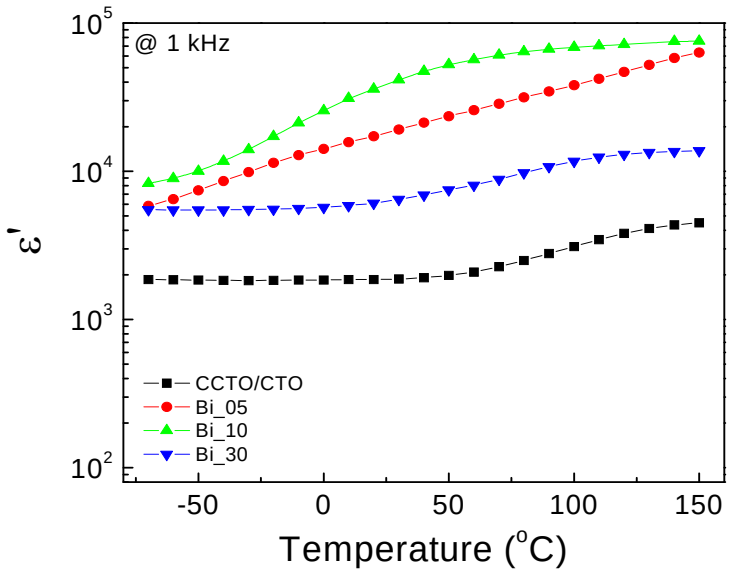

Figure 3.7.5 ε' as a function of temperature at 1 kHz.

To understand the possible mechanism(s) of the strongly enhanced dielectric response in Bi-doped CCTO/CTO composites, impedance spectroscopy was used to evaluate the electrical resistances of the grains and internal interfaces. Figure 3.7.6 and its inset show impedance complex plane (Z*) plots at 120°C and an expanded view near the origin. The total resistance (R_{tot}) estimated from the diameter of a large semicircle arc of the CCTO/CTO ceramic was greatly reduced by doping with Bi^{3+}. In general, R_{tot} is governed by the resistance of GBs (R_{gb}) [6]. In CCTO/CTO composites, GBs or interfaces between different types of grains consisted of interfaces between CCTO-CCTO grains, CCTO-CTO grains, and CTO-CTO grains. The value of R_g is usually determined from the non-zero intercept on the Z' axis [6]. It was also found that substitution of Bi^{3+} ions can reduce the resistance of grains (R_g), as shown in Fig. 3.7.7.

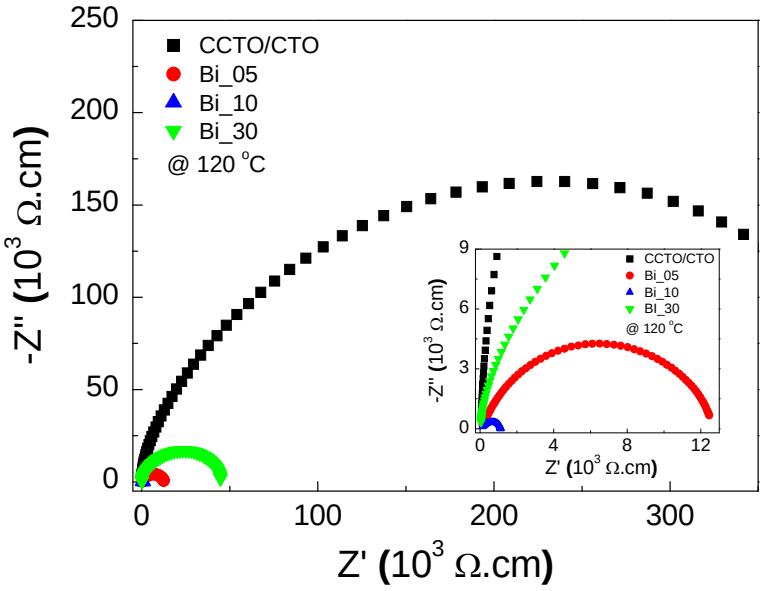

Figure 3.7.6 Impedance complex plane plots (Z* plots) of Bi-doped CCTO/CTO composites at 120 °C; inset shows an expanded view near the origin to reveal the impedance spectra of Bi_05 and Bi_10 samples.

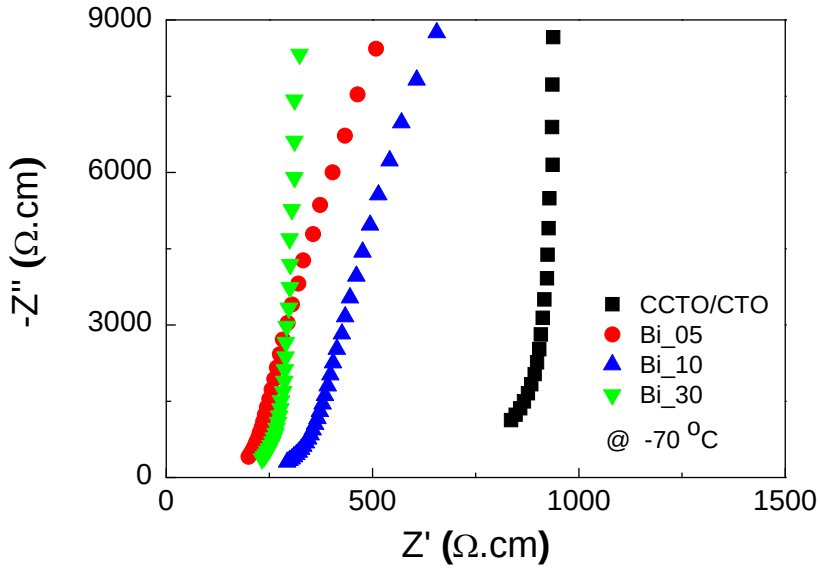

Figure 3.7.7 Z* plots at high frequencies of Bi-doped CCTO/CTO composites at -70 °C, showing the non-zero intercept on the Z′ axis.

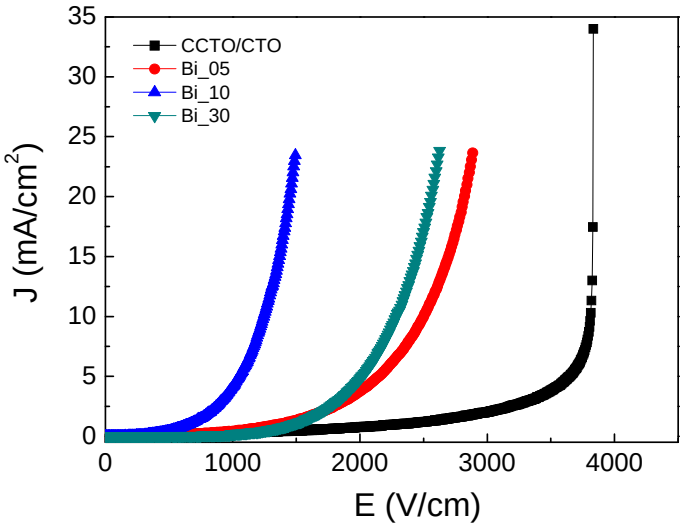

Figure 3.7.8 Nonlinear *J-E* characteristics of Bi-doped CCTO/CTO composites.

Fig. 3.78 shows the nonlinear electrical characteristics of the CCTO/CTO and Bi-doped CCTO/CTO composites. Although all the composite samples exhibited nonlinear *J-E* behavior, different characteristics were observed in Bi-doped CCTO/CTO composites. Two important parameters (α and E_b) of all the composites were calculated. At room temperature, α values of the CCTO/CTO, Bi_05, Bi_10, and Bi_30 samples were found to be 9.9, 3.79, 3.60, and 5.22, respectively. E_b values of CCTO/CTO composites were greatly reduced by Bi^{3+} doping ions. These results indicate that the nonlinear *J-E* properties were degraded by doping with Bi^{3+} ions.

In CCTO and CTO ceramics, Bi^{3+} substitution for Ca^{2+} requires charge compensation. This may be achieved by one or more of the following mechanisms: (1) filling oxygen vacancies, (2) decrease of cation valence, (3) creation of cation vacancies, or (4) creation of conduction electrons. It is likely that creation of conduction electrons may be primarily responsible for the observed decrease in R_g of Bi-doped CCTO/CTO composites. Ramirez *et al*. [1] used electrostatic force microscopy (EFM) to characterize possible electrical responses in a CCTO/CTO composite system. It was found that a CTO-CTO interface was electrically inactive, whereas, CCTO-CTO and CCTO-CCTO interfaces were electrically active. This indicates the presence of potential barriers at the CCTO-CTO and CCTO-CCTO interfaces. Thus, the degradation in the nonlinear electrical properties of CCTO/CTO due to substitution of Bi^{3+} may have been related to weak electrical responses at these active interfaces. The reduction of the breakdown field in Bi-doped CCTO/CTO composites is primarily associated with a

decrease in the potential barrier height (Φ_B) at internal interfaces. For a single phase of CCTO ceramics, the Schottky barrier at GBs can be expressed as [8]:

$$\Phi_B = \frac{qN_s^2}{8\varepsilon_0\varepsilon' N_d}, \tag{3.7.1}$$

where N_s and N_d are the acceptor (surface charge) concentration and the charge carrier concentration in semiconducting grains (*i.e.*, CCTO grains), respectively. ε' is the relative permittivity of materials, and q is the electronic charge. Using Eq. (3.7.1), the large reduction in Φ_B observed in CCTO/CTO composites is clearly attributable to an increase in N_d. Generally, an increase in N_d can cause a decrease in resistance of grain interiors (R_g). This is clearly observed in Fig. 3.7.7 showing a decrease in R_g of Bi-doped CCTO/CTO composites. It is reasonable to conclude that the increase in tanδ (inset of Fig. 3.7.4) was due to the reduction of total resistance of internal interfaces. Greatly enhanced dielectric response in Bi-doped CCTO/CTO composites (especially for the Bi_05 and Bi_10 samples) may be due to the increase in charge carriers inside the grains. Under an applied electric field, more charge carries were accumulated at the internal interfaces (CCTO-CTO and CCTO-CCTO interfaces) of Bi-doped CCTO/CTO composites. This produces a relatively high intensity of interfacial polarization compared to that of the un-doped CCTO/CTO sample. This is responsible for the observed large increase in ε' in the Bi-doped CCTO/CTO composites. It is notable that the total resistance of the Bi_30 sample was found to be larger than those of the Bi_05 and Bi_10 samples. This resulted in a lower tanδ value of the Bi_30 sample compared to those of the Bi_05 and Bi_10 samples. For the Bi_30 sample, a high value of R_{tot} compared the other samples might be due to precipitation of Bi_2O_3 at interfaces, just as was observed in commercial ZnO-Bi_2O_3 varistor ceramics [9].

References

[1] M.A. Ramírez, P.R. Bueno, R. Tararam, A.A. Cavalheiro, E. Longo, J.A. Varela, J. Phys. D: Appl. Phys. 42 (2009) 185503.

[2] P. Thongbai, B. Putasaeng, T. Yamwong, S. Maensiri, J. Alloys Compd. 509 (2011) 7416-7420.

[3] J. Jumpatam, B. Putasaeng, T. Yamwong, P. Thongbai, S. Maensiri, J. Am. Ceram. Soc. 97 (2014) 2368-2371.

[4] J. Jumpatam, B. Putasaeng, T. Yamwong, P. Thongbai, S. Maensiri, J. Eur. Ceram. Soc. 34 (2014) 2941-2950.

[5] M.N. Rahaman, Ceramic processing and sintering, 2nd ed., M. Dekker, New York, 2003.

[6] R. Schmidt, M.C. Stennett, N.C. Hyatt, J. Pokorny, J. Prado-Gonjal, M. Li, D.C. Sinclair, J. Eur. Ceram. Soc. 32 (2012) 3313-3323.

[7] J. Wu, C.-W. Nan, Y. Lin, Y. Deng, Phys. Rev. Lett. 89 (2002) 217601.

[8] T. Adams, D. Sinclair, A. West, Phys. Rev. B 73 (2006) 094124.

[9] A.J. Moulson, J.M. Herbert, Electroceramics : materials, properties, applications, 2nd ed., Wiley, West Sussex ; New York, 2003.

CHAPTER IV
CONCLUSIONS AND SUGGESTIONS

4.1 $(Na_{1/3}Ca_{1/3}Ln_{1/3})Cu_3Ti_4O_{12}$ ceramics (Ln = La^{3+}, Bi^{3+}, Sm^{3+}, Gd^{3+}, Y^{3+}, Yb^{3+}, Nd^{3+}, and Dy^{3+})

A new NCBCTO perovskite compound was successfully prepared using a solid state reaction method. This NCBCTO ceramic exhibited a high ε' value of $\sim 2.5\times10^4$ and low $\tan\delta$ of ~0.038 at 1 kHz and 20 °C with a temperature coefficient less than $\pm$15% in the range of -70 to 110 °C. The observed dielectric relaxation behaviors were similar to those reported for other $ACu_3Ti_4O_{12}$ compounds. Nonlinear *J-E* characteristics were observed, suggesting the existence of Schottky barriers at the grain boundaries. Polyvalent cations, *i.e.*, Cu^+, Cu^{3+}, or Ti^{3+} ions were detected in the NCBCTO ceramics. This ceramic compound was found to be electrically heterogeneous, consisting of semiconducting grains and insulating grain boundaries. The origin of the giant dielectric response in the NCBCTO was likely caused by an electrical response at grain boundaries.

4.2 $CaCu_{3-x}Mg_xTi_4O_{12}/CaTiO_3$

The dielectric properties of CCTO/CTO composites were improved by doping with Mg^{2+} ions. It was found that Mg^{2+} was incorporated into only the CCTO phase. An enhanced ε' of 3,550 with good temperature stability ($\Delta\varepsilon' \leq \pm$15% in the temperature range of -60 - 160°C) and a reduced $\tan\delta$ value to ~0.014 (at 30°C and 1 kHz) were achieved in a $CaCu_{2.7}Mg_{0.3}Ti_4O_{12}$/CTO ceramic sintered at 1100 °C for 6 h. Furthermore, the nonlinear coefficient of this ceramic was greatly enhanced to 27.2. Using impedance spectroscopy analysis, it was suggested that improved dielectric and nonlinear properties were attributed to the enhanced electrical responses of CCTO-CTO and CCTO-CCTO interfaces resulting from the presences of Mg^{2+} doping ions.

4.3 $CaCu_{3-x}Zn_xTi_4O_{12}/CaTiO_3$

In conclusion, the dielectric and non-Ohmic properties of CCTO/CTO can be improved by doping with Zn^{2+} to deliberately create Zn-doped CCTO/CTO composites. ε' of $Ca_2Cu_{1.8}Zn_{0.2}Ti_4O_{12}$ composite was strongly enhanced to ~6513, whereas $\tan\delta$

was found to be very low, 0.015 at 1 kHz and 20°C. α and E_b of this ceramic were significantly enhanced to 12.43 and 11,689 V/cm, respectively. The maximum value of U for the CCTO/CTO_Zn1 composite was greatly increased to 39.40 kJ/m^3. The dielectric and nonlinear properties of Zn-doped CCTO/CTO composites were described and found to be influenced by Zn^{2+} doping ions influencing the electrical response of internal interfaces.

4.4 $CaCu_3Ti_{4-x}Zr_xO_{12}/CaTiO_3$

Zr^{4+}-doped CCTO/CTO ceramic composites were created from a nominal formula of $Ca_2Cu_2Ti_{4-x}Zr_xO_{12}$. Doping Zr^{4+} into CCTO/CTO composites resulted in an increase in the mean grain sizes of both the CCTO and CTO phases. Zr^{4+} ions were preferentially substituted into the CCTO phase. At Zr^{4+} dopant concentrations of more than 2.5 mol%, Zr^{4+} was found to be over the limited solid solution, leading to formation of a $CaZrTi_2O_7$ impurity phase. A strong increase in ε' of 1.03×10^4 for the 2.5 mol% of Zr^{4+}-doped CCTO/CTO composite was observed compared to that of the un-doped composite ($\varepsilon'\sim1.86\times10^3$). This result is completely different from that observed in a single phase Zr^{4+}-doped CCTO ceramic. Here, ε' was greatly reduced by doping with Zr^{4+}. Thus, the origin of the high dielectric response in CCTO/CTO composites was confirmed to be an extrinsic effect related to the electrical responses of internal interfaces, rather than being caused by an intrinsic effect originating in the grain interiors. It was found that variations of E_a and E_g values were consistent with each other. Furthermore, a change in the macroscopic dielectric relaxation time was clearly consistent with the variation of R_gC_{gb} values, following the M-W relaxation model. These results strongly support the conceptualization of an internal interface effect on the giant dielectric response in CCTO-based compounds.

4.5 $CaCu_3Ti_{4-x}Sn_xO_{12}/CaTiO_3$

Sn-doped CCTO/CTO composites were successfully prepared using a one-step process. Grain size in the CCTO phase of CCTO/CTO composites was significantly enlarged by Sn^{4+} doping. This resulted in a strong degradation of nonlinear electrical properties. The ε' value of Sn-doped CCTO/CTO composites was increased by more than a factor of 3 with a slightly changed $\tan\delta$. The influences of Sn^{4+} doping on the dielectric and electrical properties of CCTO/CTO composites were reasonably explained

by the extrinsic factors. This is proposed as the origin of the giant dielectric response in CCTO. The enhanced dielectric properties of CCTO/CTO composites likely originated from the improved electrical response at the internal interfaces and enlarged CCTO grain size, which were caused by substitution of Sn^{4+} ions.

4.6 $Ca_{1-x}La_xCu_3Ti_4O_{12}/CaTiO_3$

La^{3+} doping ions have great effects on the dielectric properties and formation of Schottky barriers at internal interfaces of a CCTO/CTO composite system. The high potential barriers at internal interfaces of the CCTO/CTO composite were greatly degraded by La^{3+} doping. The degradation of Schottky barriers resulted in a large decrease in the total resistance of internal interfaces between grains. The creation of conduction electrons due to charge compensation for La^{3+} ions substituted into Ca^{2+} sites is proposed as the primary cause. For high concentrations of La^{3+} dopant, ionic compensation by cation vacancies was another cause that further reduced the potential barrier height. The interfacial polarization mechanism at CCTO-CCTO and CTO-CCTO interfaces can be used to described the dielectric response in La^{3+}-doped CCTO/CTO composite ceramics.

4.7 $Ca_{1-x}Bi_xCu_3Ti_4O_{12}/CaTiO_3$

In conclusion, we successfully prepared CCTO/CTO composites doped with Bi^{3+} ions. Influences of Bi^{3+}substitution of the microstructure, dielectric response, and nonlinear *J—E* properties were studied. It was found that Bi^{3+} doping ions were substituted into Ca^{2+} sites in both of CCTO and CTO phases. The dielectric response in CCTO/CTO composites was greatly enhanced by doping with Bi^{3+} ions. This can be well described based on the interfacial polarization at internal interfaces of CCTO/CTO composites. The increase in $\tan\delta$ was consistent with the decrease in the total resistance of internal interfaces. The non—Ohmic properties of Bi^{3+}—doped CCTO/CTO composites were degraded, which might have resulted from a decrease in the potential barrier height at internal interfaces, *i.e.*, CCTO—CCTO and CTO—CCTO interfaces.

4.8 Suggestions

4.12.1 In this research work, although the loss tangent of CCTO and related oxide ceramics can be effectively reduced, it is likely that the temperature coefficient or variation of dielectric permittivity with temperature in a high temperature range is still a serious problem. The dielectric permittivity of the synthesized ceramics is independent on temperature only in the range of -55 – 125 ^{o}C. It is important to improve this to achieve higher-performance dielectric materials that their temperature coefficient is low in a temperature range higher than 105 ^{o}C.

4.12.2 Although the loss tangent of CCTO and related oxide ceramics can be effectively reduced into an acceptable standard value for capacitor applications, the dielectric permittivity was also decreased greatly. Ultra high dielectric permittivity in the order of >10^{5} and very low loss tangent should be investigated by engineering lattice structure and microstructure of dielectric ceramics.

Output จากโครงการวิจัยที่ได้รับทุนจาก สกว.

1. Kum-onsa P, **Thongbai P***, Putasaeng B, Yamwong T, Maensiri S. $Na_{1/3}Ca_{1/3}Bi_{1/3}Cu_3Ti_4O_{12}$: A New Giant Dielectric Perovskite Ceramic in $ACu_3Ti_4O_{12}$ Compounds. ***J. Eur. Ceram. Soc.*** 2015; **35**: 1441–1447. **(Impact Factor2013 = 2.307)**
2. Jumpatam J, Putasaeng B, Yamwong T, **Thongbai P***, Maensiri S. *A novel strategy to enhance dielectric performance and non-Ohmic properties in* $Ca_2Cu_{2-x}Mg_xTi_4O_{12}$, ***J. Eur. Ceram. Soc.*** 2014; **34**: 2941–2950. **(Impact Factor2013 = 2.307)**
3. Jumpatam J, Putasaeng B, Yamwong T, **Thongbai P***, Maensiri S. *A Novel Route to Greatly Enhanced Dielectric Permittivity with Reduce Loss Tangent in* $CaCu_{3-x}Zn_xTi_4O_{12}/CaTiO_3$ *Composites*, ***J. Am. Ceram. Soc.*** 2014; **97[8]**: 2368–2371. **(Impact Factor2013 = 2.428)**
4. Jumpatam J, **Thongbai P***, Yamwong T, Maensiri S. *Effects of* Bi^{3+} *Doping on Microstructure and Dielectric Properties of* $CaCu_3Ti_4O_{12}/CaTiO_3$ *Composite Ceramics*, ***Ceram. Int.*** 2015; http://dx.doi.org/10.1016/j.ceramint.2015.03.197. **(Impact Factor2013 = 2.086)**
5. **Thongbai P***, Jumpatam J, Putasaeng B, Yamwong T, Amornkitbamrung V, Maensiri S. Effects of La^{3+} doping ions on dielectric properties and formation of Schottky barriers at internal interfaces in a $Ca_2Cu_2Ti_4O_{12}$ composite system***. J. Mater. Sci: Mater. Electron.*** 2014; **25**: 4657–4663. **(Impact Factor2013 = 1.966)**
6. **Thongbai P***, Jumpatam J, Putasaeng B, Yamwong T, Maensiri S. Microstructural evolution and Maxwell–Wagner relaxation in $Ca_2Cu_2Ti_{4-x}Zr_xO_{12}$: The important clue to achieve the origin of the giant dielectric behavior. ***Mater. Res. Bull.*** 2014; **60**: 695–703. **(Impact Factor2013 = 1.968)**
7. Tuichai W, **Thongbai P***, Amornkitbamrung V, Yamwong T, Maensiri S. *$Na_{0.5}Bi_{0.5}Cu_3Ti_4O_{12}$ nanocrystalline powders prepared by using a glycine-nitrate process: preparation, characterization, and their dielectric properties*. ***Microelectron. Eng.*** 2014; **126**: 118–123. **(Impact Factor2013 = 1.338)**

APPENDIX

Paper publications

Available online at www.sciencedirect.com

ScienceDirect

Journal of the European Ceramic Society 35 (2015) 1441–1447

www.elsevier.com/locate/jeurceramsoc

$Na_{1/3}Ca_{1/3}Bi_{1/3}Cu_3Ti_4O_{12}$: A new giant dielectric perovskite ceramic in $ACu_3Ti_4O_{12}$ compounds

Pornsawan Kum-onsa [a], Prasit Thongbai [b,*], Bundit Putasaeng [c], Teerapon Yamwong [c], Santi Maensiri [d]

[a] *Materials Science and Nanotechnology Program, Faculty of Science, Khon Kaen University, Khon Kaen 40002, Thailand*
[b] *Department of Physics, Faculty of Science, Khon Kaen University, Khon Kaen 40002, Thailand*
[c] *National Metal and Materials Technology Center (MTEC), Thailand Science Park, Pathumthani 12120, Thailand*
[d] *School of Physics, Institute of Science, Suranaree University of Technology, Nakhon Ratchasima 30000, Thailand*

Received 4 October 2014; received in revised form 21 November 2014; accepted 21 November 2014
Available online 12 December 2014

Abstract

A new approach to achieve a novel perovskite ceramic compound, $ACu_3Ti_4O_{12}$, is presented. A-sites in the $ACu_3Ti_4O_{12}$ structure were occupied by Na^+, Ca^{2+}, and Bi^{3+} each at a level of ~33.3 at.%, leading to formation of $Na_{1/3}Ca_{1/3}Bi_{1/3}Cu_3Ti_4O_{12}$. This ceramic exhibited a low loss tangent ($\tan\delta \sim 0.038$) and a high ε' value of $\sim 2.5 \times 10^4$ at 1 kHz with good temperature stability. The high-frequency dielectric relaxation behavior showed activation energies of 0.110–0.121 eV. Nonlinear *J–E* characteristics were observed, indicating the existence of Schottky barriers at grain boundaries. Valence states of Cu cations (*i.e.*, Cu^+, Cu^{2+}, and Cu^{3+}) in $Na_{1/3}Ca_{1/3}Bi_{1/3}Cu_3Ti_4O_{12}$ ceramic were investigated using X-ray photoelectron spectroscopy. Impedance spectroscopy analysis revealed that $Na_{1/3}Ca_{1/3}Bi_{1/3}Cu_3Ti_4O_{12}$ was electrically heterogeneous and comprised of semiconducting grains and insulating grain boundaries. Interfacial polarization at the insulating layer of grain boundaries was suggested to be the origin of this high dielectric response.

Keywords: Perovskite oxide; Loss tangent; Dielectric permittivity; Microstructure

1. Introduction

Due to the requirement of many high-technology electronic devices for materials with high dielectric permittivity, $CaCu_3Ti_4O_{12}$ (CCTO) ceramics have attracted considerable attention in recent years.[1–9] This is because CCTO has very high dielectric permittivity (ε') values of 10^3–10^5 at room temperature and frequencies below 10^6 Hz. The primary impediment to the use of CCTO is that its loss tangent ($\tan\delta$) is still higher than necessary for practical application. Investigation to reduce $\tan\delta$ of CCTO ceramics has been extensively performed in recent years.[4,10–12] Additionally, there has been increasing interest in the giant dielectric properties of related-CCTO structural oxides in the family of $ACu_3Ti_4O_{12}$ compounds. In these compounds, A can be Cd,[2] $Bi_{2/3}$,[2,13,14] $La_{2/3}$,[2,13,15,16] $Y_{2/3}$,[17–19] $Na_{1/2}Bi_{1/2}$,[20–25] $Na_{1/2}Sm_{1/2}$,[26] $Na_{1/2}Y_{1/2}$,[27] and $Na_{1/2}La_{1/2}$.[28,29]

Subramanian and Sleight first reported the dielectric responses of many compounds in the family of $ACu_3Ti_4O_{12}$.[2] They found that all but CCTO exhibited ε' values at 100 kHz and 25 °C considerably less than 3600. However, further investigation showed that by varying sintering conditions, strongly enhanced ε' values were achieved, on the order of 10^4.[13,17,20,27] Furthermore, good dielectric properties of many types of these $ACu_3Ti_4O_{12}$ ceramics were observed. $Na_{1/2}Bi_{1/2}Cu_3Ti_4O_{12}$ and La-doped $Na_{1/2}Bi_{1/2}Cu_3Ti_4O_{12}$ ceramics exhibited interesting dielectric properties with high ε' values of $\sim 1.34 \times 10^4$ and $\sim 1.02 \times 10^4$ at 10 kHz, respectively, and low $\tan\delta$ values of 0.031 and 0.022 at 10 kHz, respectively.[20,21] In our previous work, high ε' (~0.61 to 0.87×10^4) and low $\tan\delta$ (0.073–0.114)

* Corresponding author. Tel.: +66 84 4190266; fax: +66 43 202374.
E-mail address: pthongbai@kku.ac.th (P. Thongbai).

http://dx.doi.org/10.1016/j.jeurceramsoc.2014.11.028
0955-2219/

were found at 1 kHz in $Na_{1/2}La_{1/2}Cu_3Ti_4O_{12}$ ceramics. The lowest $\tan\delta$ was 0.032 at 10 kHz.[28] Liang et al.[17–19] found high ε' and low $\tan\delta$ with good thermal stability at 10 kHz in $Y_{2/3}Cu_3Ti_4O_{12}$, Na-doped $Y_{2/3}Cu_3Ti_4O_{12}$, and La-doped $Y_{2/3}Cu_3Ti_4O_{12}$ ceramics. These favorable dielectric properties of $ACu_3Ti_4O_{12}$ compounds were thought to be caused by high resistance of grain boundaries (R_{gb}). Although the origin of this enhanced R_{gb} value is still unexplained, $ACu_3Ti_4O_{12}$ ceramic systems are dielectric materials with good potential for capacitor applications.

Structurally, an unusual change in the perovskite structure was observed in compounds of the type $AA'_3M_4O_{12}$. In this structure, MO_6 has a tilted octahedral structure, resulting in formation of a square planar coordination for the A′ ion.[2] As a result, the structure of many $ACu_3Ti_4O_{12}$ compounds, as well as CCTO, is very rigid. The space for the A cations (*e.g.*, Ca^{2+} for CCTO structure) in the structure is therefore essentially fixed. Thus, among A^{2+} ions, only Ca^{2+} and Cd^{2+} ions can occupy the A-site in the $ACu_3Ti_4O_{12}$ lattice structure.[2] However, it was reported that many related ceramic compounds of $A^{3+}{}_{2/3}Cu_3Ti_4O_{12}$ can be formed, where A-sites were occupied by ~66.7 at.% of A^{3+} ions and with ~33.3 at.% of the A-sites vacant to meet charge neutrality.[2,14,16,17,30] Another sub-family of $ACu_3Ti_4O_{12}$ compounds is $[Na^{+}{}_{1/2}Ln^{3+}{}_{1/2}]Cu_3Ti_4O_{12}$, where Ln^{3+} can be La, Bi, Gd, Dy, Yb, Y, or Sm.[2] Half of the A-sites are occupied by Na^+ ions, and the remained spaces in the A-sites are occupied by Ln^{3+} ions. The dielectric properties of some $ACu_3Ti_4O_{12}$ compounds are of interest. It is still very important to seek new CCTO related materials in the $ACu_3Ti_4O_{12}$ family of compounds to produce more giant dielectric compounds exhibiting good dielectric properties.

In this work, we developed a new approach to achieve a novel compound in the $ACu_3Ti_4O_{12}$ family. The A-sites in the $ACu_3Ti_4O_{12}$ structure were occupied by ~33.3 at.% of Na^+, ~33.3 at.% of Ca^{2+}, and ~33.3 at.% of Bi^{3+}, forming a new material system of $Na_{1/3}Ca_{1/3}Bi_{1/3}Cu_3Ti_4O_{12}$ (NCBCTO). Through optimization of sintering conditions, it was found that NCBCTO exhibited a high ε' value of $\sim 2.59 \times 10^4$ with a low $\tan\delta$ of ~0.038 at 1 kHz and 20 °C. The electrical responses of grains and grain boundaries were investigated using impedance spectroscopy.

2. Experimental details

$Na_{1/3}Ca_{1/3}Bi_{1/3}Cu_3Ti_4O_{12}$ (NCBCTO) ceramics were prepared using a solid state reaction method. Na_2CO_3 (99.9% purity), $CaCO_3$ (99.9% purity), Bi_2O_3 (99.9% purity), CuO (99.9% purity) and TiO_2 (99.9% purity) were selected as starting raw materials. First, stoichiometric amounts of the raw materials were weighted to produce $Na_{1/3}Ca_{1/3}Bi_{1/3}Cu_3Ti_4O_{12}$. Second, the mixture was ball milled in ethanol for 24 h. Next, the mixed slurry was dried and calcined at 900 °C for 6 h. It was found that a single phase of NCBCTO was achieved. This indicated that Na^+, Ca^{2+}, and Bi^{3+} ions substituted in the lattice structure, forming the NCBCTO crystal structure. The complete formation of NCBCTO structure can prevent Bi from evaporating at high sintering temperatures. Then, the calcined powder was ground and pressed into pellets of 9.5 mm in diameter and ~1 mm in thickness by uniaxial compression at 200 MPa. Finally, these pellets were sintered at 1050–1100 °C for 5–10 h.

Scanning electron microscopy (SEM; LEO 1450VP; Cambridge, UK) and energy dispersive X-ray spectrometry (EDS, Hitachi S-3400, Japan) were used to characterize the ceramic microstructure of the sintered ceramics. X-ray diffraction (XRD; Philips PW3040, the Netherlands) was used to study the phase composition and crystal structure of these ceramics. Valence states of cations in the NCBCTO ceramic were investigated using X-ray photoelectron spectroscopy (XPS, AXIS Ultra DLD, UK). For the dielectric measurements, surfaces of the sintered ceramics were polished until smooth and coated with Au on their surfaces at a current of 25 mA for 8 min using a Polaron SC500 sputter coating unit. The dielectric response of the sintered ceramics was determined using an Agilent E4980A Precision LCR Meter over the frequency and temperature ranges of 10^2–10^6 Hz and −70 to 200 °C, respectively, with an oscillation voltage of 0.5 V. Nonlinear current–voltage measurements were performed at room temperature using a high voltage measurement unit (Keithley Model 247).

3. Results and discussion

Fig. 1 shows the surface morphologies of NCBCTO ceramics sintered under different conditions. Abnormal grain growth was observed in all samples. Large grain sizes of ~10 to 20 μm and fine grains with sizes of 2–5 μm were observed. The overall surface morphologies of the NCBCTO ceramics were similar to those observed in $[Na^{+}{}_{1/2}Ln^{3+}{}_{1/2}]Cu_3Ti_4O_{12}$ rather than like CCTO ceramics.[19–21,25,28,29]

From the nominal formula of $Na_{1/3}Ca_{1/3}Bi_{1/3}Cu_3Ti_4O_{12}$, there are at least two possible mechanisms of the phase formation. A two-phase composite system of CCTO-$Na_{1/2}Bi_{1/2}Cu_3Ti_4O_{12}$ could form. Alternatively, a single phase may form following the nominal composition by random distribution of Na^+, Ca^{2+}, and Bi^{3+} ions in A-sites of the crystal lattice. To clarify, the XRD technique was used to determine phase composition(s). As shown in Fig. 2(a), all of the XRD patterns indicated a single phase. However, it is difficult to differentiate CCTO and $Na_{1/2}Bi_{1/2}Cu_3Ti_4O_{12}$ phases because their lattice parameters are very close (7.391 and 7.412 Å, respectively).[2] Thus, splitting of XRD peaks could not be observed using our X-ray spectrometer instrument. It is notable that these XRD patterns confirm the formation of a $CaCu_3Ti_4O_{12}$-like structure (JCPDS 75-2188). All diffraction peaks in XRD patterns for NCBCTO ceramics are well indexed based on the body-centered cubic structure within space group *Im*3. Lattice parameters were calculated and found to be 7.4007, 7.4001, 7.3960, and 7.3966 Å for NCBCTO ceramics sintered at 1060 °C for 5 h, 1070 °C for 5 h, 1080 °C for 5 h, and 1080 °C for 10 h, respectively. It was observed that these lattice parameter values were intermediate between the corresponding values of CCTO and $Na_{1/2}Bi_{1/2}Cu_3Ti_4O_{12}$.

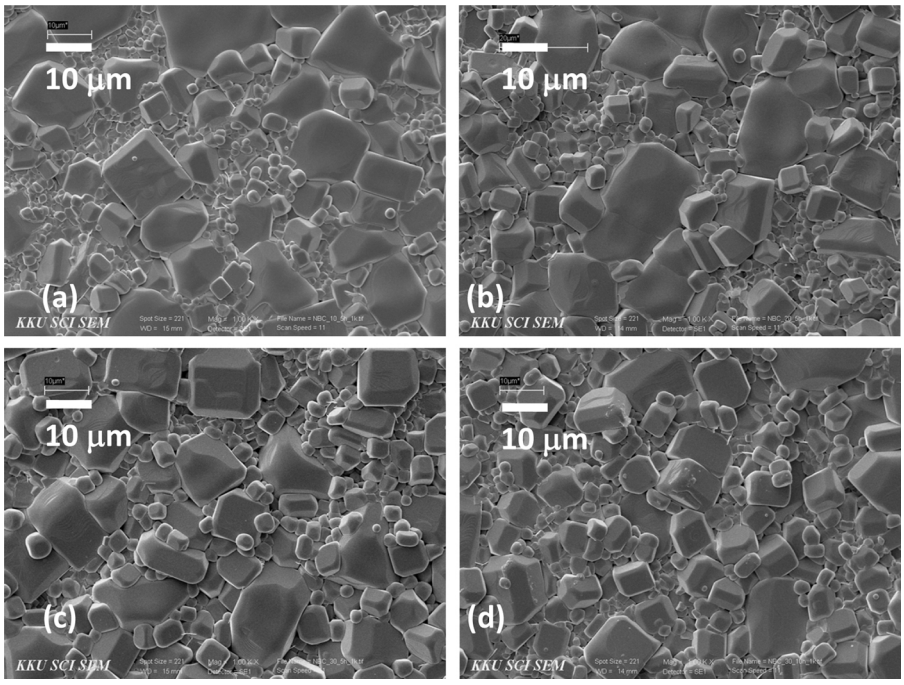

Fig. 1. SEM images of un-polished surface of NCBCTO ceramics sintered at different conditions: (a) 1060 °C for 5 h, (b) 1070 °C for 5 h, (c) 1080 °C for 5 h, and (d) 1080 °C for 10 h.

As seen in Fig. 2(b) and (c), the SEM images of the polished surfaces in the same area showed no difference in contrast in the backscattered SEM image (Fig. 2(c)). This may indicate a single phase in the NCBCTO ceramic. The microstructure was characterized using an EDS technique. The results are shown in Fig. 2(d). It was found that the EDS peaks of all metal elements (*i.e.*, Na, Ca, Bi, Cu, Ti) were detected at the same point (as marked in the circle area). These results indicate that Na^{+}, Ca^{2+}, and Bi^{3+} ions may well randomly occupy A-sites in the $ACu_3Ti_4O_{12}$ lattice structure.

As depicted in Fig. 3, all the sintered ceramics exhibited giant dielectric properties with $\varepsilon' \sim 1.5–2.75 \times 10^4$ at frequencies less than 10^5 Hz as was observed in CCTO ceramics and some $ACu_3Ti_4O_{12}$ compounds.[1,10,13,17,20,27] The frequency

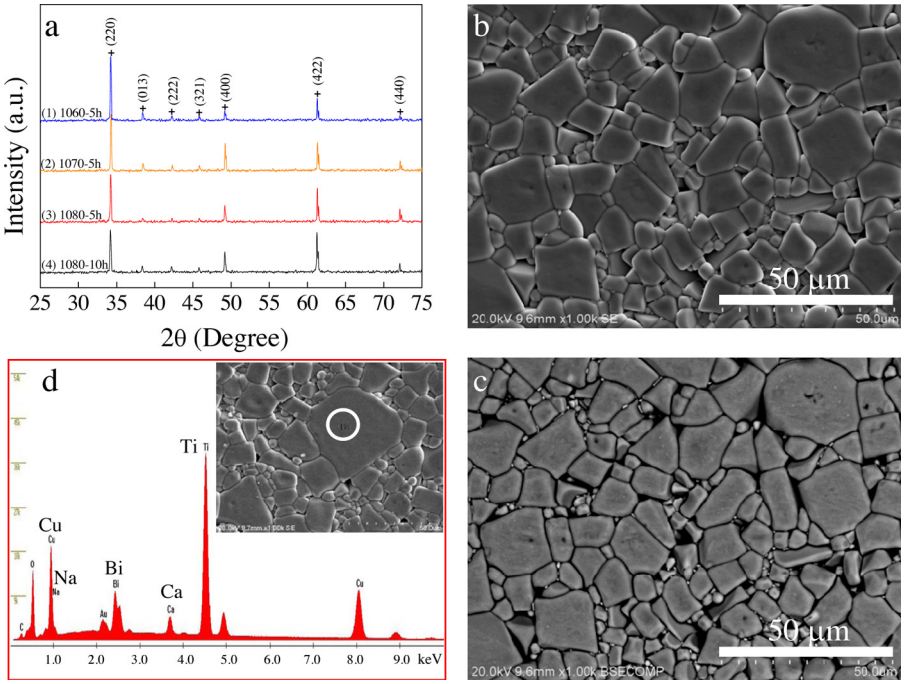

Fig. 2. (a) XRD patterns of NCBCTO ceramics. (b and c) Secondary electron and backscattered SEM images of polished surfaces of the NCBCTO ceramic sintered at 1060 °C for 5 h. (d) EDS spectrum detected in the circle area, as shown in its inset.

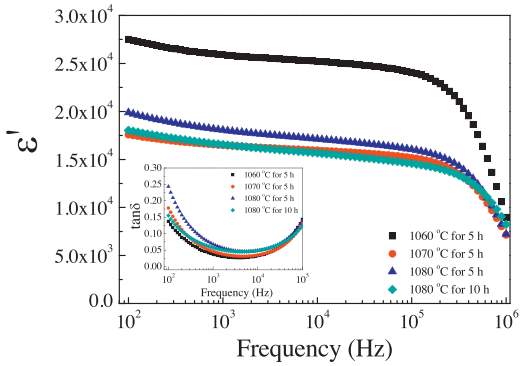

Fig. 3. Variation in ε' with frequency at 20 °C for NCBCTO ceramics sintered at different conditions; inset shows tan δ as a function of frequency at 20 °C.

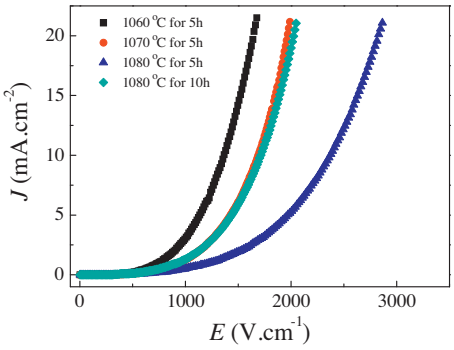

Fig. 5. Nonlinear *J–E* characteristics of NCBCTO ceramics at room temperature.

dependence of tan δ at 20 °C is demonstrated in the inset of Fig. 3. Based on the experimental results of the current study, the optimal sintering condition was 1060 °C for 5 h, resulting in values of $\varepsilon' \sim 2.59 \times 10^4$ and $\tan\delta \sim 0.038$ at 1 kHz. ε' decreased as the sintering temperature was increased. This is similar to that reported in published literature for $Na_{1/2}Bi_{1/2}Cu_3Ti_4O_{12}$ ceramics.[20] At 1 kHz, tan δ values of NCBCTO ceramics sintered at 1060 °C for 5 h, 1070 °C for 5 h, 1080 °C for 5 h, and 1080 °C for 10 h were approximately 0.038, 0.046, 0.067, and 0.057, respectively. The overall frequency dependence of ε' and tan δ behavior were similar to those observed in many compounds in the $ACu_3Ti_4O_{12}$ family.

As can be seen in Fig. 4, the frequency dependence of ε' for NCBCTO ceramics at different temperatures showed three main parts of dielectric responses. Three plateau-like features in the plots of ε' *vs.* frequency were observed in the temperature range from −70 to 190 °C, especially for the NCBCTO ceramic sintered at 1080 °C for 10 h (Fig. 4(b)). The first plateau at low frequencies was observed at the highest temperatures, whereas the high frequency plateau can only be seen in parts at the lowest temperature measured. The first plateau in a low-frequency range is attributed to an sample-electrode interface response, while the high frequency plateau is originated from the bulk response. At intermediate frequencies, the primary plateau is obvious. This is attributed to the dielectric response of the grain boundaries.[31,32] The dielectric responses of these three parts were clearly shown by Li et al.[32] A step-like decrease in ε' and a concurrent appearance of ε''-relaxation peaks [as shown in the insets] were observed. Both of a step-like decrease in ε' and ε'' peak shift to higher frequencies with increasing temperature, indicating to thermally activated dielectric relaxation process. This dielectric relaxation process is usually observed in CCTO and related ceramics.[17,28,33,34] The primary dielectric relaxation process is referred to Maxwell–Wagner relaxation. According to the Maxwell–Wagner model, Liu et al.[14] demonstrated that the dielectric relaxation behavior was governed by the electrical response of the grains. It was found that the high-frequency relaxation activation energies of the NCBCTO ceramics sintered at 1060 °C for 5 h, 1070 °C for 5 h, 1080 °C for 5 h, and 1080 °C for 10 h were 0.110, 0.116, 0.113, and 0.121 eV, respectively. These activation energy values are comparable to those observed in CCTO (0.103 eV),[35] $Bi_{2/3}Cu_3Ti_4O_{12}$ (0.095 eV),[14] and $Na_{1/2}Y_{1/2}Cu_3Ti_4O_{12}$ ceramics (0.112 eV).[27]

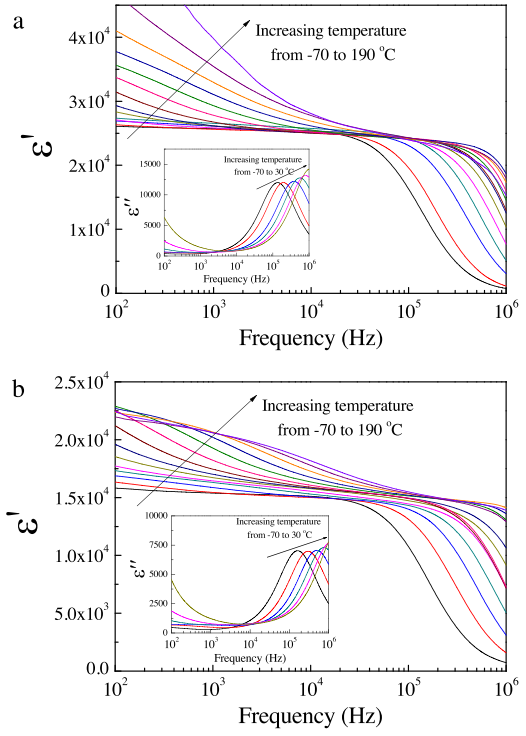

Fig. 4. Frequency dependence of ε' at various temperatures of the NCBCTO ceramics sintered at (a) 1060 °C and (b) 1080 °C for 10 h; their insets show the frequency dependence of tan δ in a temperature range from −70 to 30 °C.

Nonlinear electrical behavior was also observed in NCBCTO ceramics, as shown in Fig. 5. The breakdown electric field strength (E_b) was obtained at a current density of $J = 1$ mA cm^{-2}. The nonlinear coefficient (α) was calculated in the range of $J = 1$–10 mA cm^{-2}. The values of α in NCBCTO ceramics sintered at 1060 °C for 5 h, 1070 °C for 5 h, 1080 °C for 5 h, and 1080 °C for 10 h were found to be 3.67, 3.72, 3.19, and 3.74, respectively. E_b values were 569, 739, 836, and 704 V cm^{-2}, respectively. The nonlinear properties of NCBCTO ceramics slightly changed with sintering conditions. However, these values were still too low for practical application in varistor devices.

To describe the dielectric and electrical properties of NCBCTO ceramics, the ceramic sample with the best dielectric properties was selected for further investigation. The

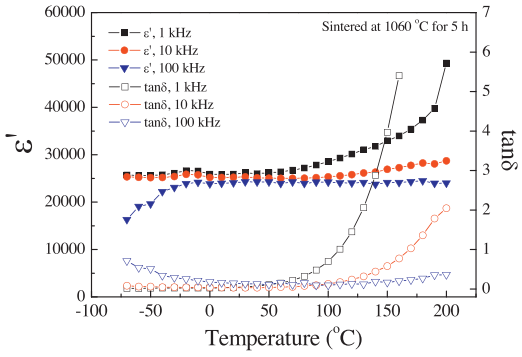

Fig. 6. Temperature dependence of ε' and $\tan\delta$ at selected frequencies of the NCBCTO ceramic sintered at 1060 °C for 5 h.

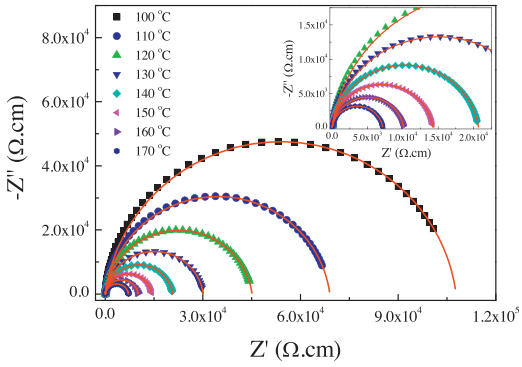

Fig. 7. Impedance complex plan plot (Z^*) at different temperatures for the NCBCTO ceramic sintered at 1060 °C for 5 h; the inset is an expanded view near the origin for high frequency data. The solid curves are the fitted data using Eq. (1).

temperature dependences of ε' and $\tan\delta$ of the NCBCTO ceramic sintered at 1060 °C for 5 h are shown in Fig. 6. At 20 °C and 1 kHz, ε' and $\tan\delta$ values of this NCBCTO ceramic were 2.59×10^4 and 0.038, respectively. Moreover, ε' was slightly dependent upon temperature in the range from −70 to 110 °C with a temperature coefficient less than ±15% (at 1 kHz). According to previous reports,[20,21] at 10 kHz, $Na_{1/2}Bi_{1/2}Cu_3Ti_4O_{12}$ and La-doped $Na_{1/2}Bi_{1/2}Cu_3Ti_4O_{12}$ ceramics showed high ε' values of $\sim 1.34 \times 10^4$ and $\sim 1.02 \times 10^4$ and low $\tan\delta$ of ~0.031 and 0.022, respectively. In these two materials, ε' at 10 kHz was slightly dependent upon temperature in the ranges of −50 to 150 °C and −60 to 120 °C, respectively. It was found that at 10 kHz, high ε' ($\sim 1.1 \times 10^4$) and low $\tan\delta$ (~0.033) with good thermal stability of ε' in the range of −60 to 150 °C were achieved in $Y_{2/3}Cu_3Ti_4O_{12}$ ceramics.[17] To compare the dielectric properties with other $ACu_3Ti_4O_{12}$ ceramics, ε' and $\tan\delta$ values as well as the temperature coefficient of the NCBCTO ceramic at 10 kHz were evaluated, *i.e.*, $\varepsilon' \sim 2.52 \times 10^4$, $\tan\delta \sim 0.032$, and temperature coefficient less than ±15% in the range of −70 to 200 °C. These results produced better dielectric properties in the NCBCTO ceramic than other $ACu_3Ti_4O_{12}$ ceramics.

Impedance spectroscopy was used to study the electrical properties of grains and grain boundaries to elucidate possible mechanisms resulting in the giant dielectric response of NCBCTO ceramics. According to the brick-work layer model for polycrystalline electroceramics,[31,32] an equivalent circuit consisting of two parallel resistor–capacitor (*R–C*) elements connected in series was presented. For CCTO ceramics, one *R–C* element represents the electrical response of semiconducting grains and other represents the electrical response of grain boundaries. It is notable that the impedance data of all the ceramic samples were calculated by considering the ratio of area of electrode/pellet thickness. As can be seen in Fig. 7 and its inset, the diameter of the large semicircle arc of the impedance complex plane plot (Z^*) decreased with increasing temperature. This indicated that the total resistance decreased as temperature increased. The total resistance might be governed by the grain boundary resistance (R_{gb}) or R_{gb} combined with the electrode interface resistance ($R_{gb} + R_e$). Generally, the grain (bulk) and grain boundary responses can each be described by a parallel *R–C* element, whereas the macroscopic dielectric response is usually represented by a series connection of two *R–C* elements.[31] To clarify, impedance data were fitted to a single *R–C* parallel circuit using the modified equation for a Z^* plot,[14]

$$Z^* = \frac{R_{gb}}{1 + (i\omega R_{gb} C_{gb})^{\alpha}}, \quad (1)$$

where C_{gb} is the capacitance of the grain boundaries, α is a constant parameter ($0 < \alpha \leq 1$), and ω is the angular frequency of an applied electric field. As shown in Fig. 7 and its inset, Z^* plots of the experimental data in the temperature range of 100–170 °C are well fitted by Eq. (1). This indicates that there are no two overlapping arcs of R_{gb} and R_e. Thus, the large semicircle arc of Z^* plots at various temperatures is attributed to the grain boundary response only. The conduction activation energy of the grain boundary determined by variation in R_{gb} was found to be 0.551 eV. The nonzero intercept of the high-frequency impedance data was also observed (not shown). Therefore, one can conclude that NCBCTO ceramics are electrically heterogeneous, consisting of conductive and insulating elements. These are the electrical properties of grains and grain boundaries, respectively. Thus, it is reasonable to suggest that the giant dielectric response of NCBCTO ceramics may be caused by the interfacial polarization at the grain boundaries. Under an applied electric field, charges inside the semiconducting grains were forced to move accumulating at the insulating grain boundaries, producing a strong interfacial polarization. This is responsible for the observed giant dielectric properties of NCBCTO ceramics.

The oxidation states of polyvalent cations were investigated using an XPS technique. Fig. 8 shows the XPS spectrum of Cu2*p* regions of the NCBCTO ceramic. The Cu2*p* peak region was divided into three peaks using Gaussian–Lorentzian profile fitting. The highest peak height represents Cu^{2+}. The other two peaks at lower and higher binding energies were produced by Cu^{+} and Cu^{3+}, respectively.[26,35,36] The XPS spectrum also indicated the presence of Ti^{3+} in the NCBCTO ceramic. Polyvalent cations, *i.e.*, Cu^{+}, Cu^{3+}, and Ti^{3+} ions, may have a remarkable effect on the electrical semiconducting properties of grains.

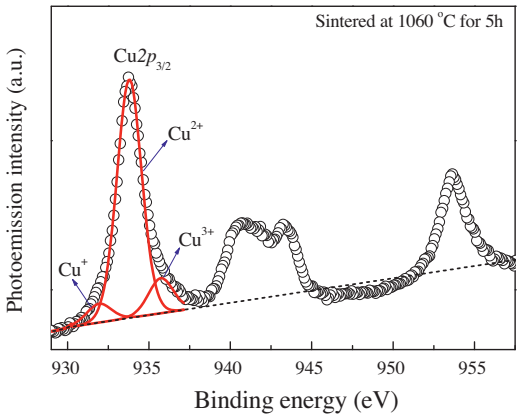

Fig. 8. XPS spectrum of the NCBCTO ceramic sintered at 1060 °C for 5 h.

For CCTO ceramics, *n*-type semiconductor characteristic of the grains was confirmed by measuring the thermoelectric power with a negative Seebeck coefficient value.[37] Thus, it is reasonable to suggest that the conduction mechanism inside the *n*-type semiconducting grains of the NCBCTO ceramics is primarily due to electron hopping between $Cu^{+} \leftrightarrow Cu^{2+}$ and $Ti^{3+} \leftrightarrow Ti^{4+}$ sites.

4. Conclusion

In conclusion, a new NCBCTO perovskite compound was successfully prepared using a solid state reaction method. This NCBCTO ceramic exhibited a high ε' value of $\sim 2.5 \times 10^4$ and low tan δ of ~0.038 at 1 kHz and 20 °C with a temperature coefficient less than ±15% in the range of −70 to 110 °C. The observed dielectric relaxation behaviors were similar to those reported for other $ACu_3Ti_4O_{12}$ compounds. Nonlinear *J–E* characteristics were observed, suggesting the existence of Schottky barriers at the grain boundaries. Polyvalent cations, *i.e.*, Cu^{+}, Cu^{3+}, or Ti^{3+} ions were detected in the NCBCTO ceramics. This ceramic compound was found to be electrically heterogeneous, consisting of semiconducting grains and insulating grain boundaries. The origin of the giant dielectric response in the NCBCTO was likely caused by an electrical response at grain boundaries.

Acknowledgments

This work was financially supported by the Thailand Research Fund (TRF) and Khon Kaen University, Thailand [grant number TRG5680047]. P.K. would like to thank the Science Achievement Scholarship of Thailand (SAST) for her Master of Science Degree scholarship.

References

1. Subramanian MA, Li D, Duan N, Reisner BA, Sleight AW. High dielectric constant in $ACu_3Ti_4O_{12}$ and $ACu_3Ti_3FeO_{12}$ phases. *J Solid State Chem* 2000;**151**:323.
2. Subramanian MA, Sleight AW. $ACu_3Ti_4O_{12}$ and $ACu_3Ru_4O_{12}$ perovskites: high dielectric constants and valence degeneracy. *Solid State Sci* 2002;**4**:347.
3. Hutagalung SD, Ibrahim MIM, Ahmad ZA. Microwave assisted sintering of $CaCu_3Ti_4O_{12}$. *Ceram Int* 2008;**34**:939.
4. Wu YJ, Su SH, Wu SY, Chen XM. Microstructures and dielectric properties of spark plasma sintered $Ba_{0.4}Sr_{0.6}TiO_3/CaCu_3Ti_4O_{12}$ composite ceramics. *Ceram Int* 2011;**37**:1979.
5. Liu Y, Chen Q, Zhao X. Dielectric response of Sb-doped $CaCu_3Ti_4O_{12}$ ceramics. *J Mater Sci: Mater Electron* 2014;**25**:1547.
6. Liu Y, Wang W, Huang J, Tang F, Zhu C, Cao Y. Dielectric properties of giant permittivity $NaCu_3Ti_3NbO_{12}$ ceramics. *Ceram Int* 2013;**39**:9201.
7. Kashyap R, Thakur OP, Tandon RP. Study of structural, dielectric and electrical conduction behaviour of Gd substituted $CaCu_3Ti_4O_{12}$ ceramics. *Ceram Int* 2012;**38**:3029.
8. Kashyap R, Mishra RK, Thakur OP, Tandon RP. Structural, dielectric properties and electrical conduction behaviour of Dy substituted $CaCu_3Ti_4O_{12}$ ceramics. *Ceram Int* 2012;**38**:6807.
9. de la Rubia MA, Leret P, del Campo A, Alonso RE, López-Garcia AR, Fernández JF, et al. Dielectric behaviour of Hf-doped $CaCu_3Ti_4O_{12}$ ceramics obtained by conventional synthesis and reactive sintering. *J Eur Ceram Soc* 2012;**32**:1691.
10. Yang Z, Zhang L, Chao X, Xiong L, Liu J. High permittivity and low dielectric loss of the $Ca_{1-x}Sr_xCu_3Ti_4O_{12}$ ceramics. *J Alloys Compd* 2011;**509**:8716.
11. Jumpatam J, Putasaeng B, Yamwong T, Thongbai P, Maensiri S. A novel route to greatly enhanced dielectric permittivity with reduce loss tangent in $CaCu_{3-x}Zn_xTi_4O_{12}/CaTiO_3$ composites. *J Am Ceram Soc* 2014;**97**:2368.
12. Kwon S, Huang C-C, Patterson EA, Cann DP, Alberta EF, Kwon S, et al. The effect of Cr_2O_3, Nb_2O_5 and ZrO_2 doping on the dielectric properties of $CaCu_3Ti_4O_{12}$. *Mater Lett* 2008;**62**:633.
13. Hao W, Zhang J, Tan Y, Su W. Giant dielectric-permittivity phenomena of compositionally and structurally $CaCu_3Ti_4O_{12}$-like oxide ceramics. *J Am Ceram Soc* 2009;**92**:2937.
14. Liu J, Duan C-G, Yin W-G, Mei W, Smith R, Hardy J. Large dielectric constant and Maxwell–Wagner relaxation in $Bi_{2/3}Cu_3Ti_4O_{12}$. *Phys Rev B: Condens Matter* 2004;**70**:144106.
15. Shri Prakash B, Varma KBR. Microstructural and dielectric properties of donor doped (La^{3+}) $CaCu_3Ti_4O_{12}$ ceramics. *J Mater Sci: Mater Electron* 2006;**17**:899.
16. Liu Z, Chao X, Liang P, Yang Z, Zhi L. Differentiated electric behaviors of $La_{2/3}Cu_3Ti_4O_{12}$ ceramics prepared by different methods. *J Am Ceram Soc* 2014;**97**:2154.
17. Liang P, Yang Z, Chao X, Liu Z. Giant dielectric constant and good temperature stability in $Y_{2/3}Cu_3Ti_4O_{12}$ ceramics. *J Am Ceram Soc* 2012;**95**:2218.
18. Liang P, Chao X, Wang F, Liu Z, Yang Z. The lowered dielectric loss and grain-boundary effects in La-doped $Y_{2/3}Cu_3Ti_4O_{12}$ ceramics. *J Am Ceram Soc* 2013;**96**:3883.
19. Liang P, Chao X, Yang Z. Low dielectric loss, dielectric response, and conduction behavior in Na-doped $Y_{2/3}Cu_3Ti_4O_{12}$ ceramics. *J Appl Phys* 2014;**116**:044101.
20. Ren H, Liang P, Yang Z. Processing, dielectric properties and impedance characteristics of $Na_{0.5}Bi_{0.5}Cu_3Ti_4O_{12}$ ceramics. *Mater Res Bull* 2010;**45**:1608.
21. Yang Z, Ren H, Chao X, Liang P. High permittivity and low dielectric loss of $Na_{0.5}Bi_{0.5-x}La_xCu_3Ti_4O_{12}$ ceramics. *Mater Res Bull* 2012;**47**:1273.
22. Tuichai W, Thongbai P, Amornkitbamrung V, Yamwong T, Maensiri S. $Na_{0.5}Bi_{0.5}Cu_3Ti_4O_{12}$ nanocrystalline powders prepared by a glycine–nitrate process: preparation, characterization, and their dielectric properties. *Microelectron Eng* 2014;**126**:118.
23. Xu B, Zhang J, Tian Z, Yuan SL. Synthesis, dielectric and nonlinear electrical properties of $Na_{1/2}Bi_{1/2}Cu_3Ti_4O_{12}$ ceramics by a sol–gel technique. *Mater Lett* 2012;**75**:87.
24. Qiu Y, Ma ZZ, Huo SX, Duan HN, Tian ZM, Yuan SL, et al. Giant dielectric and low voltage varistor behaviors of Ba-doped $Bi_{1/2}Na_{1/2}Cu_3Ti_4O_{12}$ ceramics. *J Mater Sci: Mater Electron* 2012;**23**:1587.
25. Liang P, Li Y, Li F, Chao X, Yang Z. Effect of the synthesis route on the phase formation behavior and electric property of $Na_{0.5}Bi_{0.5}Cu_3Ti_4O_{12}$ ceramics. *Mater Res Bull* 2014;**52**:42.

26. Somphan W, Thongbai P, Yamwong T, Maensiri S. High Schottky barrier at grain boundaries observed in $Na_{1/2}Sm_{1/2}Cu_3Ti_4O_{12}$ ceramics. *Mater Res Bull* 2013;**48**:4087.
27. Somphan W, Sangwong N, Yamwong T, Thongbai P. Giant dielectric and electrical properties of sodium yttrium copper titanate: $Na_{1/2}Y_{1/2}Cu_3Ti_4O_{12}$. *J Mater Sci: Mater Electron* 2012;**23**:1229.
28. Thongbai P, Yamwong T, Maensiri S. Dielectric properties and electrical response of grain boundary of $Na_{1/2}La_{1/2}Cu_3Ti_4O_{12}$ ceramics. *Mater Res Bull* 2012;**47**:432.
29. Liu Z, Chao X, Yang Z. Preparation process, microstructure and dielectric properties of $Na_{0.5}La_{0.5}Cu_3Ti_4O_{12}$ ceramics by a sol–gel method. *J Mater Sci: Mater Electron* 2014;**25**:2096.
30. Sebald J, Krohns S, Lunkenheimer P, Ebbinghaus SG, Riegg S, Reller A, et al. Colossal dielectric constants: a common phenomenon in $CaCu_3Ti_4O_{12}$ related materials. *Solid State Commun* 2010;**150**:857.
31. Schmidt R, Stennett MC, Hyatt NC, Pokorny J, Prado-Gonjal J, Li M, et al. Effects of sintering temperature on the internal barrier layer capacitor (IBLC) structure in $CaCu_3Ti_4O_{12}$ (CCTO) ceramics. *J Eur Ceram Soc* 2012;**32**:3313.
32. Li M, Shen Z, Nygren M, Feteira A, Sinclair DC, West AR. Origin(s) of the apparent high permittivity in $CaCu_3Ti_4O_{12}$ ceramics: clarification on the contributions from internal barrier layer capacitor and sample-electrode contact effects. *J Appl Phys* 2009;**106**:104106.
33. Krohns S, Lunkenheimer P, Ebbinghaus SG, Loidl A. Colossal dielectric constants in single-crystalline and ceramic $CaCu_3Ti_4O_{12}$ investigated by broadband dielectric spectroscopy. *J Appl Phys* 2008;**103**:084107.
34. Jia R, Zhao X, Li J, Tang X. Colossal breakdown electric field and dielectric response of Al-doped $CaCu_3Ti_4O_{12}$ ceramics. *Mater Sci Eng B* 2014;**185**:79.
35. Ni L, Chen XM. Enhancement of giant dielectric response in $CaCu_3Ti_4O_{12}$ ceramics by Zn substitution. *J Am Ceram Soc* 2010;**93**:184.
36. Yu R, Xue H, Cao Z, Chen L, Xiong Z. Effect of oxygen sintering atmosphere on the electrical behavior of CCTO ceramics. *J Eur Ceram Soc* 2012;**32**:1245.
37. Chung S-Y, Kim I-D, Kang S-JL. Strong nonlinear current–voltage behaviour in perovskite-derivative calcium copper titanate. *Nat Mater* 2004;**3**:774.

Available online at www.sciencedirect.com

ScienceDirect

Journal of the European Ceramic Society 34 (2014) 2941–2950

www.elsevier.com/locate/jeurceramsoc

A novel strategy to enhance dielectric performance and non-Ohmic properties in $Ca_2Cu_{2-x}Mg_xTi_4O_{12}$

Jutapol Jumpatam [a], Bundit Putasaeng [b], Teerapon Yamwong [b], Prasit Thongbai [c,d,*], Santi Maensiri [e]

[a] *Materials Science and Nanotechnology Program, Faculty of Science, Khon Kaen University, Khon Kaen 40002, Thailand*
[b] *National Metal and Materials Technology Center (MTEC), Thailand Science Park, Pathumthani 12120, Thailand*
[c] *Integrated Nanotechnology Research Center (INRC), Khon Kaen University, Khon Kaen 40002, Thailand*
[d] *Department of Physics, Faculty of Science, Khon Kaen University, Khon Kaen 40002, Thailand*
[e] *School of Physics, Institute of Science, Suranaree University, Nakhon Ratchasima 30000, Thailand*

Received 31 January 2014; received in revised form 17 April 2014; accepted 19 April 2014
Available online 13 May 2014

Abstract

A novel strategy to improve the dielectric and non-Ohmic properties of $CaCu_3Ti_4O_{12}$ ceramics that deliberately created a binary-phase system of $CaCu_{3-x}Mg_xTi_4O_{12}/CaTiO_3$ was proposed and can be performed with a starting nominal formula of $Ca_2Cu_{2-x}Mg_xTi_4O_{12}$. Mg^{2+} doping ions were preferentially incorporated only into the $CaCu_3Ti_4O_{12}$ phase. Substitution of Mg^{2+} into $CaCu_3Ti_4O_{12}/CaTiO_3$ can cause a significant increase in dielectric permittivity and a large reduction of the loss tangent to <0.015 at 1 kHz; while, retaining excellent temperature dielectric-stability. Sintering time had a slight influence on the dielectric properties, but remarkable effects upon the nonlinear electrical properties of $CaCu_{3-x}Mg_xTi_4O_{12}/CaTiO_3$ ceramics. Degradation of nonlinear properties with increased sintering time is suggested to be the result of the dominant effect of oxygen vacancies. Impedance spectroscopy analysis demonstrated that improved dielectric and nonlinear properties could be attributed to the enhanced electrical responses of $CaCu_3Ti_4O_{12}$–$CaTiO_3$ and $CaCu_3Ti_4O_{12}$–$CaCu_3Ti_4O_{12}$ interfaces resulting from Mg^{2+} doping ions.

Keywords: Ceramic composite; Dielectric properties; Varistor; Impedance spectroscopy; Loss tangent

1. Introduction

Over the past few years, $CaCu_3Ti_4O_{12}$ (CCTO) has been extensively studied in the field of high-permittivity dielectric materials. This is due to the fascinating physics underlying the origin of an ultra-high dielectric permittivity (ε') in CCTO without any detectable phase transition over a wide temperature range. It holds promise for a new generation of multilayer ceramic capacitors.[1–16] The origin of the giant dielectric response in CCTO is still unclear today. According to several elegant works, CCTO is clearly electrically heterogeneous, consisting of *n*-type semiconducting grains and relatively low conductivity at grain boundaries (GBs).[2,4] Therefore, it is believed that the overall dielectric performance can be tuned by engineering the internal interfaces at the GBs. Generally, $\tan\delta$ of CCTO ceramics is still too high (>0.05).[1,5,8–10] This is one of the most serious problems preventing the use of CCTO ceramics in practical applications. Another difficulty is the poor temperature stability of ε', $\Delta\varepsilon'(\%) = [(\varepsilon'_T - \varepsilon'_{RT})]/\varepsilon'_{RT}) \times 100$, where ε'_{RT} and ε'_T are ε' (at 10^3 Hz) at room temperature and at any selected temperature, respectively. Usually, ε' at 10^3 Hz of CCTO-based compounds is strongly dependent on temperature when temperatures are higher than 100 °C.[17–21] Such an increase in the ε' value is also accompanied by an increase in the low-frequency $\tan\delta$. These undesirable behaviors are closely associated with high dc conductivity (σ_{dc}).[22]

Generally, lowering σ_{dc} to reduce low-frequency $\tan\delta$ can be done by enhancing the resistances of internal interfaces in

* Corresponding author at: Department of Physics, Faculty of Science, Khon Kaen University, Khon Kaen 40002, Thailand. Tel.: +66 84 4190266; fax: +66 43 202374.
E-mail addresses: pthongbai@kku.ac.th, prasitphysics@hotmail.com (P. Thongbai).

http://dx.doi.org/10.1016/j.jeurceramsoc.2014.04.037
0955-2219/

CCTO-based compounds. These could be the interface between grains (GB) or the interface between a CCTO grain and a second phase particle. Enhancement may be accomplished by (1) doping CCTO with suitable metal ions to intrinsically improve electrical properties of GBs,[5,18,20,23] (2) altering Ca^{2+} and Cu^{2+} molar ratios to produce CCTO/$CaTiO_3$ (CTO) composites,[6,7,24–29] (3) filling oxygen vacancies at GBs,[30] among others. Unfortunately, improved dielectric properties of CCTO produced using these strategies rarely result in materials that fulfill all of the requirements of electronic applications, *i.e.*, high ε', low $\tan\delta$, and dielectric response with good temperature stability. It was also found that most of the metal ion substitutions or other strategies, which have been successfully used to improve a particular dielectric property, simultaneously worsen other important dielectric properties of CCTO. For example, a large decrease in $\tan\delta$ (~0.02 at 1 kHz) observed in a binary compound system of $Ca_2Cu_2Ti_4O_{12}$ (consisting of 33.3 mol% of CCTO and 66.7 mol% of CTO) caused a large decrease in ε' ($\sim 2 \times 10^3$).[6,26] Given a very low-$\tan\delta$ value of CCTO/CTO, with its low-ε' value are still acceptable values for use in capacitor applications compared to commercial $BaTiO_3$ and $Pb(Sc_{1/2}Ta_{1/2})O_3$ ceramics.[6] Unfortunately, the condition of $\Delta\varepsilon'(\%) < \pm 15\%$ within CCTO/CTO exists only in a narrow temperature range of −60 to 90 °C.[26,29] Hence, these properties are consistent with the EIA temperature standard for application in X5R capacitor only, but not for X7R or X8R capacitors.[31] It is very important to note the advantages of CCTO/CTO composite ceramics. First, this composite system can be synthesized using a one-step process from a nominal composition of $Ca_2Cu_2Ti_4O_{12}$.[6,25–29] Second, this composite ceramic showed no piezoelectricity, which is advantageous to reduce mechanical damage in ac operation.[1,6] Third, its sintering temperature is lower than that of $BaTiO_3$.[6,26,29] Thus, it is better if all of the dielectric properties of $Ca_2Cu_2Ti_4O_{12}$ ceramics can simultaneously be improved. This will support progress in communications technology. Enhanced ε', reduced $\tan\delta$, and increased $\Delta\varepsilon'(\%)$ are valuable for enhancing volumetric efficiency, reducing dissipation of stored energy into heat, and extending the temperature use range of capacitors, respectively.

It was reported that Mg^{2+} substitution in CCTO ceramics can enhance their dielectric response.[8,9] Interestingly, low-frequency $\tan\delta$ values of Mg-doped CCTO ceramics were slightly reduced to ≈0.05 compared to un-doped CCTO.[8] Although this value is still slightly higher than the standard value, these behaviors are rarely found in CCTO ceramics. Normally, the variation of both ε' and $\tan\delta$ are directly proportional.[10] It is likely that the temperature stability of Mg-doped CCTO was slightly higher than the un-doped material.[8] We hypothesize that substitution of Mg^{2+} into $Ca_2Cu_2Ti_4O_{12}$ ceramics may enhance the overall dielectric properties if the majority of Mg^{2+} doping ions are substituted into Cu^{2+} sites of the CCTO phase. Therefore, the aim of this work was to provide a novel strategy to improve the overall dielectric properties of CCTO-based ceramics by substitution of Mg^{2+} ions to a binary compound system of $Ca_2Cu_2Ti_4O_{12}$ to form $CaCu_{3-x}Mg_xTi_4O_{12}$/$CaTiO_3$ composite ceramics.

2. Experimental procedure

An Mg-doped binary compound $Ca_2Cu_2Ti_4O_{12}$ system with a nominal chemical composition of $Ca_2Cu_{2-x}Mg_xTi_4O_{12}$ ($x = 0$, 0.05, 0.10, 0.20, and 0.30) ceramics was prepared using a solid state reaction method. These materials are referred to as CCTO/CTO, Mg05, Mg10, Mg20, and Mg30 ceramics, respectively. $CaCO_3$ (Cerac, 99.95% purity), CuO (Cerac, 99.9% purity), TiO_2 (Sigma–Aldrich, 99.9% purity), and MgO (Sigma–Aldrich, 99.99% purity) were used as starting raw materials. A stoichiometric mixture of the starting materials for each composition was ball-milled in ethanol for 24 h using ZrO_2 balls. The mixed slurries were dried and then calcined at 900 °C for 15 h. The calcined powders were ground and pressed into pellets (without a binder) of 9.5 mm diameter and ~1.0 mm thickness by uniaxial compression at 200 MPa. Finally, these pellets were sintered at 1100 °C for 6 and 24 h.

X-ray diffraction (XRD; PW3040, Philips, the Netherlands) was used to characterize the phase compositions and crystal structures of the sintered $Ca_2Cu_{2-x}Mg_xTi_4O_{12}$ composite system. Scanning electron microscopy (SEM; LEO 1450VP; Cambridge, UK) and energy-dispersive X-ray spectrometry (EDS) were used to reveal the distribution of CCTO and CTO phases as well as the chemical elements in the sintered ceramics. The capacitance and dispassion factor (D or $\tan\delta$) of the ceramic samples were measured using an Agilent 4294A Precision Impedance Analyzer over the frequency and temperature ranges of 10^2–10^7 Hz and −70 to 200 °C, respectively. Current–voltage measurements were made at room temperature using a high voltage measurement unit (Keithley Model 247, Estado St. Pasadena, CA). Before measurements, Au was sputtered on each pellet face at a current of 25 mA for 8 min using a Polaron SC500 sputter coating unit (Sussex, UK). The breakdown electric field (E_b) was achieved at a current density of $J = 1$ mA cm^{-2}. The nonlinear coefficient (α) was calculated from the following formula:

$$\alpha = \frac{\log(J_2/J_1)}{\log(E_2/E_1)}, \quad (1)$$

where E_1 and E_2 represent the electric fields corresponding to $J_1 = 1$ and $J_2 = 10$ mA cm^{-2}, respectively.

3. Results and discussion

Fig. 1 shows the XRD patterns of $Ca_2Cu_{2-x}Mg_xTi_4O_{12}$ ($x = 0$, 0.05, 0.10, 0.20, and 0.30) ceramics sintered for 24 h. All of the 24 h samples (as well as the 6 h samples) consisted of two phases of CCTO (JCPDS 75-2188) and CTO (JCPDS 82-0231). This result is similar to that reported in the literature.[24–29,32,33] According to the nominal formula of $Ca_2Cu_2Ti_4O_{12}$, two phases of ~33.3 mol% of CCTO and ~66.7 mol% of CTO should be formed due to the imbalance between Ca^{2+} and Cu^{2+} ions. This is confirmed by a Rietveld quantitative analysis of a $Ca_2Cu_2Ti_4O_{12}$ ceramic as reported in the literature.[28] The ionic radius of Ca^{2+} is much larger than that of Cu^{2+}. As a result, Ca^{2+} cannot enter into Cu^{2+} sites in a planar square to form $Ca(CaCu_2)Ti_4O_{12}$ structure. Interestingly, no impurity related to Mg^{2+} doping ions

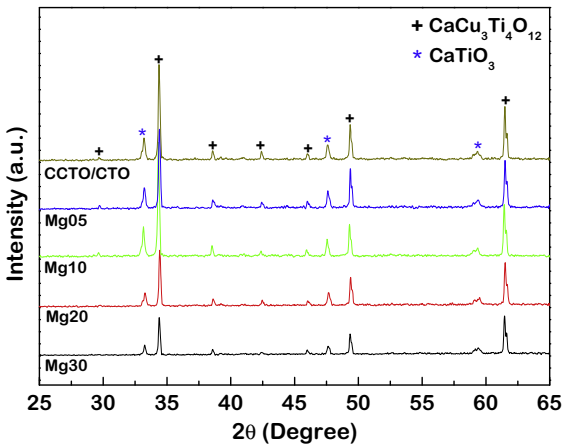

Fig. 1. XRD patterns of CCTO/CTO and Mg-doped CCTO/CTO composite ceramics sintered for 24 h.

was observed. This likely indicates the formation of a solid solution between the Mg^{2+} doping ions and CCTO, CTO or both. To clarify this, lattice parameters (a) of the CCTO phase in all composite ceramics were calculated and are summarized in Table 1. These values showed no significant change even through the Mg^{2+} concentration was increased to $x = 0.3$. There are two possible mechanisms that may be responsible for this observation. First, Cu^{2+} might form a solid solution with CTO phase, leading to an unchanged lattice parameter value of the CCTO structure. Second, Mg^{2+} ions might replace Cu^{2+} sites in the CCTO phase, forming a solid solution with the CCTO phase. In the latter explanation, the a value of a CCTO phase is unchanged due to the same ionic radii of Mg^{2+} ($r_4 = 0.57$ Å) and Cu^{2+} ($r_4 = 0.57$ Å) ions.[34]

Fig. 2(a)–(e) and (f)–(j) shows backscattered SEM images of the polished 24 h samples and 6 h samples, respectively. Two phases with different contrasts were observed, *i.e.*, darker and lighter phases. This observation is consistent with the XRD result and similar to those reported in the literature for un-doped $Ca_2Cu_2Ti_4O_{12}$ ceramics.[27–29] As shown in Fig. 3(a) and (b), the darker and lighter phases are clearly CTO and CCTO phases, respectively. Only the EDS peaks corresponding to Ca, Ti, and O appeared in the EDS spectra measured in the darker region. All possible EDS peaks for Ca, Cu, Ti, O, and Mg were detected in the lighter CCTO phase. This clearly indicates that Mg^{2+} doping ions preferentially form solid solution only within the CCTO phase. Therefore, it is likely that Mg^{2+} ions were substituted into Cu^{2+} sites in the CCTO phase. Thus, it is reasonable to suggest that the prepared $Ca_2Cu_{2-x}Mg_xTi_4O_{12}$ ceramics consist of ~33.3 mol% of $CaCu_{3-x}Mg_xTi_4O_{12}$ ($x = 0$, 0.05, 0.10, 0.20, 0.30) and ~66.7 mol% of CTO.

As shown in Fig. 2(a) and (f), the distribution of CCTO and CTO phases in the microstructures of the CCTO/CTO samples sintered for 24 and 6 h is quite uniform. The mean grain sizes of the CCTO phase in the CCTO/CTO samples sintered for 24 and 6 h were estimated to be ~2.90 ± 0.97 and ~3.07 ± 0.77 μm, respectively; whereas, the mean grain sizes of the CTO phase are of about ~1.96 ± 0.48 and ~2.09 ± 0.47 μm, respectively. The sintering time has no significant influence on the microstructural evolution of CCTO/CTO composites. It is worth noting that the mean grain sizes of CCTO phase in the CCTO/CTO samples are smaller than the mean grain size of ~7 μm for the sample sintered at 1050 °C for 0.5 h sintered using a microwave sintering method.[7] Ramírez et al.[27,28] found that the CCTO/CTO ceramic sintered at 1100 °C for 3 h using a conventional furnace exhibited two different grain size distributions for the CCTO phase with mean grain sizes of $d = 10$–15 and 3–4 μm. Grain sizes of the CTO phase of the CCTO/CTO composites sintered using a microwave and conventional furnace were found to be ~2 and ~4 μm, respectively[27] [see Figs. 2(a) and 3(a) in Ref. 27]. These values are closed to grain sizes of ~2–3 μm of the CTO phase in the CCTO/CTO samples presented in this work.

After doping adding Mg^{2+} ions with $x = 0.05$ and 0.10 (sintered for 24 h), some grains of the CCTO phase increased to sizes of ~8–20 μm with the mean grain size of ~11.1 ± 4.6 μm for the Mg05 sample. For the Mg05 sample sintered for 6 h, large grain sizes of the CCTO phase were also observed with the mean grain size of ~4.74 ± 2.46 μm. The mean grain sizes of the CTO phase in the Mg05 samples sintered for 24 and 6 h were estimated to be ~3.61 ± 0.95 and ~2.42 ± 0.69 μm, respectively. For the samples sintered for 24 h with $x = 0.20$–0.30 and the samples sintered for 6 h with $x = 0.10$–0.30, the grain sizes of CCTO and CTO phases become homogeneous. Morphologies of both CCTO and CTO phases of these samples were well dispersed and separate from each other. Large

Table 1
Lattice parameter (a), ε' and $\tan\delta$ (at 1 kHz and 30 °C), resistance at GBs (R_{gb}) at 120 °C, nonlinear coefficient (α), and breakdown field strength (E_b).

Sample	a (Å)	ε'	$\tan\delta$	R_{gb} (MΩ cm)	α	E_b (V/cm)
Sintered for 6 h						
CCTO/CTO	7.388	2182	0.023	0.62	13.1	8211
Mg05	7.386	3372	0.014	0.83	11.9	7811
Mg10	7.382	3298	0.011	1.52	20.7	10,221
Mg20	7.390	2748	0.015	2.62	18.5	10,869
Mg30	7.390	3550	0.014	1.77	27.2	8859
Sintered for 24 h						
CCTO/CTO	7.389	1877	0.075	0.33	9.9	5817
Mg05	7.391	6824	0.020	0.17	7.3	3452
Mg10	7.391	5201	0.011	0.72	8.1	5088
Mg20	7.391	4903	0.017	0.78	7.5	4486
Mg30	7.395	4810	0.023	0.46	9.5	5700

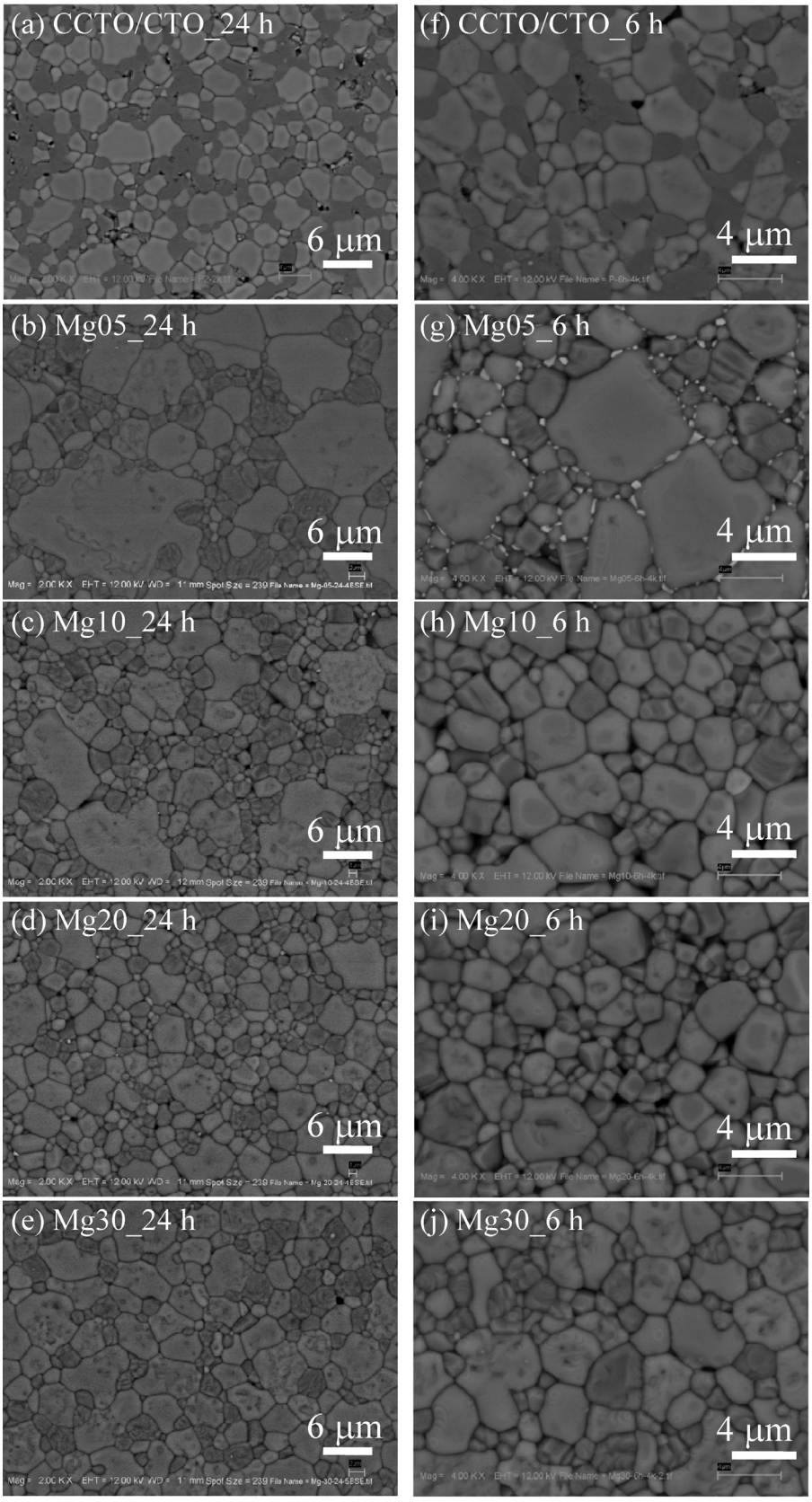

Fig. 2. (a)–(e) Backscattered SEM images of polished-surfaces of CCTO/CTO, Mg05, Mg10, Mg20, and Mg30 samples sintered for 24 h, respectively. (f)–(j) Backscattered SEM images of polished-surfaces of CCTO/CTO, Mg05, Mg10, Mg20, and Mg30 samples sintered for 6 h, respectively.

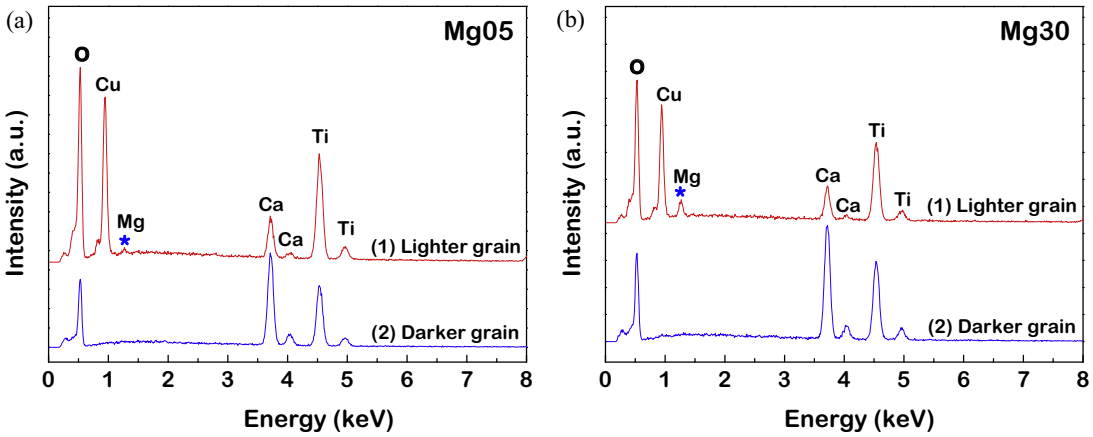

Fig. 3. EDS spectra of the (a) Mg05 and (b) Mg30 samples detected at a darker and lighter regions.

clusters of CTO grains no longer appeared. The mean grain sizes of the CCTO and CTO phases in the Mg10, Mg20, and Mg30 samples sintered for 24 h were estimated to be ~4.82 ± 2.7 and ~2.66 ± 0.74 μm, ~3.09 ± 1.04 and ~2.08 ± 0.39 μm, and ~5.11 ± 1.4 and ~3.12 ± 0.68 μm, respectively. For the 6 h samples, the mean grain sizes of the CCTO and CTO phases in these compositions were ~3.03 ± 0.86 and ~2.14 ± 0.54 μm, ~2.65 ± 0.72 and ~1.75 ± 0.32 μm, and ~3.12 ± 0.98 and ~1.88 ± 0.61 μm, respectively.

Grain sizes of the CTO phase in these samples showed slight change. As reported by Ni and Chen,[9] the mean grain size of CCTO ceramics was increased by doping with Mg^{2+}. This indicates the ability of Mg^{2+} doping ions to increase the sintering rate of CCTO ceramics through the liquid phase sintering mechanism. In CCTO-based ceramic oxides, the grain growth is widely accepted to be primarily caused by the liquid phase sintering mechanism.[35,36] It is possible that, during the sintering, the formation of MgO-related liquid phase in the microstructures of Mg^{2+}-doped CCTO/CTO composites occurred. Liquid phases have long been referred as a primary cause of abnormal grain growth. Usually, physical and chemical inhomogeneities, such as inhomogeneous packing of powders and non-uniform distribution of dopants, can result in local variation in the microstructure.[37] This was considered a main cause of abnormal grain growth. Thus, it is likely that the abnormal grain growth of CCTO phase in the Mg05 (sintered for 6 and 24 h) and Mg10 (sintered for 24 h) composite samples may be caused by a local liquid phase sintering because of non-uniform distribution of Mg^{2+} doping ions in the green body of composites. The local liquid phase sintering produces inequalities in the GB mobility, resulting in the initiation of abnormal growth.[37] When the concentration of Mg^{2+} doping ions increased, it may be well distributed throughout the compacted powders. On heating, equalities in the GB mobility are approximately equal throughout the composite microstructure, leading to a normal grain growth. Thus, homogeneous microstructure of the composite ceramics with high concentration of Mg^{2+} was achieved in this way.

Fig. 4(a)–(b) and their insets show the frequency dependence of ε' and $\tan\delta$ at 30 °C for the 6 h and 24 h samples, respectively. Interestingly, ε' values of all the samples were independent of frequency in the range from 10^2 to 10^5 Hz. ε' values of all Mg-doped CCTO/CTO ceramics were higher than for un-doped ceramics. It is worth noting that a low-frequency $\tan\delta$ of CCTO/CTO was remarkably reduced by doping with Mg^{2+}. ε' and $\tan\delta$ (1 kHz and 30 °C) of all composite ceramics are summarized in Table 1. ε' values of the un-doped

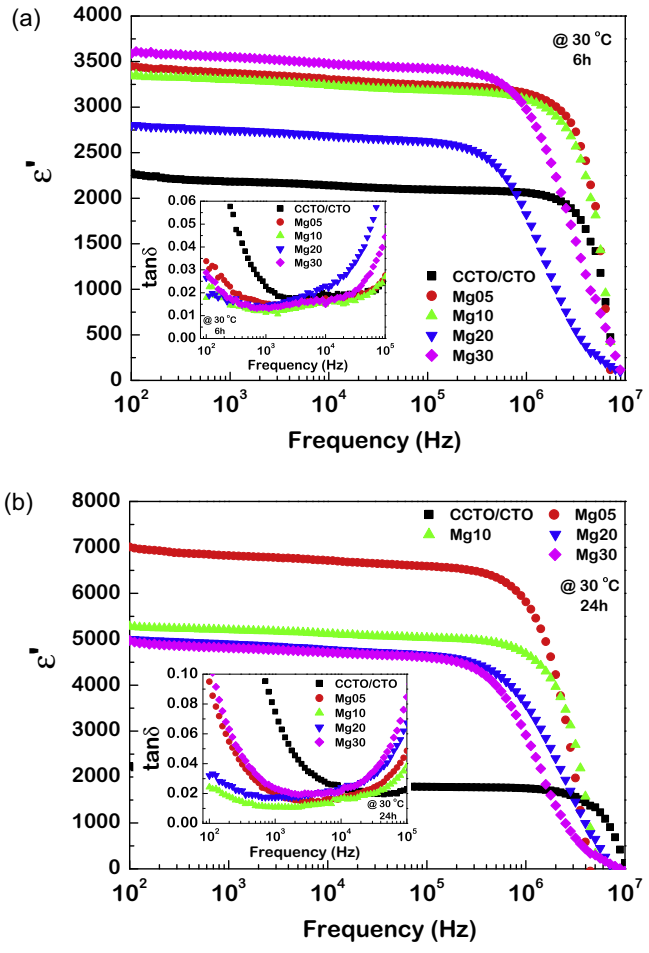

Fig. 4. Frequency dependence of ε' for the ceramic samples sintered for (a) 6 and (b) 24 h; their insets show $\tan\delta$ as a function of frequency.

CCTO/CTO samples sintered for 6 and 24 h are close to the ε' value of ~1800 for a sample sintered at 1090 °C for 24 h, as first reported by Kobayashi and Terasaki.[6] However, these two values are larger than the ε' value of ~1300 for the sample sintered at 1050 °C for 0.5 h sintered using a microwave sintering method.[7] Ramírez et al.[27] found $\varepsilon' \sim 2960$ at 1 kHz for CCTO/CTO ceramic sintered at 1100 °C for 3 h using a conventional furnace. According to our previous work,[26] $\varepsilon' \sim 2104$ at 1 kHz was obtained in a CCTO/CTO ceramic sintered at 1050 °C for 10 h. These indicate that the sintering method and sintering conditions have an influence on ε' of a CCTO/CTO ceramic system.

Interestingly, ε' values of the Mg^{2+}-doped CCTO/CTO composites sintered for 24 h were about 2–3 times larger than that of the un-doped ceramics. Notably, their tan δ values were reduced by factors of 3–6. It was seen that after increasing sintering time from 6 to 24 h, ε' of Mg-doped CCTO/CTO composites increased by a factor of 1.5–2 over that of samples sintered for 6 h, while tan δ slightly changed. At 10^2 Hz, the values of tan δ at 30 °C of the CCTO/CTO, Mg05, Mg10, Mg20, and Mg30 samples sintered at 1100 °C for 6 h were found to be 0.118, 0.034, 0.018, 0.026, and 0.029, respectively, while tan δ values of the 24 h samples were 0.303, 0.095, 0.024, 0.032, and 0.107, respectively. For the 6 h and 24 h samples, tan δ values at the low frequency of 10^2 Hz for all Mg-doped CCTO/CTO composites were significantly reduced compared to the un-doped CCTO/CTO samples sintered for the same time. As is well known, dc conduction in dielectric materials leads to an apparently high value of low-frequency tan δ at room temperature and higher,[22] *i.e.*, $\tan\delta \approx \sigma_{dc}/\omega\varepsilon_0\varepsilon'_s$, where ε'_s is the dielectric permittivity in a low-frequency range. This large reduction in tan δ is therefore attributed to a strong reduction of σ_{dc} in these samples.

For the 6 h samples, the Mg30 sample exhibited the highest ε'; while, ε' of the Mg30 sample was found to be highest among the 24 h samples. It is widely believed that the giant ε' of CCTO ceramics is attributed to the interfacial polarization at the GBs through the internal barrier layer capacitor (IBLC) effect.[2,5,12,15,18,23] This polarization is likely to be a cause of high dielectric response in CCTO/CTO composites as well. According to the IBLC model, ε' is associated with the area of insulating GB layer between grains, which is approximately equal to the mean grain size, and the GB capacitance that related to the intrinsic GB dielectric permittivity. Schmidt et al.[15] found that the GB dielectric permittivity strongly increased with sintering temperature. They have suggested this observation as a result of chemical changes, even though it is difficult to detect significant changes in defect chemistry. By using this model, a higher value of ε' for the Mg30 sample (sintered for 6 h) should be primarily attributed to stronger enhanced dielectric response of the GBs. For the 24 h samples, the mean grain size of the Mg05 samples is much larger than those of other samples. Thus, ε' of the Mg05 sample might be dominated by the grain size effect over the improved electrically active of interfaces.

The temperature dependencies of ε' at 1 kHz for all the 6 h and 24 h samples are shown in Fig. 5(a) and (b), respectively. When the temperature is higher than 100 °C, ε' rapidly increases in value. The temperature dependence of ε' in un-doped CCTO/CTO ceramics was similar to that observed in CCTO ceramics.[8–10,21] Mg^{2+} substitution into CCTO/CTO ceramics not only caused an increase in ε' and reduction of tan δ, but also can contribute to the temperature stability of ε'. The temperature dependencies of tan δ at 1 kHz for all the 6 h and 24 h samples are shown in Fig. 5(c) and (d), respectively. When the temperature is higher than 100 °C, tan δ is higher than 0.1 for Mg-doped CCTO/CTO composites. The large increase in tan δ at high temperatures is consistent with the increase in ε'. It is likely that the large value of tan δ in a high temperature range is one of the most serious problem for using CCTO-based compounds in high temperatures. Further investigation is needed to improve high-temperature tan δ of CCTO ceramics. As shown in Fig. 5(e), for the 6 h samples, the conditions of $\Delta\varepsilon' < \pm 15\%$ for the CCTO/CTO, Mg05, Mg10, Mg20, and Mg30 samples were found to be in the temperature ranges of −60 °C to 90 °C, −60 °C to 120 °C, −60 °C to 140 °C, −60 °C to 160 °C, and −60 °C to 170 °C, respectively. Dielectric properties of these samples satisfy the EIA X5R, X5R, X7R, X8R, and X8R standard capacitor specifications, respectively. It is worth noting that the temperature stability of ε' in CCTO-based compounds satisfying the X8R capacitor requirement was rarely reported.[38,39] Thus, substitution of Mg^{2+} into a $Ca_2Cu_2Ti_4O_{12}$ binary system is one of the most effective and interesting methods to improve the overall dielectric performance of CCTO ceramics, making them suitable for practical application in capacitors.

As shown in Fig. 5(f), conditions where $\Delta\varepsilon' < \pm 15\%$ for the 24 h samples were in the temperature ranges of −60 °C to 60 °C, −60 °C to 100 °C, −60 °C to 130 °C, −60 °C to 140 °C, and −60 °C to 110 °C, respectively. When the sintering time was increased to 24 h, the temperature stability of the un-doped CCTO/CTO sample greatly decreased, putting its properties out of the standard specification. Furthermore, the temperature stability of each Mg^{2+}-doped CCTO/CTO composite also decreased as the sintering time increased to 24 h. $\Delta\varepsilon'(\%)$ values of the Mg05, Mg10, Mg20, and Mg30 samples satisfy the X5R, X7R, X7R, and X5R capacitor applications, respectively. Notably, for the Mg10 and Mg20 samples, ε' increased more than 2 times with high temperature stability and tan δ was reduced by factors of ≈4–6.

Fig. 6 and its inset demonstrate the nonlinear electrical characteristics of the 6 h and 24 h samples, respectively. All the composite ceramics exhibited nonlinear *J–E* behavior. Two important parameters (α and E_b) of all the composites were calculated from these curves and are summarized in Table 1. The overall non-Ohmic results revealed that values of α and E_b for the 24 h samples slightly changed with Mg^{2+} concentration. This is in contrast to their dielectric properties. E_b and α values were reduced by increasing sintering time. Interestingly, an α value of 27.2 observed for the Mg30 sample sintered for 6 h is much larger than that of the CCTO/CTO sample ($\alpha = 13.1$). This result indicates that Mg^{2+} doping ions had significant effects on both the dielectric and nonlinear electrical properties of CCTO/CTO composites sintered for 6 h. The high value of $\alpha = 27.2$ for the Mg30 sample can be compared to

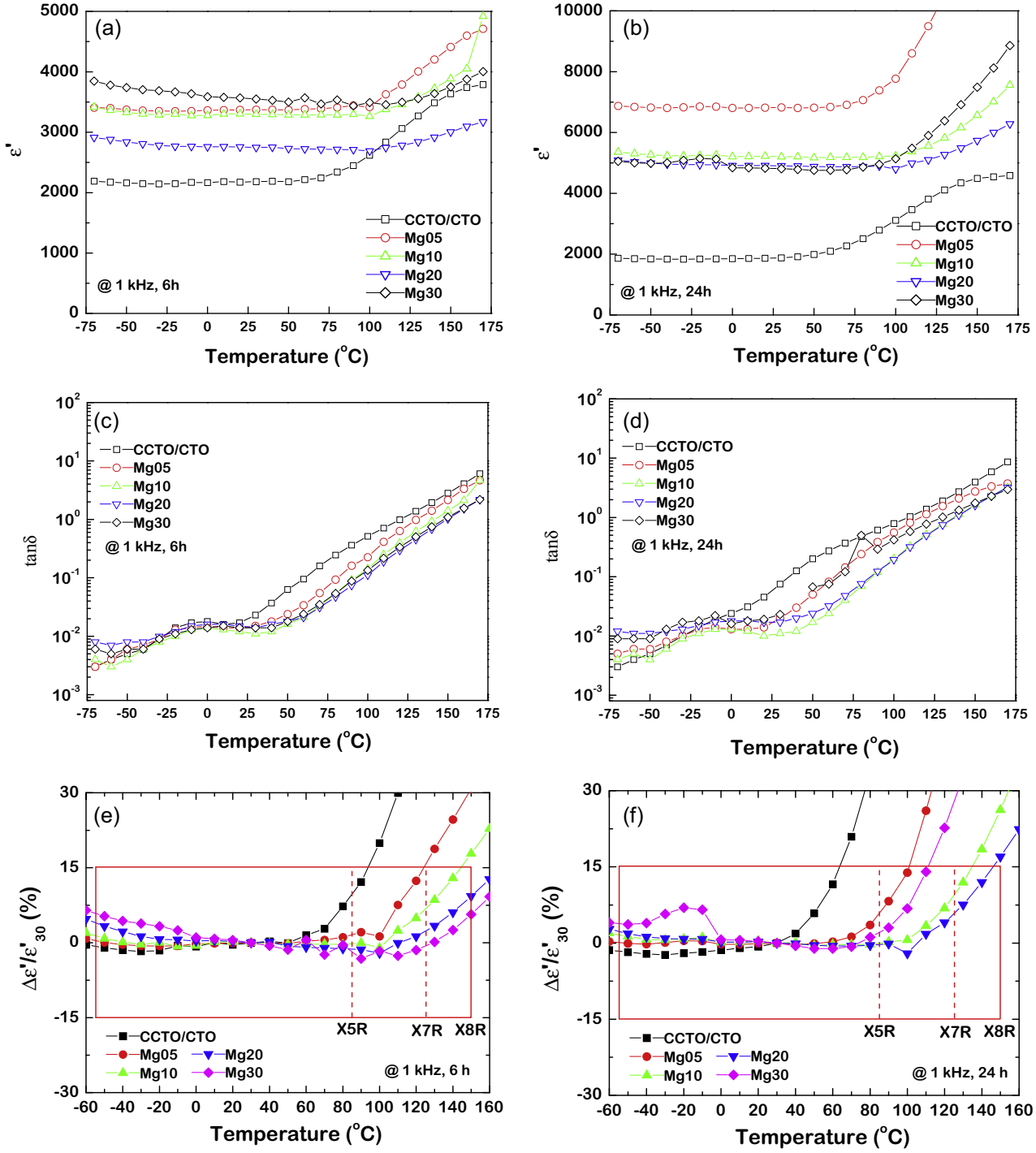

Fig. 5. (a)–(b) Temperature dependence of ε' for the composite ceramics sintered for 6 and 24 h, respectively. (c)–(d) Temperature dependence of tan δ for the composite ceramics sintered for 6 and 24 h, respectively. (e)–(f) Temperature coefficient of ε' at 10^3 Hz for the composite ceramics sintered for 6 and 24 h, respectively: ε'_{30} is the dielectric permittivity at 30 °C.

values of 29.67 and 25.3 achieved in a Tb-doped CCTO ceramic[40] and VO_2 (3 mol%)-added (66.7 mol%)CCTO/(33.7 mol%)CTO ceramic.[24] However, these values are much lower than the value of 42 for un-doped CCTO/CTO ceramic sintered at 1100 °C for 3 h reported by Ramírez et al.[27] It is worth noting that α of CCTO-based ceramics is strongly dependent on the rate increase of applied voltage.[41] α was found to decrease when this rate was increased. In this work, the rate of increase in an applied voltage was 1.33 V/s. Unfortunately, rate of voltage increase used in other work to measure *J–E* characteristics of CCTO/CTO composites has not been reported. Therefore, the large difference in α values in many reports might be due to different rates of voltage increase used in these studies.

To elucidate the possible mechanism(s) of the nonlinear properties and dielectric response in Mg^{2+}-doped CCTO/CTO composites, impedance spectroscopy was used to study

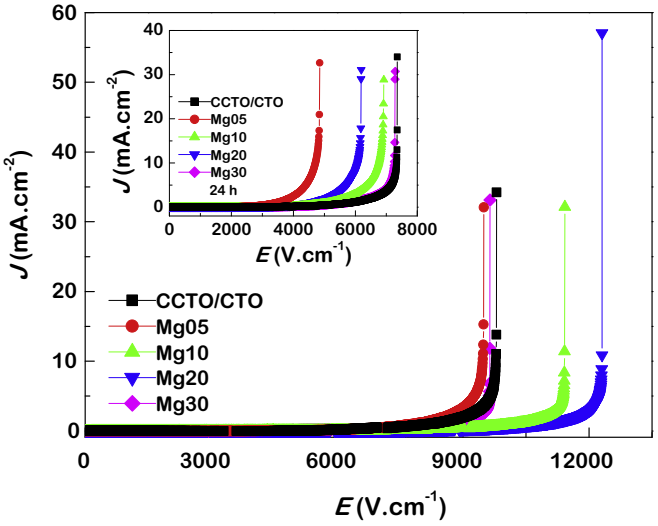

Fig. 6. *J–E* curves of the composite ceramics sintered for 6 h; inset shows *J–E* curves of the ceramics sintered for 24 h.

electrical responses inside the grains and at internal interfaces. Fig. 7 and its inset show impedance complex plane (Z^*) plots at 120 °C for 6 h and 24 h samples, respectively. The total resistance (R_{tot}) was estimated from the diameter of a large semicircle arc of the CCTO/CTO ceramic enhanced by doping with Mg^{2+}, except for the Mg05 sample sintered for 24 h.[2] Generally, R_{tot} is governed by the resistance of GBs (R_{gb}).[2,42] In this CCTO/CTO composite system, GBs or interfaces between grains consist of interfaces between CCTO–CCTO grains, CCTO–CTO grains, and CTO–CTO grains. The R_{gb} values determined at 120 °C for all the samples are summarized in Table 1. According to the microstructure analysis, Mg^{2+} doping ions prefer to form solid solution only within CCTO phase. Thus, the molar ratio and volume fraction of the CTO phase of each composition should ideally be the same. Thus, the difference in R_{gb} values indicated a significant effect of Mg^{2+} doping ions upon the electrical responses of internal interfaces.

According to the previous work of Ramírez et al.,[28] using electrostatic force microscopy (EFM), it was clearly shown that CCTO–CTO and CCTO–CCTO interfaces were electrically

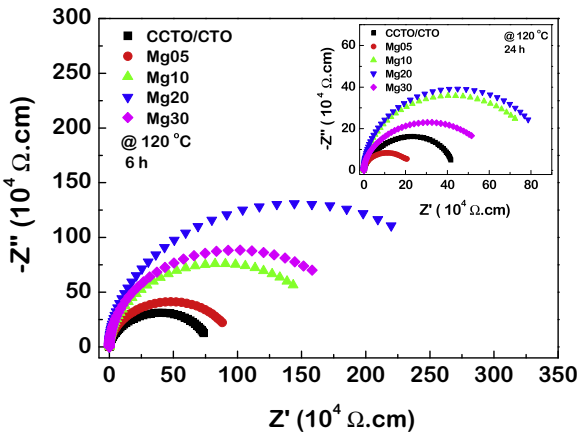

Fig. 7. Impedance complex plane (Z^*) plots at 120 °C for the composites sintered for 6 h; inset shows Z^* plots at 120 °C for the composites sintered for 24 h.

active, indicating the presence of potential barriers. However, a CTO–CTO interface was electrically inactive. This indicates the important role of Cu atoms in generating potential barriers. Mg^{2+} doping ions might improve the electrical responses of these active interfaces. This is because of undetectable Mg^{2+} doping ions in CTO grains, which make the CTO–CTO interfaces electrically inactive. The improved electrically active of interfaces can cause increases in both R_{gb} and E_b of 6 h samples. This indicates to the effect of Mg^{2+} doping ions on the intrinsic properties of the interfaces (GBs) of the CCTO/CTO composites.

Generally, both the intrinsic and geometric properties of the GBs of CCTO ceramics are key factors determining their overall properties. The geometric properties of the GBs are also important as well and cannot be ignored. Using the geometric approach, the increase in the GB density due to the reduction in grain size can cause enhancement of R_{gb} and E_b. For the 6 h samples, as shown in Table 1, it is clear that variations of R_{gb} and E_b values of the Mg05, Mg10, Mg20, and Mg30 samples are both closely related to the changes in their mean grain sizes. The geometric approach cannot describe the difference in values of R_{gb} between the un-doped CCTO/CTO sample and Mg-doped CCTO/CTO samples (especially for the Mg05 sample). As mentioned above, the increase in R_{gb} of the Mg05 sample compared to the CCTO/CTO sample is mainly attributed to the improved intrinsic properties of the GBs, which may be caused by the modified electrically active interfaces. These results indicate that both the geometric and intrinsic properties of the GBs have a remarkable effect on the electrical properties of the CCTO/CTO composites.

For the 24 h samples, changes in R_{gb} and E_b values of the CCTO/CTO and Mg05 samples are both correlated with the variation of their grain sizes. R_{gb} and E_b values of the CCTO/CTO sample were reduced as the mean grain size increased for the Mg05 sample. Interestingly, variation of R_{gb} values of the Mg05, Mg10, Mg20, and Mg30 samples sintered for 24 h are closely correlated with the changes in their mean grain sizes just as observed in the Mg-doped CCTO/CTO composites sintered for 6 h. Note that, both of the 6 h and 24 h samples, R_{gb} of the Mg30 samples is lower than that of the Mg20 samples. This result is primarily attributed to the increase in the mean grain size of the Mg30 samples. Variation of E_b values of the Mg05, Mg10, Mg20, and Mg30 samples cannot be explained by using the geometric approach. Generally, the formation mechanism of electrostatic barrier at GBs of traditional metal oxide non-Ohmic materials and CCTO ceramics is closely related the oxygen content at GBs.[7,30] As shown in Table 1, E_b and α values of each sample were reduced by increasing sintering time from 6 to 24 h. The concentration of oxygen vacancy at GBs of the ceramic composites sintered for 24 h may be higher than that of the 6 h samples, resulting in the degradation of nonlinear properties. This indicates that the effect of oxygen vacancies on the nonlinear properties in the 24 h samples is dominant.

It was observed that the E_b value of the Mg30 sample is larger than that of the Mg20 sample; while, the mean grain size of the Mg30 sample is larger than of the Mg20 sample. It is possible that substitution of Mg^{2+} ions into CCTO/CTO composites with

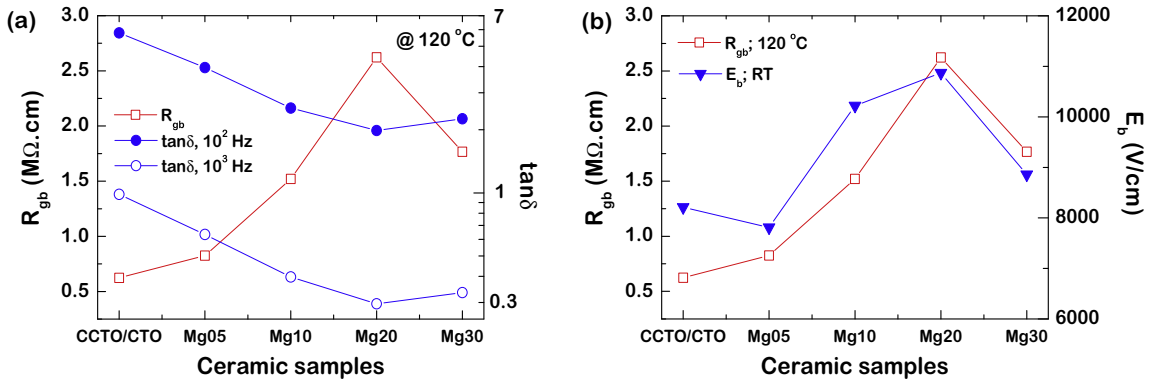

Fig. 8. (a) Correlation between R_{gb} and tan δ at 120 °C of composite ceramics sintered for 6 h. (b) Correlation between R_{gb} (at 120 °C) and E_b (measured at room temperature) of composite ceramics sintered for 6 h.

a suitable high-concentration might suppress the existence of oxygen vacancies at the GBs during sintering process at high temperatures and long reaction time. This can retain a high value of E_b. However, further work is needed to explore the exact origin of this observation.

As mentioned above, a high value of low-frequency tan δ at high temperatures is primarily caused by long-range migration of charges (σ_{dc}) of CCTO/CTO composites. This is governed by σ_{gb}. Thus, a low-frequency tan δ value should be inversely proportional to R_{gb}, as clearly seen in Fig. 8(a). With increasing Mg^{2+} concentration, tan δ values decreased while those of R_{gb} increased. With increasing Mg^{2+} concentration ($x = 0.20$–0.30), tan δ increased as R_{gb} decreased. Although R_{gb} values at 30 °C for all the samples could not be calculated, it is reasonable to suggest that a reduction of tan δ at 30 °C for Mg^{2+}-doped CCTO/CTO composites can be attributed to enhancement of R_{gb}, as a result of the presence of Mg^{2+} doping ions. As shown in Fig. 8(b), although E_b of the Mg05 sample is slightly lower than that of the un-doped CCTO/CTO composite, a correlation between R_{gb} and E_b likely exists. From the results in Fig. 8, it is clearly demonstrated that a low-frequency tan δ value of CCTO-based compounds was closely related to resistances of internal interfaces. However, for the R_{gb}–E_b relationship, these two parameters may not be correlated with each other. As shown in the inset of Fig. 6 and in Table 1, E_b values of all the Mg^{2+}-doped CCTO/CTO composites sintered for 24 h were found to be lower than those of the un-doped CCTO/CTO sample. On the other hand, the R_{gb}-tan δ relationship is still quite similar to that observed in the 6 h samples. This means that E_b or nonlinear properties may not have any relationship to R_{gb} or tan δ. As reported by Ramírez et al.,[28] E_b and α values of a CCTO/CTO composite that possessed higher volume fraction of CTO phase were less than those of the values obtained in a sample with a lower CTO volume fraction. For the 24 h samples, E_b and α were slightly changed by variation in the concentration of Mg^{2+}. It is possible that the effect of oxygen vacancies in the 24 h samples is more dominant than the effect of Mg^{2+}-modified GB response. This may make some electrically active interfaces weakly active or inactive. Evidence of a strong effect of oxygen vacancies on low-frequency tan δ values is clearly observed in the inset of Fig. 4(b).

4. Conclusions

The dielectric properties of CCTO/CTO composites were improved by doping with Mg^{2+} ions. It was found that Mg^{2+} was incorporated into only the CCTO phase. An enhanced ε' of 3550 with good temperature stability ($\Delta\varepsilon' \leq \pm 15\%$ in the temperature range of −60 to 160 °C) and a reduced tan δ value to ~0.014 (at 30 °C and 1 kHz) were achieved in a $CaCu_{2.7}Mg_{0.3}Ti_4O_{12}$/CTO ceramic sintered at 1100 °C for 6 h. Furthermore, the nonlinear coefficient of this ceramic was greatly enhanced to 27.2. Using impedance spectroscopy analysis, it was suggested that improved dielectric and nonlinear properties were attributed to the enhanced electrical responses of CCTO–CTO and CCTO–CCTO interfaces resulting from the presences of Mg^{2+} doping ions.

Acknowledgments

This work was financially supported by the Thailand Research Fund (TRF) and Khon Kaen University, Thailand (Grant No. TRG5680047). J.J. would like to thank the Thailand Graduate Institute of Science and Technology (TGIST) for his Master of Science Degree scholarship.

References

1. Subramanian MA, Li D, Duan N, Reisner BA, Sleight AW. High dielectric constant in $ACu_3Ti_4O_{12}$ and $ACu_3Ti_3FeO_{12}$ phases. *J Solid State Chem* 2000;**151**:323.
2. Sinclair DC, Adams TB, Morrison FD, West AR. $CaCu_3Ti_4O_{12}$: one-step internal barrier layer capacitor. *Appl Phys Lett* 2002;**80**:2153.
3. Yang J, Shen M, Fang L. The electrode/sample contact effects on the dielectric properties of the $CaCu_3Ti_4O_{12}$ ceramic. *Mater Lett* 2005;**59**:3990.
4. Chung S-Y, Kim I-D, Kang S-JL. Strong nonlinear current–voltage behaviour in perovskite-derivative calcium copper titanate. *Nat Mater* 2004;**3**:774.
5. Patterson EA, Kwon S, Huang C-C, Cann DP. Effects of ZrO_2 additions on the dielectric properties of $CaCu_3Ti_4O_{12}$. *Appl Phys Lett* 2005;**87**:182911.

6. Kobayashi W, Terasaki I. $CaCu_3Ti_4O_{12}/CaTiO_3$ composite dielectrics: Ba/Pb-free dielectric ceramics with high dielectric constants. *Appl Phys Lett* 2005;**87**:032902.
7. Ramírez MA, Bueno PR, Varela JA, Longo E. Non-Ohmic and dielectric properties of a $Ca_2Cu_2Ti_4O_{12}$ polycrystalline system. *Appl Phys Lett* 2006;**89**:212102.
8. Li M, Cai G, Zhang DF, Wang WY, Wang WJ, Chen XL. Enhanced dielectric responses in Mg-doped $CaCu_3Ti_4O_{12}$. *J Appl Phys* 2008;**104**:074107.
9. Ni L, Chen XM. Enhanced giant dielectric response in Mg-substituted $CaCu_3Ti_4O_{12}$ ceramics. *Solid State Commun* 2009;**149**:379.
10. Ni L, Chen XM. Enhancement of giant dielectric response in $CaCu_3Ti_4O_{12}$ ceramics by Zn substitution. *J Am Ceram Soc* 2010;**93**:184.
11. Kadyrova NI, Medvedeva NI, Zainulin YG, Ivanovskii AL. Multicomponent perovskite-type oxides $CaCu_3V_{4-x}Mn_xO_{12}$: synthesis and electronic properties. *Solid State Commun* 2013;**162**:57.
12. Li J, Jia R, Tang X, Zhao X, Li S. Enhanced electric breakdown field of $CaCu_3Ti_4O_{12}$ ceramics: tuning of grain boundary by a secondary phase. *J Phys D: Appl Phys* 2013;**46**:325304.
13. Liu Y, Wang W, Huang J, Tang F, Zhu C, Cao Y. Dielectric properties of giant permittivity $NaCu_3Ti_3NbO_{12}$ ceramics. *Ceram Int* 2013;**39**:9201.
14. Ouyang X, Huang S, Zhang W, Cao P, Huang Z, Gao W. Investigation of phase evolution of $CaCu_3Ti_4O_{12}$ (CCTO) by in situ synchrotron high-temperature powder diffraction. *J Solid State Chem* 2014;**211**:58.
15. Schmidt R, Stennett MC, Hyatt NC, Pokorny J, Prado-Gonjal J, Li M, Sinclair DC. Effects of sintering temperature on the internal barrier layer capacitor (IBLC) structure in $CaCu_3Ti_4O_{12}$ (CCTO) ceramics. *J Eur Ceram Soc* 2012;**32**:3313.
16. de la Rubia MA, Leret P, del Campo A, Alonso RE, López-Garcia AR, Fernández JF, de Frutos J. Dielectric behaviour of Hf-doped $CaCu_3Ti_4O_{12}$ ceramics obtained by conventional synthesis and reactive sintering. *J Eur Ceram Soc* 2012;**32**:1691.
17. Li M, Zhang DF, Wang WY, Wang G, Chen XL. The effects of grain boundary response and electrode contact response on the dielectric properties of $CaCu_3Ti_4O_{12}$. *J Phys D: Appl Phys* 2010;**43**:295405.
18. Yang Z, Zhang L, Chao X, Xiong L, Liu J. High permittivity and low dielectric loss of the $Ca_{1-x}Sr_xCu_3Ti_4O_{12}$ ceramics. *J Alloys Compd* 2011;**509**:8716.
19. Liang P, Yang Z, Chao X, Liu Z, Chen XM. Giant dielectric constant and good temperature stability in $Y_{2/3}Cu_3Ti_4O_{12}$ ceramics. *J Am Ceram Soc* 2012;**95**:2218.
20. Liang P, Chao X, Wang F, Liu Z, Yang Z. The lowered dielectric loss and grain-boundary effects in La-doped $Y_{2/3}Cu_3Ti_4O_{12}$ ceramics. *J Am Ceram Soc* 2013;**96**:3883.
21. Li Y, Liang P, Chao X, Yang Z. Preparation of $CaCu_3Ti_4O_{12}$ ceramics with low dielectric loss and giant dielectric constant by the sol–gel technique. *Ceram Int* 2013;**39**:7879.
22. Wu J, Nan C-W, Lin Y, Deng Y. Giant dielectric permittivity observed in Li and Ti doped NiO. *Phys Rev Lett* 2002;**89**:217601.
23. Thongbai P, Putasaeng B, Yamwong T, Amornkitbamrung V, Maensiri S. Liquid phase sintering behavior and improvement of giant dielectric properties by modifying microstructure and electrical response at grain boundaries of $CaCu_3Ti_{4-x}Mo_xO_{12}$ ceramics. *J Alloys Compd* 2014;**582**:747.
24. Ramajo L, Parra R, Varela JA, Reboredo MM, Ramírez MA, Castro MS. Influence of vanadium on electrical and microstructural properties of $CaCu_3Ti_4O_{12}/CaTiO_3$. *J Alloys Compd* 2010;**497**:349.
25. Li T, Fang K, Hao J, Xue Y, Chen Z. The effect of Ca-rich on the electric properties of $Ca_{1+x}Cu_{3-x}Ti_4O_{12}$ polycrystalline system. *Mater Sci Eng B* 2011;**176**:171.
26. Thongbai P, Putasaeng B, Yamwong T, Maensiri S. Improved dielectric and non-Ohmic properties of $Ca_2Cu_2Ti_4O_{12}$ ceramics prepared by a polymer pyrolysis method. *J Alloys Compd* 2011;**509**:7416.
27. Ramírez MA, Bueno PR, Longo E, Varela JA. Conventional and microwave sintering of $CaCu_3Ti_4O_{12}/CaTiO_3$ ceramic composites: non-Ohmic and dielectric properties. *J Phys D: Appl Phys* 2008;**41**:152004.
28. Ramírez MA, Bueno PR, Tararam R, Cavalheiro AA, Longo E, Varela JA. Evaluation of the effect of the stoichiometric ratio of Ca/Cu on the electrical and microstructural properties of the $CaCu_3Ti_4O_{12}$ polycrystalline system. *J Phys D: Appl Phys* 2009;**42**:185503.
29. Jumpatam J, Thongbai P, Kongsook B, Yamwong T, Maensiri S. High permittivity, low dielectric loss, and high electrostatic potential barrier in $Ca_2Cu_2Ti_4O_{12}$ ceramics. *Mater Lett* 2012;**76**:40.
30. Yu R, Xue H, Cao Z, Chen L, Xiong Z. Effect of oxygen sintering atmosphere on the electrical behavior of CCTO ceramics. *J Eur Ceram Soc* 2012;**32**:1245.
31. Moulson AJ, Herbert JM. *Electroceramics: materials, properties, applications*. 2nd ed. West Sussex/New York: Wiley; 2003. p. xiv.
32. Cheng B, Lin Y-H, Yang H, Lan J, Nan C-W, Xiao X, He J. High dielectric permittivity behavior in Cu-doped $CaTiO_3$. *J Am Ceram Soc* 2009;**92**:2776.
33. Oliveira LH, Paris EC, Avansi W, Ramírez MA, Mastelaro VR, Longo E, Varela JA, Chen XM. Correlation between photoluminescence and structural defects in $Ca_{1+x}Cu_{3-x}Ti_4O_{12}$ systems. *J Am Ceram Soc* 2013;**96**:209.
34. Shannon RD. Revised effective ionic radii and systematic studies of interatomie distances in halides and chaleogenides. *Acta Cryst* 1976;**A32**:751.
35. Kim K-M, Kim S-J, Lee J-H, Kim D-Y. Microstructural evolution and dielectric properties of SiO_2-doped $CaCu_3Ti_4O_{12}$ ceramics. *J Eur Ceram Soc* 2007;**27**:3991.
36. Romero JJ, Leret P, Rubio-Marcos F, Quesada A, Fernández JF. Evolution of the intergranular phase during sintering of $CaCu_3Ti_4O_{12}$ ceramics. *J Eur Ceram Soc* 2010;**30**:737.
37. Rahaman MN. *Sintering of ceramics*. Boca Raton, FL: CRC Press; 2008. p. 388.
38. Shao SF, Zhang JL, Zheng P, Wang CL, Li JC, Zhao ML. High permittivity and low dielectric loss in ceramics with the nominal compositions of $CaCu_{3-x}La_{2x/3}Ti_4O_{12}$. *Appl Phys Lett* 2007;**91**:042905.
39. Vangchangyia S, Yamwong T, Swatsitang E, Thongbai P, Maensiri S. Selectivity of doping ions to effectively improve dielectric and non-Ohmic properties of $CaCu_3Ti_4O_{12}$ ceramics. *Ceram Int* 2013;**39**:8133.
40. Thongbai P, Boonlakhorn J, Putasaeng B, Yamwong T, Maensiri S. Extremely enhanced nonlinear current–voltage properties of Tb-doped $CaCu_3Ti_4O_{12}$ ceramics. *J Am Ceram Soc* 2013;**96**:379.
41. Lu Z-Y, Li X-M, Wu J-Q, Winter M. Voltage–current nonlinearity of $CaCu_3Ti_4O_{12}$ ceramics. *J Am Ceram Soc* 2012;**95**:476.
42. Adams TB, Sinclair DC, West AR. Influence of processing conditions on the electrical properties of $CaCu_3Ti_4O_{12}$ ceramics. *J Am Ceram Soc* 2006;**89**:3129.

J. Am. Ceram. Soc., 97 [8] 2368–2371 (2014)
DOI: 10.1111/jace.13048

journal
Rapid Communication

A Novel Route to Greatly Enhanced Dielectric Permittivity with Reduce Loss Tangent in $CaCu_{3-x}Zn_xTi_4O_{12}/CaTiO_3$ Composites

Jutapol Jumpatam,[‡] Bundit Putasaeng,[§] Teerapon Yamwong,[§] Prasit Thongbai,[¶,‖,†] and Santi Maensiri[††]

[‡]Materials Science and Nanotechnology Program, Faculty of Science, Khon Kaen University, Khon Kaen 40002, Thailand

[§]National Metal and Materials Technology Center (MTEC), Thailand Science Park, Pathumthani 12120, Thailand

[¶]Department of Physics, Faculty of Science, Khon Kaen University, Khon Kaen 40002, Thailand

[‖]Nanotec-KKU Center of Excellence on Advanced Nanomaterials for Energy Production and Storage, Khon Kaen 40002, Thailand

[††]School of Physics, Institute of Science, Suranaree University, Nakhon Ratchasima 30000, Thailand

Dielectric and nonlinear properties of a binary compound derived from $Ca_2Cu_2Ti_4O_{12}$ were greatly improved by doping with Zn^{2+} to deliberately create $CaCu_{3-x}Zn_xTi_4O_{12}/CaTiO_3$ composites. $Ca_2Cu_{1.8}Zn_{0.2}Ti_4O_{12}$ composition can exhibit an enhanced ε′, ~6,513, with a strong reduction in tanδ to ~0.015 (at 1 kHz). The nonlinear coefficient and breakdown field strength were significantly enhanced. The dielectric and nonlinear properties were described based on the effect of Zn^{2+} substitution on electrical response of internal interfaces.

I. Introduction

Recently, there have been extensive studies of the giant dielectric permittivity of $CaCu_3Ti_4O_{12}$ (CCTO) materials.[1–7] This is because CCTO holds promise for use in development of a new generation of multilayer ceramic capacitors. They also have fascinating physics underlying the exact origin of giant dielectric permittivity (ε′) in CCTO without any detectable phase transition over a wide temperature range. CCTO polycrystalline ceramics are electrically heterogeneous, consisting of *n*-type semiconducting grains and insulating layers of grain boundaries.[2,3] Unfortunately, tanδ of CCTO ceramics is still too large (>0.05). This is one of the most serious problems preventing the use of CCTO in capacitor applications.[1,6]

A large decrease in tanδ of ~0.02 (1 kHz) was observed in a binary compound system of $Ca_2Cu_2Ti_4O_{12}$, which consists of 33.3 mol% of CCTO and 66.7 mol% of $CaTiO_3$ (CTO).[8,9] However, such a decrease in tanδ also caused a large decrease in ε′ of CCTO (~1800 at 300 K and 1 kHz). It is notable that this CCTO/CTO composite can be fabricated using a one-step process starting with a nominal composition of $Ca_2Cu_2Ti_4O_{12}$ at a relatively lower sintering temperature than $BaTiO_3$ ferroelectric oxide. Furthermore, this material system showed no piezoelectricity, which is helps reduce mechanical damage during AC operation.[8] Therefore, elucidation of ways to enhance ε′ of CCTO/CTO composites while retaining a low tanδ value is very important.

The aim of this work was to provide a new strategy to enhance the dielectric performance of CCTO/CTO composites by doping with Zn^{2+}. $CaCu_{3-x}Zn_xTi_4O_{12}/CTO$ composites with strongly enhanced ε′ and lower tanδ can be synthesized from a binary compound system with a nominal composition of $Ca_2Cu_{2-x}Zn_xTi_4O_{12}$ (x = 0, 0.2, and 0.3).

II. Experimental Section

$Ca_2Cu_{2-x}Zn_xTi_4O_{12}$ ceramics, where x = 0, 0.20, and 0.30 (referred to as CCTO/CTO, CCTO/CTO_Zn1, and CCTO/CTO_Zn2 composites, respectively), were prepared using a solid-state reaction method. First, a stoichiometric mixture of the starting materials ($CaCO_3$, CuO, ZnO, and TiO_2) for each composition was ball-milled in ethanol for 24 h. Second, the resulting slurries were dried and calcined at 900°C for 15 h. Then, the calcined powders were pressed into pellets of 9.5 mm diameter and ~1.0 mm in thickness. Finally, these green body pellets were sintered at 1100°C for 24 h.

X-ray diffraction (XRD; PW3040 Philips; Eindhoven, the Netherlands) was used to characterize phase compositions of the sintered $Ca_2Cu_{2-x}Zn_xTi_4O_{12}$ composites. Scanning electron microscopy (SEM; LEO 1450VP; Cambridge, UK) and energy dispersive-X-ray spectrometry (EDS) were used to characterize ceramic microstructure. Au was sputtered on to each pellet face for dielectric and current–voltage measurements. The dielectric properties were measured using an Agilent 4294A Precision Impedance Analyzer over the frequency range of 10^2–10^7 Hz. Current–voltage measurements were carried out using a high voltage measurement unit (Keithley Model 247, Estado St Pasadena, CA). The breakdown electric field (E_b) was calculated at a current density of J = 1 mA/cm^2. The nonlinear coefficient (α) was calculated in the range of 1–10 mA/cm^2.

III. Results and Discussion

The XRD patterns of $Ca_2Cu_{2-x}Zn_xTi_4O_{12}$ ceramics are shown in Fig. 1. All the samples consisted of CCTO (JCPDS 75-2188) and CTO phases (JCPDS 82-0231). This observation is similar to those reported in the literature.[9–12] Considering the nominal formula of $Ca_2Cu_2Ti_4O_{12}$, phases of CCTO (~33.3 mol%) and CTO (~66.7 mol%) should be formed. This was further confirmed by a Rietveld quantitative analysis.[10] The reason for this is that the ionic radius of Ca^{2+} is much larger than that of Cu^{2+}. Thus, Ca^{2+} cannot

C. M. Chen—contributing editor

Manuscript No. 34800. Received April 4, 2014; approved May 12, 2014.
[†]Author to whom correspondence should be addressed. e-mail: pthongbai@kku.ac.th

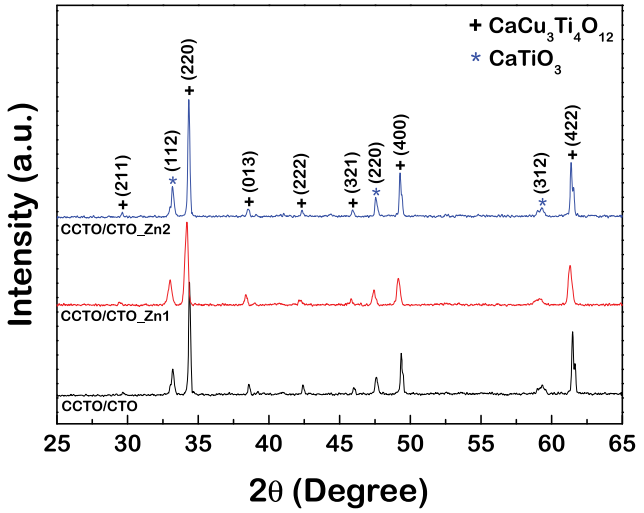

Fig. 1. XRD patterns of $Ca_2Cu_{2-x}Zn_xTi_4O_{12}$ (x = 0, 0.20, and 0.30) ceramics.

enter into Cu^{2+} sites in a planar square to create a Ca $(CaCu_2)Ti_4O_{12}$ structure. Interestingly, an impurity phase related to Zn^{2+} doping ions was not observed. Lattice parameters (a) of the CCTO phase were calculated and found to be 7.3893, 7.3929, and 7.4002 Å for CCTO/CTO, CCTO/CTO_Zn1, and CCTO/CTO_Zn2 composites, respectively. The increase in the value of a for the CCTO phase may be due to different ionic radii being formed between Zn^{2+} (r_4 = 0.60 Å) and Cu^{2+} (r_4 = 0.57 Å) ions.[13]

Figures 2(a)–(c) show backscattered SEM images of the polished CCTO/CTO, CCTO/CTO_Zn1, and CCTO/CTO_Zn2 composites, respectively. Darker and lighter phases were observed, which is consistent with the XRD results and similar to those reported in the literature for undoped $Ca_2Cu_2Ti_4O_{12}$ ceramics.[10,12] Figure 2(d) reveals unpolished surface of the CCTO/CTO_Zn2 composite, showing the smooth and rough surfaces, which were expected as CCTO and CTO phases,[12] respectively.

As seen in Fig. 3(a) for the EDS spectra [spectra (#1)-(#3)] of the CCTO/CTO and CCTO/CTO_Zn2 composites, the lighter and darker phases are clearly CCTO and CTO phases, respectively. Grain sizes of CCTO and CTO phases

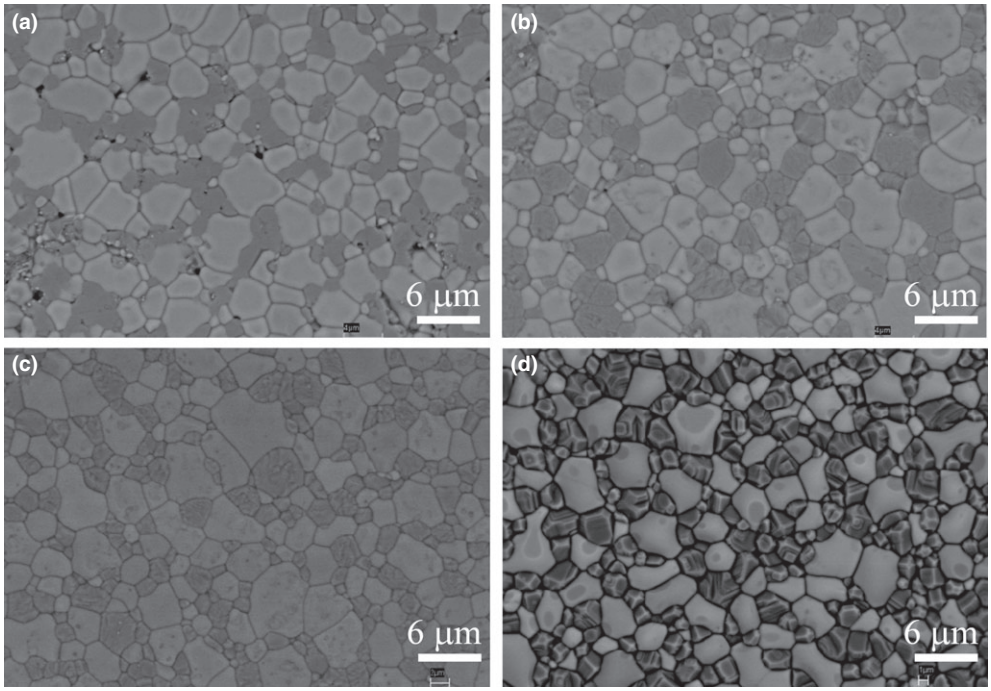

Fig. 2. Backscattered SEM images of polished surfaces of (a) CCTO/CTO, (b) CCTO/CTO_Zn1, and (c) CCTO/CTO_Zn2 composites. (d) Backscattered SEM image of unpolished surface of CCTO/CTO_Zn2 composite.

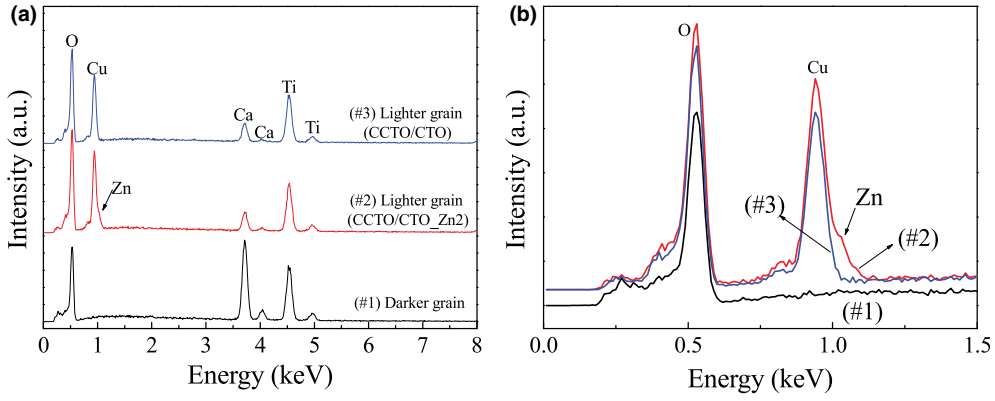

Fig. 3. (a) Energy-dispersive X-ray spectrometry spectra of CCTO/CTO and CCTO/CTO_Zn2 composites. (b) Enlarged view of (a).

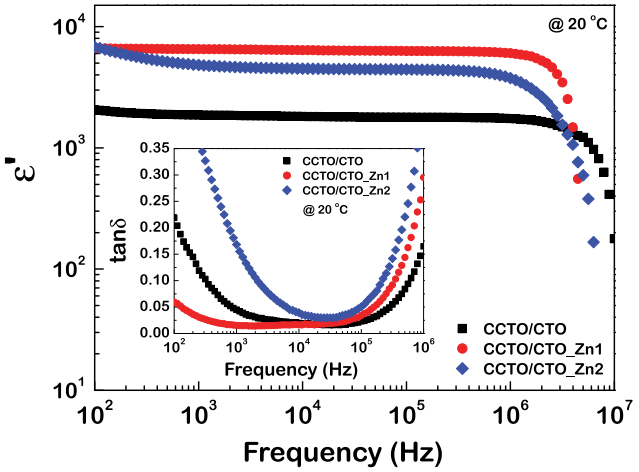

Fig. 4. Frequency dependence of ε′ at 20°C for $Ca_2Cu_{2-x}Zn_xTi_4O_{12}$ (x = 0, 0.20, and 0.30) ceramics; inset shows tanδ at 20°C.

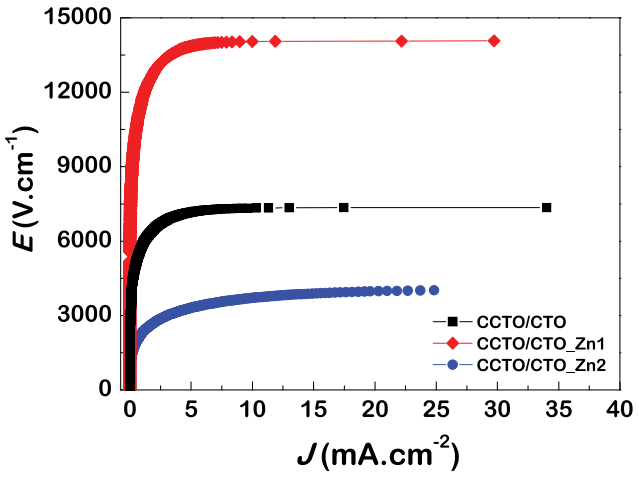

Fig. 5. Nonlinear properties of $Ca_2Cu_{2-x}Zn_xTi_4O_{12}$ ceramics.

are slightly changed. Notably, highly dense microstructure of CCTO/CTO composites was obtained by doping with Zn^{2+}. However, the EDS peak of Zn cannot be observed in either phase. This was due to similarity of values of the energy of the X-ray emissions for $L\alpha$ of Cu^{2+} (~0.929 keV) and Zn^{2+} (~1.011 keV) ions. In Fig. 3(b), the shoulder of EDS-Cu peak detected at the lighter grain of the CCTO/CTO_Zn2 composite was observed. This indicates to Zn^{2+} ions, which were preferentially substituted into Cu^{2+} sites but only in the CCTO phase. It was estimated that the $Ca_2Cu_{2-x}Zn_xTi_4O_{12}$ ceramics prepared in this study consisted of ~33.3 mol% of $CaCu_{3-x}Zn_xTi_4O_{12}$ (x = 0, 0.20, and 0.30) and ~66.7 mol% of CTO.

As shown in Fig. 4, ε′ at 20°C of the CCTO/CTO and CCTO/CTO_Zn1 composites was independent of frequency in the range from 10^2 to 10^6 Hz. Notably, ε′ of CCTO/CTO composites was strongly enhanced by doping with Zn^{2+}, whereas, tanδ was significantly reduced [inset of Fig. 4]. The ε′ values at 20°C and 1 kHz of CCTO/CTO, CCTO/CTO_Zn1, and CCTO/CTO_Zn2 composites were found to be 1863, 6513, and 4821, respectively. Values of tanδ were found to be 0.045, 0.015, and 0.168, respectively. It was noted that ε′ of the CCTO/CTO composite sample was close to the ε′ value of ~1800 for a sample sintered at 1090°C for 24 h as was reported in the literature.[8] Interestingly, the CCTO/CTO_Zn1 composite exhibited a greatly enhanced ε′ with a significantly reduced tanδ. High-performance dielectric properties of the CCTO/CTO_Zn1 composite can be comparable to that observed in $CaCu_{3-x}La_{2x/3}Ti_4O_{12}$ ceramics (ε′~7500 and tanδ~0.02 at 1 kHz).[14]

The effect of Zn^{2+} doping ions on non-Ohmic properties of CCTO/CTO composites was also investigated. The results are shown in Fig. 5. All the composite ceramics of this study exhibited nonlinear E–J behavior. α and E_b of the CCTO/CTO, CCTO/CTO_Zn1, and CCTO/CTO_Zn2 composites were calculated and found to be 9.89 and 5817 V/cm, 12.43 and 11 689 V/cm, and 4.77 and 2295 V/cm, respectively. Interestingly, improved nonlinear electrical properties were achieved in the CCTO/CTO_Zn1 composite. Zn^{2+} doping ions had significant influences on both the dielectric and nonlinear electrical properties of CCTO/CTO composites.

Using electrostatic force microscopy,[10] it was clearly shown that CCTO–CCTO and CCTO–CTO interfaces were electrically active. This indicated the presence of potential barriers at these interfaces. However, a CTO–CTO interface was electrically inactive. Enhancement of non-Ohmic properties of the CCTO/CTO_Zn1 composite was therefore attributed to the improved electrical response of these interfaces, resulting from substitution of Zn^{2+}. Higher concentrations of Zn^{2+} doping ions caused degradation of nonlinear properties in the CCTO/CTO_Zn2 composite. This result is similar to that reported in literature for Zn-doped CCTO ceramics with high Zn^{2+} content.[15] It was reported that ε′ and E_b of the CCTO/CTO system decreased as the content of the CTO phase increased.[10] For CCTO ceramics, the giant ε′ response is now widely accepted to be caused by the interfacial polarization at the CCTO–CCTO interface.[2,3] Therefore, a strong increase in ε′ of Zn-doped CCTO/CTO composites may be primarily caused by the enhanced electrical response at the CCTO–CCTO interface alone. This is reasonable because ε′ of CCTO/CTO was found to be slightly dependent on sintering temperature.[11] Although the mechanism responsible for these observations is still unclear, this work provides an important novel route to strongly enhance the dielectric response and non-Ohmic properties of CCTO-based ceramics.

IV. Conclusions

In conclusion, the dielectric and non-Ohmic properties of CCTO/CTO can be improved by doping with Zn^{2+} to deliberately create Zn-doped CCTO/CTO composites. ε′ of $Ca_2Cu_{1.8}Zn_{0.2}Ti_4O_{12}$ composite was strongly enhanced to ~6513, whereas tanδ was found to be very low, 0.015 at 1 kHz and 20°C. α and E_b of this ceramic were significantly enhanced to 12.43 and 11 689 V/cm, respectively. The dielectric and nonlinear properties of Zn-doped CCTO/CTO composites were described and found to be influenced by Zn^{2+} doping ions influencing the electrical response of internal interfaces.

Acknowledgments

This work was financially supported by the Thailand Research Fund (TRF) and Khon Kaen University, Thailand (Grant No. TRG5680047) and Khon Kaen University, Thailand and the Nanotechnology Center (NANOTEC), NSTDA, Ministry of Science and Technology, Thailand, through its program of Center of Excellence Network. J.J. thank the Thailand Graduate Institute of Science and Technology (TGIST) for his Master of Science Degree scholarship.

References

[1]M. A. Subramanian, D. Li, N. Duan, B. A. Reisner, and A. W. Sleight, "High Dielectric Constant in $ACu_3Ti_4O_{12}$ and $ACu_3Ti_3FeO_{12}$ Phases," *J. Solid State Chem.*, **151** [2] 323–5 (2000).

[2]D. C. Sinclair, T. B. Adams, F. D. Morrison, and A. R. West, "$CaCu_3Ti_4O_{12}$: One-Step Internal Barrier Layer Capacitor," *Appl. Phys. Lett.*, **80** [12] 2153, 3pp (2002).

[3]S.-Y. Chung, I.-D. Kim, and S.-J. L. Kang, "Strong Nonlinear Current–Voltage Behaviour in Perovskite-Derivative Calcium Copper Titanate," *Nat. Mater.*, **3** [11] 774–8 (2004).

[4]H. Yu, H. Liu, H. Hao, D. Luo, and M. Cao, "Dielectric Properties of $CaCu_3Ti_4O_{12}$ Ceramics Modified by $SrTiO_3$," *Mater. Lett.*, **62** [8–9] 1353–5 (2008).

[5]J. Li, R. Jia, X. Tang, X. Zhao, and S. Li, "Enhanced Electric Breakdown Field of $CaCu_3Ti_4O_{12}$ Ceramics: Tuning of Grain Boundary by a Secondary Phase," *J. Phys. D: Appl. Phys.*, **46** [32] 325304, 6pp (2013).

[6]P. Thongbai, K. Meeporn, T. Yamwong, and S. Maensiri, "Extreme Effects of Na Doping on Microstructure, Giant Dielectric Response and Dielectric Relaxation Behavior in $CaCu_3Ti_4O_{12}$ Ceramics," *Mater. Lett.*, **106**, 129–32 (2013).

[7]L. Ni and X. M. Chen, "Enhancement of Giant Dielectric Response in $CaCu_3Ti_4O_{12}$ Ceramics by Zn Substitution," *J. Am. Ceram. Soc.*, **93** [1] 184–9 (2010).

[8]W. Kobayashi and I. Terasaki, "$CaCu_3Ti_4O_{12}/CaTiO_3$ Composite Dielectrics: Ba/Pb-Free Dielectric Ceramics with High Dielectric Constants," *Appl. Phys. Lett.*, **87** [3] 032902, 3pp (2005).

[9]M. A. Ramírez, P. R. Bueno, J. A. Varela, and E. Longo, "Non-Ohmic and Dielectric Properties of a $Ca_2Cu_2Ti_4O_{12}$ Polycrystalline System," *Appl. Phys. Lett.*, **89** [21] 212102, 3pp (2006).

[10]M. A. Ramírez, P. R. Bueno, R. Tararam, A. A. Cavalheiro, E. Longo, and J. A. Varela, "Evaluation of the Effect of the Stoichiometric Ratio of Ca/Cu on the Electrical and Microstructural Properties of the $CaCu_3Ti_4O_{12}$ Polycrystalline System," *J. Phys. D: Appl. Phys.*, **42** [18] 185503, 8pp (2009).

[11]P. Thongbai, B. Putasaeng, T. Yamwong, and S. Maensiri, "Improved Dielectric and Non-Ohmic Properties of $Ca_2Cu_2Ti_4O_{12}$ Ceramics Prepared by a Polymer Pyrolysis Method," *J. Alloys Compd*, **509** [27] 7416–20 (2011).

[12]J. Jumpatam, P. Thongbai, B. Kongsook, T. Yamwong, and S. Maensiri, "High Permittivity, low Dielectric Loss, and High Electrostatic Potential Barrier in $Ca_2Cu_2Ti_4O_{12}$ Ceramics," *Mater. Lett.*, **76**, 40–2 (2012).

[13]R. D. Shannon, "Revised Effective Ionic Radii and Systematic Studies of Interatomie Distances in Halides and Chaleogenides," *Acta Cryst.*, **32**, 751–67 (1976).

[14]S. F. Shao, J. L. Zhang, P. Zheng, C. L. Wang, J. C. Li, and M. L. Zhao, "High Permittivity and Low Dielectric Loss in Ceramics with the Nominal Compositions of $CaCu_{3-x}La_{2x/3}Ti_4O_{12}$," *Appl. Phys. Lett.*, **91** [4] 042905, 3pp (2007).

[15]D. Xu, C. Zhang, Y. Lin, L. Jiao, H. Yuan, G. Zhao, and X. Cheng, "Influence of Zinc on Electrical and Microstructural Properties of $CaCu_3Ti_4O_{12}$ Ceramics Prepared by Sol–Gel Process," *J. Alloys Compd*, **522**, 157–61 (2012). □

ARTICLE IN PRESS

Available online at www.sciencedirect.com

ScienceDirect

Ceramics International ▮ (▮▮▮▮) ▮▮▮–▮▮▮

CERAMICS INTERNATIONAL

www.elsevier.com/locate/ceramint

Effects of Bi^{3+} doping on microstructure and dielectric properties of $CaCu_3Ti_4O_{12}/CaTiO_3$ composite ceramics

Jutapol Jumpatam[a], Prasit Thongbai[b,*], Teerapon Yamwong[c], Santi Maensiri[d]

[a]*Materials Science and Nanotechnology Program, Faculty of Science, Khon Kaen University, Khon Kaen 40002, Thailand*
[b]*Department of Physics, Faculty of Science, Khon Kaen University, Khon Kaen 40002, Thailand*
[c]*National Metal and Materials Technology Center (MTEC), National Science and Technology Development of Agency, Thailand Science Park, Pathumthani 12120, Thailand*
[d]*School of Physics, Institute of Science, Suranaree University of Technology, Nakhon Ratchasima 30000, Thailand*

Received 26 October 2014; accepted 19 March 2015

Abstract

The effects of Bi^{3+} doping ions on the microstructure and dielectric properties of $CaCu_3Ti_4O_{12}/CaTiO_3$ (CCTO/CTO) composites prepared by using a conventional solid state reaction method were investigated. Microstructure analysis revealed that Bi^{3+} doping ions can be substituted into Ca^{2+} sites in both the CCTO and CTO phases. It is notable that the value of ε' at 1 kHz and 30 °C of the CCTO/CTO composite was greatly increased to 4.1×10^4 by doping with Bi^{3+} ions, compared to the un-doped sample ($\varepsilon' \sim 1.8 \times 10^3$). Non-Ohmic properties of Bi^{3+}-doped CCTO/CTO composites were also investigated. The electrical responses of grains and internal interfaces were investigated using impedance spectroscopy. Strongly enhanced dielectric responses and variation in nonlinear electrical properties can be well described based on the electrical responses at internal interfaces of the composites.

Keywords: $CaCu_3Ti_4O_{12}/CaTiO_3$; Dielectric permittivity; Non-Ohmic properties; Loss tangent

1. Introduction

In recent years, giant dielectric materials, especially $CaCu_3Ti_4O_{12}$ (CCTO), have been intensively investigated due to their very high dielectric permittivity (ε') and novel physical behavior [1–10]. The electrical responses of different internal interfaces in CCTO polycrystalline ceramics and related $ACu_3Ti_4O_{12}$ compounds (A=$Bi_{2/3}$, $La_{2/3}$, $Na_{1/2}Bi_{1/2}$, $Na_{1/2}Sm_{1/2}$, *etc.*) were investigated in order to clarify the unexpected appearance of giant dielectric properties [2,3,7,11–15]. The internal interfaces studied were domain boundaries (DBs) [16], grain boundaries (GBs) [2,3,7], planar defects due to stacking faults in the grains [17], and interfaces between the CCTO grain matrix and secondary phases of other substances [18–21]. Furthermore, CCTO can exhibit electrical properties that show a nonlinear relationship between current density and electric field strength (*J–E*) [2]. Most results suggested that the observed nonlinear *J–E* behavior of CCTO polycrystalline ceramics was caused by the electrical response of the insulating GBs [2–5,12,20]. Unfortunately, the loss tangent (tanδ) of CCTO is still too large [1,4–7,21], which is undesirable for many applications such as capacitors and memory devices.

To improve the dielectric properties of CCTO ceramics, Kobayashi and Terasaki [18] reported a strategy to greatly reduce tanδ of CCTO ceramics by producing a composite system of $CCTO/CaTiO_3$ (CCTO/CTO) from a starting composition with a nominal formula of $Ca_2Cu_2Ti_4O_{12}$. The nonlinear *J–E* properties of this composite system were improved [19,22]. Generally, tanδ values of CCTO/CTO composites are very low ($\tan\delta \sim 0.02$) [23,24]. Moreover, very high breakdown electric field (E_b) and large nonlinear coefficient (α) values were achieved in this composite system compared to a single phase of CCTO ceramics [19,22]. Enhancement of nonlinear electrical properties of CCTO/CTO composites was mainly attributed to the electrical response of

*Corresponding author.
E-mail address: pthongbai@kku.ac.th (P. Thongbai).

http://dx.doi.org/10.1016/j.ceramint.2015.03.197
0272-8842/

Please cite this article as: J. Jumpatam, et al., Effects of Bi^{3+} doping on microstructure and dielectric properties of $CaCu_3Ti_4O_{12}/CaTiO_3$ composite ceramics, Ceramics International (2015), http://dx.doi.org/10.1016/j.ceramint.2015.03.197

the CTO–CCTO interface [19,23,24], which does not appear in a single phase CCTO ceramic. It is often observed that substitution of metal ions into CCTO ceramics significantly changes both the dielectric response and nonlinear properties. Changes in properties of CCTO ceramics were ascribed to the changing electrical properties of grains and GBs as a result of dopants [4,5,25–27].

In this work, we substituted aliovalent Bi^{3+} ions in various concentrations into Ca^{2+} sites of material with a starting composition of $Ca_2Cu_2Ti_4O_{12}$. Two CCTO and CTO phases were observed in the XRD patterns. It was found that Bi^{3+} doping ions had remarkable effects on the microstructure, dielectric response, and electrical properties of CCTO/CTO composites. Very large changes in dielectric properties were described based on interfacial polarization at internal interfaces.

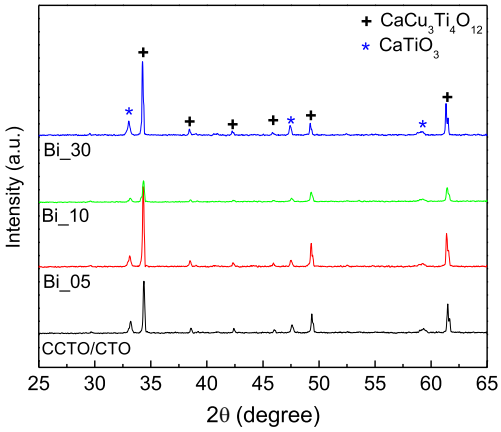

Fig. 1. XRD patterns of Bi-doped CCTO/CTO composites.

2. Experimental details

In this work, ceramic powders with nominal compositions of $Ca_2Cu_2Ti_4O_{12}$ (CCTO/CTO), $Ca_{1.95}Bi_{0.05}Cu_2Ti_4O_{12}$ (Bi_05), $Ca_{1.90}Bi_{0.10}Cu_2Ti_4O_{12}$ (Bi_10), and $Ca_{1.7}Bi_{0.30}Cu_2Ti_4O_{12}$ (Bi_30) were prepared by using a solid state reaction method. $CaCO_3$ (99.9% purity), Bi_2O_3 (99.99% purity), TiO_2 (99.9% purity), and CuO (99.9% purity) were used as starting raw materials. First, stoichiometric amounts of these raw materials were mixed by ball milling in ethanol for 24 h using 2 mm in diameter ZrO_2 balls. Next, each slurry mixture was dried and calcined in air at 900 °C for 15 h. Then, the calcined powders were ground and pressed to form green bodies each with a diameter of 9.5 mm and a thickness of ~1.2 mm. Finally, the green bodies were sintered in air at 1100 °C for 24 h at heating and cooling rates of 5 °C/min.

Phase compositions of sintered ceramics were investigated by X-ray diffraction spectrometer (XRD; Philips PW3040). Scanning electron microscopy (SEM; LEO 1450VP; Cambridge, UK) and energy-dispersive X-ray spectrometry (EDS) were used to reveal the distribution of CCTO and CTO phases as well as the chemical elements in the sintered ceramics at different areas. The dielectric properties of the sintered ceramics were measured using an Agilent 4294A Precision Impedance Analyzer over a frequency range of 10^2–10^7 Hz with an oscillation voltage of 0.5 V. The dielectric properties were measured over the temperature range of −70 to 150 °C. Each step increase in measurement temperature was 10 °C with a precision of ±0.1 °C. *J*–*E* measurements were determined at room temperature using a high voltage measurement unit (Keithley Model 247). The value of E_b was obtained at J=1 mA cm^{-2}. α values of all the samples were calculated over the range of J=1 − 10 mA cm^{-2}. Before electrical and dielectric measurements, Au was sputtered onto each pellet face at a current of 25 mA for 8 min using a Polaron SC500 sputter coating unit (Sussex, UK).

3. Results and discussion

The XRD patterns of Bi-doped CCTO/CTO composites are illustrated in Fig. 1. It is clearly seen that all of the composite samples consisted of two phases of CTO (JCPDS 82-0231) and CCTO (JCPDS 75–2188). This result is similar to those reported in the literature [19,23,24,28]. Considering the nominal formula of $Ca_2Cu_2Ti_4O_{12}$, ~66.7 mol% of CTO and ~33.3 mol% of CCTO should be created during the sintering process due to an imbalance between Ca^{2+} and Cu^{2+} ions. The creation of CCTO/CTO composites was confirmed by a Rietveld quantitative analysis of synthesized $Ca_2Cu_2Ti_4O_{12}$ ceramics as reported in the literature [19]. The formation can be explained as follows. Due to a relatively large ionic radius of Ca^{2+} compared to that of Cu^{2+}, Ca^{2+} cannot enter into Cu^{2+} sites in a planar square to form a Ca$(CaCu_2)Ti_4O_{12}$ structure [23,24].

Fig. 2 shows surface morphologies of CCTO/CTO and Bi-doped CCTO/CTO composites. It was found that some grains in the microstructure of Bi-doped CCTO/CTO grew rapidly. This indicates that an abnormal grain growth occurred in the Bi-doped CCTO/CTO composites [29]. Such grain growth may be related to the liquid phase sintering behavior as a result of a Bi-related liquid phase. This is reasonable because the melting point of Bi_2O_3 is lower than the sintering temperature of CCTO/CTO composites (1100 °C). As revealed in the insets of Fig. 2(a) and (b) for the backscattered SEM images, two phases with different contrasts were observed, *i.e.*, darker and lighter phases in the CCTO/CTO sample. This observation is consistent with the XRD results and similar to those reported in the literature for un-doped CCTO/CTO [19,23,24]. The darker and lighter phases were CTO and CCTO phases, respectively [19,23,24]. However, varying contrast could not be clearly observed in the Bi_05 sample as well as in other Bi-doped CCTO/CTO samples. As depicted in Fig. 3(a) and (b), EDS peaks corresponding to Bi, Ca, Ti, and O appeared in the EDS spectra measured in a small grain (point 2). All EDS peaks for Bi, Ca, Cu, Ti, and O were detected in the larger grain. This clearly indicates that Bi^{3+} doping ions preferentially formed solid solution within both the CCTO and CTO phases.

Fig. 4 and its inset show the frequency dependence of ε' and tanδ at 30 °C. Clearly, Bi^{3+} doping ions have a great influence on the dielectric properties of CCTO/CTO composites. The values of ε' and tanδ of CCTO/CTO composites were strongly

Please cite this article as: J. Jumpatam, et al., Effects of Bi^{3+} doping on microstructure and dielectric properties of $CaCu_3Ti_4O_{12}/CaTiO_3$ composite ceramics, Ceramics International (2015), http://dx.doi.org/10.1016/j.ceramint.2015.03.197

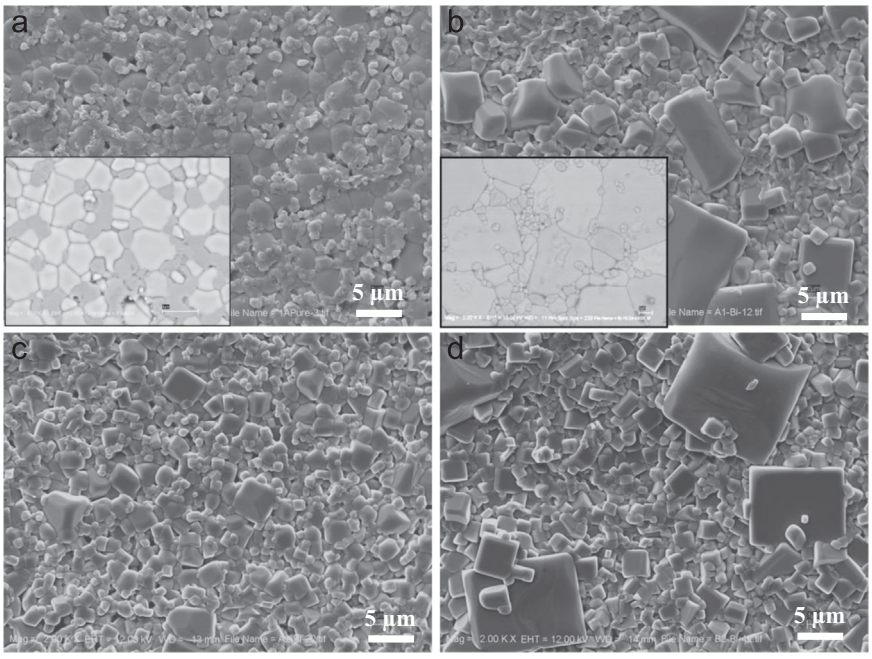

Fig. 2. SEM images of (a) CCTO/CTO, (b) Bi_05, (c) Bi_10, and (d) Bi_30 samples; insets of (a) and (b) are backscattered SEM images of the CCTO/CTO and Bi_05 samples.

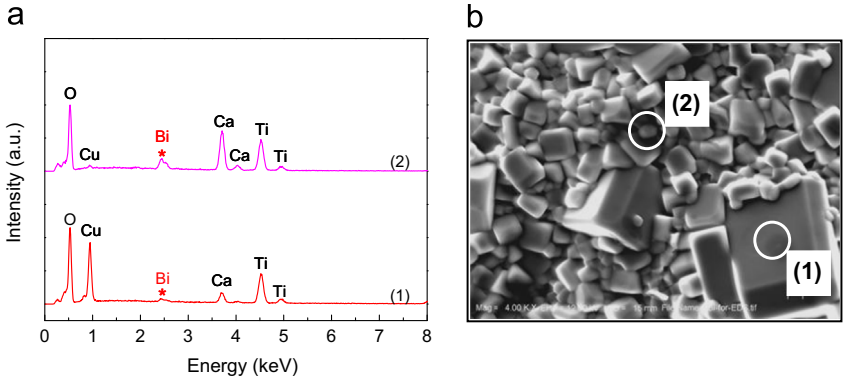

Fig. 3. (a) EDS spectra of a Bi_30 sample detected at different regions on the surface of the sample. (b) SEM image of Bi_30 sample showing EDS-detection points.

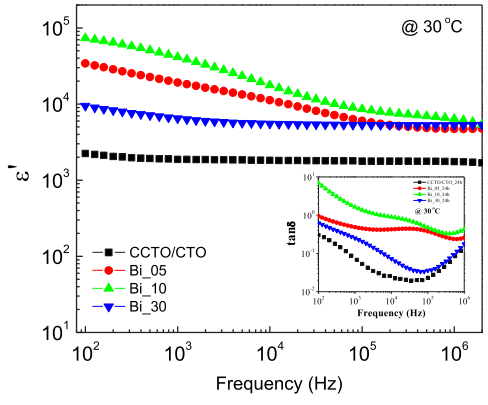

Fig. 4. Frequency dependence of ε' at 30 °C for Bi-doped CCTO/CTO composites; inset depicts tanδ as a function of frequency at 30 °C.

enhanced by doping with Bi^{3+}. This is likely due to the enhanced dielectric responses of internal interfaces [7]. At 30 °C and 1 kHz, the ε' values of the CCTO/CTO, Bi_05, Bi_10, and Bi_30 samples were found to be 1877, 19153, 41468, and 6458, respectively. Variation in tanδ due to substituted Bi^{3+} ions was similar to that observed in the change in ε'. Fig. 5 shows the temperature dependence of ε'. It was observed that ε' values of all the samples increased with increasing temperature. The increase in ε' at high temperatures for CCTO ceramics is usually observed. This may be related to the effect of dc conduction in the bulk sintered ceramic composites [30]. It is notable that strong increases in ε' were observed in the Bi_05 and Bi_10 samples.

To understand the possible mechanism(s) of the strongly enhanced dielectric response in Bi-doped CCTO/CTO composites, impedance spectroscopy was used to evaluate the electrical resistances of the grains and internal interfaces. Fig. 6 and its inset show impedance complex plane (Z^*) plots at 120 °C and an expanded view near the origin, respectively. The total resistance (R_{tot}) estimated from the diameter of a large semicircle arc of the CCTO/CTO ceramic was greatly reduced by doping with Bi^{3+}. In general, R_{tot} is governed by

Please cite this article as: J. Jumpatam, et al., Effects of Bi^{3+} doping on microstructure and dielectric properties of $CaCu_3Ti_4O_{12}/CaTiO_3$ composite ceramics, Ceramics International (2015), http://dx.doi.org/10.1016/j.ceramint.2015.03.197

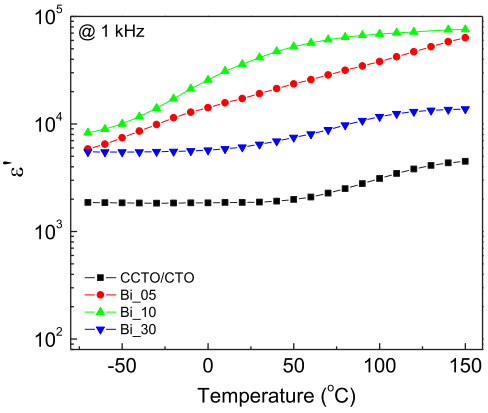

Fig. 5. ε' as a function of temperature at 1 kHz.

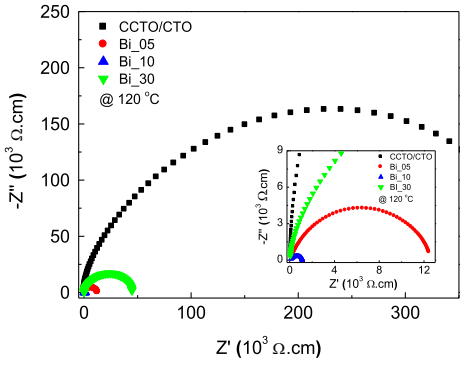

Fig. 6. Impedance complex plane plots (Z^* plots) of Bi-doped CCTO/CTO composites at 120 °C; inset shows an expanded view near the origin to reveal the impedance spectra of Bi_05 and Bi_10 samples.

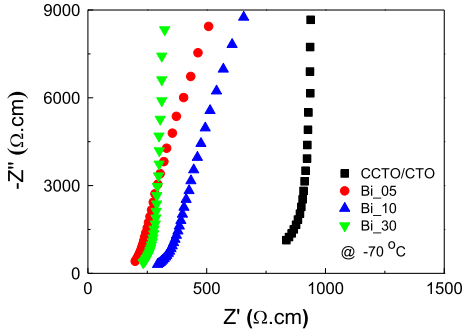

Fig. 7. Z^* plots at high frequencies of Bi-doped CCTO/CTO composites at −70 °C, showing the non-zero intercept on the Z' axis.

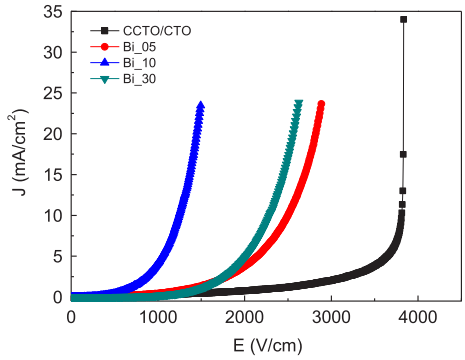

Fig. 8. Nonlinear J–E characteristics of Bi-doped CCTO/CTO composites.

the resistance of GBs (R_{gb}) [7]. In CCTO/CTO composites, GBs or interfaces between different types of grains consisted of interfaces between CCTO–CCTO grains, CCTO–CTO grains, and CTO–CTO grains. The resistance of grains (R_g) is usually determined from the non-zero intercept on the Z' axis [7]. It was also found that substitution of Bi^{3+} ions can reduce the value of R_g, as shown in Fig. 7.

Fig. 8 shows the nonlinear electrical characteristics of the CCTO/CTO and Bi-doped CCTO/CTO composites. Although all the composite samples exhibited nonlinear J–E behavior, different characteristics were observed in Bi-doped CCTO/CTO composites. Two important parameters (α and E_b) of all the composites were calculated. At room temperature, α values of the CCTO/CTO, Bi_05, Bi_10, and Bi_30 samples were found to be 9.9, 3.79, 3.60, and 5.22, respectively. E_b values of CCTO/CTO composites were greatly reduced by Bi^{3+} doping ions. These results indicate that the nonlinear J–E properties were degraded by doping with Bi^{3+} ions.

In CCTO and CTO ceramics, Bi^{3+} substitution for Ca^{2+} requires charge compensation. This may be achieved by one or more of the following mechanisms: (1) filling oxygen vacancies, (2) decrease of cation valence, (3) creation of cation vacancies, or (4) creation of conduction electrons. It is likely that the creation of conduction electrons may primarily be responsible for the observed decrease in R_g of Bi-doped CCTO/CTO composites. Ramirez et al. [19] used electrostatic force microscopy (EFM) to characterize possible electrical responses in a CCTO/CTO composite system. It was found that a CTO–CTO interface was electrically inactive, whereas, CCTO–CTO and CCTO–CCTO interfaces were electrically active. This indicates the presence of potential barriers at the CCTO–CTO and CCTO–CCTO interfaces. Thus, the degradation in the nonlinear electrical properties of CCTO/CTO due to the substitution of Bi^{3+} may have been related to weak electrical responses at these active interfaces. The reduction of the breakdown field in Bi-doped CCTO/CTO composites is primarily associated with a decrease in the potential barrier height (Φ_B) at internal interfaces. For a single phase of CCTO ceramics, the Schottky barrier at GBs can be expressed as [31]:

$$\Phi_B = \frac{qN_s^2}{8\varepsilon_0\varepsilon' N_d}, \quad (1)$$

where N_s and N_d are the acceptor (surface charge) concentration and the charge carrier concentration in semiconducting grains (*i.e.*, CCTO grains), respectively. ε' is the relative permittivity of materials, and q is the electronic charge. Using Eq. (1), the large reduction in Φ_B observed in CCTO/CTO composites is clearly attributable to an increase in N_d. Generally, an increase in N_d can cause a decrease in R_g. This is clearly observed in Fig. 7 showing a decrease in R_g of Bi-doped CCTO/CTO composites. It is reasonable to conclude that the increase in tanδ (inset of Fig. 4) was due to the reduction of total resistance of internal interfaces. Greatly enhanced dielectric response in Bi-doped CCTO/CTO

Please cite this article as: J. Jumpatam, et al., Effects of Bi^{3+} doping on microstructure and dielectric properties of $CaCu_3Ti_4O_{12}/CaTiO_3$ composite ceramics, Ceramics International (2015), http://dx.doi.org/10.1016/j.ceramint.2015.03.197

composites (especially for the Bi_05 and Bi_10 samples) may be due to the increase in charge carriers inside the grains. Under an applied electric field, more charge carries were accumulated at the internal interfaces (CCTO–CTO and CCTO–CCTO interfaces) of Bi-doped CCTO/CTO composites. This produces a relatively high intensity of interfacial polarization compared to that of the un-doped CCTO/CTO sample. This is responsible for the observed large increase in ε' in the Bi-doped CCTO/CTO composites. It is notable that R_{tot} of the Bi_30 sample was found to be larger than those of the Bi_05 and Bi_10 samples. This resulted in a lower tanδ value of the Bi_30 sample compared to those of the Bi_05 and Bi_10 samples. For the Bi_30 sample, a high value of R_{tot} compared the other samples might be due to precipitation of Bi_2O_3 at interfaces, just as was observed in commercial ZnO–Bi_2O_3 varistor ceramics [32].

4. Conclusions

In conclusion, we successfully prepared CCTO/CTO composites doped with Bi^{3+} ions. Influences of Bi^{3+} substitution of the microstructure, dielectric response, and nonlinear *J–E* properties were studied. It was found that Bi^{3+} doping ions were substituted into Ca^{2+} sites in both of CCTO and CTO phases. The dielectric response in CCTO/CTO composites was greatly enhanced by doping with Bi^{3+} ions. This can be well described based on the interfacial polarization at internal interfaces of CCTO/CTO composites. The increase in tanδ was consistent with the decrease in the total resistance of internal interfaces. The non-Ohmic properties of Bi^{3+}-doped CCTO/CTO composites were degraded, which might have resulted from a decrease in the potential barrier height at internal interfaces, i.e., CCTO–CCTO and CTO–CCTO interfaces.

Conflict of interest

We declare that we do not have any commercial or associative interest that represents a conflict of interest in connection with the work submitted.

Acknowledgments

This work was financially supported by the Thailand Research Fund (TRF) and Khon Kaen University, Thailand [Grant number TRG5680047]. This work was also supported by the Higher Education Research Promotion and National Research University Project of Thailand, Office of the Higher Education Commission, through the Advanced Functional Materials Cluster of Khon Kaen University. J. Jumpatam would like to thank the Thailand Graduate Institute of Science and Technology (TGIST) for his Master of Science Degree scholarship.

References

[1] M.A. Subramanian, D. Li, N. Duan, B.A. Reisner, A.W. Sleight, High dielectric constant in $ACu_3Ti_4O_{12}$ and $ACu_3Ti_3FeO_{12}$ phases, J. Solid State Chem. 151 (2) (2000) 323–325.
[2] S.-Y. Chung, I.-D. Kim, S.-J.L. Kang, Strong nonlinear current–voltage behaviour in perovskite-derivative calcium copper titanate, Nat. Mater. 3 (11) (2004) 774–778.
[3] V.P.B. Marques, A. Ries, A.Z. Simões, M.A. Ramírez, J.A. Varela, E. Longo, Evolution of $CaCu_3Ti_4O_{12}$ varistor properties during heat treatment in vacuum, Ceram. Int. 33 (7) (2007) 1187–1190.
[4] B. Cheng, Y.-H. Lin, J. Yuan, J. Cai, C.-W. Nan, X. Xiao, J. He, Dielectric and nonlinear electrical behaviors of La-doped $CaCu_3Ti_4O_{12}$ ceramics, J. Appl. Phys. 106 (3) (2009) 034111.
[5] F. Luo, J. He, J. Hu, Y.-H. Lin, Electric and dielectric properties of Bi-doped $CaCu_3Ti_4O_{12}$ ceramics, J. Appl. Phys. 105 (7) (2009) 076104.
[6] S. Jin, H. Xia, Y. Zhang, Effect of La-doping on the properties of $CaCu_3Ti_4O_{12}$ dielectric ceramics, Ceram. Int. 35 (1) (2009) 309–313.
[7] R. Schmidt, M.C. Stennett, N.C. Hyatt, J. Pokorny, J. Prado-Gonjal, M. Li, D.C. Sinclair, Effects of sintering temperature on the internal barrier layer capacitor (IBLC) structure in $CaCu_3Ti_4O_{12}$ (CCTO) ceramics, J. Eur. Ceram. Soc. 32 (12) (2012) 3313–3323.
[8] L. Liu, H. Fan, X. Chen, P. Fang, Electrical properties and microstructural characteristics of nonstoichiometric $CaCu_{3x}Ti_4O_{12}$ ceramics, J. Alloy. Compd. 469 (1–2) (2009) 529–534.
[9] Q. Zheng, H. Fan, Influence of fabrication parameters on the phase formation and dielectric properties of $CaCu_3Ti_4O_{12}$ ceramics, J. Mater. Sci. Technol. 28 (10) (2012) 920–926.
[10] Y.J. Wu, S.H. Su, S.Y. Wu, X.M. Chen, Microstructures and dielectric properties of spark plasma sintered $Ba_{0.4}Sr_{0.6}TiO_3/CaCu_3Ti_4O_{12}$ composite ceramics, Ceram. Int. 37 (6) (2011) 1979–1983.
[11] H. Ren, P. Liang, Z. Yang, Processing, dielectric properties and impedance characteristics of $Na_{0.5}Bi_{0.5}Cu_3Ti_4O_{12}$ ceramics, Mater. Res. Bull. 45 (11) (2010) 1608–1613.
[12] W. Somphan, P. Thongbai, T. Yamwong, S. Maensiri, High Schottky barrier at grain boundaries observed in $Na_{1/2}Sm_{1/2}Cu_3Ti_4O_{12}$ ceramics, Mater. Res. Bull. 48 (10) (2013) 4087–4092.
[13] Y. Qiu, Z.Z. Ma, S.X. Huo, H.N. Duan, Z.M. Tian, S.L. Yuan, L. Chen, Giant dielectric and low voltage varistor behaviors of Ba-doped $Bi_{1/2}Na_{1/2}Cu_3Ti_4O_{12}$ ceramics, J. Mater. Sci.: Mater. Electron. 23 (8) (2012) 1587–1591.
[14] W. Hao, J. Zhang, Y. Tan, W. Su, Giant dielectric-permittivity phenomena of compositionally and structurally $CaCu_3Ti_4O_{12}$-like oxide ceramics, J. Am. Ceram. Soc. 92 (12) (2009) 2937–2943.
[15] Y. Liu, W. Wang, J. Huang, F. Tang, C. Zhu, Y. Cao, Dielectric properties of giant permittivity $NaCu_3Ti_3NbO_{12}$ ceramics, Ceram. Int. 39 (2013) 9201–9206.
[16] T.-T. Fang, C.P. Liu, Evidence of the internal domains for inducing the anomalously high dielectric constant of $CaCu_3Ti_4O_{12}$, Chem. Mater. 17 (20) (2005) 5167–5171.
[17] W.C. Ribeiro, E. Joanni, R. Savu, P.R. Bueno, Nanoscale effects and polaronic relaxation in compounds, Solid State Commun. 151 (2) (2011) 173–176.
[18] W. Kobayashi, I. Terasaki, $CaCu_3Ti_4O_{12}/CaTiO_3$ composite dielectrics: Ba/Pb-free dielectric ceramics with high dielectric constants, Appl. Phys. Lett. 87 (3) (2005) 032902.
[19] M.A. Ramírez, P.R. Bueno, R. Tararam, A.A. Cavalheiro, E. Longo, J.A. Varela, Evaluation of the effect of the stoichiometric ratio of Ca/Cu on the electrical and microstructural properties of the $CaCu_3Ti_4O_{12}$ polycrystalline system, J. Phys. D: Appl. Phys. 42 (18) (2009) 185503.
[20] R. Jia, X. Zhao, J. Li, X. Tang, Colossal breakdown electric field and dielectric response of Al-doped $CaCu_3Ti_4O_{12}$ ceramics, Mater. Sci. Eng.: B 185 (2014) 79–85.
[21] H.E. Kim, S.-M. Choi, Y.-W. Hong, S.-I. Yoo, Improved dielectric properties of the $CaCu_3Ti_4O_{12}$ composites using $BaTiO_3$-coated powder as precursor, J. Alloy. Compd. 610 (0) (2014) 594–599.

Please cite this article as: J. Jumpatam, et al., Effects of Bi^{3+} doping on microstructure and dielectric properties of $CaCu_3Ti_4O_{12}/CaTiO_3$ composite ceramics, Ceramics International (2015), http://dx.doi.org/10.1016/j.ceramint.2015.03.197

[22] M.A. Ramírez, P.R. Bueno, J.A. Varela, E. Longo, Non-Ohmic and dielectric properties of a $Ca_2Cu_2Ti_4O_{12}$ polycrystalline system, Appl. Phys. Lett. 89 (21) (2006) 212102.
[23] J. Jumpatam, B. Putasaeng, T. Yamwong, P. Thongbai, S. Maensiri, A novel route to greatly enhanced dielectric permittivity with reduce loss tangent in $CaCu_{3-x}Zn_xTi_4O_{12}/CaTiO_3$ composites, J. Am. Ceram. Soc. 97 (8) (2014) 2368–2371.
[24] J. Jumpatam, B. Putasaeng, T. Yamwong, P. Thongbai, S. Maensiri, A novel strategy to enhance dielectric performance and non-Ohmic properties in $Ca_2Cu_{2-x}Mg_xTi_4O_{12}$, J. Eur. Ceram. Soc. 34 (12) (2014) 2941–2950.
[25] R. Kashyap, O.P. Thakur, R.P. Tandon, Study of structural, dielectric and electrical conduction behaviour of Gd substituted $CaCu_3Ti_4O_{12}$ ceramics, Ceram. Int. 38 (4) (2012) 3029–3037.
[26] S.-H. Hong, D.-Y. Kim, H.-M. Park, Y.-M. Kim, Electric and dielectric properties of Nb-doped $CaCu_3Ti_4O_{12}$ ceramics, J. Am. Ceram. Soc. 90 (7) (2007) 2118–2121.
[27] S.-Y. Chung, J.-H. Choi, J.-K. Choi, Tunable current–voltage characteristics in polycrystalline calcium copper titanate, Appl. Phys. Lett. 91 (9) (2007) 091912.
[28] P. Thongbai, B. Putasaeng, T. Yamwong, S. Maensiri, Improved dielectric and non-ohmic properties of $Ca_2Cu_2Ti_4O_{12}$ ceramics prepared by a polymer pyrolysis method, J. Alloy. Compd. 509 (27) (2011) 7416–7420.
[29] M.N. Rahaman, Ceramic processing and sintering, 2nd ed., M. Dekker, New York, 2003.
[30] J. Wu, C.-W. Nan, Y. Lin, Y. Deng, Giant dielectric permittivity observed in Li and Ti doped NiO, Phys. Rev. Lett. 89 (21) (2002) 217601.
[31] T. Adams, D. Sinclair, A. West, Characterization of grain boundary impedances in fine- and coarse-grained $CaCu_3Ti_4O_{12}$ ceramics, Phys. Rev. B 73 (9) (2006) 094124.
[32] A.J. Moulson, J.M. Herbert, Electroceramics: materials, properties, applications, 2nd ed., Wiley, West Sussex; New York, 2003.

Please cite this article as: J. Jumpatam, et al., Effects of Bi^{3+} doping on microstructure and dielectric properties of $CaCu_3Ti_4O_{12}/CaTiO_3$ composite ceramics, Ceramics International (2015), http://dx.doi.org/10.1016/j.ceramint.2015.03.197

J Mater Sci: Mater Electron (2014) 25:4657–4663
DOI 10.1007/s10854-014-2219-1

Effects of La^{3+} doping ions on dielectric properties and formation of Schottky barriers at internal interfaces in a $Ca_2Cu_2Ti_4O_{12}$ composite system

Prasit Thongbai · Jutapol Jumpatam · Bundit Putasaeng · Teerapon Yamwong · Vittaya Amornkitbamrung · Santi Maensiri

Received: 20 May 2014 / Accepted: 28 July 2014 / Published online: 7 August 2014

Abstract Influences of La^{3+} substitution on the dielectric properties and formation of Schottky barriers at internal interfaces of a $Ca_2Cu_2Ti_4O_{12}$ ($CaTiO_3/CaCu_3Ti_4O_{12}$) composite system were investigated. It was found that electrostatic potential barrier height was greatly reduced by doping with La^{3+}, leading to a large decrease in the total resistance of internal interfaces between grains. This observation was attributed to the creation of conduction electrons, which were possibly induced by electrical charge compensation of La^{3+} substitution into Ca^{2+} sites. Variations in the dielectric properties of La^{3+}-doped $CaTiO_3/CaCu_3Ti_4O_{12}$ composite ceramics and nonlinear properties can be described based on the electrical responses at the internal interfaces between $CaCu_3Ti_4O_{12}$–$CaCu_3Ti_4O_{12}$ grains and $CaTiO_3$–$CaCu_3Ti_4O_{12}$ grains. Influence of possible charge compensation due to different levels of La^{3+} dopant on the formation of potential barriers was discussed.

P. Thongbai (✉) · V. Amornkitbamrung
Department of Physics, Faculty of Science, Khon Kaen University, Khon Kaen 40002, Thailand
e-mail: pthongbai@kku.ac.th

P. Thongbai · V. Amornkitbamrung
Integrated Nanotechnology Research Center (INRC), Khon Kaen University, Khon Kaen 40002, Thailand

J. Jumpatam
Materials Science and Nanotechnology Program, Faculty of Science, Khon Kaen University, Khon Kaen 40002, Thailand

B. Putasaeng · T. Yamwong
National Metal and Materials Technology Center (MTEC), Thailand Science Park, Pathumthani 12120, Thailand

S. Maensiri
School of Physics, Institute of Science, Suranaree University of Technology, Nakhon Ratchasima 30000, Thailand

1 Introduction

Recently, $CaCu_3Ti_4O_{12}$ (CCTO) has been widely studied due to its very high dielectric permittivity (ε') and it fascinating but incompletely understood physical behavior [1–14]. Electrical responses of various CCTO internal interfaces and related compounds were investigated to elucidate the abnormal dielectric response in this material. The internal interfaces are grain boundaries (GBs) [2, 3], domain boundaries (DBs) [15], line defects due to stacking faults [16], and interfaces between the CCTO grain matrix and secondary phases of other particles [6, 9, 10, 16–21]. In addition to these interesting dielectric properties, CCTO can also exhibit non-Ohmic properties that reveal a nonlinear relationship between current density and electric field (J–E). The internal interface or GB was clearly shown to be the cause of observed nonlinear J–E behavior of CCTO polycrystalline ceramics [2, 22].

Kobayashi and Terasaki [17] improved the dielectric properties of CCTO ceramics by creating a composite system of CCTO/$CaTiO_3$ (CCTO/CTO) from a starting material with the chemical formula of $Ca_2Cu_2Ti_4O_{12}$. It was further found that improved nonlinear J–E properties were also observed in this composite system [16, 18, 19]. CCTO/CTO composites have very low loss tangents ($\tan\delta \sim 0.02$) with very high breakdown field values (E_b) and large nonlinear coefficients (α) compared to a single phase of CCTO ceramics [16–19]. The enhanced performance of nonlinear J–E properties in CCTO/CTO composites was mainly due to the electrical response of the CTO-CCTO interface, which does not appear in a single

phase CCTO ceramic. It was often observed that doping metal ions in CCTO ceramics can change macroscopic dielectric and nonlinear *J–E* properties [4, 5, 7, 8, 10–12, 23–29]. Changes in dielectric response and nonlinear properties may be due to the effect of dopants upon the electrical properties of GBs in a CCTO microstructure. Possible charge compensation due to substitution of aliovalent cations was hypothesized to responsible for the electrical properties of grains and GBs [26, 28, 29].

There are several brief reports on the giant dielectric properties of related oxides in the family of $\boldsymbol{A}Cu_3Ti_4O_{12}$ compounds, especially for $\boldsymbol{A} = La^{3+}$ and $[Na^{+}La^{3+}]_{1/2}$ [1, 30, 31]. Lattice parameters of these two ceramics (7.417 Å) and CCTO (7.391 Å) are nearly the same in value. Therefore, this indicates that La^{3+} ions can perfectly substitute into Ca^{2+} sites in related-perovskite structure of CCTO. In La^{3+}-doped $BaTiO_3$ [32], both the electronic (by electrons) and ionic compensations (by cation vacancies) can occur, depending on doping concentration levels. To our knowledge, investigation of dielectric and *J–E* properties of CCTO/CTO composites substituted by aliovalent cations (*e.g.*, for La^{3+} doping into Ca^{2+} site) has never been reported. Different charge-compensation mechanisms may have an effect on the non-Ohmic properties and/or dielectric response in CCTO/CTO composites.

In this work, we substituted aliovalent La^{3+} cations at different concentration levels into Ca^{2+} sites of CCTO/CTO composites in order to study the possible impacts of charge compensation on the dielectric and electrical nonlinear properties. It was found that La^{3+} substitution had great effects on both of dielectric and nonlinear properties. The electrostatic potential barriers at internal interfaces of CCTO/CTO composites were strongly reduced by doping with 2.5 mol % La^{3+}. Higher concentrations of 15 mol % La^{3+} dopant ions had a slight influence on the potential barrier height compared to a relatively low concentration of 2.5 mol % La^{3+}. This resulted from different mechanisms of charge compensations, *i.e.*, electronic and ionic compensations, respectively.

2 Experimental details

Ceramics with nominal compositions of $Ca_2Cu_2Ti_4O_{12}$ (La–0), $Ca_{1.95}La_{0.05}Cu_2Ti_4O_{12}$ (La–05), and $Ca_{1.7}La_{0.3}Cu_2Ti_4O_{12}$ (La–30) were prepared by a solid state reaction method using $CaCO_3$ (99.9 % purity), La_2O_3 (99.99 % purity), CuO (99.9 % purity) and TiO_2 (99.9 % purity) as starting raw materials. First, stoichiometric amounts of raw materials were mixed during ball milling in ethanol for 24 h using ZrO_2 balls. Second, the mixed slurry was dried and calcined at 900 °C for 10 h. Third, the resulting powder was ground and re-calcined at 900 °C for 5 h. Then, all calcined powders were ground and pressed into pellets to form green bodies. Finally, the green bodies were sintered at 1,100 °Cfor 24 h.

Phase compositions were investigated using X-ray diffraction (XRD) (Philips PW3040). The dielectric response of the samples was measured using an Agilent 4294A Precision Impedance Analyzer over a frequency range of 10^2–10^7 Hz with an oscillation voltage of 500 mV. The dielectric properties as a function of temperature were measured over the range of $-70 \sim 150$ °C. The step increase in each measurement temperature was 10 °C with an accuracy of ±1 °C. *J–E* measurements were determined at various temperatures using a high voltage measurement unit (Keithley Model 247). The breakdown electric field (E_b) was obtained at $J = 1$ mA cm^{-2}. The nonlinear coefficient (α) values were calculated over the range of $J = 1$–10 mA cm^{-2}.

3 Results and discussion

The XRD patterns of $Ca_{2-x}La_xCu_2Ti_4O_{12}$ ($x = 0$, 0.05, and 0.30) compositions are shown in Fig. 1. It is clearly seen that all of the ceramic compositions consisted of two main phases, CCTO (JCPDS 75-2188) and CTO (JCPDS 82-0231), forming a composite system of CCTO/CTO. These XRD patterns are similar to those reported in the literature for $Ca_2Cu_2Ti_4O_{12}$ ceramics [16, 18, 21, 33]. An impurity phase of CuO was observed in the La-30 samples. This may be due to the decomposition of CuO from the lattice [34]. Theoretically, a ceramic that was prepared using a starting composition of $Ca_2Cu_2Ti_4O_{12}$ should consist of ~33.3 mol % of CCTO and ~66.7 mol % of CTO. This was experimentally confirmed by a Rietveld

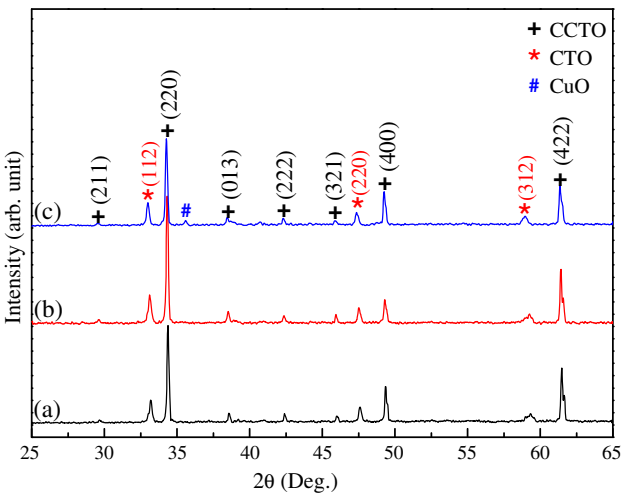

Fig. 1 XRD patterns of **a** $Ca_2Cu_2Ti_4O_{12}$ (La-0 sample), **b** $Ca_{1.95}La_{0.05}Cu_2Ti_4O_{12}$ (La-05 sample), and **c** $Ca_{1.7}La_{0.3}Cu_2Ti_4O_{12}$ (La-30 sample) ceramics

quantitative analysis [16]. Formation of a CCTO/CTO composite system was due to the much larger ionic radius of Ca^{2+} than of Cu^{2+}. Therefore, excess Ca^{2+} ions could not be substituted into Cu^{2+} sites in a planar square to create a $Ca(CaCu_2)Ti_4O_{12}$ structure. Lattice parameters of the CCTO phases of La–0, La-05 and La-30 samples were calculated and found to be 7.3891, 7.3928, and 7.3943 Å, respectively. The lattice parameter of CCTO phase in the CCTO/CTO composites increased with increasing La^{3+} doping concentration. The increase in the lattice parameter may be attributed to the different ionic radii between Ca^{2+} and La^{3+} ions.

Figure 2 and its insets show ε′ and tanδ at 20 °C as a function of frequency for the La-0, La-05, and La-30 samples. In a low frequency range of 10^2–10^3 Hz, ε′ of the La-doped samples was much higher than that of the undoped sample. ε′ values at 10^2 Hz for the La-0, La-05, and La-30 samples were found to be 2,060, 11,162, and 6,378, respectively. It was observed that these high ε′ values in a low frequency range decreased as the frequency was increased from 10^2 to 10^3 Hz. This result indicates the dominant effect of dc conduction and/or low-frequency dielectric relaxation [35]. As shown in the inset of Fig. 2, tanδ greatly increased as frequency was decreased. However, the increase in tanδ was not exponentially. Conversely, the magnitude of the tanδ relaxation peak was not large. Therefore, the frequency dependence of tanδ in a low-frequency range was affected by the combined effects of dc conduction and a relaxation process [36]. tanδ values of La-0, La-05, and La-30 samples at 10^2 Hz were found to be 0.219, 0.517, and 2.971, respectively. tanδ of CCTO/CTO composites increased with increasing La^{3+} doping concentration. Variations in tanδ with changing concentration of La^{3+} were not consistent with changes in ε′.

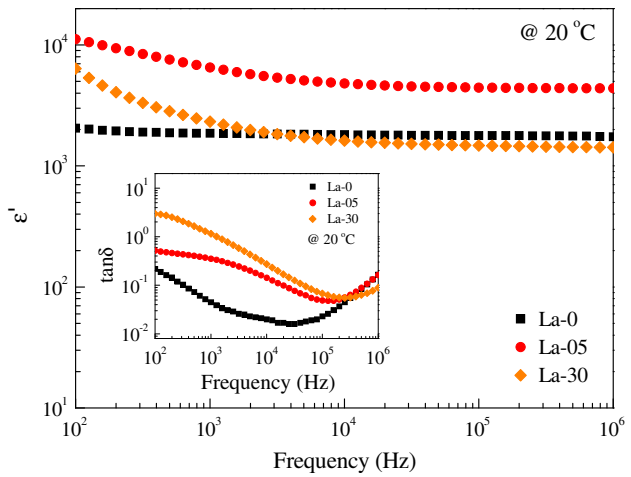

Fig. 2 ε′ at 20 °C in the frequency range of 10^2–10^6 Hz for all samples; the inset shows the frequency dependence of tanδ

Generally, variations in the properties of CCTO ceramics were consistent with each other. Increases in ε′ of CCTO ceramics were usually accompanied by an increase in tanδ [37]. This result can be described by considering interfacial polarization at GBs. High ε′ values are attributed to a large polarization intensity at the interfaces between adjacent grains, which are insulating GBs. Concurrently, a large polarization intensity indicates a high density of accumulated charges at GBs, driven by an external electric field. High concentrations of mobile charges inside semiconducting grains are a source of space charges. Conversely, high concentrations of charges not only contribute to polarization intensity and ε′, but also increase the possibility of leaked current in bulk ceramics. This is a major cause of high tanδ. Therefore, the dielectric response behavior in La^{3+}-doped CCTO/CTO composites might be significantly influenced by the electrical characteristics of GBs as well.

In the current study, the effects of La^{3+} doping on the *J*–*E* characteristics of CCTO/CTO composites were investigated. Figure 3 shows the nonlinear *J*–*E* properties of the study samples at different temperatures. E_b values at room temperature of the La-0, La-05, and La-30 samples were found to be 4,811, 732, and 665 V/cm, respectively. α values of the same samples at room temperature were found to be 7.66, 3.14, and 1.62, respectively. The nonlinear properties of CCTO/CTO composites were degraded as La^{3+} ions were substituted for Ca^{2+} sites. According to a previous work [38], substitution of La^{3+} into CCTO with nominal chemical compositions of $Ca_{1-3x/2}La_xCu_3Ti_4O_{12}$ ($x = 0-0.09$) caused a decrease in dc conduction activation energy when $x > 0.05$. Cheng et al. [5] found an increase in E_b in $Ca_{1-3x/2}La_xCu_3Ti_4O_{12}$ as La^{3+} concentration increased. From these two studies, the molar ratio of Ca^{2+} was adjusted to obtain an electrical charge equilibrium and thus freed electrons since an aliovalent dopant was not expected. In the current study, electronic charge compensation by conduction electrons may have existed due to La^{3+} ions being substituted into Ca^{2+} sites. This may have been the primary cause of the degradation of nonlinear properties. Ramirez et al. [16] used electrostatic force microscopy (EFM) to characterize possible electrical responses in a CCTO/CTO composite system. They found that a CTO–CTO interface was electrically inactive, while CCTO–CTO and CCTO–CCTO interfaces were electrically active. This indicates the presence of potential barriers.

To study the effect of La^{3+} doping ions on the formation of electrostatic potential barriers at internal interfaces of CCTO/CTO composites, nonlinear *J*–*E* properties were determined at different temperatures. As shown in Fig. 3a–c, E_b linearly decreased with increasing temperature. This indicated the influence of temperature upon the

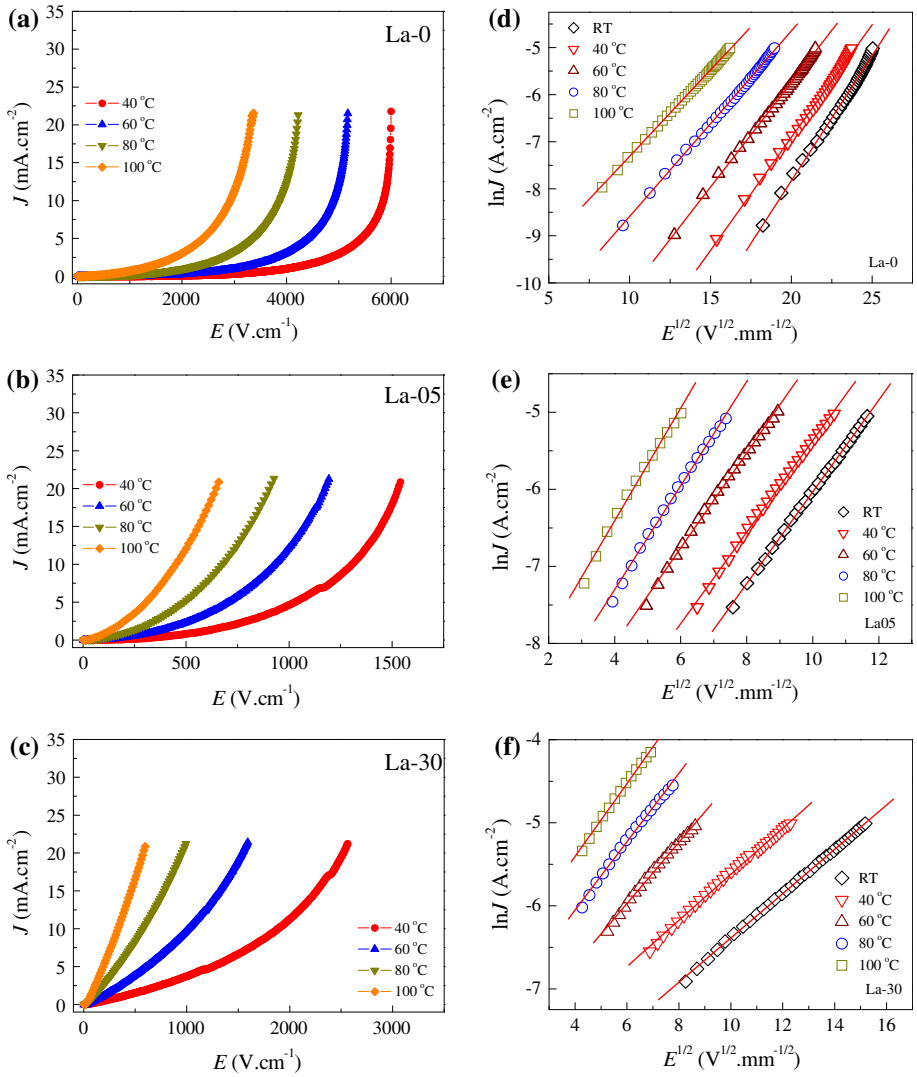

Fig. 3 **a–c** Nonlinear *J–E* characteristics at various temperatures for La-0, La05, and La30 samples, respectively. **d–f** Plots of ln*J* versus $E^{1/2}$

electrostatic potential barriers at internal interfaces. According to previous work [2, 5, 6, 20, 22], the electrical response of GBs (CCTO–CCTO interfaces) for a single phase CCTO polycrystalline ceramic clearly resulted from the Schottky effect. It was also further suggested that the potential barriers at CCTO–CTO interfaces were also Schottky-type barriers [16]. Therefore, electrical conduction at CCTO–CCTO and CCTO-CTO interfaces in the pre-breakdown region should be due to thermion emission of the Schottky barrier [5, 6]. This emission is usually affected by the electric field (E) and temperature (T). Variations of J with E and T will follow the relationship [20]:

$$\ln J = \frac{\beta E^{1/2}}{k_B T} + \left[\ln AT^2 - \frac{\Phi_B}{k_B T}\right] \quad (1)$$

where Φ_B is the Schottky potential-energy barrier height at the GBs, A is the Richardson constant, and β is a constant related to the potential barrier width. The last term on the right hand side of Eq. (1) is expressed as:

$$\ln J_0 = \ln AT^2 - \frac{\Phi_B}{k_B T}. \quad (2)$$

Values of lnJ_0 at various temperatures were calculated from the plots of ln$J$ versus $E^{1/2}$ by linearly fitting data at $E = 0$. Figure 3d–f show the fitted results, indicating a good linear relationship between ln$J$ vs. $E^{1/2}$. Using Eq. (2), Φ_B values for all the samples were calculated by fitting data of the plots of lnJ_0 versus 1,000/T. As shown in Fig. 4, a good linear relationship between J_0 and temperature was observed. Values of Φ_B were approximately 0.919, 0.321, and 0.216 eV for the La-0, La-05, and La-30 samples, respectively. It is notable that $\Phi_B \approx 0.919$ eV for the La-0 (CCTO/CTO) sample can be comparable to that observed in the CCTO/CTO composite prepared by a simple thermal decomposition method (0.856 eV) [39]. This value is also

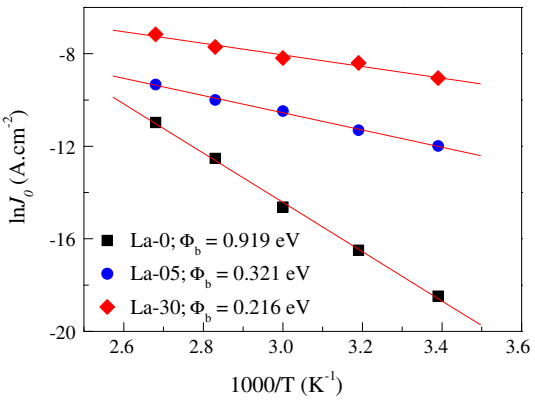

Fig. 4 Plots of lnJ_0 versus 1,000/T for all samples; the *solid lines* are results fitted to Eq. (2)

comparable to that observed in $Na_{1/2}Sm_{1/2}Cu_3Ti_4O_{12}$ ceramics (0.925–0.964 eV) [40]. Φ_B of CCTO/CTO composites was greatly reduced by doping with La^{3+}. This means that La^{3+} doping ions have an effect on the formation of electrostatic potential barriers at CCTO–CTO and CCTO–CCTO interfaces. For a single phase of CCTO ceramics, the Schottky barrier at GBs can be expressed as [22]:

$$\Phi_B = \frac{qN_s^2}{8\varepsilon_0\varepsilon' N_d}, \quad (3)$$

where N_s and N_d are the acceptor (surface charge) concentration and the charge carrier concentration in semiconducting grains (*i.e.*, CCTO grains), respectively. ε' is the relative permittivity of materials, and q is the electronic charge. Using Eq. (3), it is possible that the strong reduction of Φ_B observed in CCTO/CTO composites can be attributed to either an increase in N_d or a large decrease in N_s. Generally, an increase in N_d can cause a decrease in resistance of grain interiors (R_g). In Ta^{5+} and Nb^{5+}-doped CCTO ceramic systems [26], it was found that Ta^{5+} and Nb^{5+} doping ions had no significant effect on R_g of CCTO ceramics. Thus, the observed strong decrease in potential barriers at GBs of these materials was not related to any change of N_d and other proposed mechanism. Charge compensation mechanisms were investigated in nominal compositions of $La_xCa_{1-3x/2}Cu_3Ti_4O_{12}$ and $La_xCa_{1-x}Cu_3Ti_4O_{12}$ [38]. It was clearly shown that in the latter material, electrical compensation was found to be conduction electrons.

In the current study, impedance spectroscopy was used to investigate the electrical properties of grains and GBs. As shown in Fig. 5a, at 20 °C, the diameter of a large semicircle arc in the plot of the complex impedance plane (Z*) of CCTO/CTO composites decreased with increasing La^{3+} dopant concentration. This result indicated a large

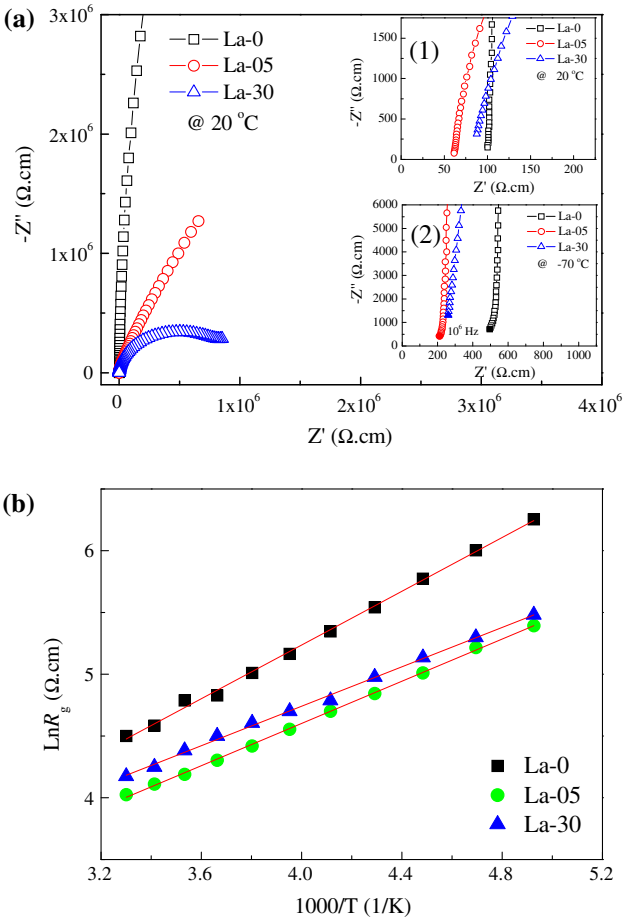

Fig. 5 **a** Comparison of impedance complex plane (Z*) plots at 20 °C for all samples; *insets* (1) and (2) show high-frequency data close to the origin at 20 and −70 °C, respectively. **b** Temperature dependence of R_g of all ceramic samples

reduction of the total resistance at internal interfaces [3], *i.e.*, GBs between CCTO–CCTO grains and CTO-CCTO grains [16]. The insets (1) and (2) of Fig. 5a show the non-zero intercept on the Z′ axis of the impedance spectra in a high-frequency range at 20 and −70 °C, respectively. The resistances of semiconducting grains or R_g values of CCTO/CTO composites can be estimated from these non-zero intercepts [3]. At −70 °C, R_g values of ∼200 Ω cm for the La-05 and La-30 samples were much lower than R_g ∼ 500 Ω.cm for the La-0 sample (un-doped CCTO/CTO composites). R_g values at various temperatures in the range from −70 to 30 °C for all the samples are shown in Fig. 5b. This result indicates that N_d values of the La-05 and La-30 samples were enhanced. Thus, substitution of La^{3+} ions to Ca^{2+} sites was electrically compensated by conduction electrons. As demonstrated in Fig. 5b, R_g decreases with increasing temperature. It was found that the temperature dependence of R_g follows the Arrhenius law:

$$R_g = R_0 \exp\left(\frac{E_g}{k_B T}\right), \quad (4)$$

where E_g is the activation energy for conduction in the grain interiors, R_0 is a constant term, T is absolute temperature (K), and k_B is Boltzmann constant. The temperature dependence of R_g is well fitted by Eq. (4). E_g values of the La-0, La-05, and La-30 samples were calculated from the fitted result and found to be 94, 74, and 69 meV, respectively.

According to Eq. (3), the strong decrease in observed Φ_B values for the La-05 and La-30 samples can be attributed to the increase in charge carrier concentration in the semiconducting grains compared to the La-0 sample. It is important to note that Φ_B of the La-30 sample was slightly reduced further to 0.216 eV. This observation is similar to that observed in Ta^{5+} and Nb^{5+}-doped CCTO systems [26]. R_g values of these two samples were nearly the same in value. R_g of the La-30 sample was slightly larger than that of the La-05 sample. This result means that N_d did not increase even though La^{3+} dopant concentration was further increased from $x = 0.05$ to 0.3. Charge compensation for La^{3+} substituted to Ca^{2+} sites by conduction electrons no longer occurred when La^{3+} concentration was increased to a higher level of 15 mol% ($x = 0.3$). In contrast, the ionic compensation by cation vacancies may have occurred in grain interiors, just as it occurred in La^{3+}-doped $BaTiO_3$ [32]. Chung et al. [26] proposed that at GBs, the positive charge of the dopant cations could efficiently make compensation of the negative charge of unknown acceptors without the creation of electrons or cation vacancies in this region. Consequently, the number of active acceptor states at GBs (CCTO–CCTO and/or CTO-CCTO interfaces) that contribute to the formation of potential barriers decreases with La^{3+} addition. It is notable that the large increase in ε' of the La-05 sample compared to the La-0 sample (un-doped CCTO/CTO composite) might be due to a high intensity of interfacial polarization at the internal interfaces. Conversely, the decrease in ε' of the La-30 sample might be due to its low Φ_B value. It is possible that this potential barrier height of the La-30 sample was not sufficient to completely restrict the motion of conduction electrons within the grains. Most of them can move across GBs. Thus, the intensity of polarization at interfaces decreased, leading to a decrease in ε'. This is consistent with its tanδ value, which was highest among these three composites under study. Such a high value of tanδ was primarily caused by a dc current that resulted from a high concentration of conduction electrons across GBs.

4 Conclusions

La^{3+} doping ions have great effects on the dielectric properties and formation of Schottky barriers at internal interfaces of a CCTO/CTO composite system. The high potential barriers at internal interfaces of the CCTO/CTO composite were greatly degraded by La^{3+} doping. The degradation of Schottky barriers resulted in a large decrease in the total resistance of internal interfaces between grains. The creation of conduction electrons due to charge compensation for La^{3+} ions substituted into Ca^{2+} sites is proposed as the primary cause. For high concentrations of La^{3+} dopant, ionic compensation by cation vacancies was another cause that further reduced the potential barrier height. The interfacial polarization mechanism at CCTO–CCTO and CTO–CCTO interfaces can be used to described the dielectric response in La^{3+}-doped CCTO/CTO composite ceramics.

Acknowledgments This work was financially supported by the Thailand Research Fund (TRF) and Khon Kaen University, Thailand (Grant No. TRG5680047) and the Integrated Nanotechnology Research Center (*INRC*), Khon Kaen University, Thailand. J. Jumpatam would like to thank the Thailand Graduate Institute of Science and Technology (TGIST) for his Master of Science Degree scholarship.

References

1. M.A. Subramanian, D. Li, N. Duan, B.A. Reisner, A.W. Sleight, J. Solid State Chem. **151**, 323 (2000)
2. S.-Y. Chung, I.-D. Kim, S.-J.L. Kang, Nat. Mater. **3**, 774 (2004)
3. R. Schmidt, M.C. Stennett, N.C. Hyatt, J. Pokorny, J. Prado-Gonjal, M. Li, D.C. Sinclair, J. Eur. Ceram. Soc. **32**, 3313 (2012)
4. S. Jin, H. Xia, Y. Zhang, Ceram. Int. **35**, 309 (2009)
5. B. Cheng, Y.-H. Lin, J. Yuan, J. Cai, C.-W. Nan, X. Xiao, J. He, J. Appl. Phys. **106**, 034111 (2009)
6. J. Yuan, Y.-H. Lin, H. Lu, B. Cheng, C.-W. Nan, J. Am. Ceram. Soc. **94**, 1966 (2011)
7. Q. Zheng, H. Fan, C. Long, J. Alloys Compd. **511**, 90 (2012)
8. Y. Wang, L. Ni, X.M. Chen, J. Mater. Sci.: Mater. Electron. **22**, 345 (2011)
9. J. Li, R. Jia, X. Tang, X. Zhao, S. Li, J. Phys. D Appl. Phys. **46**, 325304 (2013)
10. R. Jia, X. Zhao, J. Li, X. Tang, Mater. Sci. Eng. B **185**, 79 (2014)
11. Y. Liu, Q. Chen, X. Zhao, J. Mater. Sci. Mater. Electron. **25**, 1547 (2014)
12. L.F. Xu, T. Cheng, R.L. Wang, H.B. Xiao, G.Z. Liu, C.P. Yang, J. Mater. Sci. Mater. Electron. **25**, 817 (2013)
13. Y. Yang, X. Wang, B. Liu, J. Mater. Sci. Mater. Electron. **25**, 146 (2014)
14. P. Liang, Y. Li, F. Li, X. Chao, Z. Yang, Mater. Res. Bull. **52**, 42 (2014)
15. T.-T. Fang, C.P. Liu, Chem. Mater. **17**, 5167 (2005)
16. M.A. Ramírez, P.R. Bueno, R. Tararam, A.A. Cavalheiro, E. Longo, J.A. Varela, J. Phys. D Appl. Phys. **42**, 185503 (2009)
17. W. Kobayashi, I. Terasaki, Appl. Phys. Lett. **87**, 032902 (2005)
18. P. Thongbai, B. Putasaeng, T. Yamwong, S. Maensiri, J. Alloys Compd. **509**, 7416 (2011)
19. M.A. Ramírez, P.R. Bueno, J.A. Varela, E. Longo, Appl. Phys. Lett. **89**, 212102 (2006)
20. Y.-H. Lin, J. Cai, M. Li, C.-W. Nan, J. He, J. Appl. Phys. **103**, 074111 (2008)
21. J. Jumpatam, B. Putasaeng, T. Yamwong, P. Thongbai, S. Maensiri, J. Eur. Ceram. Soc. **34**, 2941 (2014)
22. T. Adams, D. Sinclair, A. West, Phys. Rev. B **73**, 094124 (2006)

23. P. Thongbai, J. Boonlakhorn, B. Putasaeng, T. Yamwong, S. Maensiri, J. Am. Ceram. Soc. **96**, 379 (2013)
24. P. Thongbai, J. Jumpatam, B. Putasaeng, T. Yamwong, S. Maensiri, J. Appl. Phys. **112**, 114115 (2012)
25. P. Thongbai, S. Vangchangyia, E. Swatsitang, V. Amornkitbamrung, T. Yamwong, S. Maensiri, J. Mater. Sci. Mater. Electron. **24**, 875 (2013)
26. S.-Y. Chung, J.-H. Choi, J.-K. Choi, Appl. Phys. Lett. **91**, 091912 (2007)
27. P. Thongbai, T. Yamwong, S. Maensiri, Microelectron. Eng. **108**, 177 (2013)
28. S.-Y. Chung, S.-I. Lee, J.-H. Choi, S.-Y. Choi, Appl. Phys. Lett. **89**, 191907 (2006)
29. J. Jumpatam, B. Putasaeng, T. Yamwong, P. Thongbai, S. Maensiri, Ceram. Int. **39**, 1057 (2013)
30. M.A. Subramanian, A.W. Sleight, Solid State Sci. **4**, 347 (2002)
31. Z. Liu, X. Chao, Z. Yang, J. Mater. Sci.: Mater. Electron. **25**, 2096 (2014)
32. F.D. Morrison, D.C. Sinclair, A.R. West, J. Am. Ceram. Soc. **84**, 474 (2001)
33. L. Ramajo, R. Parra, J.A. Varela, M.M. Reboredo, M.A. Ramírez, M.S. Castro, J. Alloys Compd. **497**, 349 (2010)
34. T.B. Adams, D.C. Sinclair, A.R. West, J. Am. Ceram. Soc. **89**, 2833 (2006)
35. S. Vangchangyia, E. Swatsitang, P. Thongbai, S. Pinitsoontorn, T. Yamwong, S. Maensiri, V. Amornkitbamrung, P. Chindaprasirt, J. Am. Ceram. Soc. **95**, 1497 (2012)
36. P. Lunkenheimer, S. Krohns, S. Riegg, S.G. Ebbinghaus, A. Reller, A. Loidl, Eur. Phys. J. Spec. Top. **180**, 61 (2010)
37. P. Thongbai, B. Putasaeng, T. Yamwong, S. Maensiri, J. Mater. Sci. Mater. Electron. **23**, 795 (2012)
38. A.K. Dubey, P. Singh, S. Singh, D. Kumar, O. Parkash, J. Alloys Compd. **509**, 3899 (2011)
39. J. Jumpatam, P. Thongbai, B. Kongsook, T. Yamwong, S. Maensiri, Mater. Lett. **76**, 40 (2012)
40. W. Somphan, P. Thongbai, T. Yamwong, S. Maensiri, Mater. Res. Bull. **48**, 4087 (2013)

Materials Research Bulletin 60 (2014) 695–703

Contents lists available at ScienceDirect

Materials Research Bulletin

journal homepage: www.elsevier.com/locate/matresbu

Microstructural evolution and Maxwell–Wagner relaxation in $Ca_2Cu_2Ti_{4-x}Zr_xO_{12}$: The important clue to achieve the origin of the giant dielectric behavior

Prasit Thongbai [a,b,*], Jutapol Jumpatam [c], Bundit Putasaeng [d], Teerapon Yamwong [d], Santi Maensiri [e]

[a] Department of Physics, Faculty of Science, Khon Kaen University, Khon Kaen 40002, Thailand
[b] Integrated Nanotechnology Research Center (INRC), Khon Kaen University, Khon Kaen 40002, Thailand
[c] Materials Science and Nanotechnology Program, Faculty of Science, Khon Kaen University, Khon Kaen 40002, Thailand
[d] National Metal and Materials Technology Center (MTEC), Thailand Science Park, Pathumthani 12120, Thailand
[e] School of Physics, Institute of Science, Suranaree University of Technology, Nakhon Ratchasima 30000, Thailand

ARTICLE INFO

Article history:
Received 6 May 2014
Received in revised form 10 September 2014
Accepted 18 September 2014
Available online 22 September 2014

Keywords:
Composite
Dielectric properties
Electrical properties
Microstructure
Impedance spectroscopy

ABSTRACT

A composite system of $CaCu_3Ti_4O_{12}/CaTiO_3$ doped with Zr^{4+} was deliberately created using a one-step processing method. Investigation of the microstructural evolution and electrical responses of internal interfaces of Zr^{4+}-doped $CaCu_3Ti_4O_{12}/CaTiO_3$ composites was performed to clarify the exact nature of its high dielectric response. Grain sizes of the $CaCu_3Ti_4O_{12}$ phase in the $CaCu_3Ti_4O_{12}/CaTiO_3$ microstructure were largely increased by doping with Zr^{4+}, resulting in an increase in ε' (at 10^3 Hz) from 1.86×10^3 to 1.03×10^4. This is in complete contrast to observations of a single phase of Zr^{4+}-doped $CaCu_3Ti_4O_{12}$. This observation confirmed an extrinsic effect as the origin of high dielectric properties of $CaCu_3Ti_4O_{12}/CaTiO_3$ composites, rather than intrinsic factors. The macroscopic dielectric relaxation was well described by the Maxwell–Wagner relaxation model. Furthermore, changes of the loss tangent resulting from different doping levels of Zr^{4+} correlated well with variation of the resistance of insulating internal interfaces. Experimental results gave an important clue indicating that electrical responses of internal interfaces were the cause of the giant dielectric response in the $CaCu_3Ti_4O_{12}$ material system.

1. Introduction

Recently, anomalously high-dielectric constants (ε') in many polycrystalline and single crystalline ceramic metal oxides have been widely associated with an electrical response of the internal interface(s) in the bulk ceramics [1–5]. $CaCu_3Ti_4O_{12}$ (CCTO) is a prototypically interesting case study for demonstrating the effects of internal interfaces on apparent macroscopic dielectric properties [1,6]. Electrical responses of various CCTO internal interfaces and related compounds were investigated to show their contribution to the overall dielectric spectra over a wide range of frequencies and temperatures. The internal interfaces are grain boundaries (GBs) [1,11–13], domain boundaries (DBs) [6,9,13], defects due to stacking faults [14,15], twin boundaries in single crystals [16], and interfaces of the CCTO grain matrix and secondary phases of other particles [7,8,17–21]. Furthermore, the internal interface between grains i.e., GBs [7,8,11,18,19] was widely accepted to be the cause of observed nonlinear current–voltage (or current density–electric field, *J–E*) behavior of CCTO polycrystalline ceramics. Generally, the nonlinear *J–E* properties or non-ohmic properties of polycrystalline ceramics can be used for application in varistor devices. Varistor is used to protect a circuit from high-voltage transients by providing a path across the power supply. It takes only a small current under normal conditions. However, if the voltage increases abnormally, it takes a large current. Thus, the circuit is protected by this way.

Dielectric properties and nonlinear *J–E* characteristics of CCTO ceramics were improved by deliberately creating a composite system of $CCTO/CaTiO_3$ (CCTO/CTO) from a starting material with the chemical formula, $Ca_2Cu_2Ti_4O_{12}$ [17,22–29]. This is because

* Corresponding author at: Department of Physics, Faculty of Science, Khon Kaen University, Khon Kaen 40002, Thailand. Tel.: +66 84 4190266; fax: +66 43 202374.
E-mail addresses: pthongbai@kku.ac.th, prasitphysics@hotmail.com (P. Thongbai).

http://dx.doi.org/10.1016/j.materresbull.2014.09.045
0025-5408/

CCTO/CTO composites have very low loss tangents ($\tan\delta \sim 0.02$) compared to a single phase of CCTO ceramics. Moreover, very high breakdown field (E_b) and nonlinear coefficient (α) were also achieved in this composite system [23–25]. Ramirez et al. [25] reported that there was no relationship between the dielectric response and nonlinear properties of the CCTO/CTO composite system. They demonstrated that high performance nonlinear *J–E* properties were caused by the electrical responses of the CCTO–CTO and CCTO–CCTO interfaces. The former interface does not appear in a single phase CCTO ceramic. Conversely, the electrical response of nanoscale barrier layer defects due to stacking faults was proposed to be the origin of the high dielectric response in this composite system. This novel model was referred to as the Nanoscale Barrier Layer Capacitance (NBLC) model [15]. The schematic representations of bulk polaronic defect that correlates the NBLC model were clearly demonstrated in literature [15,30]. NBLC effect is mechanism that operates in the nanoscale region due to polaron defects related to stacking fault in the CCTO structure. As shown in Fig. 1(b–d), it was proposed that sliding motion by half a lattice parameter, resulting in the formation of stacking fault formed inside crystal grains of CCTO. This is the structural planar defects. When the electric field was applied in the direction of perpendicular to the planar defects, conduction of charges cannot be generated. The electrical polarization is, therefore, produced at the planar defects, giving rise to a giant dielectric behavior in CCTO ceramics. Based on the NBLC model, the effective ε' of CCTO/CTO composites was primarily governed by the dielectric response inside CCTO grains. Therefore, effective ε' of CCTO/CTO composites should be dominated and directly proportional to ε' of the CCTO phase. This is because ε' of CCTO is much higher than that of CTO ($\varepsilon' \sim 200$ at 10^2 Hz) [29]. This hypothesis is reasonable because ε' values of CCTO/CTO composites were found to be dependent upon the volume fraction of the CCTO phase. The composite with the lowest CCTO fraction (referred to the CCTO/8CTO sample in Ref. [25]) exhibited the lowest ε' value.

Regarding CCTO ceramics, most researchers believed that their giant ε' response was attributed to the internal barrier (grain boundary) layer capacitor (IBLC) effect [1,7,10,12,20,31]. In this model, the dielectric response is due to the interfacial polarization (or Maxwell–Wagner (M–W) polarization) at the interface between semiconducting grains i.e., an insulating GB layer, as illustrated in Fig. 1(a). In contrast to the NBLC model, it is also possible that ε' of CCTO/CTO composites may result from the IBLC effect as is seen in a single CCTO phase ceramic. In this IBLC model hypothesis, dielectric responses of internal interfaces between CCTO/CCTO grains and/or CCTO/CTO grains should make the primary contribution to the macroscopic dielectric properties of the CCTO/CTO composite. It is notable that the dielectric response of CTO–CTO interfaces can be neglected because of the insulating nature of CTO grains. Thus, the lowest ε' value of the CCTO/8CTO sample can also considered to be caused by lower density of CCTO/CCTO and CCTO–CTO interfaces compared to the composites having higher volume fractions of a CCTO phase (CCTO/2CTO in Ref. [25]). Due to this discrepancy between the intrinsic and extrinsic effects, a novel approach was needed to systematically investigate the relationship between macroscopic dielectric properties and

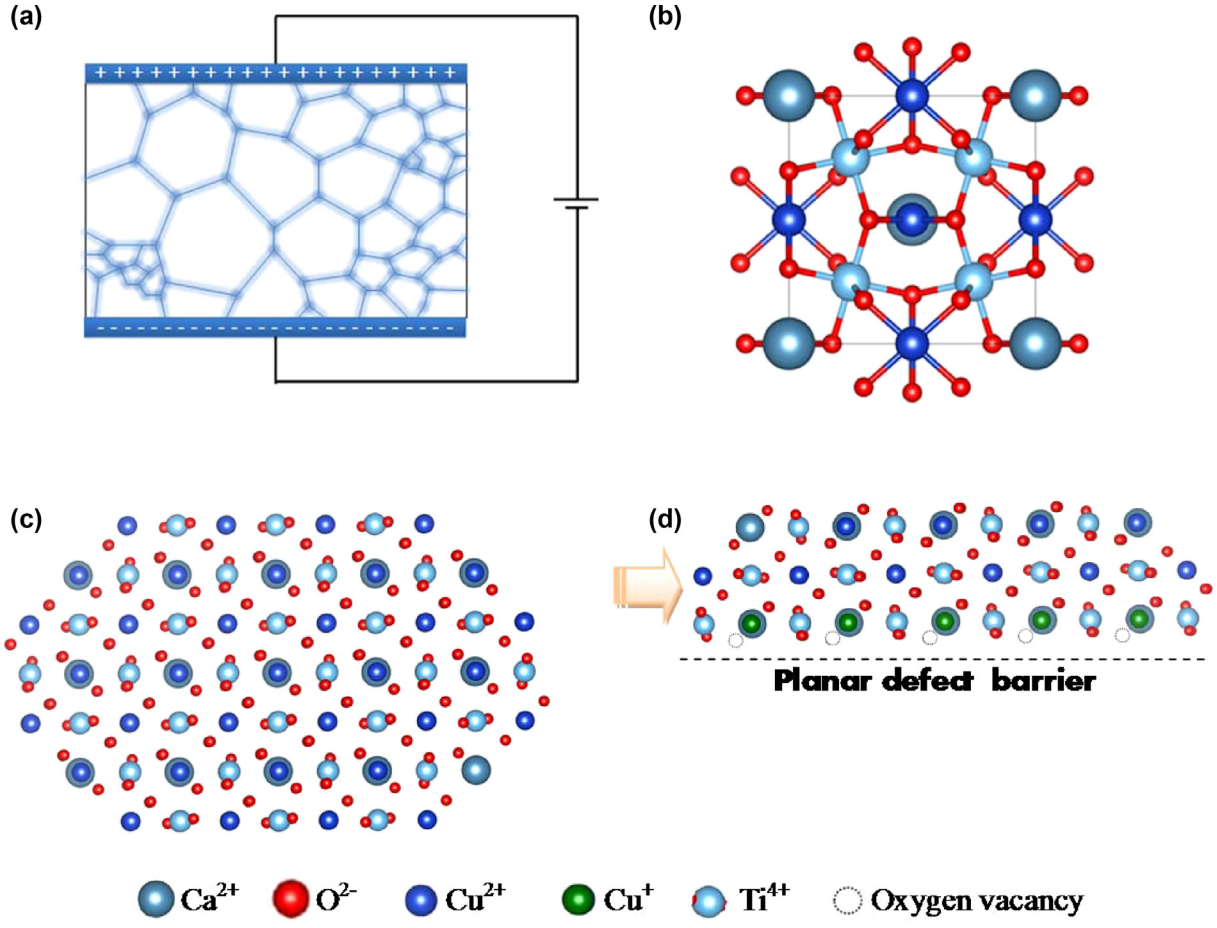

Fig. 1. (a) Schematic representation of the microstructure of CCTO polycrystalline ceramics, showing theelectrically microstructure model of internal barrier layer capacitor (IBLC) due to the electrical response of GBs. (b) Crystalline structure of CCTO. (c, d) Ideal crystalline structure of CCTO and planar defect resulting from a sliding motion by half a lattice parameter, leading to the formation of nanoscale barrier layer capacitor (NBLC) structure inside the grains of CCTO [15].

electrical responses of microscopic internal interfaces in CCTO–CTO composites. The current investigation was performed to further clarify the exact origin of giant-ε' in CCTO ceramics or at the very least to add support to a model that has already been proposed.

It is often observed that doping metal ions in CCTO ceramics can result in changes in macroscopic dielectric and nonlinear J–E properties [6,14,18,20,26,32–38]. These properties may either be enhanced or degraded. Most experimental results demonstrated that changes in the macroscopic properties of CCTO ceramics were primarily due to the effect of particular dopants upon the electrical response at GBs (CCTO–CCTO interfaces) and/or upon microstructural changes [18,20,32–35]. Some research suggested that such changes in macroscopic dielectric properties were attributed to intrinsic effects [14,36–38]. However, in both cases, nonlinear properties were still caused by GB electrical responses. Many researchers found that substitution of Zr^{4+} ions into CCTO ceramics caused a large decrease in ε' [39–41]. This result was described based on the reduction in grain size or modification of defect equilibrium at GBs [39–41]. Using an intrinsic approach assuming that the electrical response of internal interfaces had a slight influence, a reduced effective ε' of the $CaCu_3Ti_{4-x}Zr_xO_{12}$/CTO composite system was expected. This is due to a degradation of ε' in the CCTO phase. Furthermore, the effective ε' should be independent of microstructural changes. If an effective ε' of this composite system could be enhanced by doping with Zr^{4+} and was strongly dependent on ceramic microstructure, the result might not be associated with intrinsic factors. To our knowledge, the investigation of dielectric and J–E properties of CCTO/CTO composites substituted by metal ions has been rarely reported [26].

In this work, we proposed a novel conceptualization to clarify the dielectric and electrical properties of CCTO/CTO composites doped with Zr^{4+} ions. The effects of Zr^{4+} upon microstructural evolution, macroscopic ε', dielectric relaxation behavior, nonlinear J–E characteristics, and intrinsic parameters were systematically investigated. Possible mechanisms explaining the experimental results obtained are discussed.

2. Experimental

A solid state reaction method was used to prepare Zr-doped $Ca_2Cu_2Ti_4O_{12}$ ceramics with a nominal chemical composition of $Ca_2Cu_2Ti_{4-x}Zr_xO_{12}$, where $x = 0$, 0.05, 0.10, 0.20, and 0.30 (abbreviated as CCTO/CTO, Zr05, Zr10, Zr20, and Zr30 ceramics, respectively). Starting raw materials used in this work were $CaCO_3$ (99.95% purity), CuO (99.9% purity), TiO_2 (99.9% purity), and ZrO_2 (99.9% purity). First, a stoichiometric mixture of the starting materials for each x value was ball-milled in ethanol for 24 h using ZrO_2 balls. Second, the mixed slurries of all compositions were dried and then calcined in air at 900 °C for 15 h. Third, the calcined powders were carefully ground and pressed into pellets (without a binder) with a dimension of 9.5 mm in diameter and ~1.0 mm in thickness. Finally, these pellets were sintered at 1100 °C for 24 h.

To characterize the possible phase compositions of the sintered $Ca_2Cu_2Ti_{4-x}Zr_xO_{12}$ ceramics, X-ray diffraction (XRD; PW3040 Philips X-ray diffractometer with Cu K_α radiation, $\lambda = 0.15406$ nm; Philips, The Netherlands) was used to investigated. Microstructural analysis was performed using scanning electron microscopy (SEM) and energy-dispersive X-ray spectrometry (EDS) (SEM; 1450VP, LEO) to characterize the distribution of the possible phases as well as the chemical elements in the sintered ceramics. To reveal the distribution of multiple phases throughout the microstructure, the polished surfaces were characterized using SEM operating in backscattering electron mode. Before electrical measurements, Au was sputtered on each pellet face at a current of 25 mA for 8 min using a Polaron SC500 sputter coating unit. An Agilent 4294A Precision Impedance Analyzer was used to measure dielectric properties over the frequency and temperature ranges of 10^2–10^7 Hz and −70 to 220 °C, respectively. Current–voltage measurements were done at room temperature using a high voltage measurement unit (Keithley Model 247). E_b is defined as a value of an electric field at which $J = 1.0$ mA/cm^2. Thus, E_b was directly obtained from J–E data. α was calculated using the following formula:

$$\alpha = \frac{\log(J_2/J_1)}{\log(E_2/E_1)}, \quad (1),$$

where E_1 and E_2 are the applied electric fields, at which $J_1 = 1$ and $J_2 = 10$ mA/cm^{-2}, respectively. The complex impedance (Z^*) and complex electric modulus (M^*) were calculated from the relation [42],

$$\varepsilon* = \varepsilon' - i\varepsilon'' = \frac{1}{i\omega C_0 Z*} = \frac{1}{i\omega C_0 (Z' - iZ'')}, \quad (2)$$

$$M* = M' + iM'' = \frac{1}{\varepsilon*}, \quad (3)$$

where ε' and ε'' are, respectively, the real (dielectric constant) and imaginary parts (dielectric loss) of the complex permittivity (ε^*). Z' and Z'' are the real part and imaginary parts of Z^*, respectively. M' and M'' are the real and imaginary parts of M^*. ω is the angular frequency ($\omega = 2\pi f$) and $i = \sqrt{-1}$. $C_0 = \varepsilon_0 S/d$ is the empty cell capacitance, where S is the sample area, d is the sample thickness, and ε_0 is the permittivity of free space, $\varepsilon_0 = 8.854 \times 10^{-12}$ F/m.

3. Results and discussion

Ceramics with a nominal composition of $Ca_2Cu_2Ti_4O_{12}$ consisted of two phases i.e., CCTO and CTO at concentrations of ~33.3 and ~66.7 mol%, respectively [23,25]. In Fig. 2a, CCTO (JCPDS 75-2188) and CTO (JCPDS 82-0231) phases appear in all the XRD patterns of $Ca_2Cu_2Ti_{4-x}Zr_xO_{12}$ ($x = 0 - 0.3$) compositions, which is similar to that reported in literature [17,22–28]. The XRD result confirms creation of CCTO/CTO composite system. An impurity phase was not detected in the XRD patterns of the CCTO/CTO, Zr05, and Zr30 samples. This indicates substitution of Zr^{4+} into the Ti^{4+} sites of the CCTO phase. However, an impurity phase of $CaZrTi_2O_7$ (JCPDS 84-0163) was also observed in the XRD patterns of the Zr20 and Zr30 samples. This indicates a limited solid solution of Zr^{4+} in CCTO and/or CTO phases. CCTO phase lattice parameters in the CCTO/CTO, Zr05, Zr10, Zr20, and Zr30 composite samples were calculated by using Cohen's least mean square method and found to be 7.3893 ± 0.0012, 7.3933 ± 0.0003, 7.3957 ± 0.0003, 7.3914 ± 0.0005, and 7.4004 ± 0.0004 Å, respectively. These calculated values are comparable to the 7.391 Å value for CCTO crystal structure (JCPDS 75-2188) and published values of ≈7.391 Å [12,16,20,21,25,27,32–34,36,37,40,41]. Lattice parameter calculations indicated an enlarged unit cell in the CCTO phase. As shown in Fig. 2b, lattice parameters of CCTO phase in $Ca_2Cu_2Ti_{4-x}Zr_xO_{12}$ compositions tends to increase with increasing concentration of Zr^{4+} doping ions (x), except for the Zr02 sample for $x = 0.2$.

As depicted in the backscattered SEM images of Fig. 3, all the sintered ceramics consisted of at least two phases with different contrasts. According to previous work [24,28], brighter and darker grains in CCTO/CTO composites were clearly shown to be CCTO and CTO phases, respectively. In Fig. 4a and b, EDS spectra detected at the darker (point 1) and brighter (point 2) grains clearly indicate CTO and CCTO phases, respectively. This is supported by published literature [24,28]. Only EDS peaks of Ca, Ti, and O were observed in the darker grain (point 1). In the brighter grain (point 2), a small intensity Zr EDS-peak was observed as well as the main Ca, Cu, Ti,

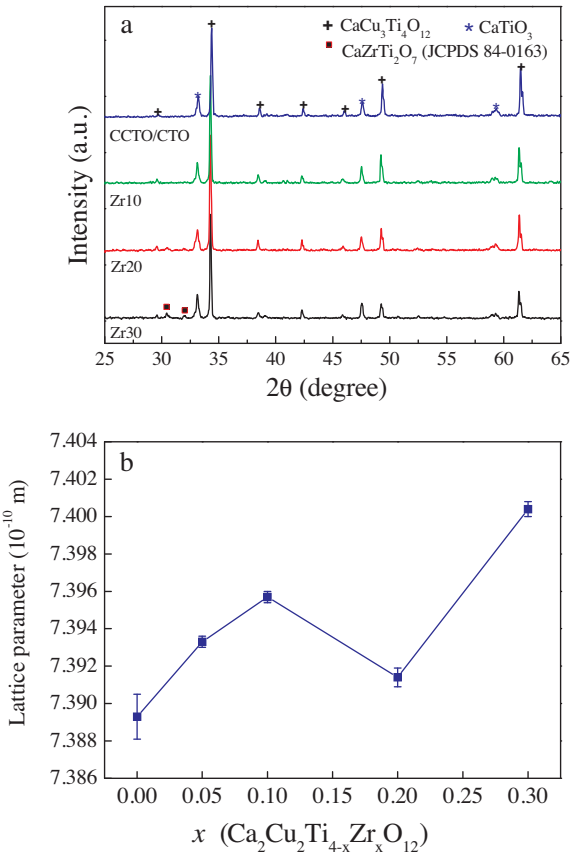

Fig. 2. (a) XRD patterns of $Ca_2Cu_2Ti_{4-x}Zr_xO_{12}$ ceramics. (b) Lattice parameter of CCTO phase in $Ca_2Cu_2Ti_{4-x}Zr_xO_{12}$ composites as a function of doping level (x).

and O EDS-peaks. This indicates that some portion of the Zr^{4+} ions was substituted into the CCTO phase. As shown in Fig. 3d and e, there is another phase in addition to CCTO and CTO that appeared in the microstructure of the Zr20 and Zr30 samples. The observation of this third phase is consistent with their XRD patterns. In Fig. 4b, the EDS spectrum detected in this phase (point 3 in Fig. 4a) confirmed the existence of Ca, Zr, Ti, and O atoms in the impurities. Thus, it is reasonable to infer that this phase was $CaZrTi_2O_7$, as it appeared in the XRD patterns.

According to the microstructure analysis shown in Figs. 3 and 4, grain sizes of the CTO and CCTO phases in Zr^{4+}-doped CCTO/CTO (Z-CCTO/CTO) composites were much larger than those observed in the CCTO/CTO composite. The mean grain sizes of the CCTO phase in the CCTO/CTO, Zr05, Zr10, Zr20, and Zr30 samples were found to be 2.9 ± 0.97, 9.04 ± 3.44, 10.99 ± 3.75, 13.40 ± 3.75, and 13.54 ± 5.22 μm, respectively. The mean grain sizes of the CTO phase in these samples were 1.96 ± 0.48, 6.22 ± 2.13, 4.63 ± 1.79, 5.85 ± 2.28, and 6.29 ± 2.21 μm, respectively. These results are particularly interesting in light of previous work [40,41], where substitution of Zr^{4+} into a single phase CCTO ceramic caused a great decrease in the mean grain size. Here, a small portion of Ca, Zr, Ti, and O reacted to form a new $CaZrTi_2O_7$ phase. Formation of a $CaZrTi_2O_7$ phase might cause an excess of CuO-rich phase within the microstructure. The grain growth of CCTO ceramics is correlated with liquid phase sintering [43,44]. A slight excess of CuO in the starting CCTO composition could promote the grain growth rate in a single phase of CCTO ceramics. The CuO-rich phase was believed to be a source of a liquid phase that existed during the sintering process of CCTO ceramics. Therefore, the larger grain growth in Z-CCTO/CTO composites may be attributed to the existence of a slight excess of CuO in their microstructure. The density of all the samples was measured by the Archimedes method. The relative densities of the CCTO/CTO, Zr05, Zr10, Zr20, and Zr30 samples were calculated and found to be 88.93, 91.33, 91.49, 89.93, and 88.96%, respectively.

Fig. 5 shows the frequency dependence of ε' and $\tan\delta$ at 20 °C for all samples of the current study. The values of ε' at $f = 1$ kHz are summarized in Table 1. The inset of Fig. 5a demonstrates the values ε' at 10^3 and 10^4 Hz as a function of doping level. $\varepsilon' \sim 1863$ of the CCTO/CTO sample was comparable to the value 1800 first reported by Kobayashi and Terasaki [17], and others [27]. According to microstructural analyses, it is likely that the Zr05 and Zr10 samples consisted of CTO and CCTO phases with concentrations roughly estimated to be about 66.7 and 33.3 mol%, respectively. This is the same as in the CCTO/CTO composite. The Zr20 and Zr30 samples consisted of three phases with an additional $CaZrTi_2O_7$ phase. According to previous work [39–41], it was found that substitution of Zr^{4+} ions into CCTO ceramics caused a large decrease in ε' values. According to simple mixing models that excluded the effect of interfacial interaction between the two phases [17],ε' of the Z-CCTO/CTO composite system should be reduced compared to the un-doped CCTO/CTO composite. This is because ε' of the un-doped CCTO grains in the CCTO/CTO composite was expected to be larger than that of the Zr-doped CCTO grains in the $CaCu_3Ti_{4-x}Zr_xO_{12}$/$CaTiO_3$ composites. Interestingly, ε' at $f < 10^5$ Hz of CCTO/CTO composites was strongly enhanced by doping with Zr^{4+}, as clearly seen in the inset of Fig. 4a. The dielectric response in Z-CCTO/CTO composite system could not be described by simple mixing models or a mixing law such as the Maxwell–Garnett model, Bruggeman self-consistent effective medium model, and Lichtenecker's logarithmic law [17,45]. This result strongly suggested that the high dielectric response of a CCTO/CTO system as well as in CCTO ceramics was not primarily due to intrinsic effects. Obviously, a high dielectric response should be caused by an electrical response of internal interfaces such as the CCTO–CCTO interface, CCTO–CTO interface, and/or domain boundaries in the large grains of CCTO. Therefore, a strongly enhanced ε' in Z-CCTO/CTO system may be attributed to the modified electrical response at these internal interfaces caused by Zr^{4+} doping ions.

The frequency dependence of $\tan\delta$ at 20 °C and $\tan\delta$ values (at $f = 1$ kHz) is shown in Fig. 5(b) and Table 1, respectively. Over the range of $f = 10^2$–10^4 Hz, $\tan\delta$ of all samples increased rapidly with decreasing frequency. This was mainly due to the effect dc conduction in the bulk ceramics [2,44]. A low-frequency $\tan\delta$ of $Ca_2Cu_2Ti_{4-x}Zr_xO_{12}$ ceramics increased as x increased from 0 to 0.1. Then, it decreases as x was further increased from 0.2 to 0.3. Interestingly, the Zr30 sample exhibited improved dielectric properties with $\varepsilon' \sim 4{,}610$ and a reduced $\tan\delta \sim 0.038$. When $f > 10^5$ Hz, $\tan\delta$ of all samples rapidly increased with increasing frequency. This was clearly due to the dielectric relaxation process [2].

To study the effect of Zr^{4+} substitution upon the dielectric relaxation mechanism in the CCTO/CTO composites, the frequency dependence of ε' and ε'' ($\varepsilon'' = \varepsilon' \tan\delta$) at different temperatures was investigated. As shown in Fig. 6, the frequency-dependence characteristics of the CCTO/CTO and Zr30 samples were quite similar. At −70 °C, a sudden drop in ε' at a relatively high-frequency was observed. This was accompanied with the ε'' peak. Frequencies at which rapidly decreasing ε' and ε''-peak were observed, shifted to higher frequencies with increasing temperature. This result indicates a thermally activated dielectric relaxation mechanism. The activation energy (E_a) required for this thermally activated relaxation could be calculated using the Arrhenius law [6],

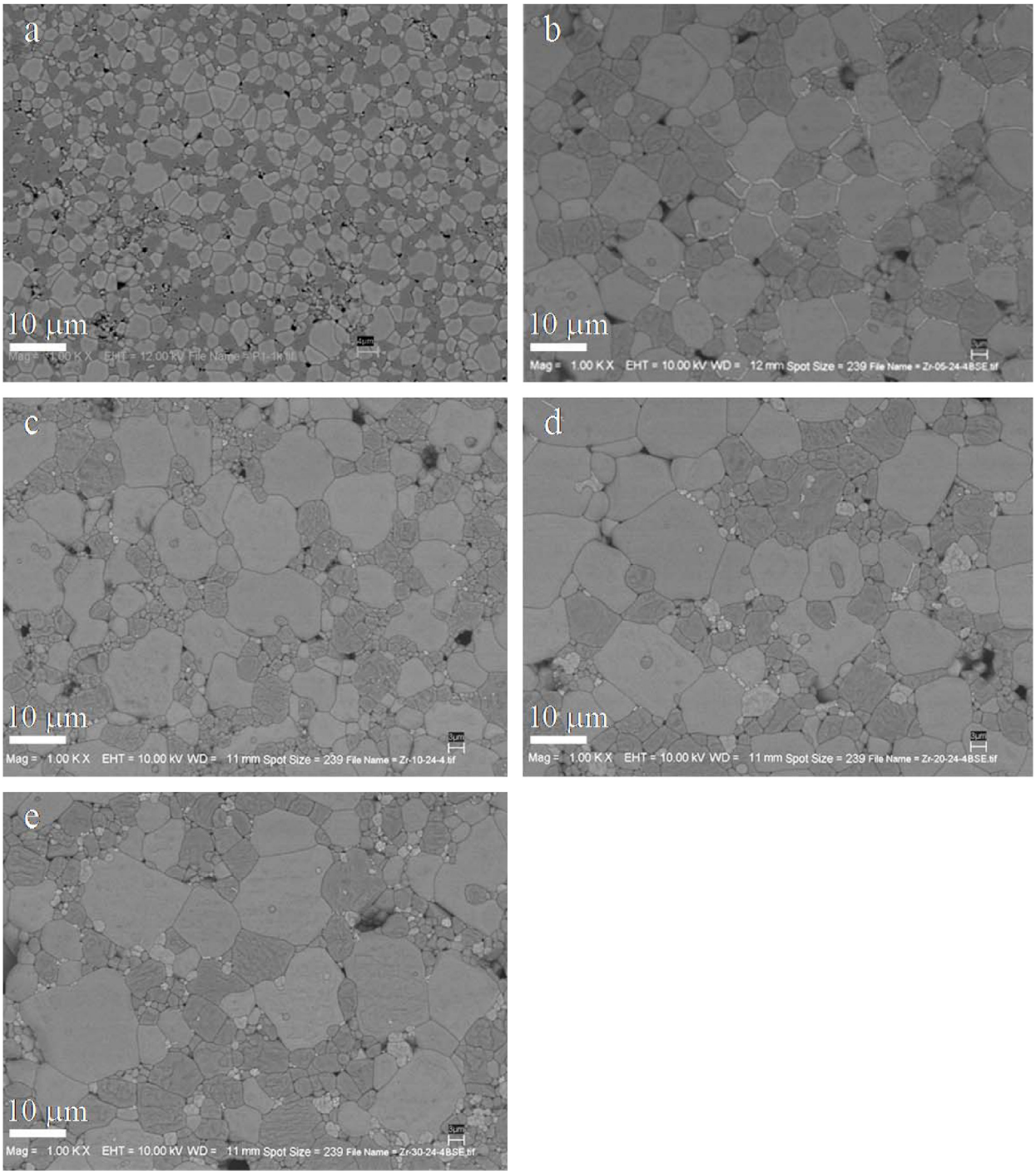

Fig. 3. Backscattered SEM images of polished-surfaces of (a) CCTO/CTO, (b) Zr05, (c) Zr10, (d) Zr20, and (e) Zr30 samples.

$$f_{\max,\varepsilon'} = f_0 \exp\left(\frac{-E_a}{k_B T}\right), \quad (4)$$

where $f_{\max,\varepsilon'}$ is the frequency at which the ε'' peak ($\varepsilon''_{\max}$) was observed, T is absolute temperature (K), k_B is the Boltzmann constant, and f_0 is a constant term. As shown in Fig. 7, the temperature dependence of $f_{\max,\varepsilon'}$ is linearly well fitted by Eq. (4). According to the fitted results, E_a values were calculated and found to be 0.122 ± 0.007, 0.137 ± 0.003, 0.139 ± 0.004, 0.144 ± 0.002, and 0.157 ± 0.002 eV for the CCTO/CTO, Zr05, Zr10, Zr20, and Zr30 composite samples, respectively. E_a tended to slightly increase with increasing Zr^{4+} concentration. As shown in Figs. 6 and 7, at a particular temperature, the $f_{\max,\varepsilon'}$ value of CCTZO/CTO composites decreased with increasing Zr^{4+} dopant concentration. For example, $f_{\max,\varepsilon'}$ values at $-70\,^{\circ}C$ for the CCTO/CTO, Zr05, Zr10, Zr20, and Zr30 samples were obtained and found to be 1.0×10^6, 2.8×10^5, 2.0×10^5, 1.0×10^5, and 0.5×10^5 Hz, respectively. This indicated the effects of Zr^{4+} doping ions on the dielectric relaxation behavior of CCTO/CTO composite systems. It is notable that the current study is the first report of dielectric relaxation behavior in CCTO/CTO composite systems. $E_a \sim 0.122$ eV for the CCTO/CTO sample was slightly higher than the value of a single CCTO phase system. Thus, the origins of the dielectric

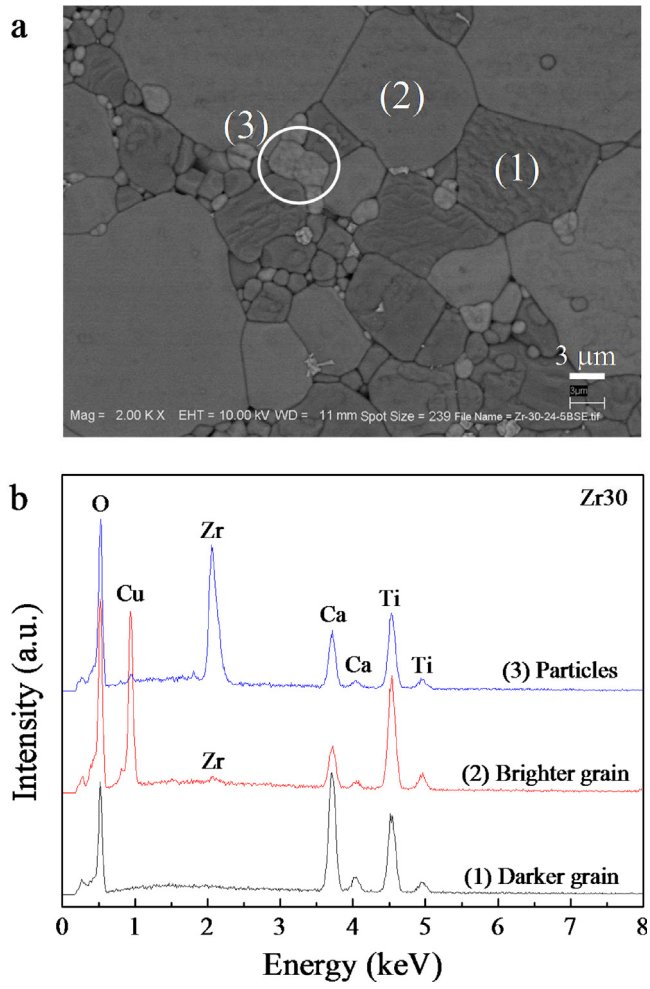

Fig. 4. (a) Backscattered SEM image of polished-surfaces of Zr30 sample, showing EDS testing points at different phases. (b) EDS spectra detected at different points on the surface of the Zr03 sample.

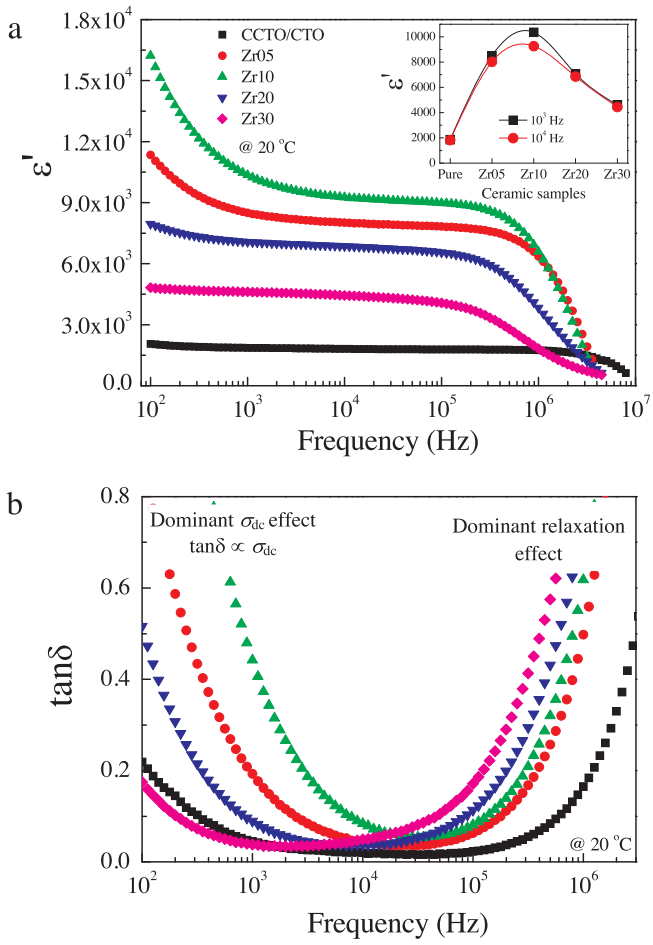

Fig. 5. (a) ε' and (b) $\tan\delta$ of $Ca_2Cu_2Ti_{4-x}Zr_xO_{12}$ ceramic at 20 °C over a measured frequency range; inset of shows ε' as a function of doping level at 10^3 and 10^4 Hz.

relaxation mechanism in CCTO/CTO composites and CCTO ceramics might have resulted from a similar cause.

Using the M–W relaxation model [46,47], the macroscopic relaxation time ($\tau = 1/2\pi f_{\max,\varepsilon'}$) was derived and estimated to correlate with the microscopic parameters of grain resistance (R_g) and GB capacitance (C_{gb}), i.e., $\tau \approx R_g C_{gb}$. Furthermore, it was demonstrated that E_a should be nearly the same value as the activation energy of conduction inside the semiconducting grains (E_g) [46]. For clarification, the dielectric relaxation behavior in Zr-CCTO/CTO composites was related to the M–W relaxation type. This was performed using impedance spectroscopy (IS) to investigate the electrical parameters of internal interfaces (or GB) and in the grain interior at different temperatures. IS data were interpreted based on the brick-work layer model [1]. In Fig. 8, the observed incomplete semicircular arcs (at 20 °C) indicate to the electrical response of insulating internal interfaces [1,31] of CCTO–CCTO and CCTO–CTO interfaces, as described by Ramirez et al. [25]. They used electrostatic force microscopy (EFM) to show that these two interfaces were electrically active, while the CTO–CTO interface was electrically inactive. Thus, the total resistance is governed by the resistance of these internal interfaces (R_{int} or R_{gb}). The non-zero intercept on Z' axis at high frequency data indicated the electrical response in the semiconducting part of CCTO/CTO composites [inset (a) of Fig. 8], which is the electrical response of CCTO grains [11]. Concurrently, the CTO phase is well known as a good insulator. In inset (b) of Fig. 8, the temperature dependence of R_g follows the Arrhenius law [46]. $R_g = R_0\exp(E_g/k_BT)$ or $\sigma_g = \sigma_0\exp(E_g/k_BT)$, where, R_0 and σ_0 are constant parameters and σ_g is the grain conductivity. E_g values were calculated and found to be 0.098 ± 0.001, 0.112 ± 0.001, 0.119 ± 0.001, 0.125 ± 0.003, and 0.144 ± 0.001 eV for the CCTO/CTO, Zr05, Zr10, Zr20, and Zr30 samples, respectively. Both E_g and E_b of the Z-CCTO/CTO composites increased as Zr^{4+} concentration increased. This result might indicate that the dielectric relaxation in CCTO/CTO composite system was of the M–W relaxation type [46].

To further investigate the relationship between the macroscopic τ values obtained from the dielectric relaxation peak of ε'' and the product of R_gC_{gb}, C_{gb} values were calculated from the M″–f plots. From the magnitude of the maximum value of $M''(f)$ (M''_{max}), it can be shown that $f_{max,M''} = 1/2\pi RC$ and $M''_{max} = C_0/2C$ [42]. As seen in Fig. 9a for the Zr20 sample, the height of M''_{max} is nearly independent of temperature. These values are proportional to the reciprocals of the associated capacitance. This result indicated that capacitance related to observed M''_{max} only weakly depended on temperature. The calculated values of capacitances at various temperatures for all samples are shown in Fig. 9b. The capacitance values of Zr-CCTO/CTO composites were in the range of ≈1.5–3.0 nF. According to the brick-work layer model for CCTO polycrystalline ceramics [1], it is reasonable to suggest that these capacitance values were a result of the dielectric response of the insulating internal interfaces or C_{gb} [31]. The grain capacitance (C_g) of CCTO is usually in the order of 10^{-12} F (or pF) [1,42]. Only C_{gb} values of the Zr05 and Zr10 samples were calculated at 20 °C, which were found to be 2.75 and 2.98 nF, respectively. Due to a

Table 1
ε' and $\tan\delta$ (at 1 kHz and 20 °C), activation energy for dielectric relaxation (E_a), activation energy for conduction inside grain (E_g), resistance of CCTO grain at 20 °C (R_g), estimated capacitance of GB at room temperature (C_{gb}), nonlinear coefficient (α), and electric breakdown field strength (E_b) at room temperature for ceramic samples.

Samples	ε'	$\tan\delta$	E_a (eV)	E_g (eV)	R_g (Ω cm)	C_{gb} (nF)	α	E_b (V/cm)
CCTO/CTO	1863	0.045	0.122	0.098	~160	~0.72	9.9	5,817
Zr05	8501	0.193	0.137	0.122	~110	~2.75	3.2	519
Zr10	10,355	0.442	0.139	0.119	~120	~2.98	2.8	396
Zr20	7073	0.089	0.144	0.125	~230	~2.28	4.1	973
Zr30	4610	0.038	0.157	0.144	~500	~1.49	3.5	917

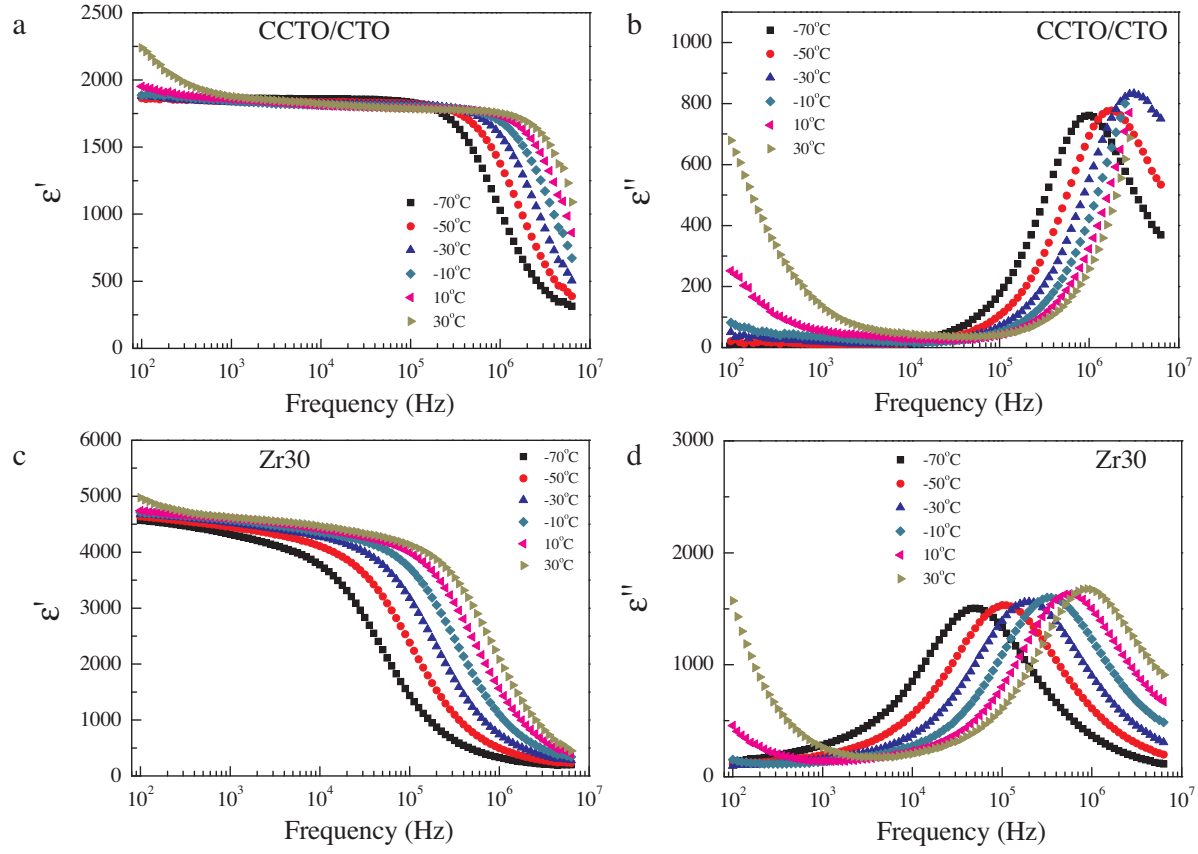

Fig. 6. Frequency dependence of (a, c) ε' and (b, d) ε'' at various temperatures over the range of −70–30 °C for the CCTO/CTO and Zr30 samples.

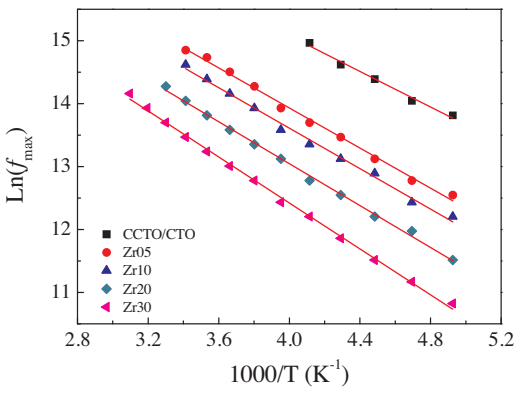

Fig. 7. Arrhenius plots of temperature dependence of f_{max}.

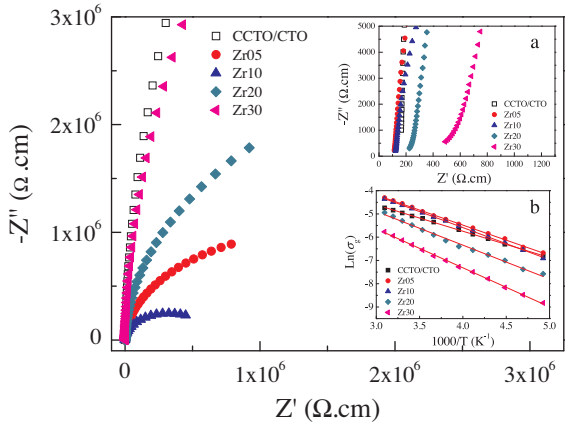

Fig. 8. Impedance complex plane plot (Z^*) at 20 °C for $Ca_2Cu_2Ti_{4-x}Zr_xO_{12}$ ceramics; inset (a) shows an expanded view of the high-frequency data close to the origin, and inset (b) shows the Arrhenius plots of temperature dependence of σ_g.

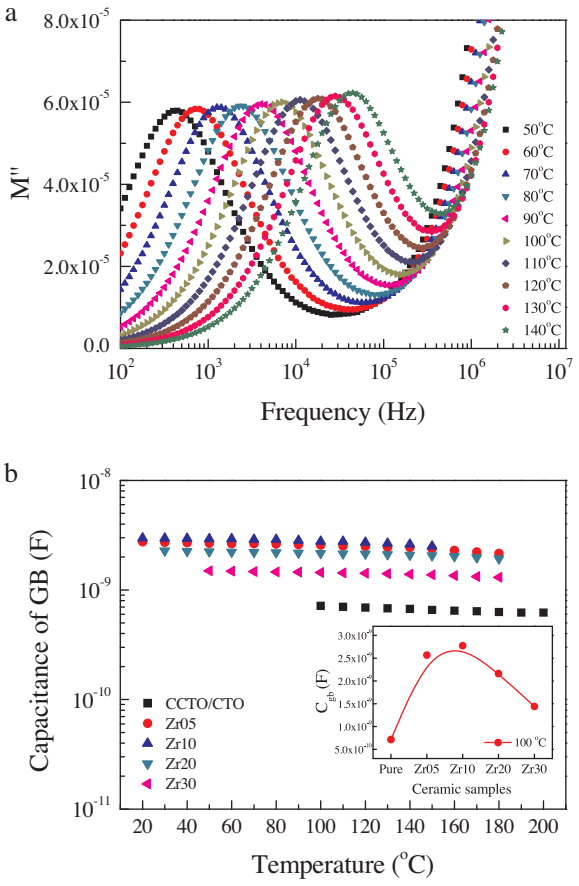

Fig. 9. (a) Frequency dependence of M'' of the Zr20 sample at various temperatures over the range of 50–140 °C. (b) Capacitance values of $Ca_2Cu_2Ti_{4-x}Zr_xO_{12}$ ceramics at different temperatures; the inset demonstrates C_{gb} values at 100 °C as a function of doping level.

small variation in temperature dependence of C_{gb}, the C_{gb} values at 20 °C of other samples were roughly estimated and are summarized in Table 1. The effect of Zr^{4+} doping ions on the value of C_{gb} of CCTO/CTO composites is clearly seen in the inset of Fig. 9b. Obviously, variations of C_{gb} values are consistent with observed variation of ε', as demonstrated in the inset of Fig. 5a. The dielectric response of CCTO/CTO composite systems might be caused by the dielectric responses at internal interfaces. The values of R_gC_{gb} were calculated using R_g values at 20 °C and the estimated values of C_{gb} at 20 °C. As shown in Fig. 10, variations of macroscopic τ values are consistent with R_gC_{gb} values. The R_gC_{gb} value of the Z-CCTO/CTO

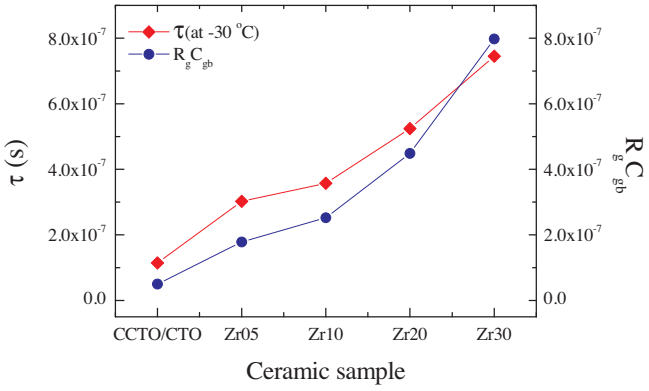

Fig. 10. Relationship between τ (calculated from $\tau = 1/\omega_{max}$) at −30 °C and the product of R_g and C_{gb} (R_gC_{gb} values) at 20 °C of $Ca_2Cu_2Ti_{4-x}Zr_xO_{12}$ ceramics.

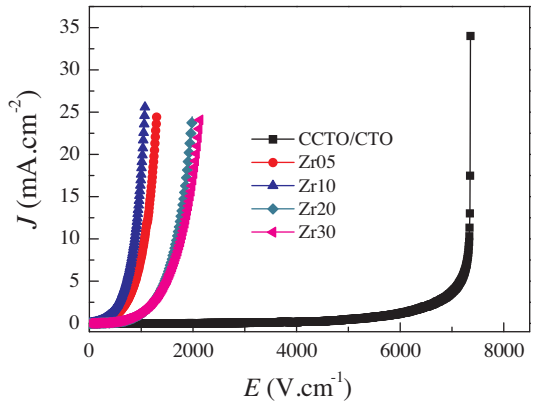

Fig. 11. J–E characteristics at room temperature of $Ca_2Cu_2Ti_{4-x}Zr_xO_{12}$ ceramics.

composites increased with increasing Zr^{4+} dopant concentration. Therefore, the dielectric relaxation behavior in CCTO/CTO composite systems may be due the M–W relaxation type, which is related to interfacial or space charged polarization [46,47]. Interfacial polarization at the internal interfaces of CCTO–CCTO and CCTO–CTO interfaces is a major cause of the observed high dielectric response in CCTO/CTO composites. Changes in ε' in the Z-CCTO/CTO composites likely resulted from modified electrical polarization at the internal interfaces. A much larger grain size of the Z-CCTO/CTO composites than un-doped CCTO/CTO composite gave rise to the space charged sheet region. This enhances polarization intensity, increases ε' magnitude of the Z-CCTO/CTO composites compared to that of CCTO/CTO samples. The decrease in ε' of the Zr20 and Zr30 samples compared to those values of the Zr05, and Zr10 samples was attributed to the incorporation of a $CaZrTi_2O_7$ phase.

To study the effect of insulating internal interfaces on tan δ of Zr-CCTO/CTO composites, the relationship between tan δ and R_{gb} was investigated. As shown in Fig. 8, R_{gb} at 20 °C of Z-CCTO/CTO composites tended to decrease strongly when increasing Zr^{4+} concentration from 1.25 and 2.5 at% (for Zr05 and Zr10 samples, respectively), indicating a decrease in R_{gb}. When the concentration of Zr^{4+} was further increased to 5.0–7.5 at% for Zr20 and Zr30 samples, respectively, R_{gb} increased. This result is consistent with variations in tan δ as a function of Zr^{4+} concentration.

The effect of Zr^{4+} doping ions on the non-ohmic properties of CCTO/CTO composites at room temperature was investigated. As illustrated in Fig. 11, E_b of nonlinear J–E curves was greatly reduced by substitution of Zr^{4+}. E_b and α values are provided in Table 1. The nonlinear properties of Z-CCTO/CTO composites were strongly degraded when compared to the un-doped CCTO/CTO samples. From SEM images, it is clear that one of the most important factors that remarkably decreases E_b is the larger mean grain sizes of the CCTO phase. This was especially true for the Zr05 and Zr10 samples when compared to the CCTO/CTO sample [11]. The increase in E_b values after further increasing Zr^{4+} concentrations may have resulted from the third $CaZrTi_2O_7$ phase. It is notable that J–E curves of the Zr20 and Zr30 samples were almost identical in the range of $J = 0$–5 mA/cm^2. The large increase in the mean grain size of CCTO phase reduced insulating GB density, resulting in a reduction of E_b [11]. Another important factor may be due to the interface of CCTO–$CaZrTi_2O_7$, but this is of lesser magnitude.

4. Conclusions

Zr^{4+}-doped CCTO/CTO ceramic composites were created from a nominal formula of $Ca_2Cu_2Ti_{4-x}Zr_xO_{12}$. Doping Zr^{4+} into CCTO/CTO composites resulted in an increase in the mean grain sizes of both

the CCTO and CTO phases. Zr^{4+} ions were preferentially substituted into the CCTO phase. At Zr^{4+} dopant concentrations of more than 2.5 mol%, Zr^{4+} was found to be over the limited solid solution, leading to formation of a $CaZrTi_2O_7$ impurity phase. A strong increase in ε' of 1.03×10^4 for the 2.5 mol% of Zr^{4+}-doped CCTO/CTO composite was observed compared to that of the un-doped composite ($\varepsilon' \sim 1.86 \times 10^3$). This result is completely different from that observed in a single phase Zr^{4+}-doped CCTO ceramic. Here, ε' was greatly reduced by doping with Zr^{4+}. Thus, the origin of the high dielectric response in CCTO/CTO composites was confirmed to be an extrinsic effect related to the electrical responses of internal interfaces, rather than being caused by an intrinsic effect originating in the grain interiors. It was found that variations of E_a and E_g values were consistent with each other. Furthermore, a change in the macroscopic dielectric relaxation time was clearly consistent with the variation of R_gC_{gb} values, following the M–W relaxation model. These results strongly support the conceptualization of an internal interface effect on the giant dielectric response in CCTO-based compounds.

Acknowledgements

This work was financially supported by the Thailand Research Fund (TRF) and Khon Kaen University, Thailand [grant number TRG5680047]. The authors would like to thank Dr. Pornjuk Srepusharawoot for providing the schematic representations of the planar defect structure. J. Jumpatam would like to thank the Thailand Graduate Institute of Science and Technology (TGIST) for his Master of Science Degree scholarship.

References

[1] D.C. Sinclair, T.B. Adams, F.D. Morrison, A.R. West, Appl. Phys. Lett. 80 (2002) 2153.
[2] J. Wu, C.-W. Nan, Y. Lin, Y. Deng, Phys. Rev. Lett. 89 (2002) 217601.
[3] Z. Wang, H.J. Li, L.L. Zhang, Y.P. Pu, Mater. Res. Bull. 53 (2014) 28–31.
[4] Y. Liu, W. Wang, J. Huang, F. Tang, C. Zhu, Y. Cao, Ceram. Int. 39 (2013) 9201–9206.
[5] P. Salame, R. Drai, O. Prakash, A.R. Kulkarni, Ceram. Int. 40 (2014) 4491–4498.
[6] W. Li, R.W. Schwartz, A. Chen, J. Zhu, Appl. Phys. Lett. 90 (2007) 112901.
[7] Y.-H. Lin, J. Cai, M. Li, C.-W. Nan, J. He, J. Appl. Phys. 103 (2008) 074111.
[8] J. Li, R. Jia, X. Tang, X. Zhao, S. Li, J. Phys. D: Appl. Phys. 46 (2013) 325304.
[9] T.-T. Fang, C.P. Liu, Chem. Mater. 17 (2005) 5167–5171.
[10] L. Liu, H. Fan, X. Chen, P. Fang, J. Alloys Compd. 469 (2009) 529–534.
[11] S.-Y. Chung, I.-D. Kim, S.-J.L. Kang, Nat. Mater. 3 (2004) 774–778.
[12] L. Liu, H. Fan, P. Fang, X. Chen, Mater. Res. Bull. 43 (2008) 1800–1807.
[13] J. Li, X. Zhao, F. Gu, S. Li, Appl. Phys. Lett. 100 (2012) 202905.
[14] W.C. Ribeiro, R.G.C. Araújo, P.R. Bueno, Appl. Phys. Lett. 98 (2011) 132906.
[15] W.C. Ribeiro, E. Joanni, R. Savu, P.R. Bueno, Solid State Commun. 151 (2011) 173–176.
[16] M.A. Subramanian, A.W. Sleight, Solid State Sci. 4 (2002) 347–351.
[17] W. Kobayashi, I. Terasaki, Appl. Phys. Lett. 87 (2005) 032902.
[18] R. Jia, X. Zhao, J. Li, X. Tang, Mater. Sci. Eng. B 185 (2014) 79–85.
[19] J. Yuan, Y.-H. Lin, H. Lu, B. Cheng, C.-W. Nan, J. Am. Ceram. Soc. 94 (2011) 1966–1969.
[20] P. Thongbai, S. Vangchangyia, E. Swatsitang, V. Amornkitbamrung, T. Yamwong, S. Maensiri, J. Mater. Sci.: Mater. Electron. 24 (2013) 875–883.
[21] H. Yu, H. Liu, H. Hao, D. Luo, M. Cao, Mater. Lett. 62 (2008) 1353–1355.
[22] M.A. Ramírez, R. Parra, M.M. Reboredo, J.A. Varela, M.S. Castro, L. Ramajo, Mater. Lett. 64 (2010) 1226–1228.
[23] M.A. Ramírez, P.R. Bueno, J.A. Varela, E. Longo, Appl. Phys. Lett. 89 (2006) 212102.
[24] M.A. Ramírez, P.R. Bueno, E. Longo, J.A. Varela, J. Phys. D: Appl. Phys. 41 (2008) 152004.
[25] M.A. Ramírez, P.R. Bueno, R. Tararam, A.A. Cavalheiro, E. Longo, J.A. Varela, J. Phys. D: Appl. Phys. 42 (2009) 185503.
[26] L. Ramajo, R. Parra, J.A. Varela, M.M. Reboredo, M.A. Ramírez, M.S. Castro, J. Alloys Compd. 497 (2010) 349–353.
[27] P. Thongbai, B. Putasaeng, T. Yamwong, S. Maensiri, J. Alloys Compd. 509 (2011) 7416–7420.
[28] J. Jumpatam, P. Thongbai, B. Kongsook, T. Yamwong, S. Maensiri, Mater. Lett. 76 (2012) 40–42.
[29] B. Cheng, Y.-H. Lin, H. Yang, J. Lan, C.-W. Nan, X. Xiao, J. He, J. Am. Ceram. Soc. 92 (2009) 2776–2779.
[30] P.R. Bueno, R. Tararan, R. Parra, E. Joanni, M.A. Ramírez, W.C. Ribeiro, E. Longo, J.A. Varela, J. Phys. D: Appl. Phys. 42 (2009) 055404.
[31] T. Adams, D. Sinclair, A. West, Phys. Rev. B 73 (2006) 094124.
[32] Y. Liu, Q. Chen, X. Zhao, J. Mater. Sci.: Mater. Electron. 25 (2014) 1547–1552.
[33] S. Vangchangyia, T. Yamwong, E. Swatsitang, P. Thongbai, S. Maensiri, Ceram. Int. 39 (2013) 8133–8139.
[34] S.-H. Hong, D.-Y. Kim, H.-M. Park, Y.-M. Kim, J. Am. Ceram. Soc. 90 (2007) 2118–2121.
[35] S.-Y. Chung, J.-H. Choi, J.-K. Choi, Appl. Phys. Lett. 91 (2007) 091912.
[36] L. Ni, X.M. Chen, J. Am. Ceram. Soc. 93 (2010) 184–189.
[37] L. Ni, X.M. Chen, Solid State Commun. 149 (2009) 379–383.
[38] C.H. Kim, Y.H. Jang, S.J. Seo, C.H. Song, J.Y. Son, Y.S. Yang, J.H. Cho, Phys. Rev. B 85 (2012) 245210.
[39] E.A. Patterson, S. Kwon, C.-C. Huang, D.P. Cann, Appl. Phys. Lett. 87 (2005) 182911.
[40] Q.G. Chi, L. Gao, X. Wang, J.Q. Lin, J. Sun, Q.Q. Lei, J. Alloys Compd. 559 (2013) 45–48.
[41] L. Zhang, Y. Wu, X. Guo, Z. Wang, Y. Zou, J. Mater. Sci.: Mater. Electron. 23 (2012) 865–869.
[42] J. Zang, M. Li, D.C. Sinclair, W. Jo, J. Rödel, J. Am. Ceram. Soc. 97 (5) (2014) 1523–1529.
[43] K.-M. Kim, S.-J. Kim, J.-H. Lee, D.-Y. Kim, J. Eur. Ceram. Soc. 27 (2007) 3991–3995.
[44] S. Vangchangyia, E. Swatsitang, P. Thongbai, S. Pinitsoontorn, T. Yamwong, S. Maensiri, V. Amornkitbamrung, P. Chindaprasirt, J. Am. Ceram. Soc. 95 (2012) 1497–1500.
[45] Z.M. Dang, Y. Shen, C.W. Nan, Appl. Phys. Lett. 81 (2002) 4814.
[46] J. Liu, C.-G. Duan, W.-G. Yin, W. Mei, R. Smith, J. Hardy, Phys. Rev. B 70 (2004) 144106.
[47] J. Liu, C.-G. Duan, W.N. Mei, R.W. Smith, J.R. Hardy, J. Appl. Phys. 98 (2005) 93703.

Microelectronic Engineering 126 (2014) 118–123

Contents lists available at ScienceDirect

Microelectronic Engineering

journal homepage: www.elsevier.com/locate/mee

$Na_{0.5}Bi_{0.5}Cu_3Ti_4O_{12}$ nanocrystalline powders prepared by a glycine–nitrate process: Preparation, characterization, and their dielectric properties

Wattana Tuichai [a], Prasit Thongbai [b,c,*], Vittaya Amornkitbamrung [b,c], Teerapon Yamwong [d], Santi Maensiri [e]

[a] Materials science and Nanotechnology Program, Faculty of Science, Khon Kaen University, Khon Kaen 40002, Thailand
[b] Department of Physics, Faculty of Science, Khon Kaen University, Khon Kaen 40002, Thailand
[c] Integrated Nanotechnology Research Center (INRC), Khon Kaen University, Khon Kaen 40002, Thailand
[d] National Metal and Materials Technology Center (MTEC), Thailand Science Park, Pathumthani 12120, Thailand
[e] School of Physics, Institute of Science, Suranaree University, Nakhon Ratchasima 30000, Thailand

ARTICLE INFO

Article history:
Received 19 October 2013
Received in revised form 16 April 2014
Accepted 1 July 2014
Available online 9 July 2014

Keywords:
Dielectric relaxation
Combustion method
Grain boundary
Ceramics

ABSTRACT

$Na_{0.5}Bi_{0.5}Cu_3Ti_4O_{12}$ nanocrystalline powders were prepared by a combustion method using glycine as a fuel. X-ray diffraction technique was used to characterize $Na_{0.5}Bi_{0.5}Cu_3Ti_4O_{12}$ nanocrystalline powders, which were obtained by firing precursors at 800–900 °C for 6 h. Dense ceramic microstructure of $Na_{0.5}Bi_{0.5}Cu_3Ti_4O_{12}$ was obtained by sintering ceramic powders at 980 °C for 12 h. The $Na_{0.5}Bi_{0.5}Cu_3Ti_4O_{12}$ ceramics exhibited high dielectric constants in the order of 10^4 at room temperature and 1 kHz. The loss tangent of the sintered $Na_{0.5}Bi_{0.5}Cu_3Ti_4O_{12}$ ceramics was found to be less than 0.2 at room temperature and 1 kHz. The impedance spectroscopy analysis revealed that $Na_{0.5}Bi_{0.5}Cu_3Ti_4O_{12}$ ceramics were electrically heterogeneous, consisting of insulating grain boundaries and conductive part of the grains. The dielectric relaxation behavior with activation energies of about 0.118–0.127 eV observed in the dielectric spectra of the $Na_{0.5}Bi_{0.5}Cu_3Ti_4O_{12}$ ceramics was suggested to be the Maxwell–Wagner relaxation type, which was originated from the polarization relaxation at grain boundaries.

1. Introduction

$CaCu_3Ti_4O_{12}$ (CCTO) attracted considerable attention since its abnormal dielectric response was disclosed [1,2]. The dielectric behavior of CCTO ceramics is very interesting. CCTO has very high dielectric permittivity (ε') in the order of 10^3–10^5 [3–8]. Furthermore, according to the first report [1], it was found that ε' at 1 MHz is nearly independent on temperature over the range from room temperature to 300 °C. Therefore, CCTO ceramic is believed to be a new promising dielectric material for capacitor applications. Recently, the dielectric properties of related oxides in the family of $ACu_3Ti_4O_{12}$ compounds, where $A = Bi_{2/3}$ [9], $La_{2/3}$ [9,10], $Y_{2/3}$ [9,11], $Na_{1/2}Bi_{1/2}$ [12–16], $Na_{1/2}La_{1/2}$ [17,18], and $Na_{1/2}Y_{1/2}$ [19] have been widely studied. According to the first report on the study of the dielectric properties of these $ACu_3Ti_4O_{12}$ compounds [20], the ε' values of $ACu_3Ti_4O_{12}$ ceramics were found to be considerably lower than 3600 at 100 kHz. However, it was found that by varying sintering conditions, ε' of some $ACu_3Ti_4O_{12}$ compounds can be enhanced to the order of 10^4, similar to that observed in CCTO ceramics [9,11,12,14,18,19].

To study CCTO ceramics and related $ACu_3Ti_4O_{12}$ compounds for applications in electronic devices, selection of the preparation method is one of the most important decisions, which can determine the final bulk properties of these materials. Usually, CCTO ceramics and related $ACu_3Ti_4O_{12}$ compounds are synthesized via a solid state reaction (SSR) method [1,2,8–10,12,13,17,19]. Na_2CO_3, $CaCO_3$, CuO, TiO_2, Bi_2O_3, La_2O_3, and Y_2O_3 were selected as the starting raw materials to synthesize ceramic powders, which were used to form a green body before sintering. As well known, the SSR method requires high temperatures and long reaction times to produce a pure phase.

In contrast to the SSR method, synthesis of ceramic powder by using chemical solutions can offer the possibility of closer stoichiometric control compared to the SSR method. Low-temperature chemical reactions with short reaction times are usually sufficient to produce a pure phase [4,5]. There have been many studies

* Corresponding author at: Department of Physics, Faculty of Science, Khon Kaen University, Khon Kaen 40002, Thailand. Tel.: +66 84 4190266; fax: +66 43 202374.
E-mail address: pthongbai@kku.ac.th (P. Thongbai).

http://dx.doi.org/10.1016/j.mee.2014.07.002
0167-9317/

investigating synthesis of CCTO ceramics by chemical methods [3–7,21,22]. Unfortunately, synthesis of $ACu_3Ti_4O_{12}$ ceramic compounds via chemical routes have been rarely reported [14–16,18]. For the synthesis of CCTO ceramic powders, some chemical methods can effectively produce a CCTO phase by firing at temperature lower than 800 °C with short reaction times such as pyrolysis of organic solutions [4], combustion method using ammonia as a fuel [5], and ethylenediaminetetraacetic acid (EDTA) precursor [21]. Although there have been reports on chemical preparation of $ACu_3Ti_4O_{12}$ ceramic compounds, it is useful to develop new methods to increase the number of design options and to support a variety of applications in the future. Therefore, a new wet chemical solution route to prepare CCTO is worthy of study.

Among chemical routes used to prepare CCTO ceramics and related $ACu_3Ti_4O_{12}$ compounds, the combustion method is one of the most interesting routes to effectively prepare these ceramic powders [5,7,21]. Normally, organic compounds such as urea, glycine, citric acid, and EDTA are widely used as fuels for gel combustion processes [23]. The glycine nitrate process (GNP) is one of the most attractive combustion methods [24], which can be used effectively to prepare homogeneous nanoparticles of ceramic powders. The advantages of the GNP process are relatively low cost, fast heating rates, short reaction times, high composition homogeneity, and high energy efficiency [25,26]. To best of our knowledge, there is no report on the preparation of $ACu_3Ti_4O_{12}$ ceramic compounds by using a combustion method. Therefore, in this work, we have prepared $Na_{1/2}Bi_{1/2}Cu_3Ti_4O_{12}$ (NBCTO) ceramics using GNP. The NBCTO powders and sintered ceramics were characterized. The dielectric properties of the sintered NBCTO ceramics were investigated and discussed.

2. Experimental procedure

NBCTO ceramics were prepared by the GNP. The starting raw materials consist of $NaNO_3$ (99.99%, Kanto Chemical), $(CH_3CO_2)_3Bi$ (99.99%, Sigma–Aldrich), $Cu(NO_3)_2{\cdot}4H_2O$ (99.5%, Carlo Erba), $C_{16}H_{28}O_6Ti$ (75 wt.% in isopropanol, Sigma–Aldrich), acetic acid, deionized water, and glycine. First, stoichiometric amounts of $NaNO_3$, $(CH_3CO_2)_3Bi$, and $Cu(NO_3)_2{\cdot}4H_2O$ with molar ratio of 0.5:0.5:3 were dissolved in an aqueous solution of acetic acid with constant stirring at room temperature. Then, a $C_{16}H_{28}O_6Ti$ solution was added into the metal ion solution under constant stirring until the formation of a clear and transparent solution was accomplished. Next, 0.5 g (or 0.75 g) of glycine powder was added into the mixed solution with stirring at 150 °C until a viscous gel was observed. Finally, the gel was dried in air at 350 °C for 30 min. It is worth noting that combustion was occurred in this step at a temperature of about 200 °C. When 1.0 g of glycine was used to prepare NBCTO powders, the reactions occurring during ignition were highly explosive and the combustion process cannot be controlled. The resulting dried porous precursors were ground and calcined at 800, 850, and 900 °C for 6 h. The NBCTO powders that were prepared by using 0.5 g of glycine and calcined at 800, 850, and 900 °C are referred to P1, P2, and P3 powders, respectively. The NBCTO powders that were prepared by using 0.75 g of glycine and calcined at 800, 850, and 900 °C are abbreviated as P4, P5, and P6 powders, respectively. All of the calcined powders were pressed into pellets with dimensions of 9.5 mm in diameter and ~1–2 mm in thickness by uniaxial compression at 200 MPa. Finally, these pellets were sintered in air at 980 °C for 12 h. The sintered NBCTO ceramics synthesized by using P1–P6 powders to form green bodies are assigned to be the S1-G0.5C800, S2-G0.5C850, S3-G0.5C900, S4-G0.75C800, S5-G0.75C850, and S6-G0.75C900 ceramic samples, respectively.

The phase formation and crystal structure of the NBCTO powders and the sintered ceramics were analyzed by X-ray diffraction (XRD) (Philips PW3040, the Netherlands) technique. Scanning electron microscope (SEM) (LEO 1450VP, UK) coupled with energy-dispersive X-ray spectrometry (EDS) were used to characterize the microstructure of the NBCTO powders and the sintered ceramics. Each pellet face of the sintered bulk ceramics was polished and sputtered with Au at a current of 25 mA for 8 min using a Polaron SC500 sputter coating unit. The dielectric properties were measured using an Agilent 4294A Precision Impedance Analyzer over the frequency and temperature ranges from 10^2 to 10^7 Hz and −70 to 220 °C with an oscillation voltage of 0.5 V.

In this work, the complex impedance (Z^*) was calculated from the equation,

$$\varepsilon^* = \varepsilon' - i\varepsilon'' = \frac{1}{i\omega C_0 Z^*} = \frac{1}{i\omega C_0 (Z' - iZ'')}, \quad (1)$$

where Z' and Z'' are the real part and imaginary parts of Z^*, respectively. ε' and ε'' are the real (dielectric constant) and imaginary parts (dielectric loss) of the complex permittivity (ε^*), respectively. ω is the angular frequency ($\omega = 2\pi f$) and $i = \sqrt{-1}$. $C_0 = \varepsilon_0 S/d$ is the empty cell capacitance, where d is the sample thickness, S is the sample area, and ε_0 is the permittivity of free space, $\varepsilon_0 = 8.854 \times 10^{-12}$ F/m.

3. Results and discussion

The phase compositions of the calcined powders were characterized by using the XRD technique. Fig. 1 shows the XRD patterns of NBCTO powders prepared by a GNP using 0.5 g and 0.75 g of glycine and calcined in air at 800, 850, and 900 °C for 6 h. As shown

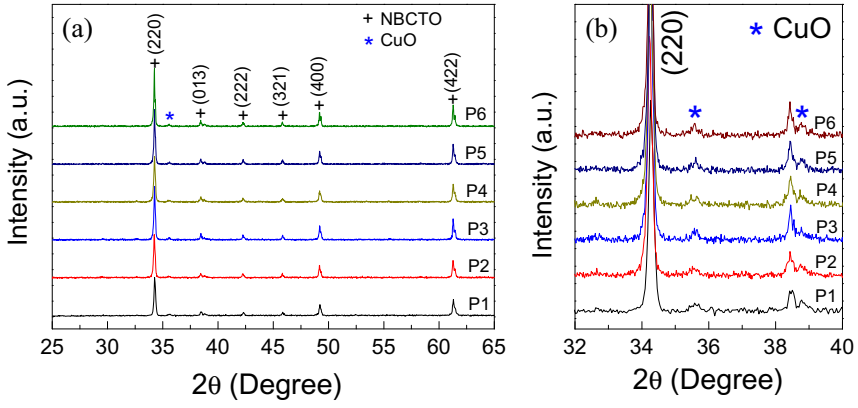

Fig. 1. XRD patterns of NBCTO powders calcined at different temperatures and prepared by using different amount of glycine. (a) and (b) represent the XRD patterns in a wide range scale of $2\theta = 25–65°$ and narrow range scale $2\theta = 32–38°$, respectively, revealing the existence of a second CuO phase.

in Fig. 1(a), the main peaks of XRD corresponding to NBCTO crystal structure were observed in all the samples. The overall XRD patterns of all the samples (P1–P6 powders) are very similar to that observed in literature for the NBCTO ceramics prepared by a conventional solid state reaction method [12,13]. Furthermore, the XRD patterns of the P1–P6 powders are also similar to those observed in NBCTO ceramics prepared by using a Pechini method [14], sol–gel method [15], and co-precipitation method [16]. As demonstrated in Fig. 1(b), however, careful inspection revealed that a very small amount of CuO secondary phase was still observed in all the NBCTO powders, which is similar to that observed in NBCTO powders prepared by using other chemical routes [14–16]. It is important to note that when the precursors were calcined at temperatures lower than 800 °C, a large amount of impurity phases were detected in XRD patterns. On the other hand, a relatively high calcination temperature (>900 °C) resulted in the existence of powder agglomeration. This can cause an inhomogeneous packing of particles in the green body, which is unsuitable for fabricating highly dense microstructure.

Lattice parameters were calculated by using Cohen's least mean square method and found to be 7.411 ± 0.0015, 7.409 ± 0.0006, 7.414 ± 0.0016, 7.407 ± 0.0004, 7.397 ± 0.0012, and 7.408 ± 0.0006 Å for the P1–P6 powders, respectively. It is important to note that all of the sintered NBCTO ceramic samples are pure phase

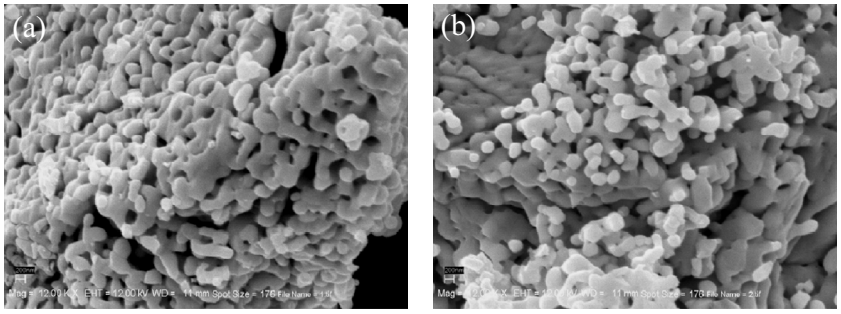

Fig. 2. SEM images of (a) P1 and (b) P4 powders calcined at 800 °C for 6 h.

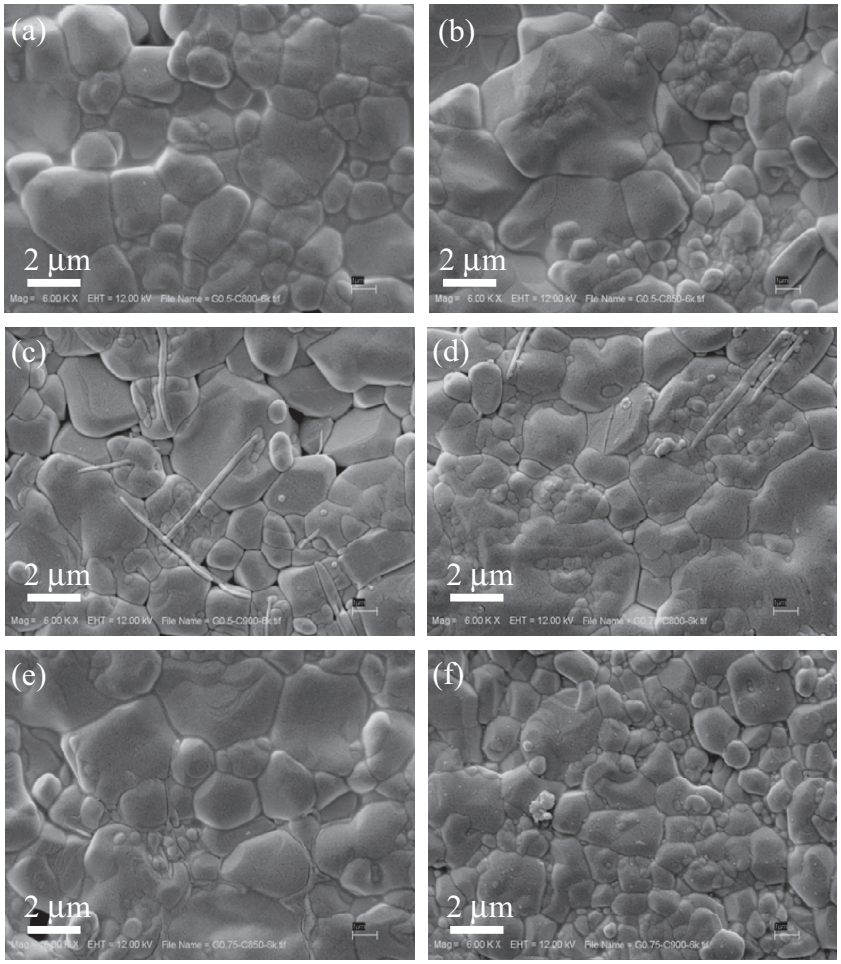

Fig. 3. SEM images of surface morphologies of NBCTO ceramics sintered at 980 °C for 12 h: (a) S1-G0.5C800, (b) S2-G0.5C850, (c) S3-G0.5C900, (d) S4-G0.75C800, (e) S5-G0.75C850, and (f) S6-G0.75C900 samples.

with lattice parameters of 7.409 ± 0.0009, 7.408 ± 0.0013, 7.407 ± 0.0007, 7.408 ± 0.0012, 7.408 ± 0.0006, and 7.407 ± 0.0008 Å for the S1-G0.5C800, S2-G0.5C850, S3-G0.5C900, S4-G0.75C800, S5-G0.75C850, and S6-G0.75C900 samples, respectively. These values of the NBCTO powders and bulk ceramics are comparable to the value of 7.412 Å reported in the literature [20]. SEM images of the P1 and P4 powders that were calcined at 800 °C are shown in Fig. 2. Particle sizes of these NBCTO powders prepared by a GNP were in the range of 100–300 nm. The surface morphologies of the sintered NBCTO ceramics are shown in Fig. 3, revealing the grain and grain boundary structure. The mean grain sizes of the S1-G0.5C800, S2-G0.5C850, S3-G0.5C900, S4-G0.75C800, S5-G0.75C850, and S6-G0.75C900 samples were estimated to be ~2.63, ~2.83, ~3.29, ~2.38, ~2.93, and ~2.09 μm, respectively. Interestingly, the microstructure with highly dense grain packing is observed in all the ceramic samples. The densities of all the NBCTO ceramic samples were calculated using Archimedes method and found to be 4.44, 4.48, 4.47, 5.01, 4.97, and 5.07 g/cm^3, respectively. These values are comparable to the value of 5.053 g/cm^3 for the theoretical density of CCTO.

To describe the dielectric properties of NBCTO ceramics, first of all, the data about the electrical properties of grains and grain boundaries must be achieved. Thus, an impedance spectroscopy was used to investigate the electrical responses of grain and grain boundary of the sintered NBCTO ceramic samples. This method is a powerful tool to separate the electrical responses of grain and the grain boundary of polycrystalline ceramics [27]. Impedance complex plane plots ($-Z''$ vs. Z' plots) at a temperature of 60 °C and their expanded view of high frequency data close to the origin

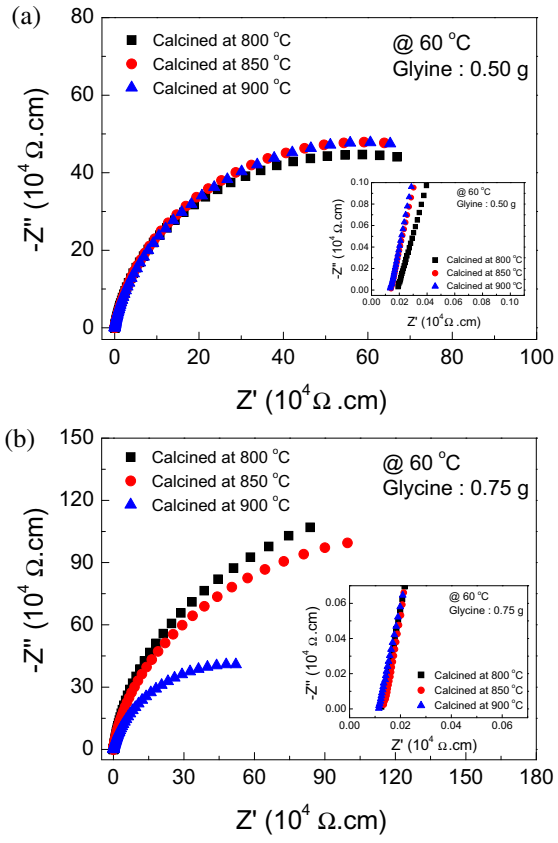

Fig. 4. Impedance complex plane plots at 60 °C of NBCTO ceramics: (a) for the S1-G0.5C800, S2-G0.5C850, S3-G0.5C900 samples, and (b) for the S4-G0.75C800, S5-G0.75C850, S6-G0.75C900 samples. Their insets show an expanded view of the high-frequency data close to the origin, indicating the electrical response of the grains.

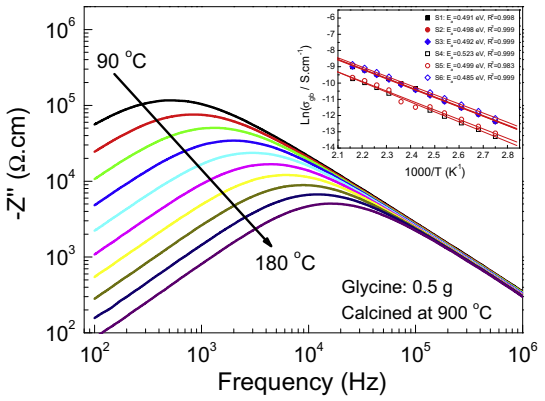

Fig. 5. Frequency dependence of Z'' in the temperature range of 90–180 °C for the S3-G0.5C900 sample (each step increase in measured temperature is 10 °C); inset shows Arrhenius plots for the grain boundary conductivity for all the ceramic samples.

for the NBCTO samples are shown in Fig. 4(a) and (b) and their insets, respectively. Basically, the grain resistance (R_g) and grain boundary resistance (R_{gb}) of a polycrystalline ceramic can be determined from the diameter of two semicircular arcs, which are observed in the impedance spectrum at high and low frequency ranges, respectively [27]. When only one arc is observed in the measured frequency range at any temperatures, R_g is usually estimated from a nonzero intercept on the Z' axis at high frequencies. As shown in Fig. 4(a) and (b), R_{gb} values of the S1-G0.5C800, S2-G0.5C850, and S3-G0.5C900 samples are nearly the same; whereas, R_{gb} of the S6-G0.75C900 sample is less than that of the S4-G0.75C800 and S5-G0.75C850 samples. R_g values of all the samples are nearly the same in value. By using the impedance spectroscopy analysis, it is strongly indicated that the NBCTO ceramics are electrically heterogeneous, consisting of insulating grain boundaries and semiconducting grains. For example, at 60 °C, it can be estimated that R_{gb} values of NBCTO ceramic samples are of about 1–2 × 10^6 Ω.cm; while, R_g values are of about 1–2 × 10^2 Ω.cm.

The frequency dependence of Z'' was used to further investigate the electrical characteristics of grain boundaries. According to the equivalent circuit represented the internal barrier layer capacitor (IBLC) electrical structure model, Z'' can be expressed as [28],

$$Z'' = R_g\left[\frac{\omega R_g C_g}{1+(\omega R_g C_g)^2}\right] + R_{gb}\left[\frac{\omega R_{gb} C_{gb}}{1+(\omega R_{gb} C_{gb})^2}\right], \quad (2)$$

As shown in Fig. 5, Z'' peak shifts to higher frequencies with increasing temperature, indicating a thermally activated electrical response. It is observed that Z'' peaks decrease with increasing temperature. At the maximum value of Z'', it can be shown that $R = 2Z''_{max}$ [29]. As shown in Fig. 4, at 60 °C, the values of R_{gb} of all the samples are of about 1–2 MΩ.cm. Thus, a step decrease in Z''_{max} represents a decrease in R_{gb}. Therefore, R_{gb} values of all the samples can be calculated at different temperatures. As demonstrated in the inset of Fig. 5, it was found that the grain boundary conductivity, $\sigma_{gb} = 1/R_{gb}$, follows the Arrhenius law,

$$\sigma_{gb} = \sigma_0 \exp\left(\frac{-E_{gb}}{k_B T}\right), \quad (3)$$

where E_{gb} is the activation energy required for conduction at grain boundaries, σ_0 is constant term, k_B is the Boltzmann constant, and T is absolute temperature. By using Eq. (3), the values of E_{gb} of all the samples can be calculated from the slope of plots of $\ln\sigma$ vs. 1000/T. E_{gb} values for the S1-G0.5C800, S2-G0.5C850, S3-G0.5C900, S4-G0.75C800, S5-G0.75C850, and S6-G0.75C900 samples are found to be 0.491, 0.498, 0.492, 0.523, 0.499, and 0.485 eV, respectively.

These values are comparable to reported values of 0.720, 0.590, and 0.639 eV for E_{gb} of the $Bi_{2/3}Cu_3Ti_4O_{12}$ [30], $La_{2/3}Cu_3Ti_4O_{12}$ [10], and $Na_{1/2}La_{1/2}Cu_3Ti_4O_{12}$ [17] ceramics, respectively. It is observed that E_{gb} of the S6-G0.75C900 sample is lower than other samples. According to the SEM images of the sintered ceramics (Fig. 3) and the impedance spectroscopy analysis (Fig. 4), R_{gb} of the S6-G0.75C900 sample is lower than R_{gb} values of the S4-G0.75C800 and S5-G0.75C850 samples even though its mean grain size is smallest. This indicates that a low R_{gb} value of the S6-G0.75C900 sample is primary caused by the intrinsic properties of the grain boundary (i.e., E_{gb} or electrostatic potential barrier height), rather than the geometric effect such as the grain boundary thickness. Thus, it is reasonable to suggest that a low R_{gb} value of the S6-G0.75C900 sample is primary attributed to a low E_{gb} value.

The dielectric properties of the sintered NBCTO ceramics were investigated as functions of temperature and frequency. Fig. 6(a) and (b) shows the frequency dependence of ε' at 20 °C for all the samples. At 10^2 Hz, ε' values at 20 °C of the S1-G0.5C800, S2-G0.5C850, S3-G0.5C900, S4-G0.75C800, S5-G0.75C850, and S6-G0.75C900 samples are of about 0.93×10^4, 1.11×10^4, 1.08×10^4, 0.88×10^4, 0.74×10^4, and 1.36×10^4, respectively. The values of ε' of all the samples synthesized from powders that were prepared by using different conditions are of about 10^4 at low frequency range and nearly the same in value. ε' values at 10^3 Hz are of about 0.76×10^4, 0.87×10^4, 0.82×10^4, 0.75×10^4, 0.60×10^4, and 1.00×10^4, respectively. Xu et al. [15] reported ε' value of $\sim 1–2 \times 10^4$ (at 10^2 Hz) for NBCTO ceramics with grain sizes of 1.0–2.2 μm prepared by a sol–gel technique using the sintering conditions of 950 and 1000 °C for 3 h. Qiu et al. [14] investigated the dielectric properties of NBCTO ceramics that were prepared by a modified Pechini method and sintered at 1000 °C for 5 h. They found that the NBCTO ceramic with average grain size of 1.9 μm exhibited a high value of $\varepsilon' \sim 2.0 \times 10^4$ at 1 kHz and room temperature. Most recently, the dielectric properties of NBCTO ceramics prepared by a co-precipitation method have been investigated [16]. At room temperature and 10^3 Hz, ε' values of NBCTO ceramics sintered at 950–1020 °C for 8 h were found to be $\sim 0.3–2.0 \times 10^4$. In this current study, ε' values of the NBCTO ceramics with grain sizes of ~2–3 μm prepared by a GNP can be comparable to ε' values for NBCTO ceramics prepared by other chemical routes. The insets of Figs. 6(a) and (b) show tanδ as a function of frequency. The values of tanδ at 10^3 Hz of all the samples are lower than 0.2, except for the S6-G0.75C900 sample. When the frequency increased to 10^6 Hz, ε' rapidly decreased. This indicates a dielectric relaxation mechanism in the NBCTO ceramics. In this work, we also found that the sintering time had effects on both microstructure and dielectric properties of NBCTO ceramics. A large amount of pores were observed in the NBCTO ceramics sintered at 980 °C for 3 h. Some residual pores were also observed in the NBCTO ceramics sintered at 980 °C for 6 h. The existence of pores in the microstructure of NBCTO ceramics resulted in a decrease in ε'.

In the low-frequency range of 10^2–10^4 Hz, ε' of the S6-G0.75C900 sample is higher than that of the S4-G0.75C800 and S5-G0.75C850 samples (Fig. 6(b)). This may be due to the effect of sample-electrode interface, i.e., interfacial polarization at the sample-electrode contact. As demonstrated by Li et al. [31], it was clearly demonstrated that the electrical response of sample-electrode contact can contribute to the low-frequency dielectric response of CCTO ceramics. They have also demonstrated that a low-frequency ε' value is dominant when R_{gb} was reduced. Therefore, in the current study, the observed higher value of ε' in a low-frequency range of the S6-G0.75C900 sample might be associated with a low value of R_{gb}, resulting in the dominant effect of sample-electrode contact.

To study the dielectric relaxation behavior in NBCTO ceramics, the frequency dependence of ε' and ε'' at various temperatures in the range from −70 to 50 °C for the S3-G0.5C900 and

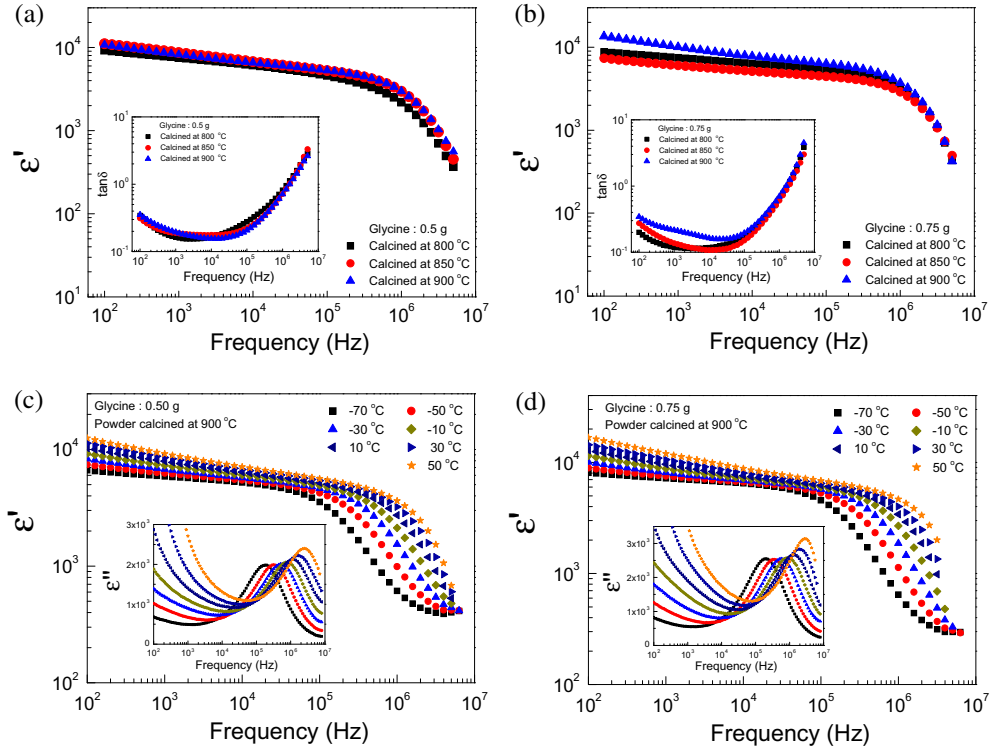

Fig. 6. (a, b) Frequency dependence of ε' at 20 °C for all of the NBCTO ceramics; insets of (a) and (b) show tanδ as a function of frequency. (c, d) Frequency dependence of ε' at various temperatures in the range from −70 to 50 °C of the S3-G0.5C900 and S6-G0.75C900 samples, respectively; their insets demonstrate the frequency dependence of ε'' at different temperatures.

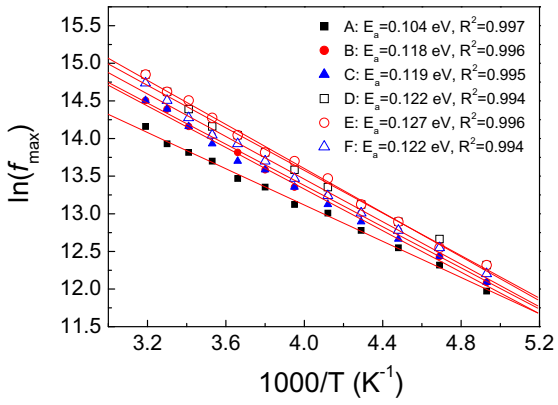

Fig. 7. Arrhenius plots of the dielectric relaxation process for all the ceramic samples: (A) S1-G0.5C800, (B) S2-G0.5C850, (C) S3-G0.5C900, (D) S4-G0.75C800, (E) S5-G0.75C850, and (F) S6-G0.75C900 samples.

S6-G0.75C900 samples was measured. As shown in Figs 6(c) and (d) and their insets, the rapid decrease (step-like decrease) in ε' and the related ε'' peak move to a higher frequency as the measuring temperature was increased. This behavior indicates a thermally activated dielectric relaxation process in the NBCTO ceramics. Note that the increase in ε'' as the frequency decreased from 10^4 to 10^2 Hz is due to the dc conduction in the NBCTO ceramics according to the relationship $\varepsilon'' = \sigma_{dc}/\varepsilon_0\omega$, where, σ_{dc} is the dc conductivity. As shown in Fig. 7, the temperature dependence of the frequency at a maxima peak of ε'' (f_{max}) follows the Arrhenius law [30],

$$f_{max} = f_0 \exp(-E_a/k_B T), \quad (4)$$

where f_0 and E_a are a constant value and the activation energy required for relaxation process, respectively. From Eq. (4), E_a can be calculated from the linear slopes in Fig. 7. The values of E_a for the S1-G0.5C800, S2-G0.5C850, S3-G0.5C900, S4-G0.75C800, S5-G0.75C850, and S6-G0.75C900 ceramic samples were found to be 0.104, 0.118, 0.119, 0.122, 0.127, and 0.122 eV, respectively. The observed dielectric relaxation in the NBCTO ceramics may be attributed to the Maxwell-Wagner polarization mechanism [30].

4. Conclusion

In conclusion, NBCTO nanocrystalline powders have successfully been prepared by using a GNP. NBCTO nanocrystalline powders were obtained by firing precursors at 800–900 °C for 6 h. Dense ceramic microstructure of NBCTO was achieved by sintering the compact ceramic powders at 980 °C for 12 h. ε' values of the NBCTO ceramics were found to be very high as in the order of 10^4 at room temperature and 1 kHz. The values of tanδ of the sintered NBCTO ceramics were found to be lower than 0.2 at room temperature and 1 kHz. By using an impedance spectroscopy, it was strongly indicated that the structure of NBCTO polycrystalline ceramics consisted of insulating grain boundaries and semiconducting grains. The dielectric relaxation behavior observed in the dielectric spectra of NBCTO ceramics with E_a of about 0.118–0.127 eV was attributed to the Maxwell–Wagner relaxation polarization at grain boundaries.

Acknowledgments

This work was financially supported by the Thailand Research Fund (TRF) and Khon Kaen University, Thailand (Grant No. TRG5680047) and the Integrated Nanotechnology Research Center (*INRC*), Khon Kaen University, Thailand. W. Tuichai would like to thank the Thailand Graduate Institute of Science and Technology (TGIST) for his Master of Science Degree scholarship.

References

[1] M.A. Subramanian, D. Li, N. Duan, B.A. Reisner, A.W. Sleight, J. Solid State Chem. 151 (2000) 323–325.
[2] A.P. Ramirez, M.A. Subramanian, M. Gardel, G. Blumberg, D. Li, T. Vogt, S.M. Shapiro, Solid State Commun. 115 (2000) 217–220.
[3] P. Jha, P. Arora, A.K. Ganguli, Mater. Lett. 57 (2003) 2443–2446.
[4] J. Liu, Y. Sui, C.-G. Duan, W.-N. Mei, R.W. Smith, J.R. Hardy, Chem. Mater. 18 (2006) 3878–3882.
[5] J. Liu, R.W. Smith, W.-N. Mei, Chem. Mater. 19 (2007) 6020–6024.
[6] C. Masingboon, S. Maensiri, T. Yamwong, P.L. Anderson, S. Seraphin, Appl. Phys. A 91 (2008) 87–95.
[7] P. Thongbai, S. Pinitsoontorn, V. Amornkitbamrung, T. Yamwong, S. Maensiri, P. Chindaprasirt, Int. J. Appl. Ceram. Technol. 10 (2013) E77–E87.
[8] P. Thongbai, T. Yamwong, S. Maensiri, Microelectron. Eng. 108 (2013) 177–181.
[9] W. Hao, J. Zhang, Y. Tan, W. Su, J. Am. Ceram. Soc. 92 (2009) 2937–2943.
[10] B. Shri Prakash, K.B.R. Varma, J. Mater. Sci.: Mater. Electron. 17 (2006) 899–907.
[11] P. Liang, Z. Yang, X. Chao, Z. Liu, X.M. Chen, J. Am. Ceram. Soc. 95 (2012) 2218–2225.
[12] H. Ren, P. Liang, Z. Yang, Mater. Res. Bull. 45 (2010) 1608–1613.
[13] Z. Yang, H. Ren, X. Chao, P. Liang, Mater. Res. Bull. 47 (2012) 1273–1277.
[14] Y. Qiu, Z.Z. Ma, S.X. Huo, H.N. Duan, Z.M. Tian, S.L. Yuan, L. Chen, J. Mater. Sci.: Mater. Electron. 23 (2012) 1587–1591.
[15] B. Xu, J. Zhang, Z. Tian, S.L. Yuan, Mater. Lett. 75 (2012) 87–90.
[16] Y. Su, J. Song, R. Liu, H. Huang, J. Electroceram. 30 (2013) 166–171.
[17] P. Thongbai, T. Yamwong, S. Maensiri, Mater. Res. Bull. 47 (2012) 432–437.
[18] Z. Liu, G. Jiao, X. Chao, Z. Yang, Mater. Res. Bull. 48 (2013) 4877–4883.
[19] W. Somphan, N. Sangwong, T. Yamwong, P. Thongbai, J. Mater. Sci.: Mater. Electron. 23 (2012) 1229–1234.
[20] M.A. Subramanian, A.W. Sleight, Solid State Sci. 4 (2002) 347–351.
[21] Y. He, T. Liu, Y. Xu, J. Zhao, Z. Du, Mater. Res. Bull. 47 (2012) 1181–1184.
[22] P. Thongbai, B. Putasaeng, T. Yamwong, S. Maensiri, J. Alloys Comp. 509 (2011) 7416–7420.
[23] S. Mukherjee, M.R. Gonal, M.K. Patel, M. Roy, A. Patra, A.K. Tyagi, M. Menon, J. Am. Ceram. Soc. 95 (2012) 290–295.
[24] L.A. Chick, L.R. Pederson, G.D. Maupin, J.L. Bates, L.E. Thomas, G.J. Exarhos, Mater. Lett. 10 (1990) 6–12.
[25] B. Liu, Y. Zhang, J. Alloys Comp. 453 (2008) 418–422.
[26] M.N. Rahaman, Ceramic Processing and Sintering, second ed., M. Dekker, New York, 2003.
[27] F.D. Morrison, D.C. Sinclair, A.R. West, J. Am. Ceram. Soc. 84 (2001) 531–538.
[28] J. Liu, C.-G. Duan, W.N. Mei, R.W. Smith, J.R. Hardy, J. Appl. Phys. 98 (2005) 093703.
[29] M. Li, A. Feteira, D.C. Sinclair, J. Appl. Phys. 105 (2009) 114109.
[30] J. Liu, C.-G. Duan, W.-G. Yin, W. Mei, R. Smith, J. Hardy, Phys. Rev. B 70 (2004).
[31] M. Li, D.C. Sinclair, A.R. West, J. Appl. Phys. 109 (2011) 084106.